COMPUTATIONAL STUDY ON POLYMERS OF UNSUBSTITUTED AND SOME SUBSTITUTED PYRROLES

COLLINS UGOCHUKWU IBEJI

COMPUTATIONAL STUDY ON POLYMERS OF UNSUBSTITUTED AND SOME SUBSTITUTED PYRROLES

By

COLLINS UGOCHUKWU IBEJI

B.Sc. Biochemistry (Benin), M.Sc. Environmental Chemistry (Ibadan)

Matric No.: 153189

A Thesis in the Department of Chemistry,
Submitted to the Faculty of science
in partial fulfillment of the requirements for the Degree of

DOCTOR OF PHILOSOPHY

of the

UNIVERSITY OF IBADAN

September 2015

ABSTRACT

Conjugated polymers which interact with biological systems have attracted interest due to their high conductivity, stability and electronic properties. Substituted polymers of 3-methyl pyrrole-4-carboxylic acid (MPC^a) have been synthesised and used as components of biosensor, while unsubstituted polypyrroles are not effective for such application. However the mechanism of interaction, nature, the relative importance of dynamic and static electron correlation of the polymers are not completely understood. This research was designed using computational approach to study the molecular properties of substituted and unsubstittued pyrrole polymers with a view to understanding what make polymers of substituted pyrroles suitable components of biosensor.

Structures of unsubstituted Pyrrole (Py); substituted pyrroles which include 3-methyl-pyrrole-4-carboxylic acid (MPC^a), 3-methyl-pyrrole-4-carboxamide (MPCam), 3-methyl-pyrrole-4-sulfonic acid ($MPSO_3H$), 3-methyl-pyrrole-1-carboxylic acid, (MPC^b), 3-methyl-pyrrole-4-carbothioic acid (MPCOSH), 3-methyl-pyrrole-4-carbaldehyde (MPCHO) and their polymers were studied using quantum mechanical approach. The molecular properties investigated were Energy gap (*Eg*), Koopman's reactivity descriptors, Fukui function, Lowest Unoccupied Molecular Orbital (LUMO), Highest Occupied Molecular Orbital (HOMO) and thermodynamic properties. These were calculated using restricted hybrid density functional theory with Becke three, Lee Yang and Parr at 6-31G(d) basis set. The calculated *Eg* were extrapolated to polymer through second order-degree polynomial equation. Spin-flip time density functional theory and coupled cluster single and double method with 6-311++G(d,p) basis set were used to calculate Coupled Cluster operator (T1) diagnostic and Vertical Singlet-Triplet (VST) gap to accurately determine polymers suitability as components of biosensor. All calculations were carried out using quantum mechanical software.

The calculated *Eg* of the polymers decreased with increasing chain length and the nature of substituent. The order of *Eg* was MPCHO > Py > MPC^b > MPC^a > MPCam > $MPSO_3H$ > MPCOSH, with MPCOSH having the lowest value of 1.7 eV. Substituted polypyrroles except MPCHO have stronger electron-electron interactions since electron-electron interaction is more when the *Eg* is low (between 1.0 and 3.0 eV). Koopman's reactivity descriptors were within the range of -3.9 to 2.4 eV (chemical

potential), 1.5 to 2.1 eV (chemical hardness) and 1.4 to 4.4 eV (electrophilicity index). Fukui function revealed a high electron density around the substituted functional groups and the LUMO and HOMO were extended over the C-C and C=C bonds. Thermodynamic parameters were enthalpy change (-4361.1 to -1045.7 $kJmol^{-}$), entropy change (540.3 to 952.2 $Jmol^{-1}K^{-1}$) and free energy change (ΔG^{0}_{f}**)** (-4361.2 to -1045.8 $kJmol^{-1}$) indicating spontaneous formation of the polymers. The T1 diagnostic of unsubstituted polypyrroles ranged from 0.0015 to 0.0013, while substituted polypyrroles ranged from 0.030 to 0.065. The T1 <0.02 indicated that unsubstituted polypyrrole had dynamic correlation with single reference (closed shell), while T1 >0.02 showed that substituted polypyrroles possessed static electron correlation with multireference (open shell) nature. The VST gap of unsubstituted polypyrroles ranged from 3.0 to 4.8 eV, while substituted polypyrroles ranged from 3.1 to 5.3 eV. The VST gap >0 revealed that all studied systems have a singlet ground state.

The presence of substituents on polypyrrole decreased the energy gaps which led to the enhancement of their molecular properties making them suitable components of biosensor.

Keywords: Conjugated polymers, Substituted and unsubstituted polypyrrole, Energy gap.

Word count: 497

ACKNOWLEDGEMENT

I am grateful to the Head of Department; Prof. A.A. Adesomoju for his fatherly advice. My profound gratitude goes to my supervisors Prof. B.B. Adeleke and Dr. I.A. Adejoro for their fatherly role and also for being there to correct and give directions when needed. Also Prof. O. Osibanjo, Prof. P.C. Onianwa, Prof. F.M. Bamiro, Prof. J.O. Woods, Prof. K.O. Adebowale, Prof. J.O. Babalola, Prof. B.I. Olu- Owolabi, Dr. G.O Adewuyi, Dr. Odozi, Dr. Ipeaiyeda, Dr. Obi-Egbedi, Dr Oladosu, Dr Oninla and other academic staff of the Department of Chemistry for contributing in one way or the other to the advancement of my knowledge base.

My appreciation also goes to CV Raman fellowship for the award of fellowship, 2013/2014. My deep gratitude goes to Dr. Debashree Gosh, my host scientist in India, for giving me an opportunity to work in her laboratory, National Chemical Laboratory (NCL, Pune, India). My appreciation goes to Delta state scholarship board for the 2011 session scholarship awarded to me. Thanks also to my lab mates in NCL, India, Samik, Baljinder, Tamal and others. I will also want to appreciate my lab mates, Mrs Adeboye, Babatunde, Eric, Gideon and others in Chemistry Department UI.

I am really grateful, to my family in the Redeemed Christain Postgraduate fellowship (RCPGF), people like Bro Aduloju, Bro Martins and Bro Henry, for their encouragement and prayers. I won't fail to appreciate my friends and fellow instrumentalist for their inspiration and making my stay a blissful one. I want to say thanks to Doyin, Toyin, Tofunmi, Omasan, Joseph (Oshooo) and others for their support and love, May God bless you all. With joy in heart, I want to say thanks to my lovely friend Geraldine, for her care and love towards me. I will not forget my best friends, Tosan and Oreva for their encouragement and support. To all my friends, I want to say a big thank you. God bless you all.

Above all my profound gratitude goes to God Almighty for His grace and enablement throughout the course of this work and also for His mercies and provision. Words are not enough to appreciate my parents Mr. and Mrs. J. Ibeji for their role and for giving me an opportunity to study. I am also grateful to my younger brothers and sisters for their understanding and love throughout my study.

CERTIFICATION

We certify that this work was carried out by IBEJI, Collins Ugochukwu (153189) under our supervision in the Department of Chemistry, Faculty of Science, University of Ibadan, Ibadan.

Supervisor	Co-supervisor
B.B. Adeleke	I.A. Adejoro
B.Sc. (Ibadan). M.Sc., Ph.D. (Queens) Professor Department of Chemistry Faculty of Science University of Ibadan, Ibadan	B.Sc., M.Sc., Ph.D (Ibadan). Senior Lecturer Department of Chemistry Faculty of Science, University of Ibadan.

DEDICATION

This work is dedicated to God Almighty the Giver of knowledge and wisdom, for His immeasurable grace and mercies towards me throughout the course of this program.

TABLE OF CONTENT

		Pages
Cover page		
Title page		
Abstract		i
Acknowledgement		iii
Certification		iv
Dedication		v
Table of content		vi
List of Tables		x
List of Plates		xii
List of Figures		xiii
List of Abbreviations		xv
List of Appendices		xvi
CHAPTER ONE		
1.0	INTRODUCTION	1
1.1	Background of study	1
1.2	Aim of study	4
1.3	Specific objectives	4
1.4	Justification of the research	4
CHAPTER TWO		
2.0	LITERATURE REVIEW	5
2.1	Overview of polymers in biosensor application	5
	2.1.1 Conjugated polymers of cholesterol biosensor	6
	2.1.2 Conjugated polymers of glucose biosensor	7
2.2	Overview of conducting Polymers	9
	2.2.1 Historical Review of Conducting Polymers	9
2.3	Conduction Mechanism in Conducting Polymers	10
2.4	Some substituted conducting polymers in biosensor applications	10

2.4.1 Polyaniline 11
2.4.2 Polypyrrole 13

2.5 Theoretical Background 15
2.6 The Schrödinger's Wave Equation 16
2.6.1 Born-Oppenheimer Approximations 19
2.6.2 Hartree-Fock Approximation 20
2.6.3 Self-consistent field method 21
2.6.4 The Variational Principle 22
2.6.5 Linear Combination of Atomic Orbitals (LCAO) Approximation 24
2.6.6 Kohn-sham (Ks) molecular orbital theory 24
2.7 Quantum mechanics approach 25
2.7.1 Semi-empirical methods 26
2.7.1.1 Modified Neglect of Diatomic Overlap (MNDO) 27
2.7.1.2 Austin Model 1 (AM1) 27
2.7.1.3 Recife Model 1 (RM1) 28
2.7.1.4 Parameterization Method 3 (PM3) 28

2.7.2 Ab initio methods 29
2.7.2.1 Density Functional Theory (DFT) 30
2.7.2.2 Local-Density Approximation (LDA) 33
2.7.2.3 Fundamental Problems in DFT 33
2.7.2.4 Time dependent Density Funtional Theory (TDDFT) 34
2.7.2.5 Time dependent Kohn-Sham system 35
2.7.3 Open-shell and excited-state methods 36
2.7.3.1 Spin Flip-Time dependent DFT (SF-TDDFT) 37
2.7.3.2 Coupled Cluster (CC) theory 37
2.8 Basis set 38

CHAPTER THREE
3.0 COMPUTATIONAL METHODS 40
3.1 Geometry definition 42
3.1.1 Geometric optimization 50
3.2 Molecular geometry 57
3.2.1 Bond Length Alternation parameter (*BLA)* 57

3.2.2 Inter-ring bond length 57
3.2.3 Intramolecular charge transfer (ICT) 57
3.3 Thermodynamic properties 58
3.3.1 Percentage difference in thermal stability 58
3.4 Determination of QSAR properties 58
3.5 Electronic properties 59
3.5.1 Determination of hardness/ softness 60
3.5.2 The global electrophilicity index (ω) 60
3.6 Electronic Transition Properties 61
3.7 Open-Shell and Excited-State (multireference) calculations 62

CHAPTER FOUR

4.0 RESULT AND DISCUSSION 62
4.1 Geometries 62
4.1.1 Geometric properties of Pyrrole 71
4.1.2 Geometric properties of MPC[a] 72
4.1.3 Geometric properties of MPC[b] 73
4.1.4 Geometric properties of MPCam 73
4.1.5 Geometric properties of MPCOSH 74
4.1.6 Geometric properties of $MPSO_3H$ 75
4.1.7 Geometric properties of MPCHO 76
4.2 Thermodynamic property 80
4.2.1 Thermodynamic properties of Pyrrole 81
4.2.2 Thermodynamic properties of MPC[a] 86
4.2.3 Thermodynamic properties of MPC[b] 87
4.2.4 Thermodynamic properties of MPCam 92
4.2.5 Thermodynamic properties of MPCOSH 95
4.2.6 Thermodynamic properties of $MPSO_3H$ 98
4.2.7 Thermodynamic properties of MPCHO 101
4.3 Quantitative Structure-Activity Relationship (QSAR) Properties 104
4.3.1 QSAR properties of Pyrrole 104
4.3.2 QSAR properties of MPC[a] 104
4.3.3 QSAR properties of MPC[b] 109

4.3.4 QSAR properties of MPCam 109
4.3.5 QSAR properties of MPCOSH 115
4.3.6 QSAR properties of $MPSO_3H$ 116
4.3.7 QSAR properties of MPCHO 120
4.4 Ionization Potential, Electron Affinity and Molecular Orbital Energy 123
4.4.1 Molecular energies of Pyrrole 123
4.4.2 Molecular energies of MPC^a 129
4.4.3 Molecular energies of MPC^b 133
4.4.4 Molecular energies of MPCam 139
4.4.5 Molecular energies of MPCOSH 144
4.4.6 Molecular energies of $MPSO_3H$ 149
4.4.7 Molecular energies of MPCHO 154
4.5 Electronic absorption Properties 159
4.5.1 Electronic absorption properties of pyrrole 159
4.5.2 Electronic absorption properties of MPC^a 152
4.5.3 Electronic absorption Properties of MPC^b 165
4.5.4 Electronic absorption Properties of MPCam 165
4.5.5 Electronic absorption Properties of MPCOSH 170
4.5.6 Electronic absorption properties of $MPSO_3H$ 173
4.5.7 Electronic absorption Properties of MPCHO 176
4.6 The nature of the ground and excited state Properties 179
4.7 Vertical Singlet-triplet gap and First excited state Dipole moment 183
CHAPTER FIVE
5.0 CONCLUSION AND RECOMMENDATIONS 185
RECOMMENDATIONS 187
REFERENCES 188
APPENDICES 204

LIST OF TABLES

Tables	Pages
Table 4.1. Selected bond length, bond angle and dihedral of studied compounds	76
Table 4.2. Calcuated BLA (δ_D), (L_B), (D_{ICT}) of studied compounds	77
Table 4.3. The heat of formation (ΔH_f) at 298.15K using different semi-empirical methods	83
Table 4.4. Thermodynamics properties of Pyrrole	85
Table 4.5. Thermodynamics properties of MPC[a]	88
Table 4.6. Thermodynamics properties of MPC[b]	90
Table 4.7. Thermodynamic properties of MPCam	93
Table 4.8. Thermodynamic properties of MPCOSH	96
Table 4.9. Thermodynamic properties of $MPSO_3H$	99
Table 4.10. Thermodynamic properties of MPCHO	102
Table 4.11. QSAR properties of pyrrole oligomers	105
Table 4.12. QSAR properties of MPC[a] oligomers	107
Table 4.13. QSAR properties of MPC[b] oligomers	111
Table 4.14. QSAR properties of MPCam oligomers	113
Table 4.15. QSAR properties of MPCOSH oligomers	116
Table 4.16. QSAR properties of $MPSO_3H$ oligomers	118
Table 4.17. QSAR properties of MPCHO oligomers	121
Table 4.18. IPs, EAs, HOMOs, LUMOs, and Band Gaps of pyrrole oligomers	125
Table 4.19. Calculated hardness, electrophilicity, and chemical potential of pyrrole	126
Table 4.20. IPs, EAs, HOMO-LUMOs, and Band Gaps of MPC[a] oligomers	130
Table 4.21. Calculated hardness, electrophilicity, and chemical potential of MPC[a]	131
Table 4.22. IPs, EAs, HOMOs-LUMOs, and Band Gaps of MPC[b] oligomers	135

Table 4.23. Calculated molecular hardness, electrophilicity, and chemical potential of MPC[b] 136
Table 4.24. IPs, EAs, HOMOs, LUMOs, and Band Gaps of MPCam oligomers 140
Table 4.25. Calculated molecular hardness, electrophilicity, and chemical potential of MPCam 141
Table 4.26. IPs, EAs, HOMOs, LUMOs, and Band Gaps of MPCOSH oligomers 145
Table 4.27. Calculated molecular hardness, electrophilicity, and chemical potential of MPCOSH 146
Table 4.28. IPs, EAs, HOMOs, LUMOs, and Band Gaps of $MPSO_3H$ oligomers 150
Table 4.29. Calculated molecular hardness, electrophilicity, and chemical potential of $MPSO_3H$ 151
Table 4.30. IPs, EAs, HOMOs, LUMOs, and Band Gaps of MPCHO oligomers 155
Table 4.31. Calculated molecular hardness, electrophilicity, and chemical potential of MPCHO 156
Table 4.32. Calculated electronic transition data for pyrrole 160
Table 4.33. Calculated electronic transition data for MPC[a] 163
Table 4.34. Calculated electronic transition data for MPC[b] 166
Table 4.35. Calculated electronic transition data for MPCam 168
Table 4.36. Calculated electronic transition data for MPCOSH 171
Table 4.37. Calculated electronic transition data for of $MPSO_3H$ 174
Table 4.38. Calculated electronic transition data for MPCHO 177
Table 4.39. T1 diagnostics for studied systems 180
Table 4.40. Vertical singlet-triplet gap (eV) and transition dipole moment (Debye) (in parenthesis) for studied systems 184

LIST OF PLATES

Plates	Pages
Plate 3.1. HP cluster machine, 132GB, at National chemical laboratory (NCl, Pune, India)	41
Plate 3.2. Optimized geometry of MPC^a	51
Plate 3.3. Optimized geometry of MPC^b	52
Plate 3.4. Optimized geometry of MPCAM	53
Plate 3.5. Optimized geometry of MPCOSH	54
Plate 3.6. Optimized geometry of $MPSO_3H$	55
Plate 3.7. Optimized geometry of MPCHO	56
Plate 4.1. Optimized structure of pyrrole pentimer	64
Plate 4.2. Optimized structure of MPC^a pentimer	65
Plate 4.3. Optimized structure of MPC^b pentimer	66
Plate 4.4. Optimized structure of MPCam pentimer	67
Plate 4.5. Optimized structure of MPCOSH pentimer	68
Plate 4.6. Optimized structure of $MPSO_3H$ pentimer	69
Plate 4.7. Optimized structure of MPCHO pentimer	70
Plate 4.8. The frontier molecular orbital plot of pyrrole	128
Plate 4.9. The frontier molecular orbital plot of MPC^a	133
Plate 4.10. The frontier molecular orbital plot of MPC^b	138
Plate 4.11. The frontier molecular orbital plot of MPCam	143
Plate 4.12. The frontier molecular orbital plot of MPCOSH	148
Plate 4.13. The frontier molecular orbital plot of $MPSO_3H$	153
Plate 4.14. The frontier molecular orbital plot of MPCHO	158
Plate 4.15. Calculated UV-VIS spectra of pyrrole	161
Plate 4.16. Calculated UV-VIS spectra of MPC^a (Pentamer)	164
Plate 4.17. Calculated UV-VIS spectra of MPC^b (Pentamer)	167
Plate 4.18. Calculated UV-VIS spectra of MPCam (Pentamer)	169
Plate 4.19. Calculated UV-VIS spectra of MPCOSH	172

Plate 4.20. Calculated UV-VIS spectra of $MPSO_3H$ (Pentamer) 175
Plate 4.21. Calculated UV-vis spectra of MPCHO (Pentamer) 178

LIST OF FIGURES

Figure **Pages**

Fig. 3.1. Structural representation of Pyrrole 43
Fig. 3.2. 3-methyl-pyrrole-4-carboxylic acid (MPC^a) 44
Fig. 3.3. Structural representation of 3-methyl-pyrrole-1-carboxylic acid (MPC^b) 45
Fig. 3.4. Structural representation of 3-methyl-pyrrole-4-carboxamide (MPCam) 46
Fig. 3.5. Structural representation of 3-methyl-pyrrole-4-carbothioic acid (MPCOSH) 47
Fig. 3.6. Structural representation of 3-methyl-pyrrole-4-sulfonic acid ($MPSO_3H$) 48
Fig. 3.7. Structural representation of 3-methyl-pyrrole-4-carbaldehyde (MPCHO) 49
Fig. 4.1. The plot of studied compounds against bond length 78
Fig 4.2. The plot of studied compounds against bond angle 79
Fig 4.3. The heat of formation (ΔH_f) of studied polymers using different semi-empirical methods compared with the experimental value 84
Fig. 4.4. Enthalpies of Pyrrole and MPC^a as a function of the number of unit 89
Fig. 4.5. Enthalpies of Pyrrole and MPC^b as a function of the number of unit 91
Fig. 4.6. Enthalpies of Pyrrole and MPCam as a function of the number of unit 94
Fig. 4.7. Enthalpies of Pyrrole and MPCOSH as a function of the number of unit 97
Fig. 4.8. Enthalpies of Pyrrole and $MPSO_3H$ as a function of the number of unit 100
Fig. 4.9. Enthalpies of Pyrrole and MPCHO as a function of the number of unit 103
Fig. 4.10. Plot of Log (1/C) vs. Log P showing the biological activity of pyrrole 106
Fig. 4.11. Plot of Log (1/C) vs. Log P showing the biological activity of MPC^a 108
Fig. 4.12. Plot of Log (1/C) vs. Log P showing the biological activity of MPC^b 112
Fig. 4.13. Plot of Log (1/C) vs. Log P showing the biological activity of MPCam 114
Fig. 4.14. Plot of Log (1/C) v Log P showing the biological activity of MPCOSH 117
Fig. 4.15. Plot of Log (1/C) vs Log P showing the biological activity of $MPSO_3H$ 119
Fig 4. 16. Plot of Log (1/C) v Log P showing the biological activity of MPCHO 122
Fig. 4.17. Plot of HOMO, LUMO energy level against 1/n of pyrrole oligomer 127
Fig. 4.18. Plot of HOMO, LUMO energy level against 1/n of MPC^a oligomer 132

Fig. 4.19. Plot of HOMO, LUMO energy level against 1/n of MPC^b oligomer 137

Fig. 4.20. Plot of HOMO-LUMO energy level against 1/n of MPCam oligomer 142

Fig. 4.21. Plot of HOMO, LUMO energy level against 1/n of MPCOSH oligomer 147

Fig. 4.22. Plot of HOMO, LUMO energy level against 1/n of $MPSO_3H$ oligomer 152

Fig. 4.23. Plot of HOMO, LUMO energy level against 1/n of MPCHO oligomer 157

Fig. 4.24. Natural orbital occupation numbers for the doubly occupied orbitals of Unsubstituted Pyrrole as a function of chain length 181

Fig. 4.25. Natural orbital occupation numbers for the doubly occupied orbitals of substituted Pyrrole as a function of chain length 182

LIST OF ABBREVIATIONS

Abbreviations

UB3LYP	Unrestricted Becke Three, Lee Yang And Parr
MO	Molecular Orbital
CNDO	Complete Neglect of Differential Overlap
MINDO	Modified Intermediate Neglect of Differential Overlap
MNDO	Modified Neglect of Diatomic Overlap
ZINDO	Zerner's Intermediate Neglect of Differential Overlap
AM1	Austin Model 1
RM1	Recife Model 1
PM3	Parameterization method 3
CCSD (T)	Coupled Cluster Single and Double (Triples)
STO	Slater Type Orbital
GTO	Gaussian Type Orbital
MPC^a	3-methyl-pyrrole-4-carboxylic acid
MPC^b	3-methyl-pyrrole-1-carboxylic acid
MPCam	3-methyl-pyrrole-4-carboxamide
MPCOSH	3-methyl-pyrrole-4-carbothioic acid
$MPSO_3H$	3-methyl-pyrrole-4-sulfonic acid
MPCHO	3-methyl-pyrrole-4-carbaldehyde
kJ/mol	Kilo Joule per mole
$Jmol^{-1}K^{-1}$	Joule per mole per Kelvin
E_0	Total energy of the system
ΔH^o_f	change in Enthalpy of formation
ΔG^o_f	change in Gibbs free energy of formation
ΔS^o_f	change in Enthropy of formation
ICT	Intramolecular charge transfer
Eg	Energy gap
E_{LUMO}	Energy of the Lowest Unoccupied Molecular Orbital
E_{HOMO}	Energy of the Highest Unoccupied Molecular Orbital

LIST OF APPENDICES

Optimized coordinates of studied compound 204

MPC 204

MPC-1-monomer 204

MPC-1-pentimer 205

MPCam-monomer 206

MPCam-Pentimer 207

MPCOSH-monomer 209

MPCOSH-Pentimer 209

$MPSO_3H$-monomer 211

$MPSO_3H$- pentimer 211

Experimental UV-VIS spectrum of pyrrole at different solvent phase (Heeralal and Krishamurthi, 2014) 213

UV/VIS Spectrum for monomers 214

UV/VIS of MPC monomer 214

UV/VIS of MPC^b monomer 214

UV/VIS of MPCam monomer 215

UV/VIS of MPCOSH monomer 216

UV/VIS of $MPSO_3H$ monomer 217

CHAPTER ONE
INTRODUCTION

1.1 Background of study

Conjugated polymers are the resonance stabilized organic polymers. They are also named as synthetic metals since they mimic the electrical, electronic, magnetic and optical properties of metals while retaining the ease of chemical and physical modification associated with ordinary polymers (Wallace *et al*., 2009).

According to Lyons, conducting electroactive polymers are generally classified under the three major types; redox polymers, ion-exchange polymers (ionomers) and electronically conducting polymers. Redox polymers are defined as conductors containing redox active groups covalently bonded to a nonelectroactive polymer backbone, for example poly (vinyl ferrocene). Conduction in these polymers is via electron hopping and they are only conducting over a narrow potential range. Ionomers are ion exchange polymers, in which redox active sites are electrostatically incorporated with the redox active component being a counter anion to a polymeric material. Conduction in ionomers is possible, either through local electron hopping between fixed redox sites or through physical diffusion of the incorporated redox moiety followed by electron transfer. Electronically conducting polymers are different from redox polymers and ionomers in that the backbones of these polymers are themselves conducting (Wallace *et al*., 2009). Electronically conducting polymers have been known to show transition from insulator to conductor and vice versa as the polymers move from one oxidation state to another and are conductive over an extended potential range.

Conjugated Polymers that could effectively interact with biological systems and applied in the areas of molecular electronics, sensors surgical plasters have attracted much interest. Conjugated polymers have been widely studied because of their foreseen technological applications. They have many advantages when compared to inorganic semiconductors such as their easy processing, their tunable optical gap and their favourable structural

properties. Novel approach has been adopted in order to study biological electron transport between polymeric materials and proteins using functionalized conducting polymers to produce thin films which has been used for the covalent binding of electrode surfaces to glucose oxidase (Schuhmann, 1991). Barker *et al.,* (1990) and Kudera *et al.,* (2000) reported experimentally the existence of reversible electron transfer between Au electrodes and peptide proteins, which in turn has opened fascinating perspectives in terms of developing conducting polymers for biosensor devices.

Conducting polymers such as polypyrrole and polyaniline have been synthesized and polymerized electrochemically or chemically (Hailin *et al*., 1993) and applied in the area of biosensor and chemisensor application. Currently improvements have been in the controlled synthesis of these polypyrrole materials, which allow the design and preparation of new chemical and biosensor systems. Inorder to obtain a long operational life of the bio-molecules, the technique of the enzyme-immobilization onto the transducer is a key process to developing a good biosensor device. Generally, the enzyme-immobilization methods such as adsorption (Jayasree *et al.,* 2012) have been applied. One of the mostly studied conducting polymers is polyaniline (PANI), this is due to the fact that it possesses interesting electrical, electrochemical and optical properties. Research reveals that the N-substituted anilines do not have pH sensitivity (Lindfors and Ivaska, 2002). This is due to the fact that the alkyl chain, which is covalently bonded to the nitrogen atom, prevents formation of the emeraldine base (deprotonated form). Most of the studies are basically experimental with few theoretical analyses.

Therefore there is a need to create a synergy between experimental studies and computer simulation studies on the properties of conducting polymers. Computer simulations assist in solving chemical problems by incorporating efficient computer programs and methods (dynamic and static situations) of theoretical chemistry to calculate the structures and properties of molecules and solids. These properties include absolute and relative (interaction) energies, electronic charge distributions, dipole and higher multipole moments, vibrational frequencies, stability, reactivity or other spectroscopic quantities. Computational chemistry applies both Ab intio methods which are entirely on quantum mechanics and basic physical constants and semi-empirical methods that employ empirical parameters. Quantum mechanical calculations such as density functional theory

gives results that are close to experimental values, basically by the use of functional (Grimme, 2011)

In recent years, quantum chemistry methods have made great progresses in studies of electronic and structural properties of conjugated polymers. In the beginning semi-empirical methods were the dominat theoretical tool to study conjugated polymers such as unsubstituted and substituted polypyrrole. More theoretical investigations have been carried out on conjugated polymers to study the electronic and structural properties. These have provided more insight into different forms of oligomers and their repeating units containing different functional groups and subtitutents (Lin and Yan, 2012).

Lin and Yan (2012) have theoretically studied the mechanisms of interaction of alcohol top polyaniline used as gas sensors. In this work, they studied the geometric properties, electronic properties and structural properties. Based on optimized structures, natural bond orbital analysis was determined to know the nature of charge distribution between the conjugated polymer and the alcohol molecule. Density functional theory method using UB3LYP (Unrestricted Becke Three, Lee Yang and Parr) was used and the influence of chain length, binding properties was appropriately discussed. It was observed that incorporation of substituents increased the chain length and other electronic properties.

Nero *et al*. (2002) carried out computational studies on the geometries and spectroscopic properties of MPC oligomers and some of its related parent's structures. The geometry was determined using semi-empirical (AM1, PM3) and methods, while spectroscopic properties were investigated using ZINDO-S/CI which are less developed methods.

Despite intense theoretical work on polypyrrole concerning structural and electronic properties, the mechanism of interaction, nature and relative importance dynamic and static electron correlation of polypyrrole, are yet to be completely understood. Therefore it is important to explain the mechanism of interaction and other molecular properties that make substituted polypyrrole suitable components of biosensors.

1.2 Aim of study

This research was designed using computational approach to study the molecular properties of substituted and unsubstittued pyrrole polymers by employing higher level of *Ab initio* theory with a view to understanding what make substituted pyrroles suitable components of biosensors

1.3 Specific objectives

i. To theoretically investigate the possiblilities of reducing band gap by replacing an atom in the parent compound with groups that have similar electronic effect
ii. To investigate the effect of introducing functional groups on the structure and function of the polymer
iii. To investigate using Koopmans theorem and fukui, the stability and reactivity of polymers under study
iv. To study the effect of substituents on the band gap and other thermodynamic properties
v. To study and evaluate the UV/VIS spectra of polymers under study
vi. To study excited states of the molecules with methods such as Spin flip TDDFT and CCSD.

1.4 Justification of the research

Diseases are detected by monitoring various biochemical compounds in the body fluids using diagnostic tools. Obtaining better polymers with low energy gap for the fabrication of more accurate, cheaper and widely available monitoring diagnostic tools, which will be accessible to people for better health control is the first step in this direction.

CHAPTER TWO
LITERATURE REVIEW

2.1 Overview of polymer-biosensor applications

Biomolecule immobilization in or on electrosynthesized polymers is carried out using various strategies involving affinity interactions, electrostatic adsorption or incorporation, chemical grafting or entrapment process during the electrochemical growth of the polymer (Cosnier, 2005).

Electrochemically deposited polymer films used for biomolecule immobilization are conducting polymers such as polyacetylene, polythiophene, polypyrrole, polyaniline and polyindole (Gerard *et al.,* 2002). Although the most used conducting polymer, polypyrrole is a good immobilization matrix, its derivatives are also widely used to enhance its properties and biocompatibility. The other most used conducting polymer is polyaniline. For instance, polyaniline nanofibers was used to immobilize glucose oxidase (Zhao *et al.,* 2009), electroactive nanostructured membranes made with polyaniline and silver nanoparticles stabilized in polyvinyl alcohol as urea biosensor matrices, ordered mesoporous polyaniline film to construct hydrogen peroxide biosensor were used and trypsin was lately entrapped in polyaniline assembled on the Fe_3O_4/CNT composite (Wang *et al.,* 2008). On the other hand, polythiophenes, especially poly(3-hexylthiophene)

and poly(3,4-ethylenedioxythiophene) were used as immobilization matrices. Langmuir-Blodgett films of poly (3- hexylthiophene) were utilized to construct glucose biosensor (Singh *et al.,* 2004) and galactose biosensor (Sharma *et al*., 2004), in addition poly(3,4-ethylenedioxythiophene) was used to physically entrap tyrosinase (Vedrine *et al.,* 2003).
Even though electrochemical synthesis allows the direct deposition of the polymer on the electrode surface while simultaneously trapping protein molecules, it is also possible to modify polymer to bind protein molecules (Gerard *et al.,* 2002). Although, biomolecules are generally physically entrapped in polypyrrole and PEDOT during electrodeposition because of the water solubility of their monomers, immobilization through adsorption or via chemical bonding is also feasible. On the other hand, biomolecules are immobilized in polyanilines and polythiophenes via either adsorption or chemical modification.
Conducting polymers are also known to be compatible with biological molecules in neutral aqueous solutions (Gerard *et al.,* 2002), thus they are widely used with or without modification.

Conducting polymers have the ability to efficiently transfer electric charge produced by the biochemical reaction to electronic circuit. They provide good detectability and fast response as the redox reaction of the substrate, catalyzed by an appropriate enzyme, taking place in the bulk of polymer layer (Gerard, *et al.,* 2002). Hence, they are widely used in amperometric sensor applications. To illustrate the applications of conducting polymers, single walled carbon nanotube/polypyrrole composite (Cosnier, *et al.,* 2008), poly(3-thiophene acetic acid) matrix (Nien, *et al.,* 2009), poly(N-3-aminopropyl pyrrole-co-pyrrole) film and poly(3,4-ethylenedioxythiophene)-poly(styrene sulfonic acid) film were recently used for amperometric glucose, cholesterol, urea, and alcohol sensing.

2.1.1 Conjugated polymers of cholesterol biosensor

Steroids are lipids with ring structures. Although they have similar backbones, their functions in the body vary with different attached groups. Cholesterol, found in animal plasma membranes, is the precursor of several other steroids, including the vertebrate and sex hormones. Cholesterol is manufactured in the liver and the small intestine, as well as derived from dietary sources. Accumulation of cholesterol under the inner linings of

arteries may lead to atherosclerosis (Mader, 1996). Cholesterol determination in blood is clinically important in the diagnosis and prevention of cardiovascular diseases.

Chronoamperometry is the preferred technique in electrochemical detection systems for cholesterol since it allows monitoring either oxygen consumption or hydrogen peroxide production. In recent years, various enzyme immobilization matrices were used in construction of amperometric cholesterol biosensors, such as self assembled monolayers (Zhou, *et al.*, 2006), sol-gel/chitosan hybrid composite films on multiwalled carbon nanotubes (Tan, *et al.*, 2005), polypyrrole (Singh, *et al.*, 2004), PPy/Prussian blue layers (Vidal, *et al.*, 2004), PPy-hydrogel membrane (Brahim, *et al.*, 2003), polyaniline (Singh, *et al.*, 2006), poly(aniline-co-pyrrole) film (Solanki, *et al.*, 2007) and polyaniline Langmuir-Blodgett film (Matharu, *et al.*, 2007).

2.1.2 Conjugated polymers of glucose biosensor

Diabetes is one of the leading causes of death and disability in the world. The complications of battling diabetes are numerous, including higher risks of heart disease, kidney failure, or blindness. Such complications can be greatly reduced through stringent personal control of blood glucose. The diagnosis and management of diabetes mellitus thus requires a tight monitoring of blood glucose levels.

Accordingly, millions of diabetics test their blood glucose levels daily; making glucose the most commonly tested analyte. Indeed, glucose biosensors account for about 85% of the entire biosensor market. Such huge market size makes diabetes a model disease for developing new biosensing concepts. The tremendous economic prospects associated with the management of diabetes along with the challenge of providing such reliable and tight glycemic control have thus led to a considerable amount of fascinating research and innovative detection strategies. (Reach and Wilson, 1992; Wang, 2001)

Amperometric enzyme electrodes, based on glucose oxidase (GOx), have played a leading role in the move to simple easy-to-use blood sugar testing and are expected to play a similar role in the move toward continuous glucose monitoring. The monitoring of the biochemical compounds in the body fluid requires typical analytical methods for biochemical test, experts to run the tests, and time for performing clinical tests. Since the

levels of various compounds in a body system are directly related to some diseases, it is possible to monitor the progress of diseases by monitoring the concentration of these compounds.

Thus, continuous, fast, and sensitive monitoring is required to measure the body fluid concentration of these compounds efficiently. In this context, electrochemical biosensor is a promising analytical method for sensitive and selective detection of biomolecules (Turner *et al.,* 1987; Schultz and Taylor, 1996; Scheller *et al.,* 1997; Cass *et al.,* 2004). The unique property of conducting polymers along with the possibility to entrap enzymes during electrochemical polymerization has been exploited for the fabrication of amperometric biosensors (Gerard *et al.,* 2002). Most biosensors described in literature use an enzyme as biological recognition element.

Amperometric enzymatic biosensors for choline and glutamate (Rahman *et al.,* 2005) have been fabricated by the covalent immobilization of choline oxidase and glutamate oxidase enzymes onto the substituted poly-5,2 ″ 2,′ 5:′ -terthiophene-3 ′-carboxylic acid, poly-TTCA (poly-CP) layers on a glassy carbon electrode. The electrochemically prepared conducting polymer layer oxidized the enzymatically generated H_2O_2 at a lower potential and was the basis of detection of choline and glutamate. The biosensors showed good selectivity towards other interfering anions. A xanthine biosensor has been fabricated by the covalent immobilization of xanthine oxidase (XO) onto a functionalized conducting polymer (Poly-5, 2': 5', 2"-terthiophine-3-carboxylic acid), poly-TTCA through the formation of amide bond between carboxylic acid groups of poly-TTCA and amine groups of enzyme (Rahman *et al.,* 2005). The applicability of the biosensor was tested by detecting xanthine in blood serum and urine real samples.

A biosensor based on cytochrome c3 (Cyt c3) has been introduced to detect and quantify superoxide radical (O_2). Cyt c3 isolated from the sulfate-reducing bacterium and its mutant were immobilized onto a conducting polymer (polyTTCA) coated electrode by covalent bonding (Darain *et al.,* 2007). A potential application of the Cyt c3 modified electrode was evaluated by monitoring the bioelectrocatalytic response towards the O_2. In another work, Cyt c has been immobilized onto lipid bonded conducting polymer (poly (3,

4-diamino-2,2:5, 2-terthiophene) (polyDATT) layers of model biomembrane for the fabrication of another O_2 biosensor (Kwon *et al.,* 2006).

A novel amperometric biosensor based on horseradish peroxidase/polypyrrole (PPy) deposited onto the surface of ferrocenecraboxylic acid functionalized sol–gel derived composite carbon electrode for the detection of H_2O_2 has been reported (Tian *et al.,* 2001). The biosensor has a fast response and a relative large linear range making it suitable for the detection of H_2O_2. The pH effect on the co-electropolymerization of glucose oxidase and polypyrrole (PP) on the characteristics of glucose oxidase/PP biosensor has been studied. Glucose oxidase-based ultra microelectrodes fabricated via sonication and deposition of polysiloxane coating onto the working glucose oxidase/polyaniline electrode coated with insulating diaminobenzene has been reported for the improved response. Arslan et al. have fabricated a polysiloxane/polypyrrole/ tyrosinase electrode by entrapment of tyrosinase in conducting matrix by electrochemical copolymerization for determining the phenolic content of green and black tea (Arslan *et al.,* 2005).

2.2 Overview Conducting Polymers

Organic conducting polymers have recently attracted interest because they exhibit a wide range of novel electrochemical properties (Bidan *et al*., 1999; Gerard *et al.,* 2002; Brahim *et al*., 2003).

2.2.1 Historical Review of Conducting Polymers

Polyacetylene was synthesized in 1958 by as a black powder possessing semi-conductor properties depending on how the polymer was processed (Shirakawa, 2001). The scientific curiosity was elucidated in 1967 by Hideki Shirakawa's group; they succeeded in synthesizing polyacetylene directly in the form of a thin silvery semiconductor film using Zieglar-Natta catalyst nearly a thousand times greater than that usually needed. Upon treating with halogens the conductivity drastically increased. It is discovered that polyacetylene can be converted from an insulator to a semiconductor, to a full metal depending on the concentration of dopant. On the other hand, in University of Pennsylvania Alan Heeger, physicist, and Alan MacDiarmid, chemist, have been working

on (SN)x having strong electronic properties and they have discovered that bromine addition increased the conductivity tenfold. Actually, the inorganic sulfur nitride polymer discovered in 1973 showed properties very close to those of metal; however its explosive nature prevented it from becoming commercially important (Walatka *et al.*, 1973).

These three scientists cooperated and the Nobel Prize for the year 2000 went to them "for the discovery and development of electrically conducting polymers" (Shirakawa, 2001; Heeger, 2001). Although polyacetylene exhibits very high conductivity in its doped state, it is not stable in open air. Hence, in 1980s polyheterocycles, which were more air stable than polyacetylene, due to lower oxidation potential, were developed. Even if none has exhibited higher conductivity than the parent organic conducting polymer, these polymers have been helpful in designing new functionalized monomers that are soluble and stable.

2.3 Conduction Mechanism in Conducting Polymers

In conjugated polymers the electronic configuration is different since the chemical bonding leads to one unpaired electron per carbon atom. Moreover, the bonding in which the orbital of successive carbon atoms overlap results in electron delocalization. This electronic delocalization provides the highway for charge mobility along the backbone of the polymer chain. The electrical conductivity results from the existence of doping induced charge carriers and their motion along the bonded highway (Heeger, 2001).

The movement of charge carriers such as electrons and holes through a medium (metal, polymer, etc.) under influence of an electric field is named as electronic conduction.

Conductivity is not only the result of charge transfer along the backbone, but it is also due to electron transfer between chains and between different conjugated fragments of the same chain.

2.4 Some substituted conducting polymers in biosensor applications

The synthesis of polyacetylene was a starting point for a considerable number of studies. Electrodeposition of free standing films of polypyrrole from organic environment opened a new way to research on polyheterocyclic and polyaromatic conducting polymers (Waltman, 1986). After the oxidation of polypyrrole, aromatic systems have been synthesized for producing conducting polymers. Heterocyclic polymers such as

polythiophene, polypyrrole, polyaniline, and many substituted, multi-ring and polyaromatic systems have a conjugated backbone, which is required for electroactivity.

Conducting polymers due to the amplification by a total system response are sensitive to very minor perturbations and offer an advantage over small-molecule (Petrova *et al.,* 2012 and Kim *et al*., 2012). Currently progresses have been in the controlled synthesis of these polymeric materials, which allow the rational design and preparation of new chemical and biological biosensor systems. To obtain a long operational life of the bio-molecules, the technique of the enzyme-immobilization onto the transducer is a key process to developing a good biosensor device. Generally, the enzyme-immobilization methods (Majumdar *et al*., 2005) include adsorption (Jayasree *et al.,* 2012 and Molino *et al*., 2012), covalent attachment (Bax *et al*., 2012) and (Sadekar *et al*., 2012), cross-linking (Karim and Fakhruddin, 2012). Conducting polymers have been applied in the fabrication of biosensor devices in various fields, such as health care, immunosensors, DNA sensors, environmental monitoring and food analysis (Lin and Yan, 2012)

2.4.1 Polyaniline

Among the most studied electronically conducting polymers is polyaniline (PANI), which has been studied extensively as an important conducting material that possesses interesting electrical, electrochemical and optical properties (Mu *et al.,* 1997). It has also generated considerable interest because of the many routes to its production, its chemical stability and ease of redox doping. The continuous growing interest in the study of PANI is caused by these diverse, unique properties and its promising potential in commercial applications. The potential applications of PANI include anti-corrosive coatings (Bernard, *et al.,* 2001; Kraljić *et al.,* 2003), secondary batteries (Mirmohseni and Solhjo, 2003) and electrochromic devices (Malta *et al.,* 2002) and electrochemical biosensors (Iwuoha *et al.,* 2004). Some examples of the innumerable sensors prepared using polyaniline include glucose oxidase-based biosensor (Iwuoha *et al.,* 2004), cholinesterase-based biosensor (Ivanov *et al.,* 2002), horseradish peroxidase-based biosensors (Iwuoha *et al*., 1997; Yang and 1997) and CYP2D6-based biosensor (Iwuoha *et al.,* 2004).

Advantages of utilizing polyaniline-coated electrodes in biosensors are acceleration of electron transfer reactions, impressive signal amplification and elimination of electrode

fouling (Wang, 1991). This polymer also provides a suitable environment for immobilisation of biological components.

Polymer films can be deposited on electrode surfaces very readily. Polymerisation of the monomer aniline can be achieved by either chemical or electrochemical methods. However, electrochemical synthesis is rapidly becoming the preferred method for preparing electrically conducting polymers because of its simplicity and reproducibility. In both cases, that is, chemical and electrochemical methods, the polymer is prepared from a dilute monomer solution containing a suitable counter anion that serves as the dopant. The method chosen depends on the form of the polymer required. Chemical synthesis generally yields a powdered material or solution of low molecular weight oligomers whereas electrochemical synthesis yields an insoluble film on an electrode surface (Chaubey and Malhotra, 2002)

An important advantage of the electropolymerisation technique in the fabrication of biosensors is that the film thickness and characteristics can be controlled by monitoring polymerisation charge (Iwuoha and Smyth, 1996) and also the process is localised at the electrode surface. Electropolymerisation also offers an effective route for creating highly controllable size exclusion films (Wang, 1991)

Electrochemically, the polymer can be grown on the electrode surface by pulse (Genies and Tsintavis, 1985) galvanostatically, potentiostatically (Iwuoha *et al.,* 2004) or potentiodynamically (Iwuoha *et al.,* 1997; Yang and Mu, 1997).

Recent research reveals that the N-substituted anilines do not have pH sensitivity (Lindfors and Ivaska, 2002). This is due to the fact that the alkyl chain, which is covalently bonded to the nitrogen atom, prevents formation of the EB form. Another derivative of PANI, self-doped PANI, which is usually referred to sulfonated PANI, shows redox activity even in solutions with neutral pH (Mazeikiene *et al.,* 2003). Sulfonated PANI was used in amperometric enzyme sensors with a sensitivity of 24.91 uA cm^2 to detect H_2O_2 in pH 6.4 buffer solutions (Ngamna *et al.,* 2005). It has also been demonstrated that the PANI blends that included negatively charged co-components such as sulfonic acid or polyacrylic acids exhibit redox activity in neutral aqueous solutions (Bartlett and Wang, 1996; Bartlett and Simon, 2000; Bartlett and Wallace, 2001). Shi *et*

al. reported poly (aniline-aniline boronic acid) wires generated on double-strand (ds) DNA templates applied in immunosensor application (Shi *et al.,* 2004). These wires are deposited on an electrode by means of electrostatic interactions, in which PANI exhibits redox activity also in solutions with neutral pH. The redox activity behaviour at neutral pH values was also observed by Granot *et al.* (2006). They have developed PANI/single walled carbon nanotube hybrid systems, and these composites as matrices give enhanced bioelectrocatalytic activation of enzymes. These modifications are potentially useful in electroanalytical applications of PANI in biosensors. However, PANI has already been used to detect different biological compounds by using its properties such as pH sensitivity (Hoa *et al.,* 1992), electrochromism (Malinauskas *et al.,* 2004) and conductivity (Muhammad-Tahir and Alocilja, 2003).

A nanobiodetector has been developed based on the changes of conductivity of PANI Micro- and nano-fibrils in the presence of micro-organisms (Langer and Langer, 2005). It was found that the electrical response depends on the number of cells deposited on the PANI nanonetwork, and is specific to different kinds of micro-organisms. The minimum number of cells to be detected by this sensor is below 100.

2.4.2 Polypyrrole

Polypyrrole is among the most widely studied conducting organic polymers, experimentally and theoretically, this is due to their chemical stability, high conductivity upon doping and non-linear optical properties (Salzner *et al.,* 1998). Molecular design of low band-gap polymers is of current interest in research into electrically conducting polymers. It has been reported in literature that there is a direct electronic communication between functionalized, conducting polypyrrole and a redox protein in solution (Ryder *et al.,* 2000; Swann *et al.,* 2000; Nero *et al.,* 2002). Novel approach has been adopted in order to study biological electron transport between polymeric materials and proteins using functionalized conducting polymers to produce thin films.

Polymers with low band gaps are expected to show not only good intrinsic conductivity but also good non-linear optical properties (Havinga *et al.,* 1992). The experimental band gap values of polypyrrole and polythiophene had been investigated (Zotti *et al.,* 1992)

Polypyrrole films have been used for the covalent binding of electrode surfaces to glucose oxidase. (Schuhmann, 1991)

Theoretical studies of 2-phenylpyrrole (PhPy) for its neutral and mono-charged states have been performed using density functional theory. Results of this showed that C-C bond lengths in the phenyl ring are practically identical for the neutral state. The electric charging leads to significant changes in the geometry with respect to neutral states. The C-N bonds in PhPy are elongated and the negative charging produces the out-of-plane distortion of N-H bond from the aromatic ring plane. (Rottmannováa *et al*., 2012)

Ab initio quantum mechanical calculations at the MP2 level were used for an extensive study concerning the stability of hydrogen-bonded complexes formed by pyrrole and thiophene, which are the most common building blocks of conducting polymers, and DNA bases (Zanuy and Alemán, 2008). Results showed that very stable complexes were formed with pyrrole, which shows a clear tendency to form specific hydrogen-bonding interactions with nucleic acid bases. The strength of such interactions depends significantly on the base, increasing in the following order: thymine < adenine ≈ cytosine < guanine. On the contrary, thiophene formed complexes stabilized by nonspecific interactions between the π-cloud of the ring and the N−H groups of the nucleic acid bases rather than specific hydrogen bonds. An overall result shows that polypyrrole is able not only to stabilize adducts with DNA but also to interact specifically, while the interactions of the latter with polythiophene and their derivatives are weaker and nonspecific (Zanuy and Alemán, 2008).

Menges *et al*. (2013), studied the design and synthesis of pyrrolotriazepine derivatives, in their findings pyrrole derivatives having carbonyl groups at the C-2 position were converted to N-propargyl pyrroles. The reaction of those compounds with hydrazine monohydrate resulted in the formation of 5H-pyrrolo[2,1-d][1,2,5]triazepine derivatives. The synthesis of these compounds was accomplished in three steps starting from pyrrole. The formation mechanism of the products was investigated, and the results obtained were also supported by theoretical calculations.

Quantum chemical analysis (MP2/6-31+G*) of the pyrrole anions addition to carbon disulfide and the substitution effects therein was carried out by Vladimir *et al*., (2002). Results show that pyrrole-2 (5)-carbodithioates are thermodynamically the most stable compounds, while 1-isomer obtained from the unsubstituted pyrrole is likely a kinetic product. Steric hindrances destabilize N-adducts when a methyl substituent appears in a 2(5) position and the 2,5-dimethyl-1-pyrrolecarbodithioate anion turns out to be even less stable than the 2,5-dimethyl-3-pyrrolecarbodithioate anion. By contrast, pyrrole-1-carboxylates are calculated to be the most stable adducts of CO_2 with pyrrole anions.

Santos *et al.,* (2013), reported a combined thermochemical experimental and computational study of 2-pyrrolecarboxylic acid and 1-methyl-2-pyrrolecarboxylic acid. Static bomb combustion calorimetry and Knudsen mass-loss effusion technique were used to determine the standard molar enthalpies of combustion, and sublimation, respectively, from which the standard molar enthalpies of formation, in the gaseous phase, at T = 298.15 K, were derived. For comparison purposes, the gas-phase enthalpies of formation of these two compounds were also estimated by G3 (MP2)//B3LYP and MP2 approaches, using a set of gas-phase working reactions; the results were in agreement with experimental data. (Santos *et al.,* 2013), G3b (MP2)//B3LYP computations were also extended to the calculation of N−H bond dissociation enthalpies, gas-phase acidities and basicities, proton and electron affinities and adiabatic ionization enthalpies.

2.5 Theoretical background

Computational chemistry is the application of chemical, mathematical and computing skill to the solution of interesting chemical problems. It uses computer to generate information such as properties of molecules or simulated experimental results. The term computational chemistry is usually used when a mathematical method to solve a chemical problem is well developed, that it can be automated for implementation on a computer (Labanowski, 2004).

Computational chemistry has become a useful way to investigate materials that are too difficult to find or too expensive to purchase. It also helps chemists to make predictions before running the actual experiments, to predict the expected outcome. Quantum and classical mechanics as well as statistical physics and thermodynamics are the foundation

for most of the computational chemistry theory and computer programs. This is because they model the atoms and molecules using mathematical theorems (Labanowski, 2004).

There are many approaches of computational chemistry that are popular in molecular modelling. We can divide these approaches to two broad parts, empirical and quantum approaches (Labanowski, 2004) Empirical approaches use simple models of harmonic potential, electrostatic interaction and dispersion forces for basic comparisons of energetics and geometry optimisation.

2.6 The Schrödinger's Wave Equation

Approach to quantum mechanics postulates the fundamental principles and then uses these postulates to deduce experimental results (Levine, 2013). The state of a system in quantum mechanics is a function of the coordinates of particles called the wavefunction Ψ (Levine, 2013). This state changes with time. Thus for one particle, one-dimensional system, we have $\Psi = \Psi_{(x,\ t),}$ thus, the wavefunction contains all possible information about the system Suppose we have a single particle of an electron of mass, m, moving in field of space under the influence of a potential, V. To find the future state of a system from the knowledge of its first state, we need an equation that tells us how the wavefunction changes with time. This particle is described by a wavefunction $\Psi_{(x,\ t),}$ that satisfies the Schrödinger's time dependent equation (Levine, 2013).

$$\frac{\hbar}{2m}\frac{\delta^2\Psi_{(x,t)}}{\delta x^2} + V_{(x)}\Psi_{(x.t)} = i\hbar\frac{\delta\Psi_{(x,t)}}{\delta t} \qquad (2.6.1)$$

Where $\hbar = \frac{h}{2\pi}$; h is Planck's constant and $i^2 = -1$.

The time dependent Schrödinger's equation might look very difficult, however many applications of quantum mechanics to chemistry derive their model from simpler Schrödinger's time independent equation (Levine, 2013).

$$-\frac{\hbar^2}{2m}\frac{\delta^2\Psi_{(x)}}{\delta x^2} + V_{(x)}\Psi_{(x)} = E\Psi_{(x)} \qquad (2.6.2)$$

Where the first represent the Halmitonian (H), Ψ is called the wavefunction which is a function of the coordinates of particles, E is the Eigen value, which represents the exact energy or the solution of the Schrödinger's time independent equation.

Quantum mechanics explain how entities like electron have both particle and wave-like characteristics. The Schrodinger equation describes the wave function of the particle (warren, 2003):

$$(-\frac{1}{2m}\nabla^2 + \mathrm{V})\ \Psi(\tilde{r},t) = ih\frac{\partial\Psi(\tilde{r},t)}{\partial t} \qquad (2.6.3)$$

In this equation; Ψ is the wave function, m is the mass of the particle, ħ is the Planck's constant over 2π, and v is the potential field in which the particle is moving. The product of Ψ with its complex conjugate (Ψ*Ψ, often written as $/\Psi/^2$) is interpreted as the probability distribution of the particle. The Schrodinger equation for a collection of particles like a molecule is very similar. In this case the Ψ would be a function of the coordinates of all the particles in the system as well as time (t). The energy and many other properties can be obtained by solving the Schrodinger equation for Ψ, subject to the appropriate boundary conditions. Many possible wave functions are solution to it, corresponding to different state of the system.

If V is not a function of time, the Schrodinger equation can be simplified using the mathematical techniques known as separation of variables. Then we obtain two equations, one of which depends on the position of the particles independent of the time and other of which is a function of time alone.

$$\Psi(\tilde{r},t) = \Psi(\tilde{r})f(t)$$

$$= \frac{d}{dt}f(t) = Ef(t)$$

$$= (-\frac{h^2}{2m}\nabla^2 + V(\tilde{r})\Psi(\tilde{r}) = E\Psi(\tilde{r})) \qquad (2.6.4)$$

The latter one is known as the familiar time independent Schrodinger equation. The various solutions to the time independent Schrodinger equation correspond to different stationary states of the particles. The one with the lowest energy is called ground state.
The generalized Schrödinger equation for a multinuclear and multielectron system is a simple looking expression shown in equation (2.6.5).

$$H\,\Psi = E\,\Psi \qquad (2.6.5)$$

H is called the "Hamiltonian operator" which describes kinetic energies of both the nuclei and electrons that make up the molecules, as well as the electrostatic interactions felt between the nuclei and electrons. The nuclei are positively charged and the electrons are negatively charged, both attracting each other. The quantity, E, is the energy of the system, and Ψ is termed the wavefunction. The wavefunction has no obvious physical meaning; the square of the wavefunction multiplied by a small volume gives the probability of finding the system at a particular set of coordinates. The "Hamiltonian Operator", H, is given by equation (2.6.6).

$$H = \frac{1}{2}\sum_{i}^{es}\nabla_i^2 - \frac{1}{2}\sum_{A}^{nu}\frac{1}{M_A}\nabla_i^2 - \sum_{i}^{es}\sum_{A}^{nu}\frac{Z_A}{r_{iA}} + \sum^{e}{}_{i<}\sum_{j}^{e}\frac{1}{r_{ij}} + \sum_{A<}^{n}\sum_{B}^{n}\frac{z_A z_B}{R_{AB}} \qquad (2.6.6)$$

Z is the nuclear charge, M_A is the ratio of mass of nucleus A to the ratio of mass of an electron, R_{AB} is the distance between nuclei A and B, r_{ij} is the distance between electron i and nucleus A.

The many electron Schrödinger equation cannot be solved exactly for a simple two-electron system such as helium atom or hydrogen molecule. So, approximations are introduced to provide practical methods. These approximations include; Born-Oppenheimer approximations, Hartree Fork Approximations, (warren, 2003) etc.

2.6.1 Born-Oppenheimer Approximations

The Born-Oppenheimer approximation is a way to simplify the complicated Schrödinger equation for a molecule. The nucleus and electrons are attracted to each other with the same magnitude of electric charge, thus they exert the same force and momentum. While exerting the same kind of momentum, the nucleus, with a much larger mass in comparison to electron's mass, will have a very small velocity that is almost negligible. Born-Oppenheimer takes advantage of this phenomenon and makes the assumption that since the nucleus is heavier compared to the electron, its motion can be ignored while solving the electronic Schrödinger equation; that is, the nucleus is assumed to be stationary while electrons move around it. The motion of the nuclei and the electrons can be separated and the electronic and nuclear problems can be solved with independent wavefunctions. The principle of Born-Oppenheimer can be applied to calculate the bond length between molecules. By focusing on the specific separation between nucleus and electron, their wavefunction can be calculated. Thus, a molecule's energy in relationship with its bond length can be examined. (Que, 2000)

The wavefunction for the molecule thus becomes:

$$\Psi_{\text{molecule}} = \Psi_{\text{electron}} \text{ x } \Psi_{\text{nuclei}}$$

This leads to an electronic Schrödinger's expression given in (2.6.6). Where the Hamiltonian operator collapses to equation (2.6.7)

$$\hat{\mathrm{H}}^{ei}\Psi^{ei} = E^{ei}\Psi^{ei} \tag{2.6.7}$$

$$\hat{\mathrm{H}}^{ei} = -\frac{1}{2}\sum_i^e \nabla_i^2 - \sum_i^e \sum_A^n \frac{Z_A}{r_{iA}} + \sum_{i<}^e \sum_j^e \frac{1}{r_{ij}} \tag{2.6.8}$$

Equation 2.6.6 describes the nuclear kinetic energy which is missing in equation 2.6.8 or given as zero, and the nuclear coulumbic term in equation 2.6.6 is a constant. The latter needs be added to the electronic energy, E^{ei}, to yield the total energy, E, for the system (equation 2.6.9).

$$E = E^{ei} + \sum_{A<}^{nuclei} \sum_{B}^{nuclei} \frac{Z_A Z_B}{R_{AB}} \qquad (2.6.9)$$

2.6.2 Hartree-Fock approximation

The most common type of ab initio calculation is called a Hartree-Fock calculation (abbreviated HF), in which the primary approximation is the central field approximation. This means that the Coulombic electron-electron repulsion is taken into account by integrating the repulsion term. This gives the average effect of the repulsion, but not the explicit repulsion interaction. This is a variational calculation, meaning that the approximate energies calculated are all equal to or greater than the exact energy. The energies are calculated in units called Hartrees. Because of the central field approximation, the energies from HF calculations are always greater than the exact energy and tend to a limiting value called the Hartree-Fock limit as the basis set is improved.

The electronic Schrödinger's equation is still difficult to solve and needs further approximations. We first assume that electrons move independently of each other; Individual electrons are confined to functions termed molecular orbitals, each of which is determined by assuming that the electron is moving with the average field of all electrons. The total wavefunction is written in form of a single determinant (Slater determinant) which means that, it is antisymmetric upon interchange of electron coordinates. The total wavefunction is given in equation (2.6.10).

$$\Psi = \frac{1}{\sqrt{N!}} \begin{matrix} X_{1(1)} & X_{2(1)} \dots\dots\dots\dots\dots\dots.. & X_{n(1)} \\ X_{1(2)} & X_{2(2)} \dots\dots\dots\dots\dots\dots.. & X_{n(2)} \\ X_{1(3)} & X_{2(3)} \dots\dots\dots\dots\dots\dots\dots & X_{n(3)} \end{matrix} \quad (2.6.10)$$

The term X_i is called a spin orbital and is the product of a spatial function or molecular orbital, Ψ, and a spin function, α and β. The set of molecular orbitals leading to the lowest energy are obtained by a process referred to as "Self-consistent field" or SCF procedure. All SCF procedures lead to equations of the form (2.6.11).

$$f_i X_{\chi_i} \quad = \quad \sum X_{\chi_i} \quad (2.6.11)$$

The Fock operator f_i is given by the expression (2.6.12).

$$f_{(i)} \quad = \quad \frac{1}{2}\nabla_i^2 \; + \; V^{eff} \quad (2.6.12)$$

X= spin and spatial co-ordinates of the electron, i and χ are the spin orbitals while V^{eff} is the effective potential "seen" by the electron, i. (Levine, 2013)

2.6.3 Self consistent field method

Self-consistent field (SCF) method is used to find approximate solutions to the many-body problem in quantum mechanics. The procedure starts with an approximate solution for particle moving in single partial potential which derives from average interaction with all the other particles. This average interaction is determined by the wave function of all the other particles. The equation describing this average interaction is solved and the

improved solution obtained is used in the calculation of the interaction term. This procedure is repeated for wave functions until the wave functions and associated energies are not significantly changed in the cycle, self-consistency having been attained (Levine, 2013).

2.6.4 THE VARIATIONAL PRINCIPLE

The strength of quantum theory ($H\Psi = E\Psi$) is that given a molecular wave function, one can calculate physical quantities by application of approximate Hamiltonian operator in a manner analogous to that shown below (Levine, 2013) :

$$\int \Psi_j H \Psi_i dr = \int \Psi_j E \Psi_i dr \qquad (2.6.13)$$

Unfortunately, none of those equations offers a prescription for obtaining the orthonormal set of the moment, however, we can pick an arbitrary function, Φ, which is indeed a function of the appropriate electronic and nuclear coordinates to be operated upon by the Hamiltonian. Since we defined the set of orthonormal wave functions Ψ to be complete, the function Φ must be some linear combination of the Ψ, i.e.

$$\Phi = \sum_i ci\Psi i \qquad (2.6.14)$$

Since we don't yet know the individual Ψ_i, we certainly don't know the coefficients C_i either. Note that the normality of Φ imposes a constraint on the coefficients, however, deriving from

$$\int \emptyset^2 dr = 1 = \int \sum_i C_i \Psi_i \sum_j C_j \Psi_j dr$$

$$= \sum_{ij} c_i c_j \int \Psi_i \Psi_j dr$$

$$= \sum_{ij} C_i C_j dij$$

$$= \sum_i C_i^2 \qquad (2.6.15)$$

Now, consider evaluating the energy associated with wave function Φ. Taking the approach of multiply on the left and integrating as outlined above, we have

$$\int \emptyset_I H \emptyset_j dr = \int (\sum_i C_i \Psi_i) H (\sum_j C_j \Psi_j) dr$$

$$= \sum_{ij} C_i C_j \int \Psi_i H \Psi_j dr$$

$$= \sum_{ij} C_i C_j \in_j d_{ij}$$

$$= \sum_i C_i^2 \in_i \qquad (2.6.16)$$

Combine the result from equation 2.6.15 and 2.6.16 to become

$$\int \emptyset H \emptyset dr - \in_0 \int \emptyset^2 dr = \sum_i C_i^2 (\in_i - \in_0) \qquad (2.6.17)$$

Assuming the coefficients to be real numbers, each term C^2i must be greater than or equal to zero. By definitions of $\in_0$, the quantity $(\in_i - \in_0)$ must also be greater than or equal to zero.

$$\int \emptyset H \emptyset dr - \in_0 \int \emptyset^2 dr \geq 0$$

Rearrange to

$$\frac{\int \emptyset H \emptyset dr}{\int \emptyset^2 dr} \geq \in_0 \qquad (2.6.18)$$

This result is critical because it shows us that we do not have to construct our guess wave function Φ as a linear combination of (unknown) orthonormal wave functions Ψ_i, but we may construct it in any manner we wish. The quality of our guess will be determined by how low a value we calculated for the integral in equation 2.6.18 (Levine, 2013).

2.6.5 Linear Combination of Atomic Orbitals (LCAO) Approximation

This approximation takes advantage of the notion that the individual one electron solutions for many- electron atoms and molecules will closely resemble the one electron solutions for the hydrogen atom. In practice, the molecular orbitals are expected as linear combinations of a finite set of one electron functions known as basis function Φ. The LCAO Approximation is given in equation (2.6.19) (Levine, 2013).

$$\Psi_i = \sum_{\mu=1}^{Basisfunction} C_{\mu,i}\, \phi_\mu \qquad (2.6.19)$$

Where c is the molecular orbital coefficient; simply called molecular orbital. This is because the Φ is usually centred at the nuclear positions, generally called atomic orbitals (Levine, 2013).

Hartree-Fock models differ in the number and kind of atomic basis functions, and their computational cost increases as the fourth power of the number of basis function.

2.6.6 Kohn-sham (Ks) molecular orbital theory

The discussion above has emphasized that the density determines the external potential, which determines the Hamiltonian, which determines the wave function. And, of course, with the Hamiltonian and wave function in hand, the energy can be computed. However, if one attempts to proceed in this direction, there is no simplification over MO theory since the final step is still solution of the Schrodinger equation, and this is ver difficult in most

instances. The difficulty derives from the electron-electron interaction term in the correct Hamiltonian. In a key breakthrough, Kohn and Sham (1965) realized that things would be considerably simpler if only the Hamiltonian operator were one for a non-interacting system of electrons. Such a Hamiltonian can be expressed as a sum of one electron operator, has Eigen functions that are Slater determinant of individual one-electron Eigen functions, and has Eigen values that are simply the sum of one-electron Eigen values.

The Kohn-Sham (KS) one electron operator is defined as

$$hiks = \left[-\frac{1}{2}\nabla_{\mathrm{i}}^{2} - \sum_{\mathrm{k}}^{\mathrm{nuclei}} \frac{\mathrm{z_k}}{|\mathrm{r_i}-\mathrm{r_k}|} + \int \frac{\rho(\acute{\mathrm{r}})}{|\mathrm{r_i}-\acute{\mathrm{r}}|} \mathrm{d}\acute{\mathrm{r}} + \mathrm{v_{xc}}\right] \emptyset_i(r_i) = \varepsilon_i \emptyset_i(r_i) \qquad (2.6.20)$$

And $V_{xc} = \frac{\partial \in_{xc}}{\partial \rho}$

V_{xc} is called functional derivative. A functional derivative is analogous in spirit to more typical derivatives, and V_{xc} is perhaps best described as the one-electron operator for which the expectation value of the Ks Slater determinant is $\in_{xc}$

As for determination of the Ks orbital, we may take a productive approach along the lines that developed within the context of MO theory. We express them within a basis set of functions (Φ), and we determine the individual orbital coefficients by solution of a secular equation entirely analogous to that employed for HF-thre replaced by the elements $K_{\mu v}$defined by

$$K_{\mu v} = \langle \emptyset_N | -\frac{1}{2}\nabla^2 - \sum_{k}^{nuclei} \frac{z_k}{|r-\acute{r}|} + \int \frac{\rho(\acute{r})}{|r-\acute{r}|} d\acute{r} + V_{XC} | \emptyset_V \rangle$$

Indeed, the similarities with HF-theory extend well beyond the mathematical technology offered by common variation principle.

2.7 Quantum mechanics approach

Quantum approaches are roughly divided into semi-empirical methods and non-empirical (or ab initio) methods. Semi empirical methods are the approximate methods in which some quantities are taken from experiment, some small quantities are neglected, and some quantities are estimated by fitting to experimental data. Ab initio methods do not require empirical parameters and can be used for a lot of molecular systems (Levine, 2013).

2.7.1 Semiempirical methods

Semiempirical calculations are set up with the same general structure as a HF calculation. Within this framework, certain pieces of information, such as two electron integrals, are approximated or completely omitted. In order to correct for the errors introduced by omitting part of the calculation, the method is parameterized, by curve fitting in a few parameters or numbers, in order to give the best possible agreement with experimental data. The good side of semiempirical calculations is that they are much faster than the ab initio calculations. The bad side of semiempirical calculations is that the results can be eratic. If the molecule being computed is similar to molecules in the data base used to parameterize the method, then the results may be very good. If the molecule being computed is significantly different from anything in the parameterization set, the answers may be very poor (Young, 2001).

Semiempirical calculations have been very successful in the description of organic chemistry, where there are only a few elements used extensively and the molecules are of moderate size. However, semiempirical methods have been devised specifically for the description of inorganic chemistry as well. Most commonly used semiempirical methods (Young, 2001) include: Huckel, Extended Huckel, The Pariser-Parr-Pople (PPP) method (an extension of Huckel method), Complete Neglect of Differential Overlap (CNDO) method, Modified Intermediate Neglect of Differential Overlap (MINDO) methods (which are MINDO/1, MINDO/2, and MINDO/3), Modified Neglect of Diatomic Overlap (MNDO) method, Intermediate Neglect of Differential Overlap (INDO) method, Zerner's INDO method (ZINDO)(also called spectroscopic INDO: INDO/S), Symmetrically Orthogonalized Intermediate Neglect of Differential Overlap method (SINDO1), Partial Retention of Diatomic Differential Overlap(PRDDO) method, Austin Model 1 (AM1) method, Parameterization method 3 (PM3), PM3/TM (an extension of the PM3 method to include d orbitals for use with transition metals), Fenske-Hall method (a modification of crystal field theory), Typed Neglect of Differential Overlap (TNDO) method (of two versions namely TNDO/1 and TNDO/2), Semi-Ab Initio method 1 (SAM1), and Gaussian

methods (G1, G2, and G3) (Sadlej, 1985). This study employed four of these semiempirical methods and they are discussed below.

2.7.1.1 Modified Neglect of Diatomic Overlap (MNDO)

The modified neglect of diatomic overlap (MNDO) method has been found to give reasonable qualitative results for many organic systems. It has been incorporated into several popular semiempirical programs as well as the MNDO program. Today, it is still used, but the more accurate AM1 and PM3 methods have surpassed it in popularity. There are some known cases where MNDO gives qualitatively or quantitatively incorrect results. Computed electronic excitation energies are under-estimated. Activation barriers tend to be too high (Young, 2001). The correct conformer is not always computed to be lowest in energy. Barriers to bond rotation are often computed to be too small. Hypervalent compounds and sterically crowded molecules are computed to be too unstable. Four-membered rings are predicted to be too stable. Oxygenated functional groups on aromatic rings are predicted to be out-of-plane. The peroxide bond is too short by about 0.17Å. The ether C-O-C bond angle is too large by about 9^0. Bond lengths between electro-negative elements are too short. Hydrogen bonds are too weak and long (Young, 2001).

A variation on MNDO is MNDO/d. This is an equivalent formulation including d orbitals. This improves predicted geometry of hypervalent molecules. This method is sometimes used for modeling transition metal systems, but its accuracy is highly dependent on the individual system being studied. There is also a MNDOC method that includes electron correlation (Young, 2001).

2.7.1.2 Austin Model 1 (AM1)

The Austin Model 1 (AM1) method is still popular for modeling organic compounds. AM1 generally predicts the heats of formation ΔH_f more accurately than MNDO, although a few exceptions involving Br atoms have been documented. Depending on the nature of the system and information desired, either AM1 or PM3 will often give the most accurate results obtainable for organic molecules with semiempirical methods. There are some known strengths and limitations in the results obtained from these methods. Activation

energies are improved over MNDO. AM1 tends to predict results for aluminum better than PM3. It tends to poorly predict nitrogen paramidalization. AM1 tends to give O-Si-O bonds that are not bent enough (Young, 2001).

There are some known limitations to AM1 energies, such as predicting rotational barriers to be one-third the actual barrier and predicting five-membered rings to be too stable. The predicted heat of formation tends to be inaccurate for molecules with a large amount of charge localization. Geometries involving phosphorus are predicted poorly. There are systematic errors in alkyl group energies predicting them to be too stable. Nitro groups are too positive in energy. The peroxide bond is too short by about 0.17 Å. Hydrogen bonds are predicted to have the correct strength, but often the wrong orientation. On average, AM1 predicts energies and geometries better than MNDO, but not as well as PM3. Computed bond enthalpies are consistently low (Young, 2001).

2.7.1.3 Recife Model 1 (RM1)

RM1 is a new parameterization within the AM1 theoretical framework, using a more carefully chosen data set and new optimization algorithms. RM1 is a fully disclosed and public domain semiempirical molecular orbital model, capable of modeling most molecular systems of importance to organic chemistry, biochemistry and pharmaceutical research. Essentially this method is identical to the AM1 method, but with improved performance, much newer and better parameters. A known error in PM3 nitrogen charges is corrected in RM1 (Young, 2001). In most cases, RM1 yields superior results to both AM1 and PM3 for both organic and biomolecules. RM1 is different from PM5 and PM6, which use dissimilar equations, mainly affecting the way the core-core interaction is defined. RM1 is one of the most widely available semiempirical methods (Young, 2001).

2.7.1.4 Parameterization Method 3 (PM3)

Parameterization method 3 (PM3) uses nearly the same equations as the AM1 method along with an improved set of parameters. The PM3 method is also currently extremely popular for organic systems. It is more accurate than AM1 for hydrogen bond angles, but

AM1 is more accurate for hydrogen bond energies. The PM3 and AM1 methods are also more popular than other semi-empirical methods due to the availability of algorithms for including solvation effects in these calculations (Young, 2001).

There are also some known strengths and limitations of PM3. Overall heats of formation are more accurate than with MNDO or AM1. Hypervalent molecules are also predicted more accurately. PM3 tends to predict that the barrier to rotation around the C-N bond in peptides is too low. Bonds between Si and the halide atoms are too short. PM3 also tends to predict incorrect electronic states for germanium compounds. It tends to predict sp^3 nitrogen as always been pyramidal. Some spurious minima are predicted. Proton affinities are not accurate. Some polycyclic rings are not flat. The predicted charge on nitrogen is incorrect. Nonbonded distances are too short. Hydrogen bonds are too short by about 0.1 Å, but the orientation is usually correct. On average, PM3 predicts energies and bond lengths more accurately than AM1 or MNDO (Meuwly and Karplus, 2004).

An extension of the PM3 method is PM3/TM. PM3/TM includes d orbitals for use with transition metals. Unlike the case with many other semiempirical methods, PM3/TM's parameterization is based solely on reproducing geometries from X-ray diffraction results. Results with PM3/TM can be either reasonable or not depending on the coordination of the metal center. Certain transition metals tend to prefer a specific hybridization for which it works well (David, 2001).

2.7.2 Ab initio methods

The term *ab initio* comes from a Latin word, meaning from the beginning. Ab initio methods use the Hartree- Fock method as a starting point, i.e., the wave function is used to describe electronic structure. Lately, density functional approaches have come into major use as part of the non-empirical methods (Labanowski, 2004).

The principles of density functional theory of electronic structure are conveniently expounded by making reference to conventional wave function theory. Therefore, it is worthwhile briefly reviewing several key concepts, and developing a systematic nomenclature and notation, so the remainder of the chapter is devoted to this. This next section summarizes the details of density functional theory.

2.7.2.1 Density Functional Theory (DFT)

The density functional theory (DFT) is presently the most successful (and also the most promising) approach to compute the electronic structure of matter. Its applicability ranges from atoms, molecules and solids to nuclei and quantum and classical fluids. In its original formulation, the density functional theory provides the ground state properties of a system, and the electron density plays a key role. In chemistry for example, DFT predicts a great variety of molecular properties such as molecular structures, vibrational frequencies, atomization energies, ionization energies, electric and magnetic properties, reaction paths, etc. The original density functional theory has been generalized to deal with many different situations like spin polarized systems, multicomponent systems such as nuclei and electron hole droplets, free energy at finite temperatures, superconductors with electronic pairing mechanisms, relativistic electrons, time-dependent phenomena and excited states, bosons, molecular dynamics, etc (Juan, 2003).

This theory was developed in the mid 1960s by Hohenberg, Kohn and Sham (Hohenberg and Kohn, 1964; Kohn and Sham, 1965) and states that "The energy, E, of a system can be expressed as a functional of the electron density $\rho_{(r)}$ of the system.

$$E = F\left[\rho_{(r)}\right] \tag{2.6.21}$$

The theory further states that the functional is exact and universal which implies that it is applicable to any molecular system. This can be written as the sum of the following energy terms:

$$E = E_T + E_V + E_J + E_{XC} \tag{2.6.22}$$

E_T is the kinetic energy of non-interacting electrons, E_V is the classical electron repulsion, E_J is the electron-nucleus interaction and E_{XC} is the quantum mechanical contributions to the potential energy (self-interaction correction, exchange and correlation and the part of the kinetic energy that is not included in the E_T). The exact form of the exchange – correlation functional, E_{XC}, is unknown and all attempts to determine the total energy of the system rely on the approximations to this term.

Except for $E_{T,}$ all the components depend on the total electron density $\rho_{(r)}$, (equation 2.6.23).

$$\rho_r \quad = \quad 2\sum_i^{orbital}\left|\Psi_{i\,(r)}\right|^2 \qquad (2.6.23)$$

Where Ψ_i is called Kohn-Sham orbitals and the summation is carried out over pairs of electrons.

DFT is today one of the most important tools for calculating ground state properties of metals, semiconductors, and insulators. The principal aim of any many-body theory is to reduce the number of parameters needed to describe the system. In such a system, which may contain anywhere between 2 and may be more than 1023 particles, each particle is described by its three coordinates in space, which may be time-dependent, and possibly a spin coordinate. So, it involves great expense to solve the equations of motion of such a system (Blom *et al.*, 2002; Parr and Yang, 1989).

It is imperative to say that, density functional theory is only able to predict the ground state energy and properties. Since the ground state energy is a function of a number of parameters of the system, we may also use density functional theory to find other ground state properties such as bond lengths and angles.

In principle, DFT is able to produce these quantities exactly, however, in application it is necessary to introduce some approximations (Blom *et al.*, 2002) Fortunately, even the simplest reasonable, the local density approximation, (LDA), gives notably correct results, even for systems for which this approximation does not seem to be valid. One of the fundamental reasons for this good performance is that the large kinetic energy is treated exactly (Levine, 2013; Cramer, 2002). This accuracy, beside the fact that the DFT transforms the many-body problem to a one-particle problem, is the major attractiveness of the theory.

In contrast to the Hartree-Fock picture, which begins conceptually with a definition of individual electrons interacting with the nuclei and all other electrons in the system, DFT starts with a consideration of the entire electron system. The total electron density is

decomposed into one-electron densities in DFT; these are constructed from one-electron wave functions (Kohn and Sham, 1965; Jensen, 1999; Koch and Holthausen, 2001).

DFT has been successfully extended to open-shell systems and magnetic solids (Gunnarsson *et al.*, 1972). In these cases, the local exchange-correlation energy depends not only on the local electron density, but also on the local spin density if the densities of spin-up and spin-down electrons are not same, LDA changes to the local spin density approximation (LSDA). LSDA treats the densities of spin-up and spin-down electrons separately.

It is not clear which of the two pictures, the Hartree-Fock approach or the local density functional approach gives better results. Actually, the applicability of the Hartree-Fock picture versus the local density approximation depends on the effective range of many-body interactions between electrons. If these interactions are of dimensions of several interatomic distances, then the Hartree-Fock approximation is better. If, however, these many-body effects are of a more shortrange nature, then the local density approximation is more appropriate. Experience shows that for many systems, the LDA gives surprisingly good results, especially for the prediction of structural properties. This may be taken as evidence of the more local character of many-body interactions for many systems of interest (Levine, 2013; Cramer, 2002; Chong, 1995).

DFT, originally intended for metallic solid-state systems, turned out to be also surprisingly successful for describing the structure and energetics of molecules. The clear evidence for the capabilities of the local density functional approach for molecular systems was given already in the 1970's, but only recent systematic calculations on a large number of typical molecules together with the introduction of gradient corrected density functionals (like Becke's (B88). Lastly, hybrid methods became popular which involves a mixture of Hartree-Fock exchange and DFT exchange. In this new method, the exchange-correlation energy term is corrected and calculated by the help of the exact exchange at the Hartree-Fock level (Jensen, 1999; Kose, 2001). B3LYP is hybrid functional, the combination of Becke's three parameter gradient corrected hybrid functional and the LYP (developed by Lee, Yang, and Parr) is very popular (Jensen, 1999).

2.7.2.2 Local-Density Approximation (LDA)

In the local-density approximation (LDA), the many-electron problem is approximated by a set of single-particle equations which are solved with the self-consistent field method. The total energy is minimized. The total energy is taken to be the sum of a kinetic energy, T, the classical Hartree term for the electron density, E_{ed}, the electron-nucleus energy, E_{EN}, and the exchange-correlation energy, E_{XC}, which takes into account approximately the fact that an electron does not interact with itself, and that electron correlation effects occur (Young, 2001).

2.7.2.3 Fundamental problems in DFT

DFT offers a powerful and excellent method for calculating the ground-state total energy and electron density of a system of interacting electrons. The whole theory is based on functionals of the electron density, which therefore plays the central role. However, the key functional, which describes the total energy of the electrons as a function of their density, is not known exactly: the part of it that describes electronic exchange and correlation has to be approximated in practical calculations. In 1986, Michael Schlüter, Lu Sham and R. W. Godby (Godby *et al.,* 1986; Knorr and Godby, 1992) calculated an accurate exchange-correlation potential for silicon using many-body perturbation theory, and they showed the "band-gap problem", the observation that the electronic band gap of semiconductors in DFT calculations was only about half of the experimental band gap. They concluded that the band gap problem was inherent in DFT and not due to the approximations used in the various functional. But due to poor description of unoccupied orbital energy levels in Hartree-Fock approximation, the band gap values are overestimated by several electron volts in low band gap polymers (Rochefort *et al.,* 1999). On the other hand, DFT based methods tend to systematically underestimate the band gaps of low band gap polymers (Rochefort *et al.,* 1999; Dreizler and Gross, 1990).

However, recent developments of DFT/hybrid functionals that include a weighted contribution of Hartree-Fock and DFT exchange allow a better evaluation in the band gap results (Salzner *et al.,* 1997; Rochefort *et al.,* 1999). In order to improve the calculated band gap values, Salzner *et al.,* (1998) for instance, studied DFT/hybrid approach and they came to the conclusion that the best extrapolated band gaps of polymers are obtained with

hybrid functionals containing 30% of Hartree-Fock exchange in combination with the P86 correlation functional. Since exact exchange tends to reduce the self interaction, the band gaps are corrected in the direction of larger band gaps, which was the desired effect in the case of the work of Salzner *et al.,* (Salzner *et al.,* 1998)

2.7.2.4 Time dependent Density Funtional Theory (TDDFT)

TDDFT is a quantum mechanical approach applied in Physics and Chemistry to explore the properties and dynamics of many-body systems in the presence of time-dependent potentials, such as electric or magnetic fields. TDDFT is an extention of DFT but provides formally exact and basically convenient methods to evaluate electronic excitation energies of isolated systems and less commonly, solids. By distinction, density-functional theory (DFT) is a ground-state theory. In other words, it is used to determine the ground state energies of a quantum system and estimate related quantities of importance, such as the ground-state energy (Ullrich and Yang, 2014).

The formal foundation of TDDFT is Rung-Gross (RG) theorem (Rung and Gross, 1984), which is the time dependent analogue of Hohenberg-Kohn (HK) theorem (Hohenberg and Kohn, 1964).

The Rung and Gross approach considers a single component system in the presence of time –dependent scalar field where the Hamiltonian is rpresented in the form

$$\hat{\mathrm{H}}\,(t) \;=\; T + \; V_{exact}\,(t) + \; W \qquad (2.6.24)$$

Where T is the kinetic energy operator, W is the electron-electron interaction, V_{exact} (t) the external potential which along with the number of electrons defines the system.The many-body wavefunction emanates from the time-dependent Schrödinger equation

$$(-\frac{1}{2m}\nabla^2 + \mathrm{V})\;\Psi\;(\tilde{r},t) = ih\frac{\partial\Psi(\tilde{r},t)}{\partial t} \quad |\Psi(0)\rangle = |\Psi\rangle \qquad (2.6.25)$$

In explaining the Rung-Gross theorem employing the Schrödinger equation is the starting point.

2.7.2.5 Time dependent Kohn-Sham system

The Kohn-Sham formalism has been immensely thriving in ground-state DFT. Its time dependent complement appears very similar in the sense that it chooses a non-interacting system (that for which the interaction potential is zero) in which to form the density that is equal to the interacting system. This is based on the fact that the non-interacting systems can be solved and the wavefunction can be represented as a Slater determinant of single-particle orbitals.

The difficulty is to determine a potential, denoted as $V_s(\boldsymbol{r},t)$ or $V_{KS}(\mathbf{r},t)$, which in turn gives rise to a non-interacting Hamiltonian, H_s,

$$\hat{H}_s\,(t) \;=\; T + \;V\,(t) \qquad (2.6.26)$$

This determines a wavefuntion

$$\hat{H}_s\,(t)|\Psi(t)\rangle, \;=\; i\frac{\partial}{\partial t}|\Psi(t)\rangle,\;\; |\Psi(0)\rangle = |\Psi\rangle \qquad (2.6.27)$$

Which is contructed in terms of a set of N orbitals which obeys the equation,

$$(-\frac{1}{2m}\nabla^2 + \nu_s\,(\boldsymbol{r},t)\,\Psi_i\,((\boldsymbol{r},t)\;i\frac{\partial}{\partial t}\Psi_i\,((\boldsymbol{r},\,t)\;\;\Psi_i(\mathbf{r},0)\rangle = |\Psi\rangle \qquad (2.6.28)$$

and generate a time-dpendent density ρ_s

$$\rho_s\,(\mathbf{r}, t) = \sum_{i=1}^{n} \Psi_i\,(\boldsymbol{r}, t)\ |^2 \qquad (2.6.29)$$

where ρ_s is the density of the interacting system.

The challenge is determining the approximations to Kohn-sham potential. The time-dependent KS potential is deposed to exact the external potential of the system and the time-dependent Coulomb interaction, V_J. The component left is the exchange-correlation potential

$$\nu_s\,(\boldsymbol{r}, t) = \nu_{ext}\,(\boldsymbol{r}, t) + V_J\,(\boldsymbol{r}, t) + \nu_{xc}\,(\boldsymbol{r}, t) \qquad (2.6.30)$$

2.7.3 Open-shell and excited-state methods

Open shell refers to a valence shell which is not completely filled with electrons or that has given all of its valence electrons through chemical bonds with other atoms or molecules during a chemical reaction. With respect to molecules it signifies that there are unpaired electrons. In molecular orbital theory, this leads to molecular orbitals that are singly occupied most of which are characterized by static correlation. Open shell systems are more difficult to study computationally because of their static correlation and multireference nature (Shao *et al.*, 2003). In quantum chemistry such systems are treated with restricted open-shell Hartree-Fock method or the unrestricted Hartree-Fock method. The methods that can be used are spin flip Time-dependent Density Functional Theory and Equation of motion coupled cluster single and double (EOM-CCSD)

2.7.3.1 Spin Flip-Time dependent Density Funtional Theory (SF-TDDFT)

Standard TDDFT also does not yield a good description of static correlation effects, because it is based on a single reference configuration of Kohn-Sham orbitals. Recently, a new variation of TDDFT called spin-fip density functional theory (SFDFT) was developed by (Shao *et al.,* 2003) to address this issue. SFDFT is different from standard TDDFT in two ways: The reference is a high-spin triplet (quartet) for a system with an even (odd) number of electrons; One electron is spin-flipped from an alpha Kohn-Sham orbital to a beta orbital during the excitation.

SF-TDDFT can describe the ground state as well as a few low-lying excited states, and has been applied to bond-breaking processes, and di- and tri-radicals with degenerate or near-degenerate frontier orbitals.

The fundamental hypothesis of spin flip approach is based on the starting from a high-spin reference state, which is inherently less multireference in nature, to a difference target singlet configurations.

The equation can be represented as follows:

$$\left|\Psi_{target}\right\rangle = R^{SF}\left|\Phi_{ref}\right\rangle \qquad (2.6.31)$$

Where R^{SF} is the spin-flip operator, $\Psi_{target,}$ refers to the different target states and φ_0, represents the high spin reference state at DFT level of theory

2.7.3.2 Coupled Cluster (CC) theory

Coupled cluster theory is a quantum mechanics approach used for describing many-body systems. It is a post-Hartree-Fock ab initio method in quantum chemistry wich basically takes Hatree-Fock molecular orbital methods and contruct multi-electron wavefunctions using the exponential cluster operator to account for electron correlation. This method is most suitable for small to medium sized molecules. Single reference coupled cluster equation is given by (Shao *et al.,* 2003)

$$\Psi_0 = e^{\hat{T}} \left| \Phi_0 \right\rangle \qquad (2.6.32)$$

Where Ψ_0 is the CCSD wave function, φ_0 is the uncorrelated Hartree−Fock wave function and the operator T is given by;

$$T = T_1 + T_2 + T_3 + \ldots \qquad (2.6.33)$$

$$T_1 = \sum_{ia} t_i^a \{ a_a^\dagger a_i \}$$

$$T_2 = \frac{1}{4!} \sum_{ijab} t_{ij}^{ab} \{ a_a^\dagger a_b^\dagger a_j a_i \} \qquad (2.6.34)$$

$T=T_1+T_2$ → CCSD → scales as N^6 the most commonly used model

$T=T_1+T_2+T_3$ → CCSDT → scales as N^8

$T=T_1+T_2+T_3$ (partial) → CCSD (T) → scales as N^7

Where CCSD (T) is regared as Coupled Cluster Single and Double (Triple), T is the coupled cluster operator.

2.8 Basis set

Basis sets are mathematical functions which are used to construct the wave function (Levine, 2013; Cramer, 2002). Hartree-Fock calculations make use of the complete set of basis functions known as the the complete set of basis functions. Slater type orbitals (STOs) are similar to hydrogen atomic orbitals; nevertheless, they suffer from a fairly significant limitation. In STOs there are no analytical solutions for the general four-centre

integrals. For there to be an analytical solution of the general four-index integral formed from such functions, the radial decay of the STOs has been changed to Gaussian type functions (GTOs) (Cramer, 2002). The basis sets often used in Hartree-Fock, Density Functional, Moller-Plesset and configuration interaction calculations is Guassian-type functions (Hehre and Ohlinger, 2003). The quality of a basis set can be increased by the addition of extra basis functions. Important additions to basis sets are *polarisation functions* and *diffuse functions*.

CHAPTER THREE
COMPUTATIONAL METHODS

Quantum mechanical calculations of the ground state molecular structures of pyrrole and its derivatives were carried out using Spartan 10 software package (Shao *et al.,* 2011) Gaussian 09 (Frisch *et al.*, 2009), and Q-Chem 4.2 (Shao *et* al., 2014) and on a 2.50 GHz personal computer and HP cluster machine of 132GB, at National Chemical Laboratory (NCl, Pune, India). Calculations were done using Semi-empirical methods (MNDO, AM1. PM3, PM6 and RM1) (Stewart. 1989), ab initio restricted hybrid Density Functional Theory (DFT) method at B3LYP/6-31G*, Time Dependent Density Functional Theory (TDDFT), Spin-flip Time Dependent Density Functional Theory (DFT) and Coupled Cluster Single and Double Theory (CCSD). Literature reveals that DFT at B3LYP/6-31G (d) level of theory (Romanova *et al*., 2010; Salzner and Aydin, 2011; Mishra and Tandon, 2009; Ullah *et al*., 2013) can calculate the geometric and electronic (band structure) properties due to its electron correlation effect. Our confidence based on the literature led us to use the B3LYP method of DFT with 6-31G (d) basis set to calculate the molecular properties of the oligomers. We have calculated the ionization potential (IP), electron affinities (EAs), energies of highest occupied molecular orbital (HOMO) and lowest unoccupied molecular orbital (LUMO), and band gap of studied compounds up to five repeating units, where n is the number of repeating unit. For UV−VIS calculations and excited energies, TDDFT calculations have been used at B3LYP/6-31G*. The hybrid Density Functional Theory (DFT) method at B3LYP/6-31G* levels of theory, refers to the combination of functional hybrid exchange of Becke's three, (Becke, 1993) with functional correlation gradient of Lee and Yang (Lee *et al*., 1988). Due to multireference and open shell nature of higher pyrrole derivatives we have used methods that can accurately determine the excited energies, vertical excitation energies and Coupled cluster operator (T1) diagnostic using Spin-flip TDDFT methods and CCSD (6-311++G (d,p)) method. These methods help to accurately determine polymers suitability as components of biosensor

Plate 3.1. HP cluster machine, 132GB, at National Chemical Laboratory (NCl, Pune, India)

3.1 Geometry definition

The geometry of pyrrole derivatives is defined in terms of the structure below; in these structures,

$R_1 = CH_3$

R_2 = COOH, SO_3^-, $CONH_2$, COSH, and CHO.

Systems studied are unsubstituted and some substituted pyrroles.

Substituted Pyrroles include;

A. 3-methyl-pyrrole-4-carboxylic acid (MPC^a)
B. 3-methyl-pyrrole-1-carboxylic acid (MPC^b)
C. 3-methyl-pyrrole-4-carboxamide (MPCam)
D. 3-methyl-pyrrole-4-carbothioic acid (MPCOSH)
E. 3-methyl-pyrrole-4-sulfonic acid ($MPSO_3H$)
F. 3-methyl-pyrrole-4-carbaldehyde (MPCHO)

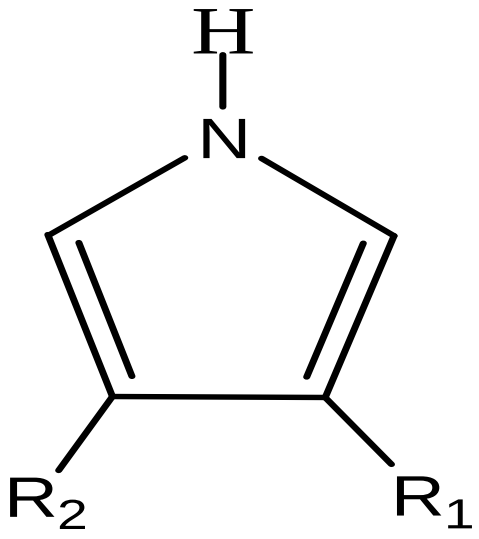

Fig. 3.1. Structural representation of pyrrole

$R_1 = CH_3$

R_2 = COOH, SO_3^-, $CONH_2$, COSH, and CHO.

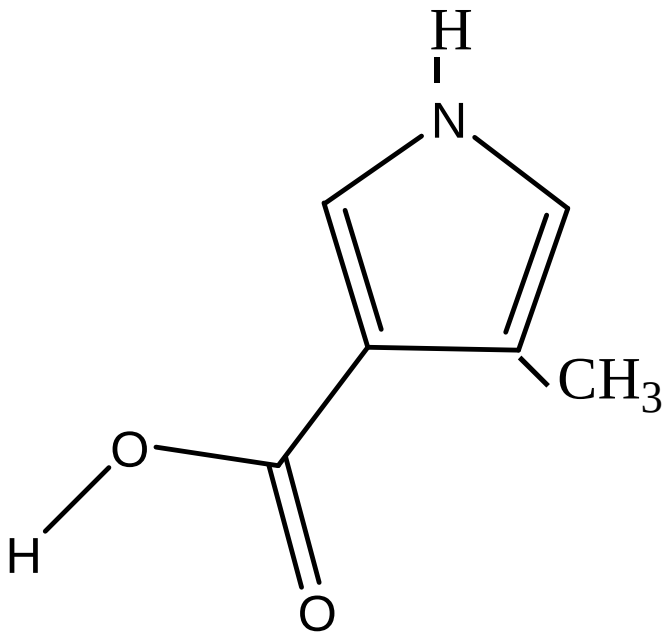

Fig. 3.2. Structural representation of 3-methyl-pyrrole-4-carboxylic acid (MPC[a])

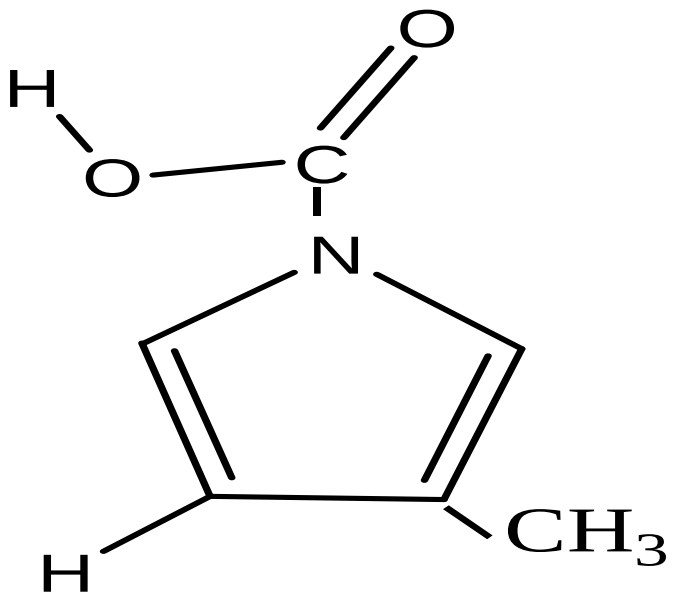

Fig. 3.3. Structural representation of 3-methyl-pyrrole-1-carboxylic acid (MPC[b])

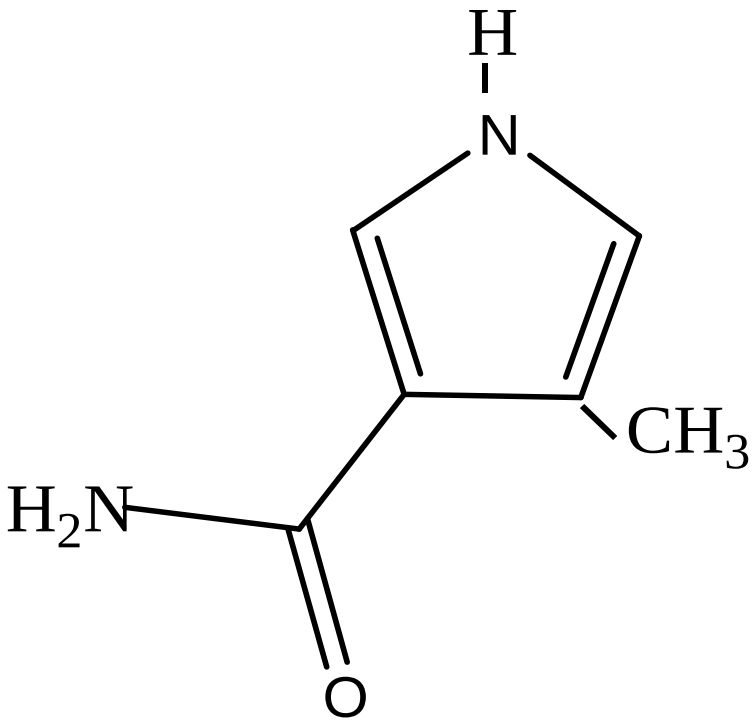

Fig. 3.4. Structural representation of 3-methyl-pyrrole-4-carboxamide (MPCam)

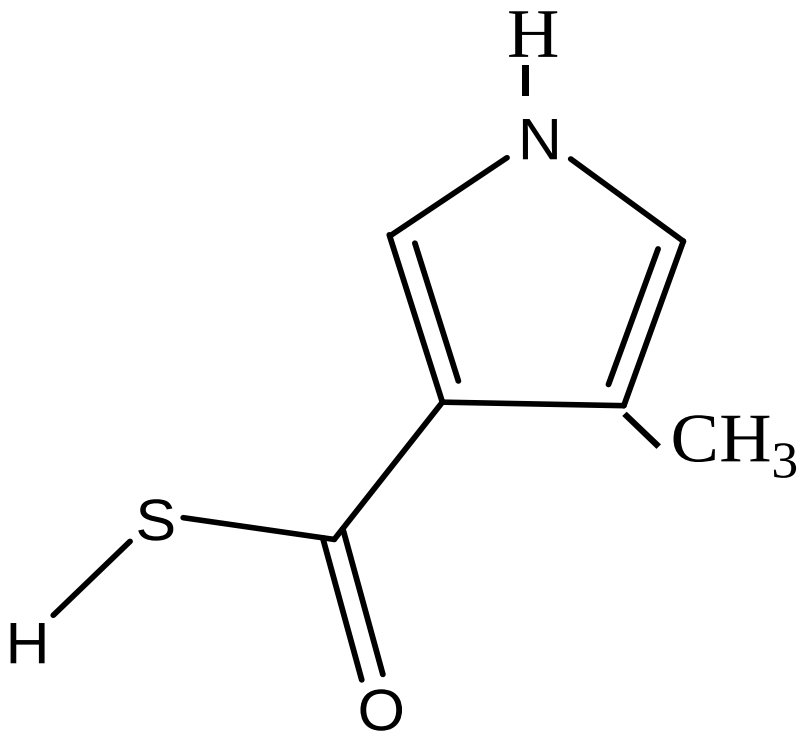

Fig. 3.5. Structural representation of 3-methyl-pyrrole-4-carbothioic acid (MPCOSH)

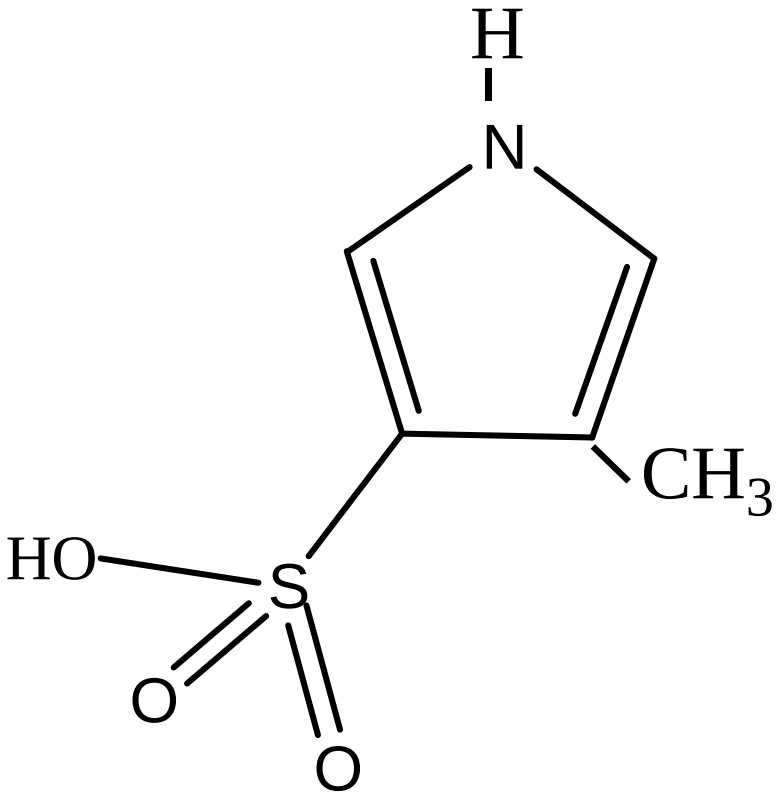

Fig. 3.6. Structural representation of 3-methyl-pyrrole-4-sulfonic acid ($MPSO_3H$)

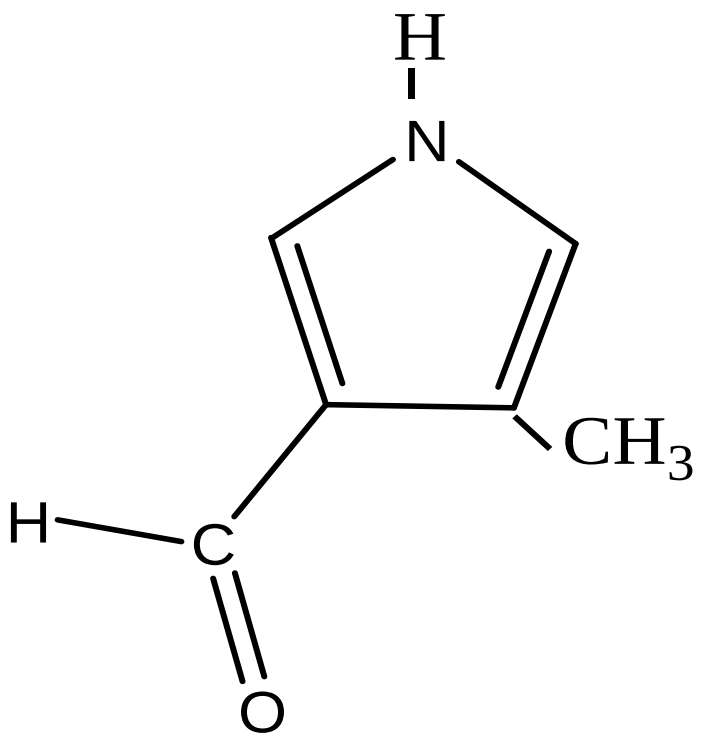

Fig. 3.7. Structural representation of 3-methyl-pyrrole-4-carbaldehyde (MPCHO)

3.1.1 Geometric optimization

Geometry optimization is an iterative process in which the energy gradients (first derivatives of the energy with respect to all coordinatates) are calculated for the initial geomtetry. For geometry corresponding to an energy minimum, the curvature of the energy surface must be positive.

The survace curvature (second derivatives of the energy with respect to coordinates) is Hessian curvature. Therefore finding the absolute or global minimum requires repeated optimization starting with initial (guess) geometry. In principle, optimization is often carried out in the absence of symmetry, i.e C1 symmetry. Local minima yield geometry with the lowest energy. To verify local minima in structures, vibrational frequencies on the final optimized geometry was carried out if there are one or more imaginary frequencies (Hehre and Ohlinger, 2011). The optimized geometries are:

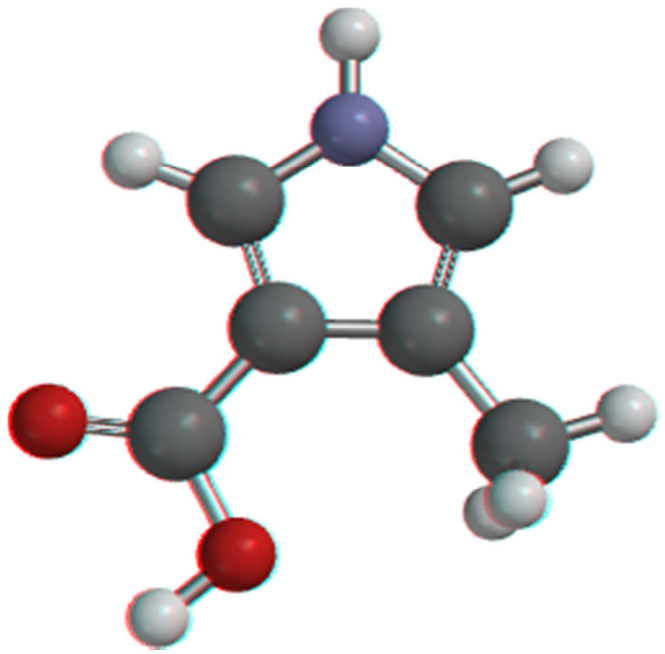

Plate 3.2. Optimized geometry of MPC[a]

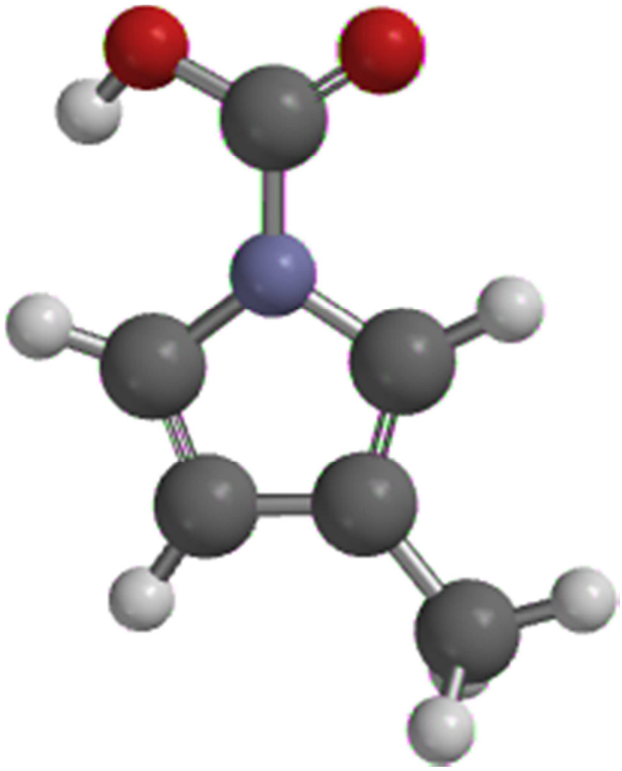

Plate 3.3. Optimized geometry of MPC[b]

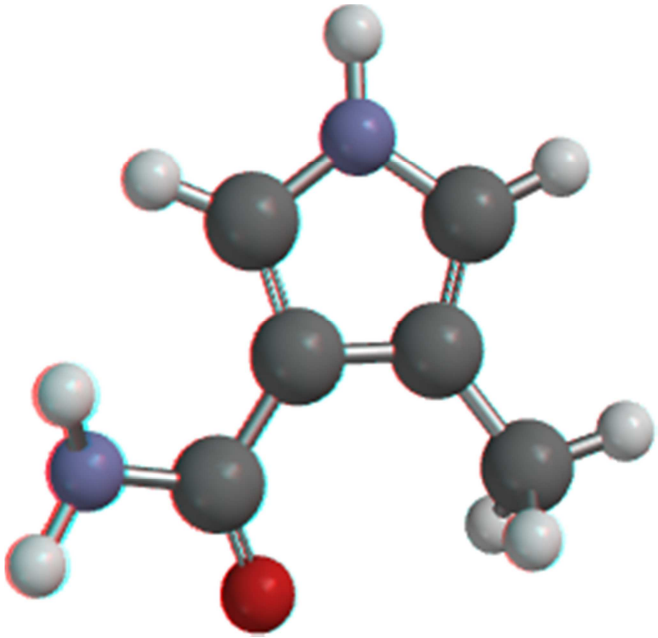

Plate 3.4. Optimized geometry of MPCAM

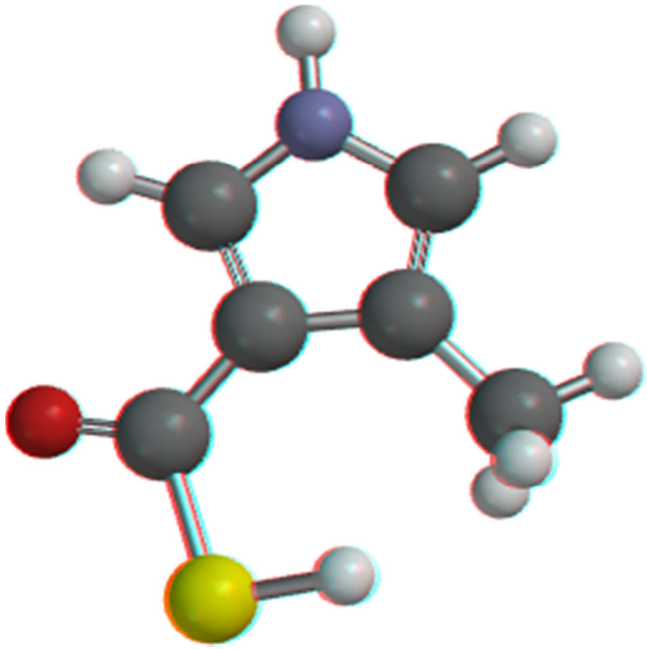

Plate 3.5. Optimized geometry of MPCOSH

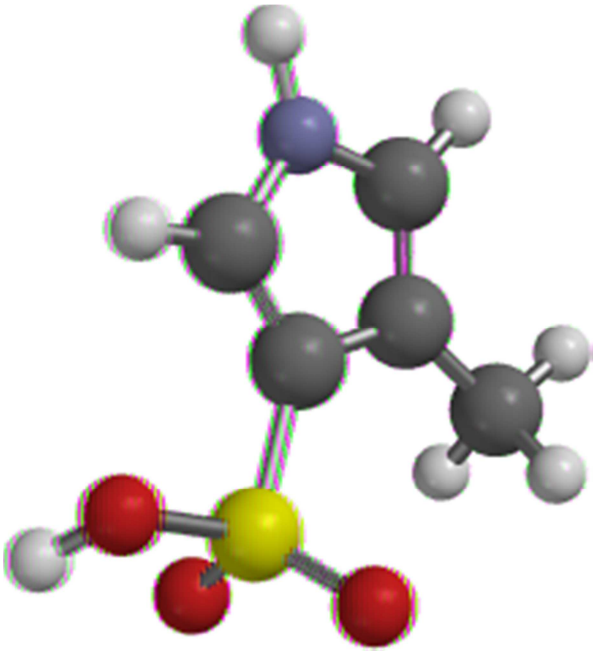

Plate 3.6. Optimized geometry of $MPSO_3H$

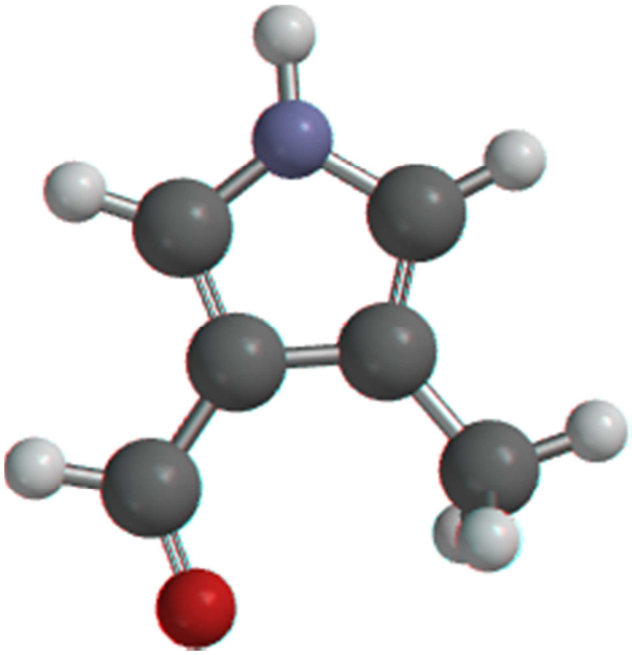

Plate 3.7. Optimized geometry of MPCHO

3.2 Molecular geometry

The geometric properties studied at ground state were selected bond length, bond angle, dihedral angle (torsional angle) and the intermolecular charge transfer (ICT). These were determined using Ab initio restricted hybrid Density Functional Theory (DFT) method at B3LYP/6-31G*.

3.2.1 Bond Length Alternation parameter (*BLA)*: In order to characterize the alternation of single or double carbon-carbon bonds within the two ring moieties, the Bond Length Alternation parameter (*BLA*) was used (Jacquemin et al., 2007). This parameter might be defined as the average of absolute values of the differences between the *i*-th bond length d_i and average bond length $\bar{d}$ (Jacquemin et al., 2007).

$$BLA = \frac{\sum / di - \bar{d} /}{N} \qquad (3.2.1)$$

3.2.2 Inter-ring bond length: The inter-ring bond length was also determined using Badger's rule (Cuff and Kertesz, 2007). An estimated inter-ring bond length based on Badger's rule of 1.42 Å indicates that the average structure is about 30% quinoid like. Cuff and Kertesz, (2007) determined bond distances through the application of Badger's rule. Accordingly,

$$F^{-1/3} = ar+b \qquad (3.2.2)$$

Where F is the stretching force constant in mdyn/A^{o}, r is the C-C bond length in Å, and a and b are constants

3.2.3 Intramolecular charge transfer (ICT): This was calculated as the average of the summation of Mulliken charge distribution of studied compounds (Malki *et al*., 2012).

$$ICT = \frac{\sum e}{2} \quad (3.2.3)$$

Where e represent summation of mulliken charge

3.3 Thermodynamic properties

Thermodynamic properties considered in this work include: Calculated energies (E_0), Zero Point Energy (ZPE), the specific heat capacity at constant volume (CV), Enthalpy (ΔH^o) Entropy change (ΔS), Heat of formation (ΔH_f^o) and Gibbs free enegy change (ΔG_f^o). These were determined using Ab initio restricted hybrid Density Functional Theory (DFT) method at B3LYP/6-31G*. The Heat of formation (ΔH_f^o), was calculated using Semi-empirical methods (MNDO, AM1, PM3 and PM6)

3.3.1 Percentage difference in thermal stability

The percentage difference in the thermal stability of titled compounds were determined using the following expression

$$\%\Delta H^o = \frac{\Delta H_f - \Delta H_i}{\Delta H_i} \times 100 \quad (3.31)$$

ΔH^o_f = Enthalpy change after adding the substituent

ΔH^o_i = Enthalpy change before adding the substituent

3.4 Determination of QSAR properties

The quantitative structure activity relationship parameters determined in this work include: Polarizability α (Å3), Log P and area (Å2). These were determined using Ab initio restricted hybrid Density Functional Theory (DFT) method at B3LYP/6-31G*. Polarizability was determined using the following equation (Targema *et al*., 2013)

$$\alpha' = 2\sum_n \frac{/\mu_{on}/^2}{E_n^{(0)} - E_0^{(0)}} \quad (3.4.1)$$

Because μ = qR where q is the charge on the system and R is the distance separating the charges on the system (molecular radius), and $E_n^{(0)} - E_0^{(0)}$ can be approximated to be difference between the energies of the frontier molecular orbitals $E_{\mathrm{LUMO}} - E_{\mathrm{HOMO}}$) denoted as ΔE, then equation 3.4.1 becomes;

$$\alpha = \frac{2(qR)^2}{\Delta E} \qquad (3.4.2)$$

Biological activity normally expressed as 1/C, where C = [drug] or compound required to achieve a defined level of biological activity. A more active compound require lower concentration (Hughes *et al.*, 2011)

$$\text{Log } 1/C = 0.75 \log P + 2.30 \qquad (3.4.3)$$

Where Log P is Partition coefficient

3.5 Electronic properties

The Ionization potential (IP), Electron affinity (EA), HOMO, LUMO, and band gap calculations were performed on these optimized structures. The oligomers were extrapolated to polymer through second-degree polynomial fit equation (Salzner, 2010). The band gap (or the π−π* lowest electron transition) was estimated as the difference between the HOMO and LUMO orbital energies. The negative of HOMO is estimated as IP, (Salzner *et al.*, 2008; Foresman and Frisch, 1996) whereas the negative of LUMO is estimated as EA (Salzner, 2008; Becke, 1988). All calculations were performed in the gas phase.

3.5.1 Determination of hardness

There is also relationship between hardness and aromaticity (Zhou and Navangul, 1990, Bird, 1997). DFT method provides definitions of important universal concept of molecular structure stability and reactivity. It was developed by (Parr and Chattaraj, 1991; Pearson, 1985; Parr and Pearson, 1983) and approximation for absolute hardness η is as follows:

$$\eta = \frac{1}{2}(I - A) \quad (3.6.1)$$

η=Absolute hardness

I= Vertical Ionization energy

A= Vertical electron affinity

According to the Koopman's theorem (Koopmans, 1933) associated within the framework of HF self-consistent field molecular orbital theory, the ionization energy and electron affinity can be expressed through frontier orbital HOMO and LUMO orbital energy.

$$I = -\varepsilon_{HOMO} \quad (3.6.1.2)$$

$$A = -\varepsilon_{LUMO} \quad (3.6.1.3)$$

$$\eta = -\frac{1}{2}(\varepsilon_{LUMO} - \varepsilon_{HOMO}) \quad (3.6.1.4)$$

3.5.2 The global electrophilicity index ω: This was introduced by Domingo *et a*l., (2002) and calculated using the electronic chemical potential μ and chemical hardness η:

$$\omega = \frac{\mu^2}{2\eta} \quad (3.6.2)$$

According to the definition, this index measures the propensity of a species to accept electrons. Under Domingo *et al*., (2002; (Parr and Yang 1989), the high nucleophility and electrophility of heterocycles corresponds to opposite extremes of the scale of global

reactivity indexes. A good, more reactive, nucleophile is characterized by a lower value of μ, ω; and conversely a good electrophile is characterized by a high value of μ, ω.

The hard and soft acids and bases (HSAB) principle has been very useful to predict the reactivity of chemical systems. The HSAB principle has been used in a local sense in terms of DFT concepts such as Fukui function *f(r)*.

$$f(r) = \left(\frac{\delta\rho(r)}{\delta N}\right)_v = \left(\frac{\delta\mu}{\delta v}\right)_N \tag{3.6.3}$$

Where μ is electronic chemical potential defined above, v is the external potential, ρ corresponds to the electronic density, and N is the total number of electrons of the system.

For nucleophilic attack

$$f^{+}(r) = \left(\frac{\delta\rho(r)}{\delta N}\right)_v^{+} = [\rho_{N+1}(r) - \rho_N(r)] \tag{3.6.4}$$

For electrophilic attack

$$f^{-}(r) = \left(\frac{\delta\rho(r)}{\delta N}\right)_v^{-} = [\rho_N(r) - \rho_{N-1}(r)] \tag{3.6.5}$$

$$I(r) = \sum_i \frac{\rho_i(r)|\varepsilon_i|}{\rho(r)} \tag{3.6.6}$$

Where $\rho i(\boldsymbol{r})$ is the electron density of the *i*-th molecular orbital (MO), and εi is its energy.

3.6 Electronic transition properties

The detailed electronic transitions, including excitation energies, oscillator strength, MO/character (configurations for the main $S_0 \rightarrow S_1$ electronic transitions) and maximum absorption in UV-Vis spectrum (denoted as λ_{max}) are presented in this work. For UV−Vis calculations, TDDFT calculations have been used at B3LYP/6-31G*

3.7 Open-Shell and Excited-State (multireference) calculations

Due to multireference nature of higher members of pyrrole derivatives, T1 diagnostic calculation was performed to ascertain the single or multireference character in studied systems. Vertical excitation energies and first exited dipole moments using Spin-flip TDDFT methods and CCSD method

CHAPTER FOUR
RESULTS AND DISCUSSION

4.1 Geometries of studied systems

The structure of pyrrole and six derivatives from monomer up to pentimer was optimized; the optimized geometric structure of pyrrole and its six derivatives (pentimers) are given in Plate 4.1-4.7.

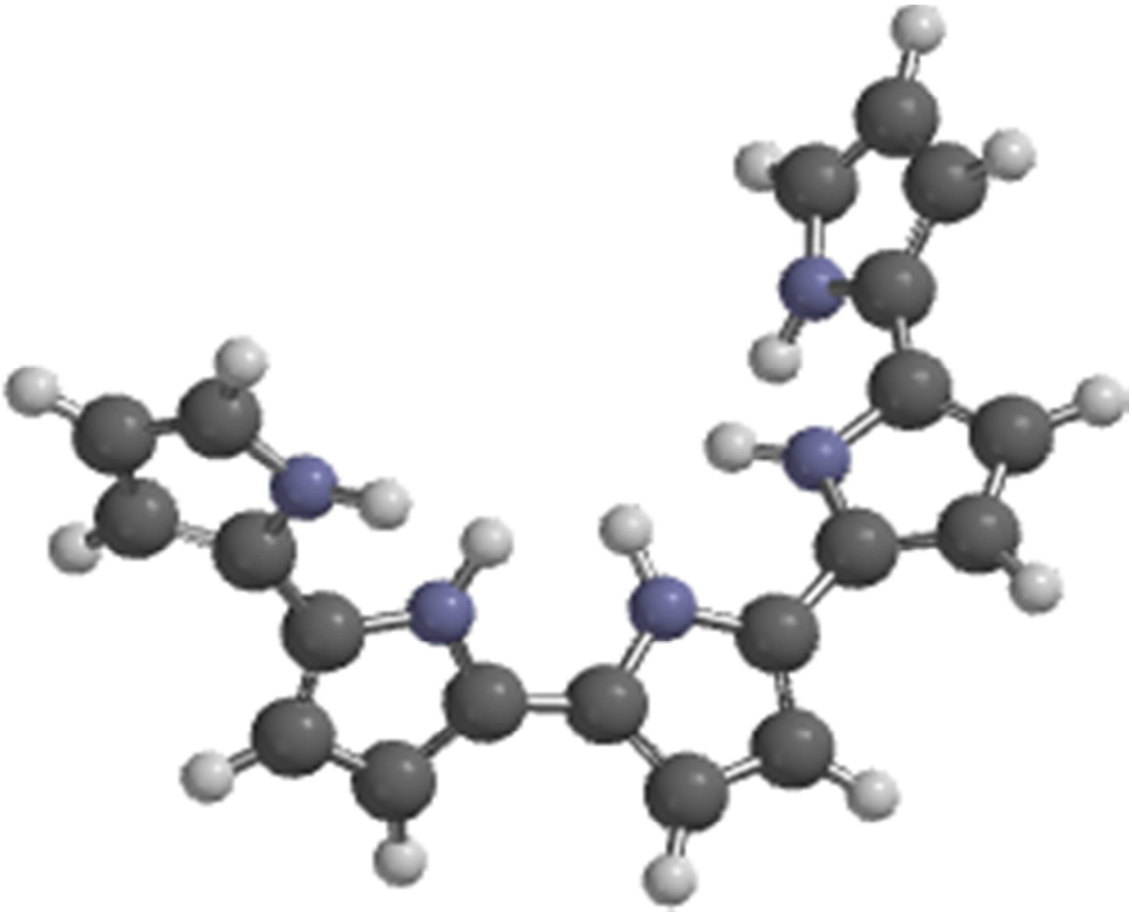

Plate 4.1. Optimized structure of pyrrole pentimer

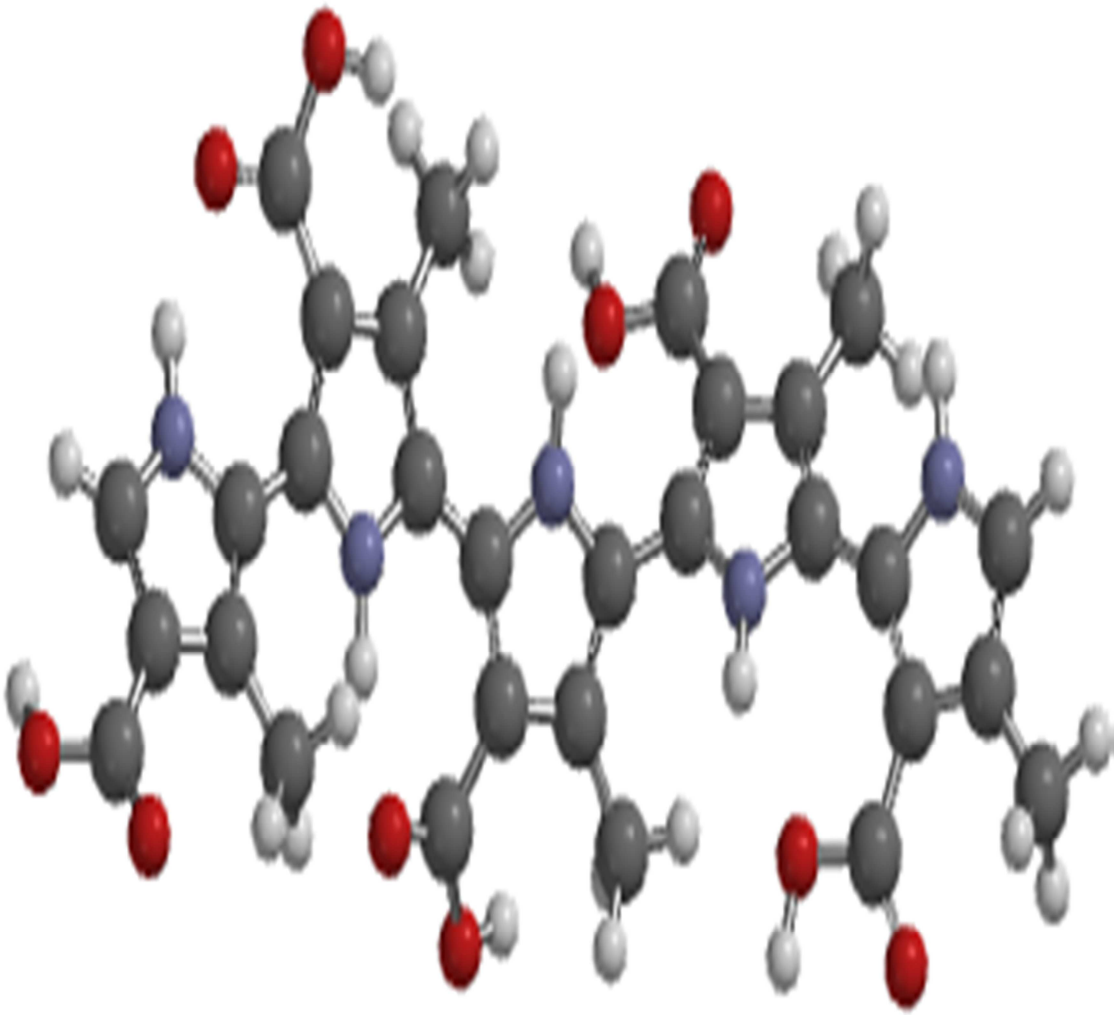

Plate 4.2. Optimized structure of MPC[a] pentimer

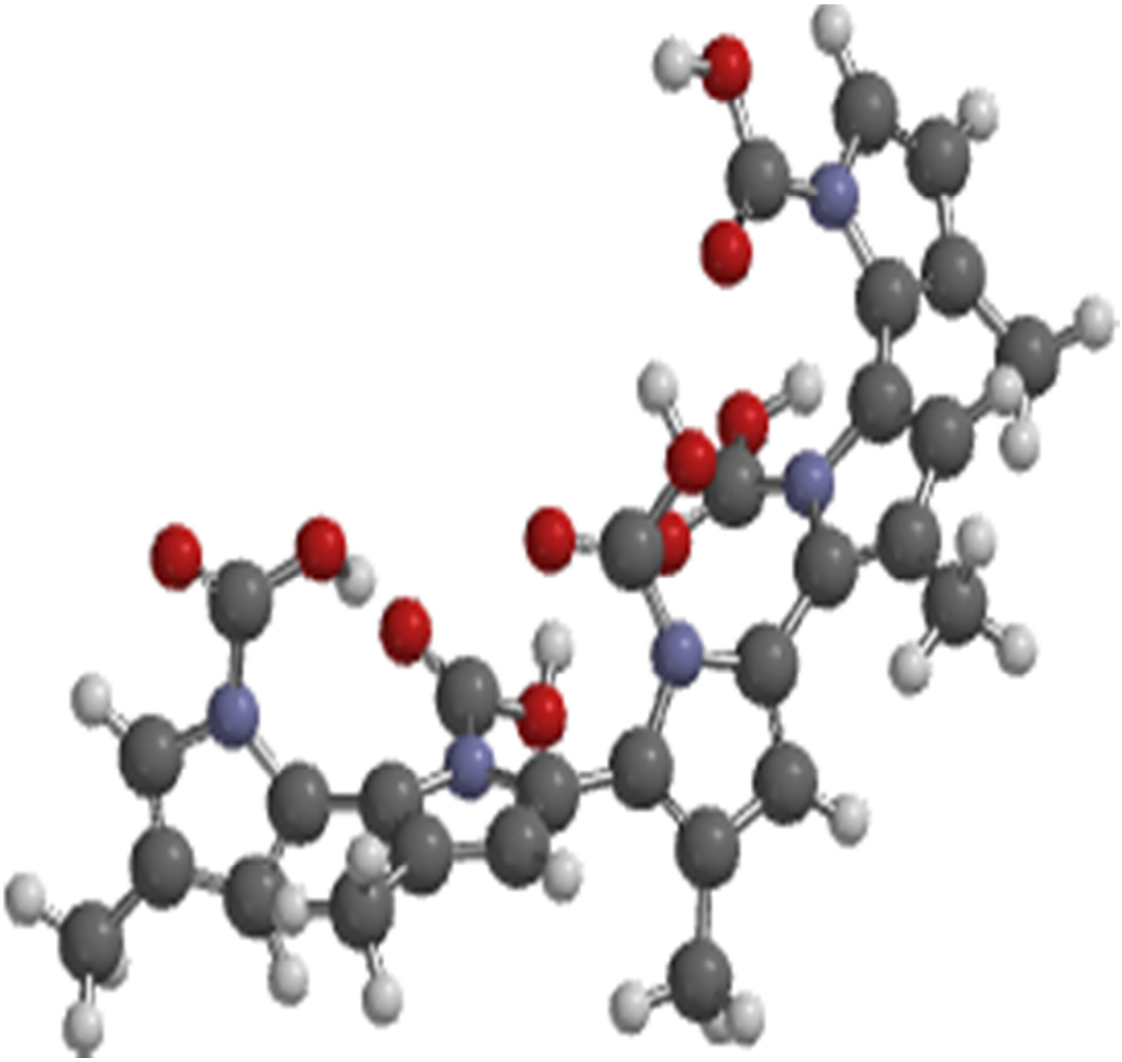

Plate 4.3. Optimized structure of MPC[b] pentimer

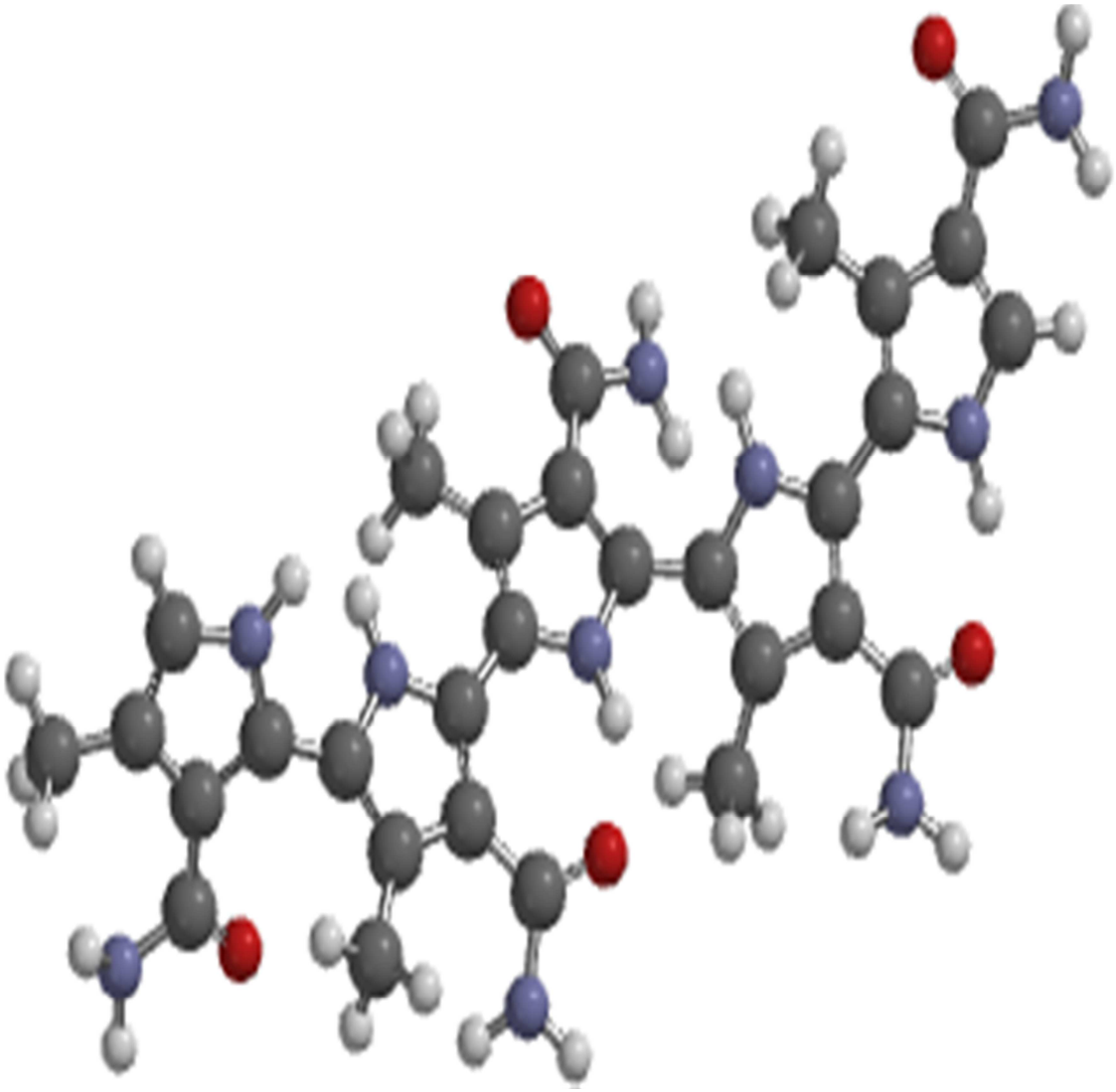

Plate 4.4. Optimized structure of MPCam pentimer

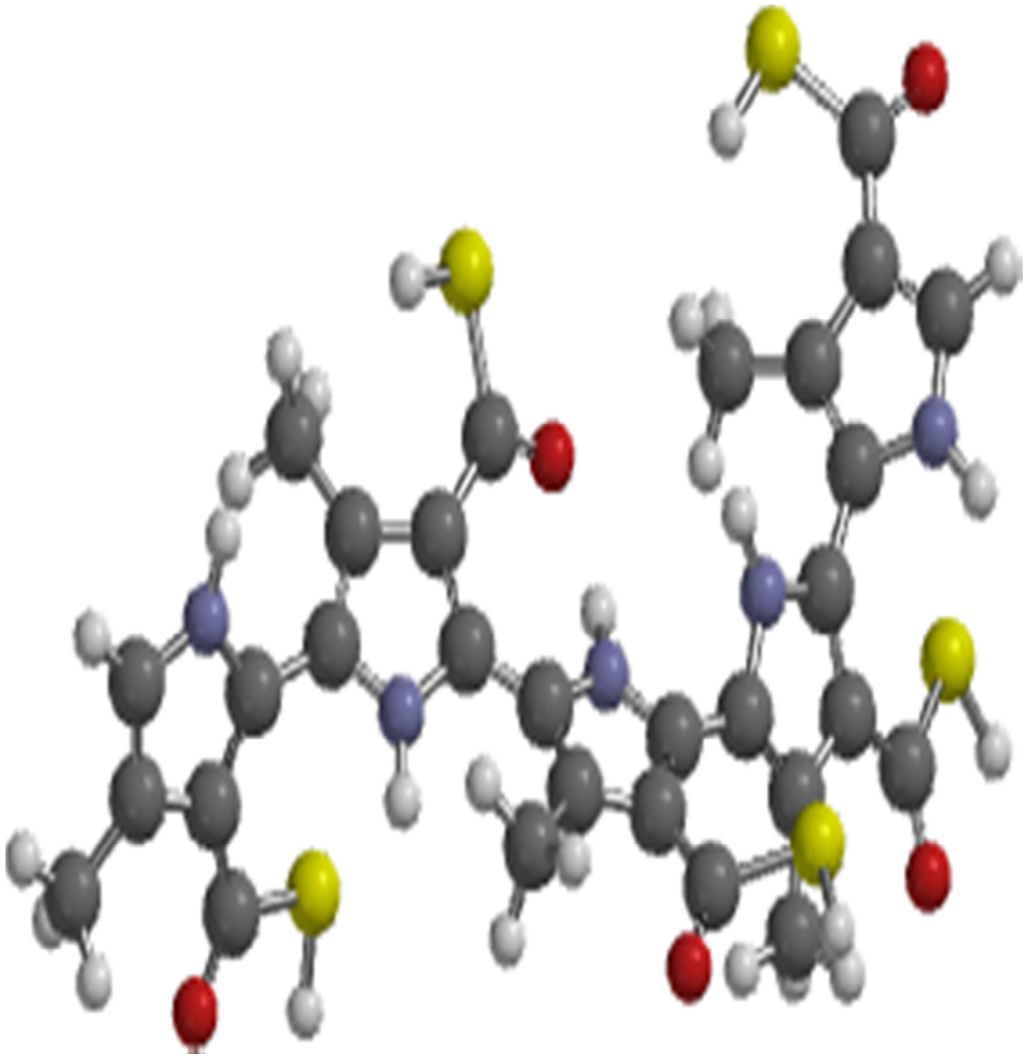

Plate 4.5. Optimized structure of MPCOSH pentimer

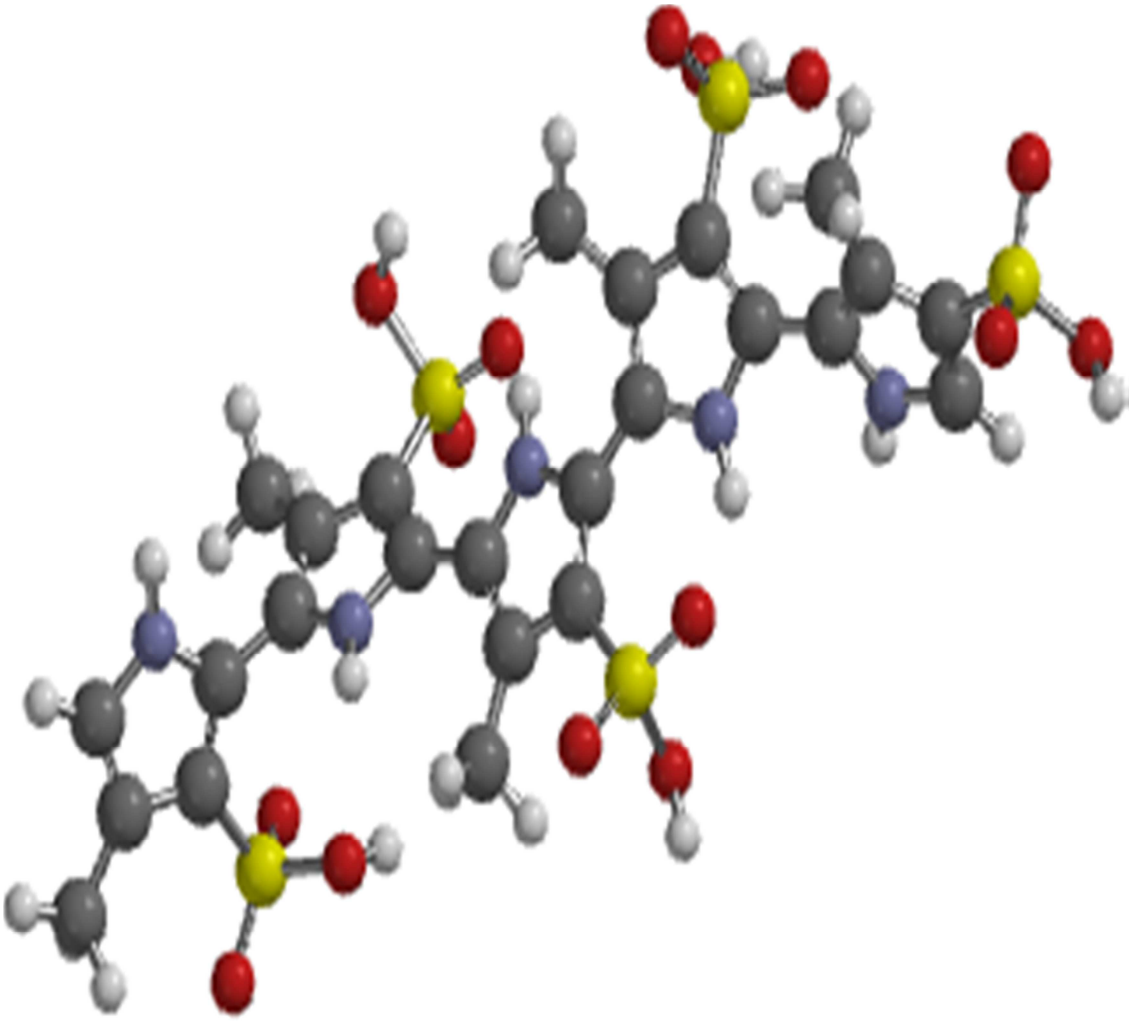

Plate 4.6. Optimized structure of $MPSO_3H$ pentimer

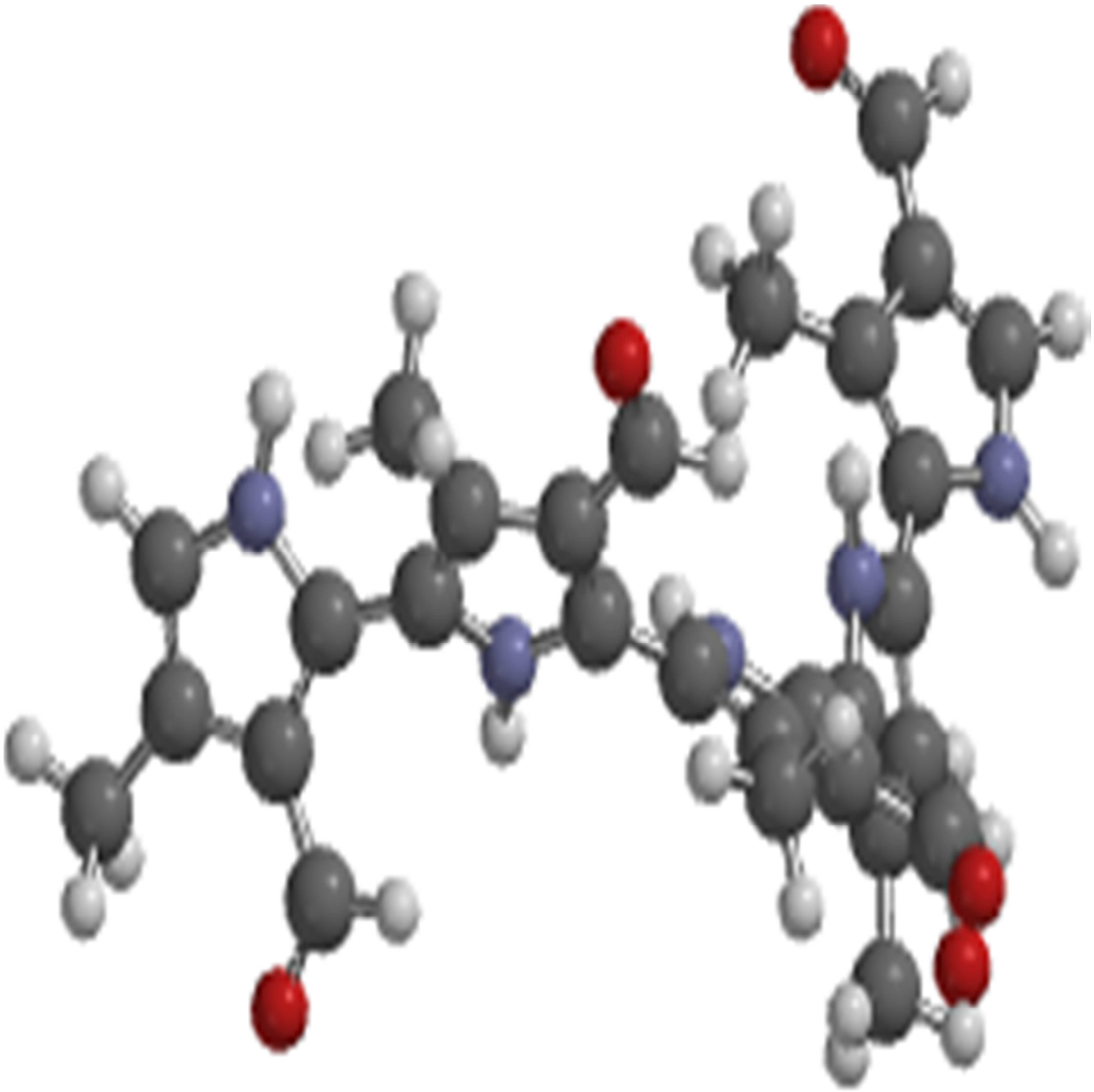

Plate 4.7. Optimized structure of MPCHO pentimer

The calculated values may be slightly different from experimental results because of the condensed phase nature of solid polymers. Several important simulated geometric parameters (bond lengths, bond angles, and dihedral angles) at B3LYP/6-31G (d) level of theory are given in Table 4.1.

4.1.1 Geometric properties of Pyrrole

The C−C bond length was found to be in the range of 1.378 to 1.425 Å, the C−H bond length was 1.082 Å, the C−N bond length was 1.375 Å and the N−H bond was 1.01 Å. The C−C−C is 107.7° (107.4°), H-N-C bonds are 125.1 ^{o} (125.1°) and those of C−N−C are 107.7 to 109.8^{o} (107.4°). The dihedral angles of C−C−N-C are in the range of 0.03 to 0.79^{o}. The calculated bond angles of pyrrole are all similar to the experimental value as seen in Table 4.1 and in Fig 4.2

The C-C bond lengths (C2-C3 bond; 1.378 Å) are closer to experimental value (1.370) (Nandeesh *et al* 2013), C3-C4 bond is about 0.007Å shorter than experimental value (I.432), C5-N1 is about 0.026Å longer than experimental value (1.349) as shown in Table 4.1 and Figure 4.1

In order to characterize the alternation of single or double carbon-carbon bonds within the two ring moieties, the Bond Length Alternation parameter (*BLA*) can be used (Jacquemin *et al*., 2007). This is defined as the average sum of absolute values of the differences between the *i*-th bond length d_i and average bond length $\bar{d}$ (Jacquemin *et al*., 2007)

N stands for the number of conjugated C—C bonds. For the Pyrrole ring, the summation in Equation above runs over the bonds N1—C2, C2—C3, C3—C4, C4—C5, C5—N1 with $N = 5$. With respect to this definition, a very small *BLA* value indicates an effective aromatic structure. As it can be seen in Table 4.2, the *BLA* value is 0.0154(Å), which is in agreement with that predicted by Rottmannováa *et al*., 2012 (0.009-0.032(Å)).

Intramolecular charge transfer (ICT) was calculated as the average of the summation of Mulliken charge distribution of studied compounds. For pyrrole, the Intramolecular charge transfer value is 0.001e.

The tortional angle calculated for pyrrole is 0° Eclipsed bonds are characterized by a torsion angle of 0° which shows that pyrrole is planar molecule due to delocalization of

the pi electrons and the nitrogen lone pair. The planarity of the chain structure is shown to be important for high conductivity in pyrrole polymers which appears to involve spinless carriers perhaps associated with bipolarons

4.1.2 Geometric properties of MPC[a]

The C−C bond length was found to be in the range of 1.375 to 1.442 Å, the C−H bond length is 1.082 Å to 1.098Å, the C−N bond length is 1.370 Å to 1.384 Å, and the N−H bond is 1.010 Å to 1.023 Å. The C−C−C is 108.6° and those of C−N−C are 107.7^{o} to 111.36^{o}. The dihedral angles of C−C−N-C are in the range of -0.17 to 0.37^{o}

Substitution of hydrogen atom in pyrrole by a methyl group at C3 (in 3-methylpyrrole) and the carboxylic group at C4 induces fairly small changes in ring inter atomic distances. The calculated C-C bond lengths of MPC are closer to the experimental value of pyrrole, but there are no experimental values for MPC

The C3-C4 bond is about 0.01Å longer than the experimental value of pyrrole (I.432) and 0.017Å longer than the calculated value. C5-N1 bond is about 0.009Å longer than experimental value (1.349) and 0.017 Å shorter than the calculated value. Substitution of hydrogen atom in pyrrole by a methyl and carboxylic group at C3 and C4 respectively lead to a slight increase in C−C−C bond angle as compared to the experimental value of pyrrole (107.4^{o}) as seen in Table 4.1 and Figure 4.1-42

In MPC[a], C3-C4 (1.442 Å) and C4-C5 (1.387Å) bond lengths are longer, and weaker than the C3-C4 and C4-C5 (1.425 and 1.378 Å respectively) bond length for pyrrole. The electron-withdrawing character of the carboxyl group and electron releasing groups methyl group affects the π-conjugation in the pyrrole ring, causing some asymmetries and changes in the strength of the adjacent bonds to the atoms in which these groups are attached and, consequently, an alteration of the bond lengths.

The Bond Length Alternation parameter (*BLA*) was also calculated to be 0.021(Å), which is slightly higher than that of pyrrole and which is in agreement with the value of pyrrole predicted by Rottmannováa *et al*., 2012. The mulliken charge distribution for modeled compound was also obtained, which gave a higher D_{CT} than pyrrole, this is due to the presence of the carboxylic group at the C-4 position.

4.1.3 Geometric properties of MPC^{b}

For MPC^{b} the C−C bond length was found to be in the range of 1.366 to 1.440 Å, the C−H bond length is 1.079 Å to 1.082Å and the C−N bond length is 1.392 Å to 1.396 Å.

The C−C−C is 107.9°, H2-N1-C3 is 119.4 and that of C−N−C is 108.8^{o}. The dihedral angles of C−C−N-C are in the range of -0.65 to 0.11^{o}

In MPC$^{\mathbf{b}}$, the carboxyl group is attached to the N atom of the pyrrole ring, the adjacent bonds N−C2 (1.392 Å) and N−C5 (1.392 Å) bond length are symmetric and their lengths are similar. However, this is because of the presence of the electron withdrawing carboxyl group, which are weaker and, consequently, longer than C2−C3 (1.369 Å) and C4−C5 (1.366 Å) bond length. A similar behaviour is observed in comparison to MPC^{a} and pyrrole, in which the N−C2 is longer than the C2-C3 and C4−C5 bond lengths. The bond angle of H2-N1-C3 calculated was observed to show a significant decrease from the experimental value of 125.1^{o} as seen in Table 4.1 and Figure 4.2

The Bond Length Alternation parameter (*BLA*) was also calculated to be 0.020(Å) which is similar to MPC^{a} and also which is slightly higher than that of pyrrole and also in agreement with the value of pyrrole predicted by Rottmannováa *et al*., (2012). The charge distribution for MPC^{b} was also obtained; this gave a similar result as MPC^{a} (0.002e). It is imperative to note that a specific pattern of charge redistribution could be an important feature of conducting and superconducting polymers.

4.1.4 Geometric properties of MPCam

The C−C bond length in MPCam**,** range from 1.378 to 1.439 Å, the C−H bond length is 1.082Å and the C−N bond length is 1.364 Å to 1.381 Å. The C−C−C is 106.4°, C−N−C is 107.8 to 109.70^{o} and that of H2-N1-C3 is 125.1°. The dihedral angles of C−C−N-C are in the range of -0.33 to -0.37^{o}

The calculated C-C bond lengths of MPCam are closer to the experimental value of pyrrole, but there are no experimental values for this compound. The C3-C4 bond is about 0.007Å longer than the experimental value of pyrrole (I.432). The C4-C5 bond is about 0.01Å shorter than experimental value for (1.397). C3-C4 (1.439 Å) and C4-C5 (1.387Å) bond lengths in MPcam are longer, and hence the bonds weaker than the corresponding

bonds in pyrrole. The substitution of hydrogen atom by an amide group at C4 ($CONH_2$) brings about a deactivation effect. When the amide group is attached to the ring through the carbonyl carbon, the partial positive charge on the carbon removes electron from the ring leading to a weakening of the bonds.

The Bond Length Alternation parameter (*BLA*) was also calculated to be 0.0198Å which is similar to that of pyrrole and also in agreement with the value obtained for pyrrole by Rottmannováa *et al*., 2012. The D_{CT} was found to be 0.003e higher than pyrrole and 0.002e than MPC^a and MPC^b (0.002e), this is due to the amide group in the at the C-4 position.

4.1.5 Geometric properties of MPCOSH

The C−C bond length was found to be in the range of 1.376 to 1.448 Å, the C−H bond length is 1.0792 Å to 1.081Å, the C−N bond length is 1.356 Å to 1.380 Å, and the N−H bond is 1.009Å. The C−C−C is 106.10° and those of C−N−C are 108.9 to 125.1. The dihedral angles of C−C−N-C are in the range of -0.38 to 0.14^o

The calculated C-C bond lengths of MPCOSH are closer to the experimental value of pyrrole, but there are no experimental values for modeled compound. The C3-C4 bonds is about 0.016Å longer than the experimental value of pyrrole (I.432) and also 0.008 Å longer than MPC^b, 0.006Å longer than MPC^a and 0.009Å longer than MPCam. The C4-C5 has a similar bond distance as do the experimental value (Fig. 4.1)

In MPCOSH, C3-C4 (1.448 Å) and C4-C5 (1.397Å) bond lengths are longer, and weaker than the C3-C4 and C4-C5 (1.425 and 1.378 Å respectively) bond length for pyrrole. This can also be attributed to be as a result of the close proximity of the electron-withdrawing, which removes electronic density from the ring.

The BLA for MPCOSH was also calculated to be 0.0234Å which is slightly higher than other modeled compound and also slightly higher than that of pyrrole and also in agreement with the value of pyrrole predicted by Rottmannováa *et al*., (2012). The D_{CT} is 0e, which is the smallest compared to other studied systems.

4.1.6 Geometric properties of $MPSO_3H$

The C−C bond length is found to be in the range of 1.376 to 1.435 Å, the C−H bond length is 1.078Å to 1.081Å, the C−N bond length is 1.364 Å to 1.380 Å, and the N−H bond is 1.009Å. The C−C−C is 106.1°, C−N−C are 106.61 to 110.13^o and that of H2-N1-C3 is 125.1. The dihedral angles of C−C−N-C are in the range of -0.08 to 0.16^o. The neighboring atoms around the 4-position are relatively close to the 4-position substituent. When the substituent is bulky, as in this case, with the methyl and the sulphonate group, the strong steric effect forces this substituent to twist out of the molecular plane of the core. All values obtained are similar to the experimental value determined by Frenkel *et al.*, (1994).

The calculated C-C bond lengths of the compound are also in the same range as that of the experimental value of pyrrole, but there are no experimental values for modeled compound. The bond length of atom C3-C4 is similar to the experimental value of pyrrole (I.432) and smaller than other modeled compounds (Fig. 4.1)

The BLA for $MPSO_3$ was also calculated to be 0.019Å which is also slightly higher than that of pyrrole and also in agreement with the value of pyrrole predicted by Rottmannováa *et al*., (2012). The D_{CT} is 0.009e, which is higher compared to other modeled compounds.

4.1.7 Geometric properties of MPCHO

The C−C bond length was found to be in the range of 1.373 to 1.442 Å, the C−H bond length is 1.081Å to 1.091Å, the C−N bond length is 1.359 Å to 1.386 Å, and the N−H bond is 1.009Å (Table 4.1). The C−C−C is 107.7°, C−N−C are 108.6^{o}and that of H2-N1-C3 is 125.0. The dihedral angles of C−C−N-C is 0°

The C-C bond lengths are also in the same range as that of the experimental value of pyrrole, but there are no experimental values for modeled compound. The bond length of atom C3-C4 is similar to the experimental value of pyrrole (I.432).

The BLA for MPCHO was also obtained to be 0.0208Å which is similar to compound A, B and D and also slightly higher than that of pyrrole and also in agreement with the value of pyrrole predicted by Rottmannováa *et al*., 2012. The D_{CT} is 0.001e, which is similar to pyrrole.

Table 4.1. Selected bond length, bond angle and dihedral of studied compounds

	Pyrrole	A	B	C	D	E	F	*Expt*
Selected Bonds (Å)								
N1-C2	1.375	1.384	1.392	1.381	1.380	1.380	1.386	
C2-C3	1.378	1.375	1.369	1.378	1.376	1.376	1.373	1.370[a]
C3-C4	1.425	1.442	1.440	1.439	1.448	1.435	1.442	1.432[a]
C4-C5	1.378	1.387	1.366	1.387	1.391	1.381	1.390	
C5-N1	1.375	1.358	1.396	1.364	1.356	1.364	1.359	1.349[a]
Selected angles								
N1-C3-C5	107.70	107.70	108.80	107.80	108.90	106.60	108.60	107.7[b]
C2-C3-C4	107.70	108.60	107.90	106.40	106.10	108.90	107.70	107.4[b]
H2-N1-C3	125.10	125.10	119.40	125.10	125.10	124.80	125.00	125.1[b]
Selected dihedral angles								
N1-C2-C3-C4	0	-0.17	-0.65	-0.37	0.14	0.16	0	
C3-C4-C5-N1	0	0.37	-0.11	-0.33	-0.38	-0.08	0	

Expt[a] (Nandeesh *et al.*, 2013), [b](Frenkel *et al.*, 1994)

Table 4.2. Calcuated BLA (δ_D), (L_B), (D_{ICT}) of studied compounds

Compounds	δ_D(Å)	L_B (Å)	D_{ICT} (e)
Pyrrole	0.015	-	0.001
A	0.021	1.457	0.002
B	0.020	1.410	0.002
C	0.019	1.478	0.004
D	0.023	1.473	0
E	0.019	1.761	0.009
F	0.021	1.458	0.001

δ_D = BLA; L_B = inter-ring bond length; D_{ICT}= intramolecular charge transfer

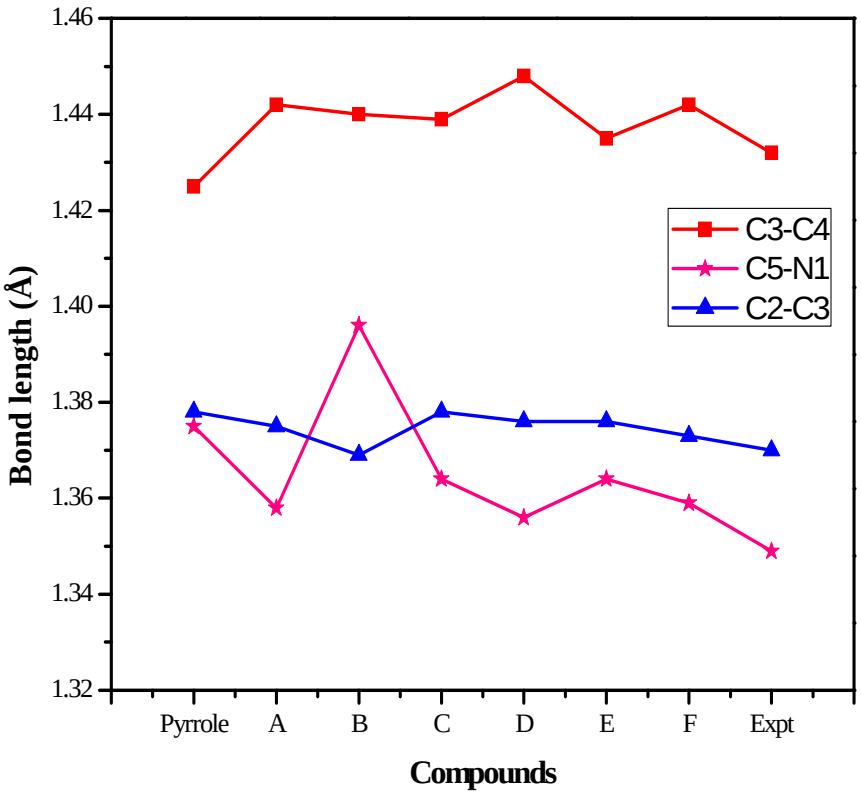

Fig. 4.1. The plot of studied compounds against bond length

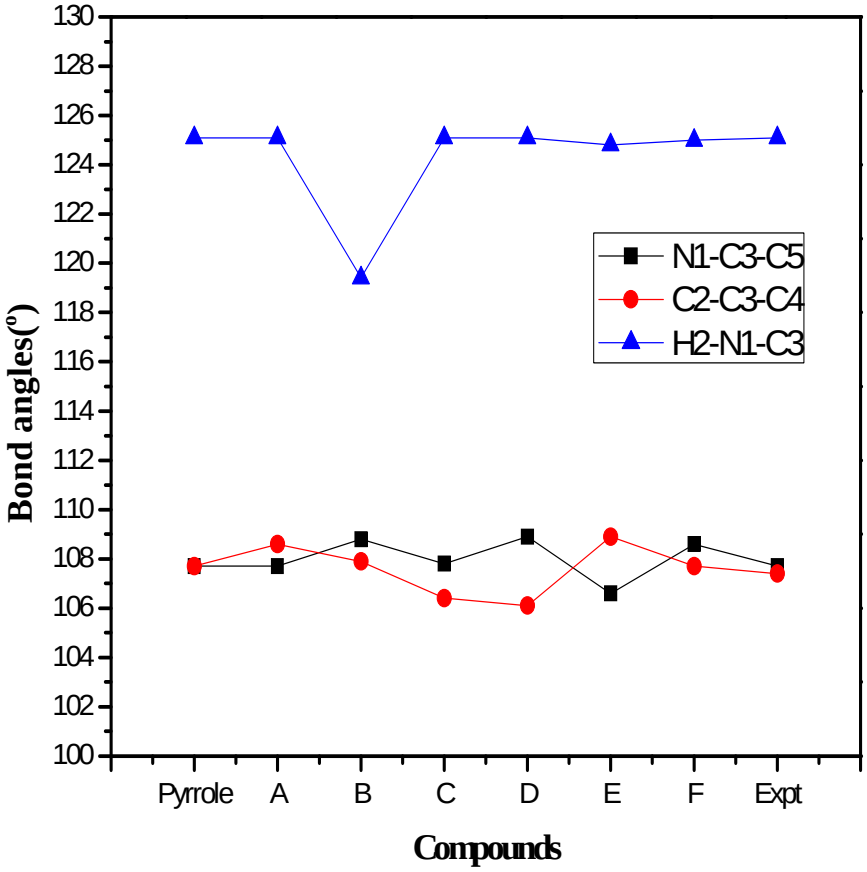

Fig. 4.2. The plot of studied compounds against bond angle

4.2 Thermodynamic property

Tables 4.3-4.10 shows the results of the standard thermodynamic functions, ZPE, total energies, entropy, free energy change, enthalpy change and specific heat capacity (Cv) of titled compounds

Table 4.3 shows the standard heat of formation (ΔH^o_f) of pyrrole and other compounds studied computationally using different methods. Standard enthalpy of formation is the change in enthalpy when one mole of a substance, in the standard state of 1 atm of pressure and temperature of 298.15 K, is formed from its pure elements under the same conditions. It can also be referred to as a measure of the energy released or consumed when one mole of a substance is formed.

Heat of formation (ΔH^o_f) is one of the most important thermochemical properties of conducting polymers because it is related directly with detonation parameters, though ΔH_f can be measured by experiments. In the past several theoretical procedures such as group additive method, molecular mechanics and semi-empirical MO methods have been used to estimate the ΔH_f of pyrrole and its derivatives. Majorly these are all parameterized methods, the results obtained strongly dependent on the parameter used. In this study, the heat of formation (ΔH^o_f), was calculated using Semi-empirical methods (MNDO, AM1, PM3 and PM6).

The other parameters were calculated using DFT at B3LYP/6-31G (d) level of theory

4.2.1 Thermodynamic properties of Pyrrole

The result obtained for pyrrole agrees reasonably with the experimental results. From the result shown in Table 4.3, the ΔH^o_f of pyrrole using PM6 is 107.70 KJ/mol which agrees with the experimental value of 108.20 KJ/mol (Frenkel *et al.,* 1994). According Dewar, and Thiel, (1977), MNDO is the oldest model that parameterized one-center two-electron integrals based on spectroscopic data for isolated atoms, and evaluates other two-electron integrals using multipole-multipole interactions from classical electrostatics. MNDO is generally not reliable in predicting heat of formation of compounds; this can be seen in Table 4.3. From the result it can be seen that PM3 and PM6 gave a better result than MNDO and AM1 when compared to the experimental value (Fig. 4.3). The ΔH^o_f obtained for pyrrole agrees with that of Guimarães *et al*., (2008) who determined the heat of formation of the monomeric form of pyrrole using AM1 as 39.80 Kcal/mol. From Table 4.3 the ΔH^o_f of pyrrole using AM1 method is 166.85 KJ/mol, which is equivalent to 39.87 Kcal/mol.

Zero-point energy (ZPE), also called quantum vacuum zero-point energy, is the lowest possible energy that a quantum mechanical physical system may have; it is the energy of its ground state. All quantum mechanical systems undergo fluctuations even in their ground state and have associated zero-point energy, a consequence of their wave-like nature. The uncertainty principle requires every physical system to have a zero-point energy greater than the minimum of its classical potential well. ZPE is also a measure of the thermodynamic stability, the more positive the ZPE, the more stable the polymer (Li and Iiao, 2009). With reference to Table 4.4, increased stability is also expected in the polymer as the number of monomer units increases (from 216.89 to 879.43 KJ/mol).

Analyzing the results of the thermodynamic function listed in Table 4.4, we see that the ΔH^o, E_0, and ΔG^o obtained using DFT and B3LYP levels are close. The negative value of ΔH^o obtained indicates that the reaction is exothermic. Since ΔG^o is negative it is also an indication that the reaction is spontaneous. For the calculated total energies E_0, there was also a progressive increase as the number of monomers increases.

Entropy (S) is a thermodynamic property which originates from the second law of thermodynamics. This property is particularly useful in determining the spontaneous

direction of a process and for establishing maximum possible efficiencies. From the result obtained in table 4.2b, the standard entropy (ΔS^o) is positive, and the entropy increases as the number of monomer also increases. The calculated entropy using DFT functional is in agreement with experimental value obtained for pyrrole as shown in table 4.4.

The specific heat capacity at constant volume (Cv) is also an important parameter and a property of a compound. From the result obtained, it can be seen that the calculated value is close to the experimental value, the calculated value is 10.92 KJ/mol more than the experimental value. As seen in other parameters, there is also an increase in the heat capacity as the number of monomers increase.

Enthalpy (ΔH^o) is the thermodynamic function that accounts for heat flow in a system. Thermodynamic stability is expected when ΔH is negative, and the more negative the value of ΔH, the more stable the compound (Li and Iiao, 2009). The value obtained range from -210.8 to -1045.73kJ/mol. As seen in Table 4.4, there is an increase in ΔH^o as the number of rings is increased

Table 4.3. The heat of formation (ΔH_f) at 298.15K using different semi-empirical methods

No of monomer	Compounds	MNDO	AM1	PM3	PM6	*Expt*
	Pyrrole	135.78	166.85	113.40	107.70	108.20
1	A	-289.50	-252.30	-309.00	-316.4	
	B	-249.70	172.80	-277.08	-263.87	
	C	-78.20	-32.10	-76.00	-120.8	
	D	119.95	27.06	-35.19	-87.02	
	E	-6.15	393.80	445.70	-477.30	
	F	-51.07	-3.96	-72.99	-56.13	
2	A	-570.30	-453.80	-620.21	-599.10	
	B	-500.50	-317.10	-542.70	-531.20	
	C	-160.80	-58.92	-75.20	-342.00	
	D	239.70	66.71	-80.80	-192.10	
	E	149.88	-791.50	-888.80	-975.80	
	F	-105.60	-8.77	-146.40	-124.44	
	A	-857.60	-672	-928.70	-903.80	
3	B	-743.90	-465.1	-806.60	-803.00	
	C	-239.60	-88.82	-250.50	-405.41	
	D	353.80	94.98	-124.60	-306.60	
	E	174.09	-1172.54	-1344.28	-1488.50	
	F	-162.01	22.27	-218.19	-190.33	
	A	-1152.66	-912.15	-1232.12	-1235.05	
4	B	-987.56	-612.92	-1071.16	-1073.22	
	C	-327.76	-144.76	-359.44	-578.39	
	D	476.06	146.67	-159.24	-386.79	
	E	0.73	-1563.30	-1786.86	-1996.43	
	F	-217.14	36.07	-289.27	-255.85	
	A	-1446.56	-1179.13	-1553.96	-1593.16	
5	B	-1238.77	-774.65	-1347.51	1359.94	
	C	-406.61	-146.04	-448.9	-689.90	
	D	526.09	189.87	-202.42	-522.21	
	E	-112.56	-1956.81	-2224.27	-2467.55	
	F	-283.81	43.24	361.25	-320.88	

*Exp*t (Frenkel *et al.*, 1994)

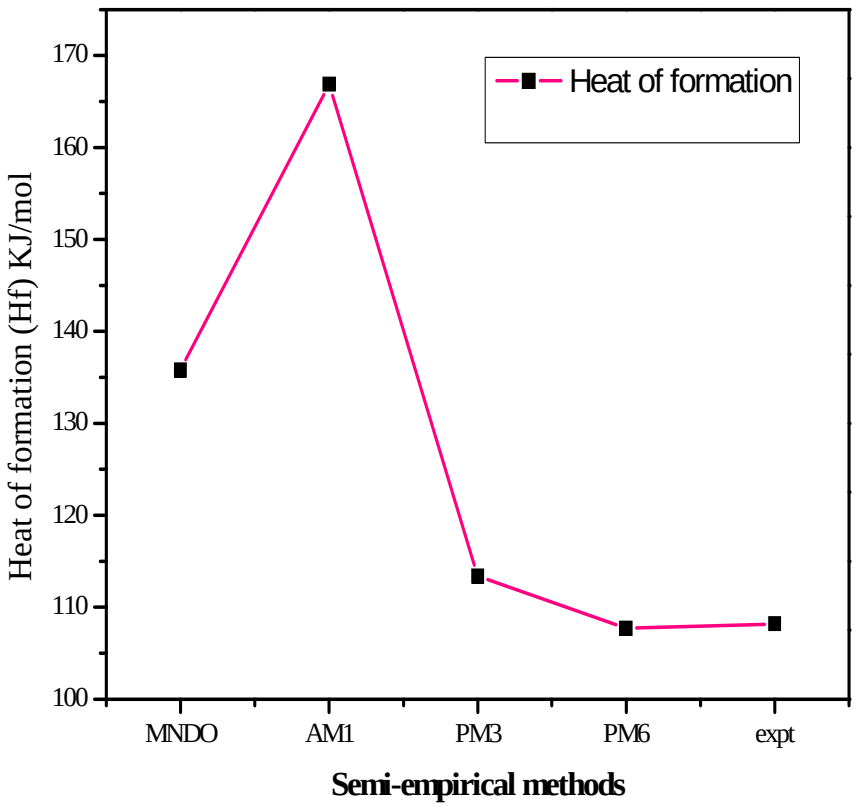

Fig. 4.3. The heat of formation (ΔH_f) of studied polymers using different semi-empirical methods compared with the experimental value

Table 4.4. Thermodynamics properties of Pyrrole

No. of Monmers	E_0 (kJ/mol)	ΔH^o_f (kJ/mol)	ZPE (kJ/mol)	ΔS^o_f ($Jmol^{-1}K^{-1}$)	ΔG^o_f (kJ/mol)	C_v (J/mol)
1	-210.17	-210.08	216.89	270.52	-210.11	60.68
2	-419.15	-418.99	383.33	346.37	-419.03	111.02
3	-628.13	-627.91	548.54	418.70	-627.95	161.45
4	-837.11	-836.82	714.48	480.49	-836.87	211.44
5	-1046.10	-1045.73	879.43	540.34	-1045.79	261.69
Expt				270.72		71.60

*Exp*t (Frenkel *et al.*, 1994)

4.2.2 Thermodynamic properties of MPC^a

The heat of formation ΔH^o_f of MPC^a using PM6 is -316.40 kJ/mol, the negative value obtained indicates an exothermic reaction as compared to 107.70 kJ/mol of pyrrole which is a positive value. Substitution of hydrogen atom in pyrrole by a methyl group at C3 (in 3-methylpyrrole) causes changes in the ring, leading to the negative value observed in the product (MPC^a). The ΔH^o_f obtained for MPC^a using AM1 (-60.20 kcal/mol) also agrees with the results of Guimarães *et al*., 2008 (-60.80 kcal/mol). The heat of formation per ring increases as the number of rings increases (Table 4.3) indicating that there is an effective electronic stabilization as expected from the pi electron character of these structures.

The calculated ZPE values for MPC^a range from 328.80 kJ/mol to 1451.20 kJ/mol as the number of ring increases as shown in Table 4.5. This value is higher than the calculated ZPE of pyrrole (216.9 kJ/mol), therefore a higher thermodynamic stability than pyrrole.

The total energy (E_0), enthalpy change (ΔH^o_f), entropy change (ΔS^o_f) and free energy change (ΔG^o_f) using DFT method, have closely related values as shown in Table 4.5. E_0 values range from -435.60 kJ/mol to -2185.60 kJ/mol (monomer to pentimer) as seen in Table 4.5. The values of ΔS^o (Table 4.5) also increases positively as the number of ring is increased as also seen in pyrrole.

The Cv of MPC^a from monomer to pentimer is 128.8(J/mol) to 663.7(J/mol) respectively as shown in Table 4.5. The Cv value obtained for MPC^a is more than the Cv value for pyrrole and also higher than the experimental value this is due to the presence of electron withdrawing carboxylic group in the structure of MPC^a.

The enthalpy change for poly-MPC^a range from -435.50 to -2184.90 kJ/mol as the number of ring is increased as shown in Table 4.5 and Fig. 4.4. Thermodynamic stability is expected when ΔH^o_f is negative, and the more negative the value of ΔH^o_f, the more stable the polymer (Li and Iiao, 2009). MPC^a is more stable thermodynamically than polypyrrole since it has a more negative ΔH^o_f value. The ΔG^o_f of MPC^a was found to be -435.50 kJ/mol which also decreases from as the number of ring increases. This is lower than that of pyrrole (210.11 kJ/mol). This increase is due to the substitution of hydrogen atom by an electron withdrawing carboxylic group at the C-4 position and methyl group at the C-3

position. This also implies that the polymer-protein formation and binding effect in poly-MPC will be more spontaneous compared to that in polypyrrole. About 107% increase in the thermal stability was also observed between polypyrrole and poly MPC^a.

4.2.3 Thermodynamic properties of MPC^b

The heat of formation ΔH^o_f of MPC^b using PM6 was observed to be -263.80 kJ/mol and higher than the ΔH^o_f of MPC^a, as shown in Table 4.3. The negative value obtained indicates an exothermic reaction as compared to 107.70 kJ/mol for pyrrole. This difference observed will be due to the presence of an electron withdrawing group at N atom carrying the lone pair of electron. This result is also comparable to earlier findings of Guimarães *et al*., (2008). The heat of formation per ring also increases as the number of rings increases (Table 4.6 and Fig 4.11) indicating also an effective electronic stabilization.

ZPE values for poly-MPC^b range from 328.40 kJ/mol to 1439.40 kJ/mol as the number of ring increases as shown in Table 4.6. The result obtained is higher than the calculated value for pyrrole (216.90 kJ/mol), and similar to that of MPC^a, therefore a similar thermodynamic stability is expected for both compounds.

Based on DFT methods, the total energy (E_0), enthalpy change (ΔH^o_f), entropy change (ΔS^o_f) and free energy change (ΔG^o_f) also have closely related values as shown in Table 4.5. E_0 values range from -438.10 kJ/mol to -2185.00 kJ/mol (monomer to pentimer) as seen in Table 4.6. The ΔG^o_f of MPC^a was found to be -438.00 kJ/mol which also increases as the number of ring is increased.

The C_v for MPC^b from monomer to pentimer is 127.90 J/mol to 659.50 J/mol respectively as shown in Table 4.6.

The enthalpy change for MPC^b range from -437.5 to -2184.90 kJ/mol as the number of ring is increased as shown in Table 4.6 and Fig. 4.5. The difference in stability was between pyrrole and MPC^b was 108%.

Table 4.5. Thermodynamics properties of MPC[a]

No. of Monomers	E_0 (kJ/mol)	ΔH^o_f (kJ/mol)	ZPE (kJ/mol)	ΔS^o_f ($Jmol^{-1}K^{-1}$)	ΔG^o_f (kJ/mol)	C_v (J/mol)
1	-435.59	-435.45	328.80	357.92	-435.49	128.83
2	-874.92	-874.67	608.70	490.31	-874.733	266.18
3	-1311.79	-1311.42	887.80	610.70	-1311.49	402.15
4	-1748.67	-1748.19	1168.10	723.13	-1748.27	535.73
5	-2185.56	-2184.96	1451.20	826.57	-2185.06	663.68

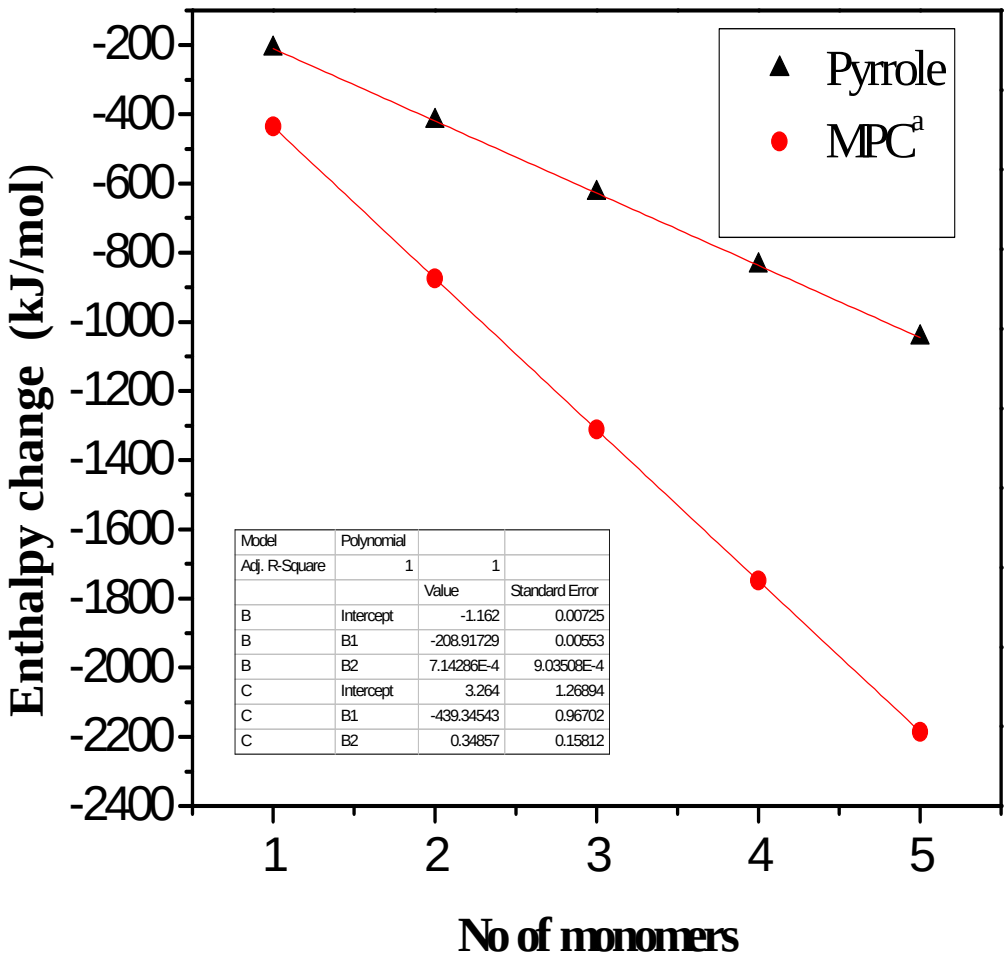

Model	Polynomial		
Adj. R-Square	1	1	
		Value	Standard Error
B	Intercept	-1.162	0.00725
B	B1	-208.91729	0.00553
B	B2	7.14286E-4	9.03508E-4
C	Intercept	3.264	1.26894
C	B1	-439.34543	0.96702
C	B2	0.34857	0.15812

Fig. 4.4. Simulated Enthalpies of Pyrrole and MPC[a] as a function of the number of monomer unit

Table 4.6. Thermodynamics properties of MPC[b]

No. of Monomers	E_0 (kJ/mol)	ΔH^o_f (kJ/mol)	ZPE (kJ/mol)	ΔS^o_f ($Jmol^{-1}K^{-1}$)	ΔG^o_f (kJ/mol)	C_v (J/mol)
1	-438.04	-437.92	328.39	356.77	-437.96	127.91
2	-874.90	-874.67	606.68	483.82	-874.72	261.60
3	-1311.80	-1311.42	884.15	600.53	-1311.50	395.56
4	-1748.70	-1748.17	1160.96	712.37	-1748.30	526.81
5	-2185.50	-2184.93	1439.38	822.03	-2185.00	659.47

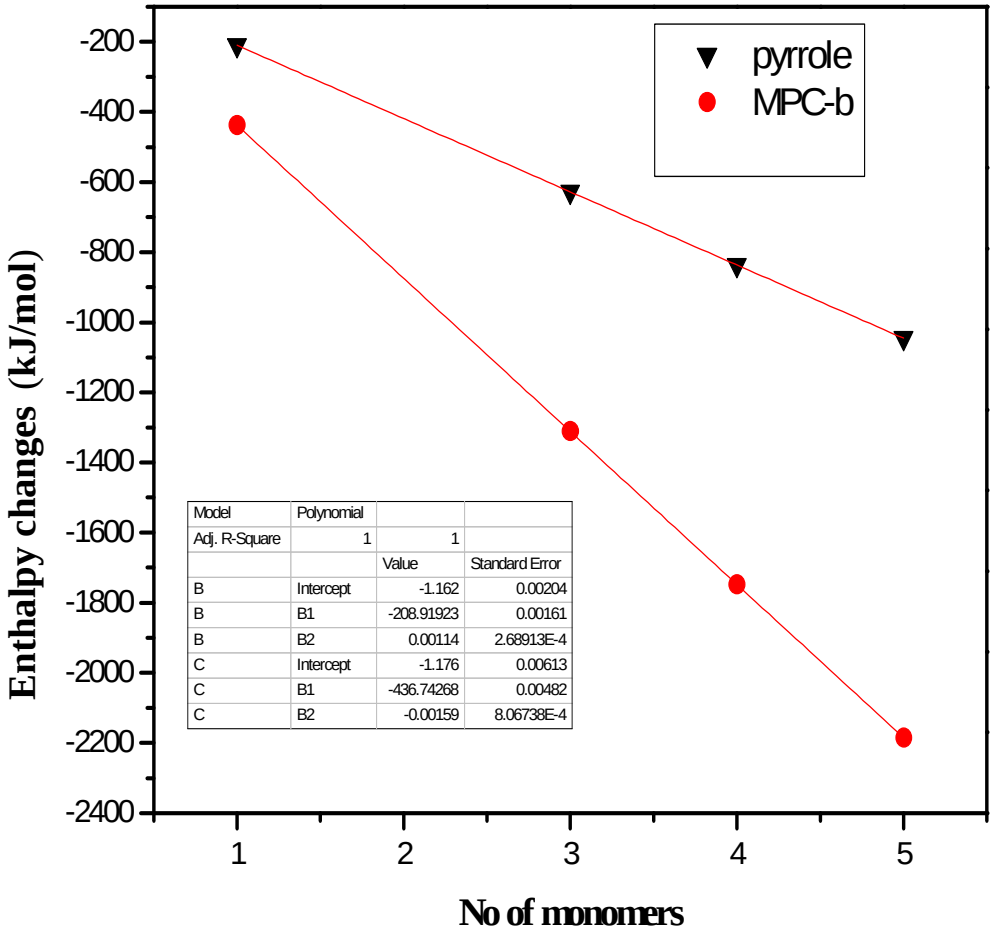

Fig. 4.5. Simulated Enthalpies of Pyrrole and MPC^{b} as a function of the number of monomer unit

4.2.4 Thermodynamic properties of MPCam

The heats of formations ΔH^o_f of MPCam using different semi-empirical methods are presented in Table 4.3. Result shows that ΔH^o_f of this substituted pyrrole is lower than the ΔH^o_f of pyrrole, and higher than that of MPC^a and MPC^b as shown in Table 4.3. The negative value obtained indicates an exothermic reaction and as well as a spontaneous process as compared to 107.70 kJ/mol of pyrrole which gave positive value. This change attributed to the proximity of the amide group attached to the ring, which removes electronic density from the ring.

The result shown in Table 4.7 reveals a higher ZPE values for MPCam as compared to MPC^a and MPC^b. This change is due to the presence of an amine group in the carbonyl atom, when a hydrogen atom is substituted in the pyrrole ring which withdraws electron from the ring.

The result based on DFT shown in Table 4.7 indicated that the total energy ($E_{0)}$, enthalpy change (ΔH^o_f), entropy change (ΔS^o_f) and free energy change (ΔG^o_f) are closely related and have higher values than MPC^a and MPC^b. E_0 values range from -418.20 to -2086.00 kJ/mol (monomer to pentimer) as seen in Table 4.7. The ΔG^o_f values was found to be in the range -418.10 to -2085.70 kJ/mol which also increases as the number of ring is increased. These results obtained show a spontaneous process for the formation of MPCam.

The specific heat capacity at constant volume (Cv) for MPCam from monomer to pentimer is 135.71 J/mol to 696.50 J/mol respectively as shown in Table 4.7.

The ΔH^o_f obtained for MPCam range from -418.00 to -2085.60 kJ/mol as the number of ring is increased as shown in Table 4.7 and in Fig. 4.6. A significant difference in stability was also observed between pyrrole and MPCam. MPCam shows a lower percentage as compared to MPC^a and MPC^b. Since thermodynamic stability is expected when ΔH^o_f is negative, and the more negative the value of ΔH, the more stable the compound (Li and jiao, 2009) From this features, MPCam will show a lower thermodynamic stability than MPC^a and MPC^b but higher compared to pyrrole. There are no experimental data for the studied systems.

Table 4.7. Thermodynamic properties of MPCam

No. of monomers	E_0 (kJ/mol)	ΔH^o_f (kJ/mol)	ZPE (kJ/mol)	ΔS^o_f ($Jmol^{-1}K^{-1}$)	ΔG^o_f (kJ/mol)	C_v (J/mol)
1	-418.19	-418.04	362.86	362.24	-418.08	135.71
2	-835.20	-834.93	676.36	493.76	-834.98	274.47
3	-1252.21	-1251.81	987.09	620.16	-1251.88	418.16
4	-1669.23	-1668.70	1301.49	730.91	-1668.79	554.42
5	-2086.23	-2085.58	1613.87	845.11	-2085.68	696.50

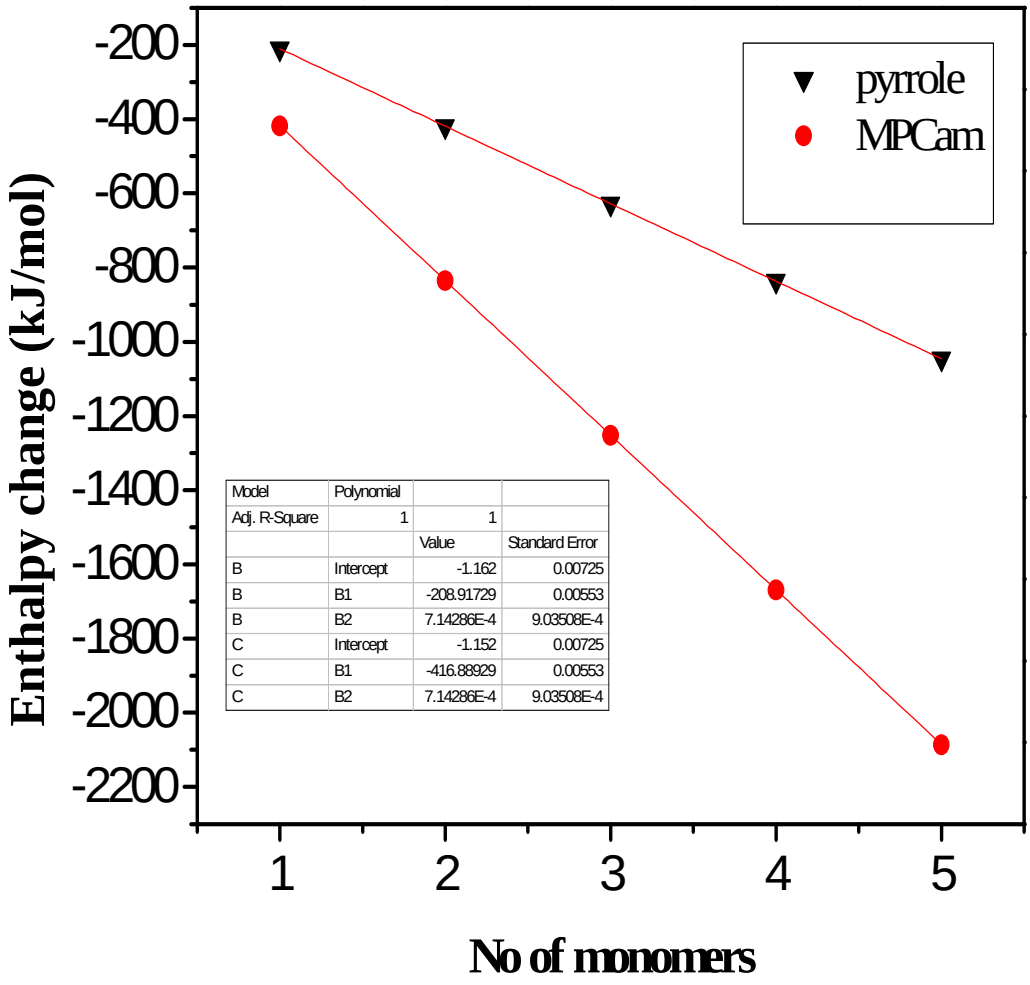

Model	Polynomial		
Adj. R-Square	1	1	
		Value	Standard Error
B	Intercept	-1.162	0.00725
B	B1	-208.91729	0.00553
B	B2	7.14286E-4	9.03508E-4
C	Intercept	-1.152	0.00725
C	B1	-416.88929	0.00553
C	B2	7.14286E-4	9.03508E-4

Fig. 4.6. Simulated Enthalpies of Pyrrole and MPCam as a function of the number of monomer unit

4.2.5 Thermodynamic properties of MPCOSH

The results for the heats of formations ΔH^o_f of MPCOSH using different semi-empirical methods are presented in Table 4.3. Result shows that ΔH^o_f of this substituted pyrrole is also lower than the ΔH^o_f of pyrrole, and higher than that of MPC^a, MPC^b, as shown in Table 4.3. The negative value obtained also indicates an exothermic process as compared to 107.70 kJ/mol of pyrrole.

ZPE values for MPCOSH as shown in Table 4.8, is lower when compared to MPC^a, $MPC^b$and MPCam This change is due to the fact that –SH group is a moderate electron withdrawing group and therefore an increased inductive effect is observed toward the positive end. (+I effect).

The result shown in Table 4.8 using DFT indicated that the total energy ($E_{0)}$, enthalpy change (ΔH^o_f), entropy change (ΔS^o_f) and free energy change (ΔG^o_f) are closely related and have higher negative values than MPC^a, MPC^b and MPCam. E_0 values range from -761.00 to -3800.3 kJ/mol (monomer to pentimer) as seen in Table 4. The ΔG^o_f values were found to be in the range -760.90 to -3799.90 kJ/mol which also decreases as the number of ring is increased. These results obtained shows that a spontaneous process will occur between the polymer and protein molecule.

The specific heat capacity at constant volume (Cv) for MPCOSH from monomer to pentimer is 137.30 J/mol to 711.80 J/mol respectively as shown in Table 4.8.

Result presented in Table 4.8 and Fig. 4.7 using DFT shows ΔH^o_f obtained for MPCOSH also increases as the number of ring is increased. A significant difference was observed between pyrrole and MPCOSH of about 262% in thermal stability. MPCOSH shows a higher percentage as compared to MPC^a, MPC^b and MPCam. From this features, MPCOSH is more thermodynamically stable than MPC^a, MPC^b, MPCam and pyrrole. This change attributed to the proximity of the thiol group attached to the ring, which removes electronic density from the ring, thereby deactivating the ring making it electron deficient. There are no experimental data for the studied systems.

Table 4.8. Thermodynamic properties of MPCOSH

No. of Monomers	E_0 (kJ/mol)	ΔH^o_f (kJ/mol)	ZPE (kJ/mol)	ΔS^o_f ($Jmol^{-1}K^{-1}$)	ΔG^o_f (kJ/mol)	C_v (J/mol)
1	-761.01	-760.88	316.08	371.17	-760.92	137.29
2	-1520.83	-1520.59	582.01	507.35	-1520.65	280.40
3	-2280.66	-2280.31	845.98	636.76	-2280.39	425.22
4	-3040.49	-3040.03	1111.90	756.14	-3040.12	566.44
5	-3800.31	-3799.75	1376.37	877.88	-3799.85	711.77

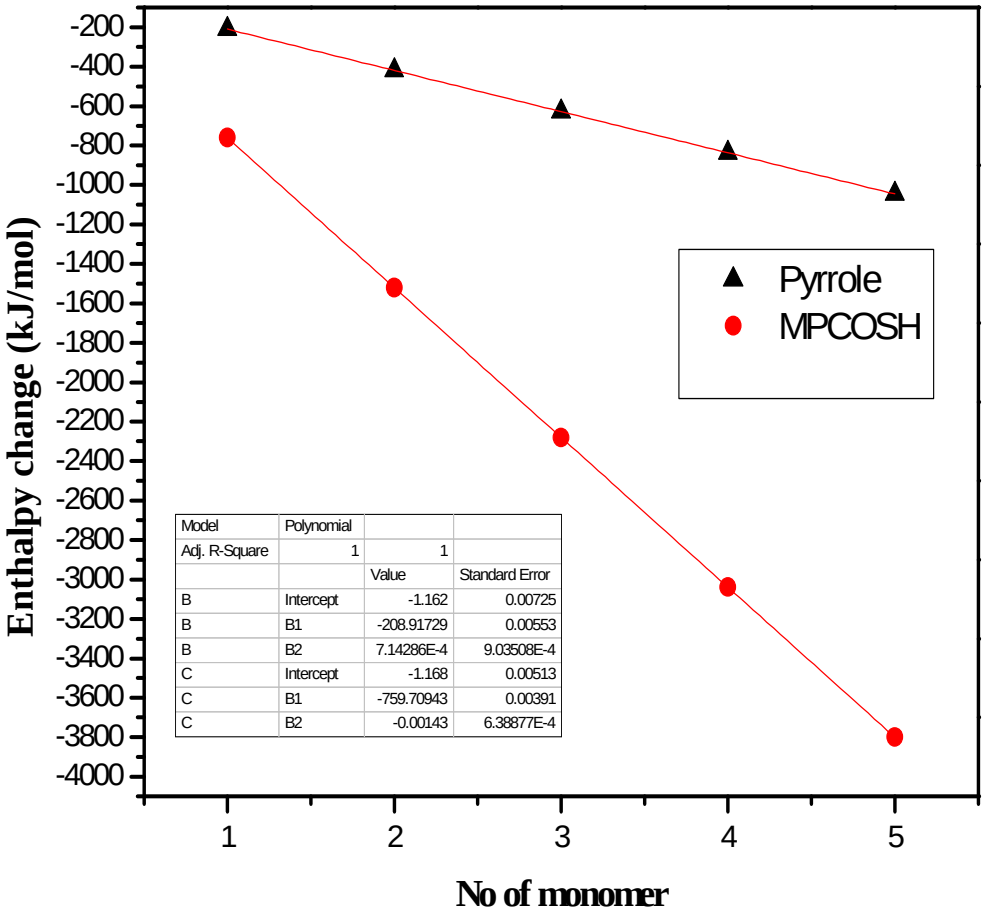

Model	Polynomial		
Adj. R-Square	1	1	
		Value	Standard Error
B	Intercept	-1.162	0.00725
B	B1	-208.91729	0.00553
B	B2	7.14286E-4	9.03508E-4
C	Intercept	-1.168	0.00513
C	B1	-759.70943	0.00391
C	B2	-0.00143	6.38877E-4

Fig. 4.7. Simulated Enthalpies of Pyrrole and MPCOSH as a function of the number of monomer unit

4.2.6 Thermodynamic properties of $MPSO_3H$

The heats of formations ΔH^o_f of $MPSO_3H$ using different semi-empirical methods are presented in Table 4.3. This shows that ΔH^o_f of $MPSO_3H$ is -477.30 kJ/mol and it is also lower than the ΔH^o_f of pyrrole, and more negative than that of MPC^a, MPC^b, MPCam and MPCOSH as shown in Table 4.3. The higher negative value obtained indicates a more exothermic and spontaneous process as compared to 107.70 kJ/mol of pyrrole. This is because SO_3H is a functional group that removes electron density from a conjugated π system via resonance effect, thus making the π system more electrophilic.

The calculated ZPE values for $MPSO_3H$ obtained from this work as shown in Table 4.9, are lower than the ZPE of MPCam, but have a closely related value to that of MPC^a, MPC^b. This is also due to the fact that sulfonate (SO_3H) groups are moderately electron withdrawing groups as compared to amide groups, therefore a more resonance effect is observed.

The result shown in Table 4.9 using DFT also indicated that the total energy ($E_{0)}$, entropy change (ΔS^o_f), enthalpy change (ΔH^o_f), entropy change (ΔS^o_f) and free energy change (ΔG^o_f) are closely related and have more negative values than MPC^a, MPC^b, MPCam and MPCOSH.

The specific heat capacity at constant volume (Cv) for $MPSO_3H$ as shown in Table 4.9 from monomer to pentimer is 153.80 J/mol to 794.30 J/mol respectively

The ΔH^o_f obtained for $MPSO_3H$ as shown in Table 4.9 and in Fig. 4.8, ranged from -418.00 to -2085.60 kJ/mol as the number of ring is increased and. A 316% significant difference was also observed between pyrrole and $MPSO_3H$, this difference in stability shows that $MPSO_3H$ has the highest percentage when compared to other studied systems. These features, indicates that $MPSO_3H$ is more thermodynamically stable than other studied systems. There are no experimental data for the studied systems.

Table 4.9. Thermodynamic properties of $MPSO_3H$

No. of Monomers	E_0 (kJ/mol)	ΔH^o_f (kJ/mol)	ZPE (kJ/mol)	ΔS^o_f ($Jmol^{-1}K^{-1}$)	ΔG^o_f (kJ/mol)	C_v (J/mol)
1	-873.28	-873.14	329.04	386.64	-873.19	153.77
2	-1745.37	-1745.12	607.11	539.96	-1745.20	313.20
3	-2617.48	-2617.11	886.46	679.43	-2617.20	471.34
4	-3489.56	-3489.08	1162.48	817.42	-3489.20	633.01
5	-4361.65	-4361.05	1439.72	952.21	-4361.20	794.30

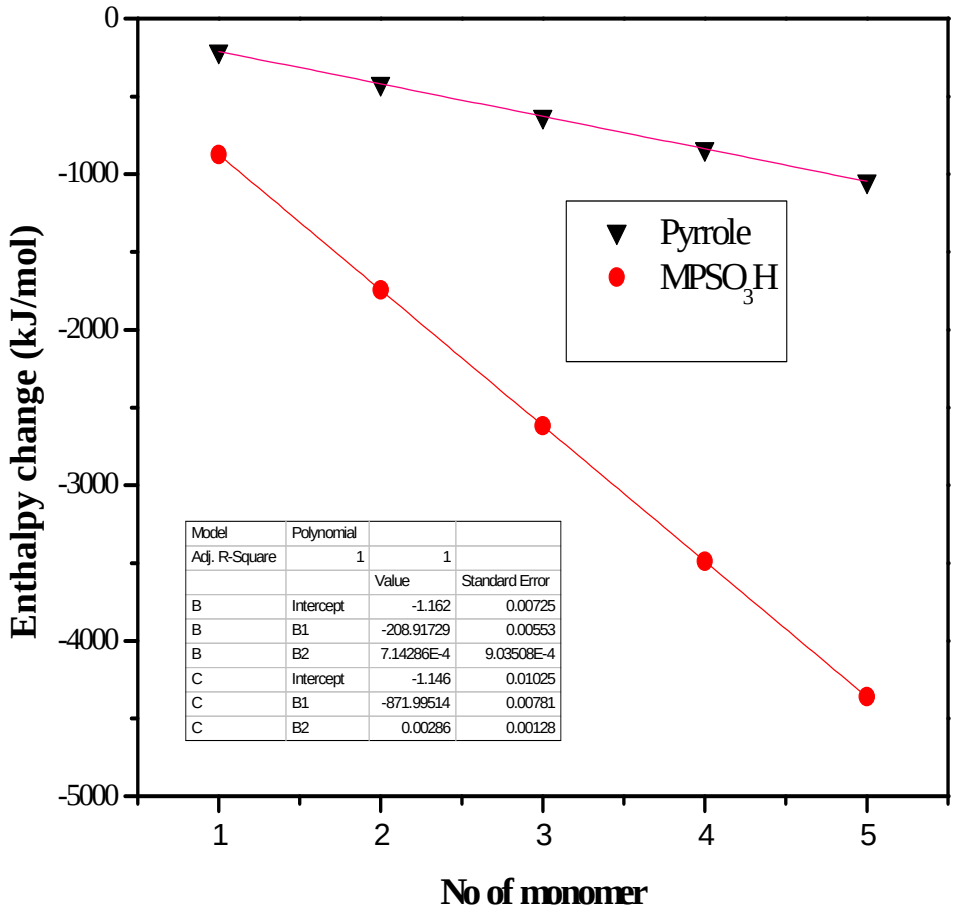

Fig 4.8. Simulated Enthalpies of Pyrrole and $MPSO_3H$ as a function of the number of monomer unit

4.2.7 Thermodynamic properties of MPCHO

Calculated heats of formations ΔH^o_f of MPCHO using different semi-empirical methods are presented in Table 4.3. This shows that ΔH^o_f of $MPSO_3H$ is -56.13 kJ/mol (PM6) and it is also lower than the ΔH^o_f of pyrrole, and less negative than that of MPC^a, MPC^b, MPCam and MPCOSH as shown in Table 4.3. The negative value obtained indicates a more exothermic and spontaneous process as compared to 107.70 kJ/mol of pyrrole.

The ZPE values for MPCHO are presented in Table 4.10. Results show that the ZPE are lower than that of MPC^a, MPC^b, MPCam and MPCOSH, but have a closely related value to that of MPCOSH. This is also due to the fact that CHO groups are moderately electron withdrawing groups as compared to amide groups, therefore a more resonance effect is observed and the atom that is attached to the molecule is involved in a multiple bond.

The result shown in Table 4.10 using DFT also indicated that the total energy ($E_{0)}$, enthalpy change (ΔH^o_f), entropy change (ΔS^o_f) and free energy change (ΔG^o_f) are closely related and have lesser negative values than MPC^a, MPC^b, MPCam and MPCOSH.

The specific heat capacity at constant volume (Cv) as shown in Table 4.9 from monomer to pentimer is 113.80 J/mol to 600.10 J/mol respectively

The enthalpy (ΔH^o_f) obtained are presented in Table 4.10 and in Fig. 4.9, ranged from -362.70 to -1808.70 kJ/mol as the number of ring is increased and. Analysis of the result shows a difference of 72.6% stability between pyrrole and MPCHO. These shows that MPCHO has the lowest percentage difference when compared to other studied systems.

Table 4.10. Thermodynamic properties of MPCHO

No. of Monomers	E_0 (kJ/mol)	ΔH^o_f (kJ/mol)	ZPE (kJ/mol)	ΔS^o_f ($Jmol^{-1}K^{-1}$)	ΔG^o_f (kJ/mol)	Cv (J/mol)
1	-362.82	-362.69	316.45	343.47	-362.73	113.84
2	-724.44	-724.21	581.37	465.83	-724.26	235.39
3	-1086.07	-1085.72	845.81	577.90	-1085.80	357.19
4	-1447.69	-1447.24	1110.76	685.37	-1447.30	478.50
5	-1809.32	-1808.76	1374.65	788.65	-1808.90	600.06

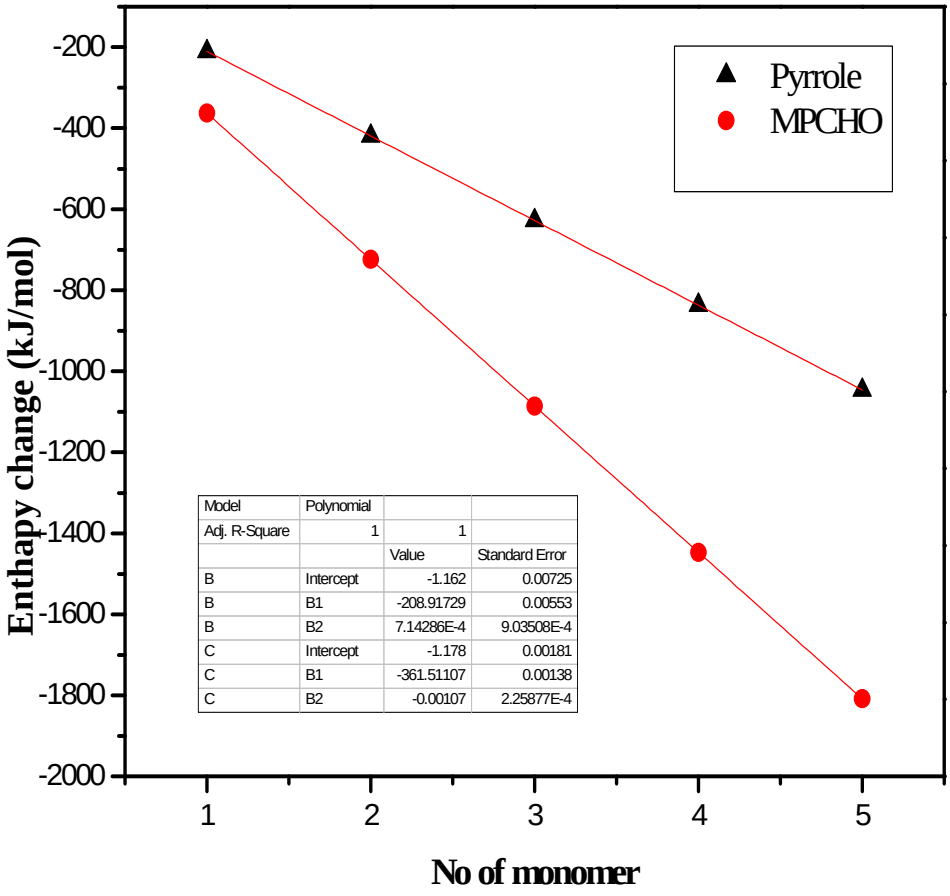

Fig. 4.9. Simulated Enthalpies of Pyrrole and MPCHO as a function of the number of monomer unit

4.3 Quantitative Structure-Activity Relationship (QSAR) Properties

Quantitative Structure-Activity Relationship (QSAR), attempts to identify and quantitate physicochemical properties of a conducting polymer in relation to its biological activity or binding. The parameters considered in this section include; Log P, Log 1/C, polarizability, and molecular area.

4.3.1 QSAR properties of Pyrrole

The polarizability of a compound is the measure of the distortion of a molecule in an electric field. This property enables the determination of the strength of molecular interactions. It is generally associated with a high chemical reactivity and high electro-optic response (Targema *et al*., 2013). These properties for the studied compounds are presented in Table 4.11. It is observed that the polarizability of the studied molecules increases as the number of ring increases. This is due to the increase in size and planarity of the molecules as the ring is increased. The molecular area also increases as the number of ring also increased.

Results of Log P and Log 1/C are presented in Table 4.11. Typically over a small range of Log P, a straight line is obtained as seen in Fig. 4.10**.** A high Log P value indicates poor solubility in aqueous phase, trapped in fat deposit and more susceptibility to metabolism. Log P and Log 1/C values of pyrrole as shown in Table 4.11 are low which indicate that pyrrole will be soluble in aqueous phase and is less susceptible to metabolism.

4.3.2 QSAR properties of MPC^{a}

The results of studied compound are presented in Table 4.12. It is observed that the polarizability of MPC^{a} is about 3.1 Å^{3} higher than that of pyrrole, the value also increases as the number of ring is increased, this indicates that MPC^{a} will have a higher chemical reactivity than pyrrole, this is comparable to the work of Targema *et al*., 2013. This increase is due to the substitution of hydrogen atom with carboxylic group at the C-4 position and methyl group at the C-3 position.

The molecular area of MPC^{a} was found to be 50 Å^{2} higher than pyrrole, this also increases as the number of ring is increased. This is also due to the presence of electron withdrawing carboxylic group in place of hydrogen atom at the C-4 position.

Table 4.11. QSAR properties of pyrrole oligomers

No. of monomers	Polarizability α ($Å^3$)	Molecular area ($Å^2$)	Log P	Log 1/C
1	46.31	99.89	0.44	2.63
2	52.05	168.43	-0.79	1.71
3	57.53	237.00	-2.02	0.79
4	62.93	305.54	-3.26	-0.15
5	68.33	374.07	-4.49	-1.07

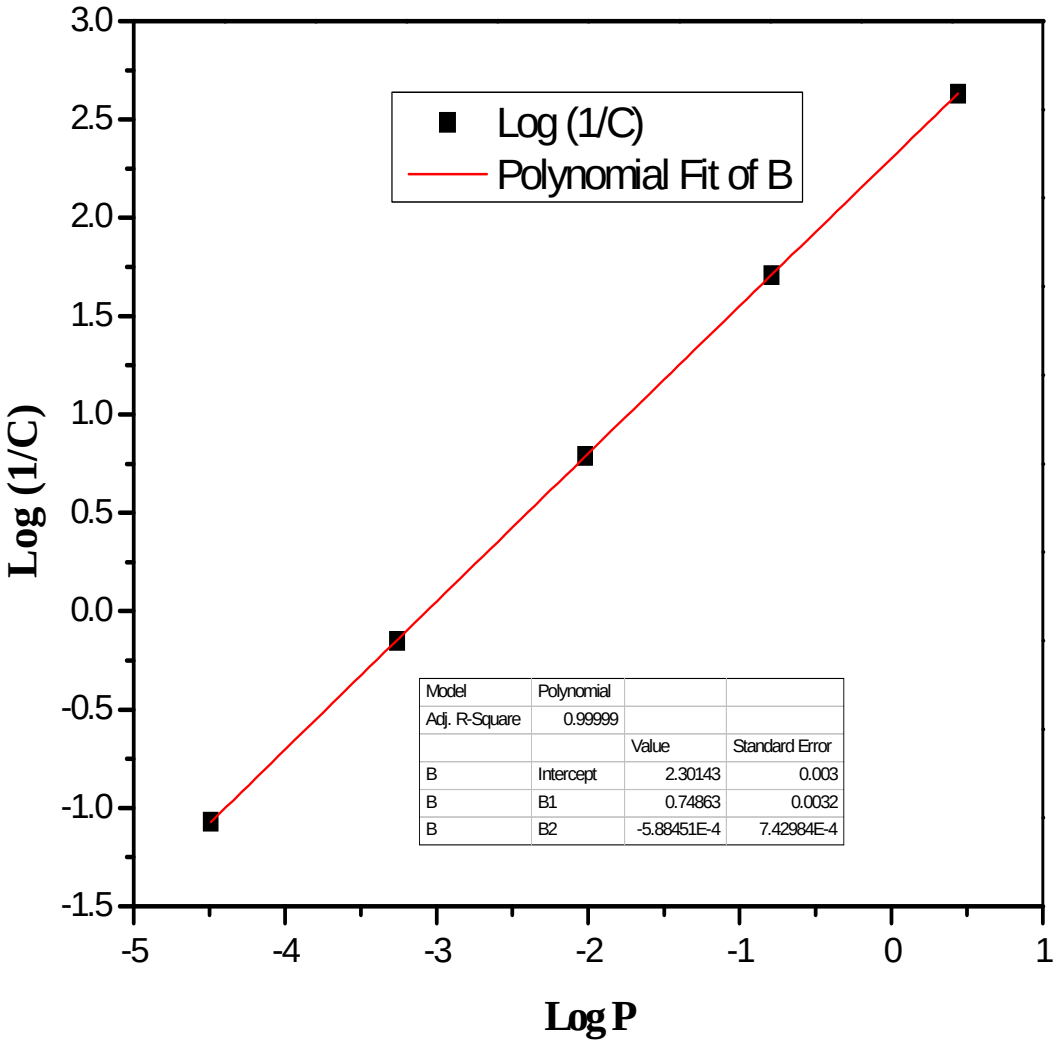

Fig. 4.10. Plot of Log (1/C) vs. Log P showing the biological activity of pyrrole

Table 4.12. QSAR properties of MPC[a] oligomers

No. of monomers	Polarizability α ($Å^3$)	Molecular area ($Å^2$)	Log P	Log (1/C)
1	49.38	149.86	-0.14	2.20
2	59.53	259.94	-1.95	0.84
3	68.64	368.51	-3.76	-0.52
4	77.62	478.81	-5.57	-1.88
5	40.50	578.84	-7.38	-3.24

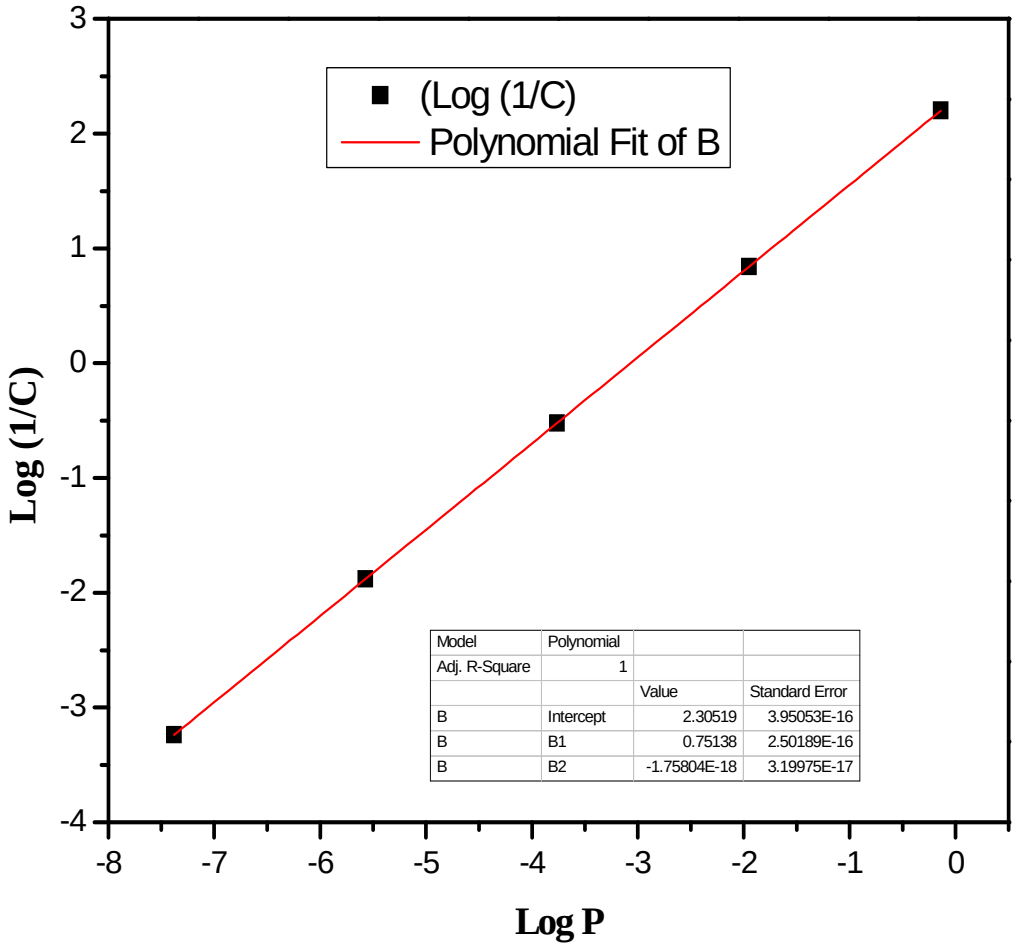

Fig. 4.11. Plot of Log (1/C) vs. Log P showing the biological activity of MPC[a]

Log (1/C) is a measure of the biological activity of molecule and the lower the value of C the more active the molecule (conducting polymer) or drugs and the lesser its binding to serum protein. From the results in Table 4.12, MPC^a has lower values of Log P and Log (1/C) than pyrrole; therefore MPC^a is more biologically active than pyrrole and lower binding effect ability. As shown in Fig 4.11, a straight line graph was observed, which indicates high solubility in aqueous phase, low ability to be trapped in fat deposit and low susceptibility to metabolism.

4.3.3 QSAR properties of MPC^b

The results of studied compound are presented in Table 4.13. It is observed that the polarizability of MPC^b is about 3.1 $Å^3$ higher than that of pyrrole; the value also increases as the number of ring is increased, and this indicates that MPC^b will have a higher chemical reactivity than pyrrole. The molecular area was also found to the higher than pyrrole, and its value increases as the value increase as the number of ring is increased.

The Log P value was found to be higher than that of pyrrole and MPC^a. The higher value obtained, indicates a higher hydrophobicity and higher binding effect to serum protein. The straight line plot as shown in Fig. 4.12 also indicates a higher solubility in aqueous phase and lower susceptibility to metabolism. The relationship between Log P and the hydrophobicity of molecules are in agreement with the work of Waterhouse, (2003).

4.3.4 QSAR properties of MPCam

Table 4.14 shows the result of QSAR properties of MPCam polymer. From the result presented it can be seen that the polarizability and the molecular area is slightly higher than that of MPC^a and MPC^b, and that the polarizability increases as the number of ring increases except for the pentimer which is decreased, these facts also indicates a higher reactivity and molecular interaction with the protein during binding is expected in MPCam compared to MPC^a and MPC^b. This change is attributed to the substitution of hydrogen atom with carboxylic group at the C-4 position and methyl group at the C-3 position.

The Log P value was found to be lower than that of pyrrole and MPC^a and MPC^b. The low value obtained, indicates a lower hydrophobicity and binding ability to serum protein. The straight line plot as shown in Fig. 4.13 also indicates a high solubility in aqueous phase and lower susceptibility to metabolism.

Table 4.13**.** QSAR properties of MPC[b] oligomers

No. of monomers	Polarizability α(Å^3)	Molecular area (Å^2)	Log P	Log (1/C)
1	50.47	150.94	0.58	2.74
2	59.76	259.93	-0.50	1.93
3	68.93	366.1	-1.59	1.11
4	77.89	470.86	-2.67	0.30
5	40.49	575.29	-3.76	-0.52

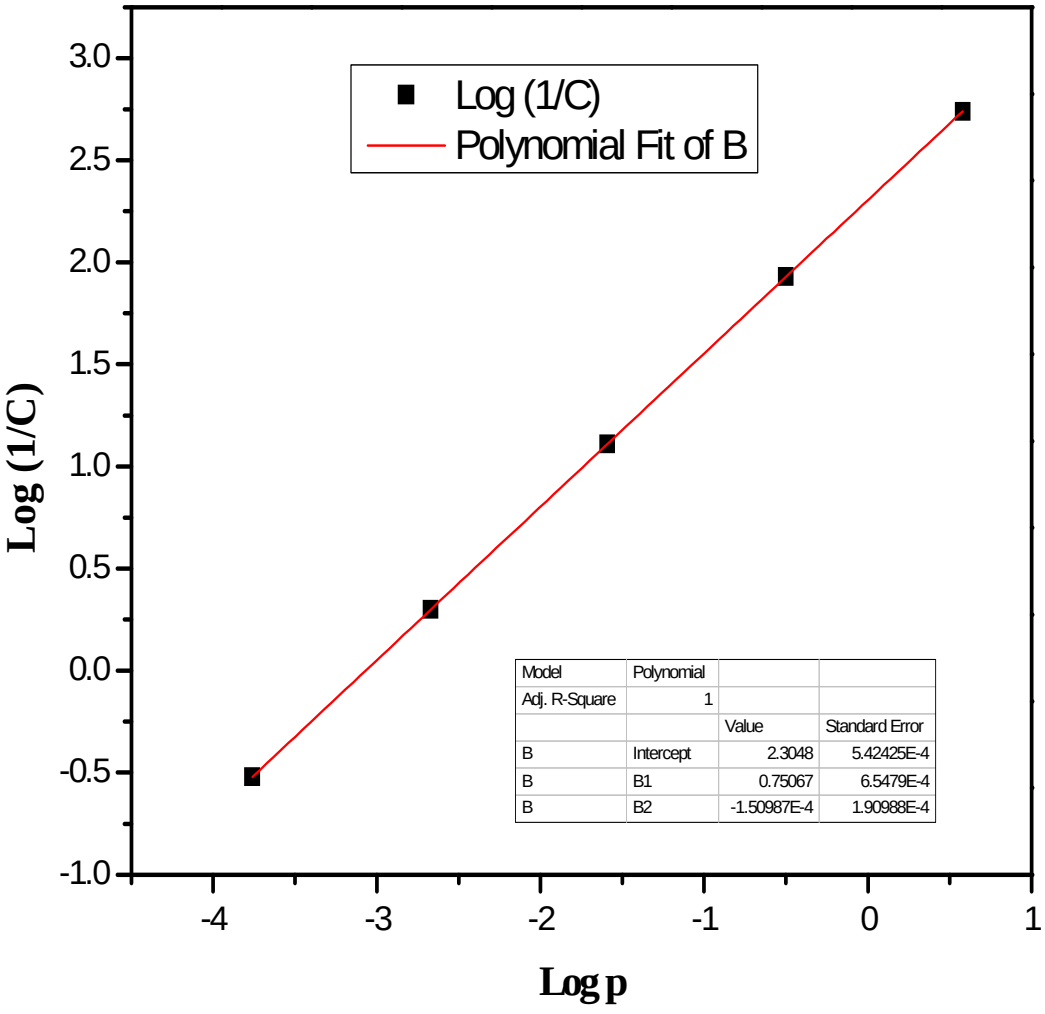

Fig. 4.12. Plot of Log (1/C) vs. Log P showing the biological activity of MPC[b]

Table 4.14. QSAR properties of MPCam oligomers

No. of monomers	Polarizability α ($Å^3$)	Molecular area ($Å^2$)	Log P	Log (1/C)
1	50.56	154.02	-0.79	1.71
2	60.11	256.55	-3.25	-0.14
3	69.26	377.41	-5.71	-2.01
4	78.51	483.82	-8.17	-3.83
5	40.49	596.94	-10.63	-5.65

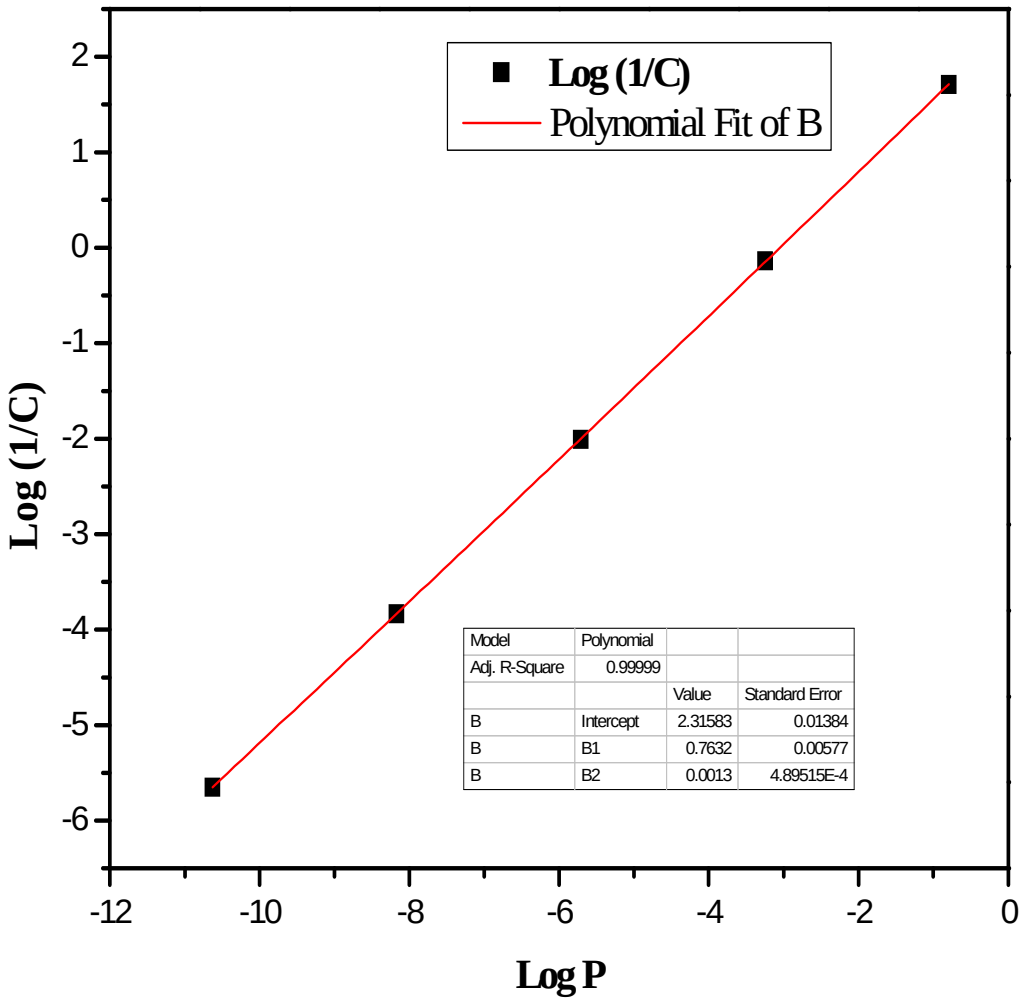

Fig. 4.13. Plot of Log (1/C) vs. Log P showing the biological activity of MPCam

4.3.5 QSAR properties of MPCOSH

The results of studied compound are presented in Table 4.15. It was observed that the polarizability of MPCOSH is about 4.9 $Å^3$ higher than that of pyrrole; the value also increases as the number of ring is increased, and this indicates that MPCOSH will have a higher chemical reactivity than pyrrole, MPC^a MPC^b and MPCam. This increase is due to the substitution of hydrogen atom with amide group at the C-4 position and methyl group at the C-3 position.

The molecular area was found to be higher than pyrrole, this also increase as the number of ring is increased.

From the results presented in Table 4.15, MPCOSH has slightly higher values of Log P and Log (1/C) than pyrrole; therefore MPC^a will be less biologically active than pyrrole and a higher binding ability is expected. As shown in Fig. 4.14, a straight line graph was observed, which indicates higher solubility in aqueous phase, lower ability to be trapped in fat deposit and lower susceptibility to metabolism.

4.3.6 QSAR properties of $MPSO_3H$

The results of studied compound are presented in Table 4.16. Result reviews that the polarizability is about 4.8 $Å^3$ higher than that of pyrrole, and also 1.1 $Å^3$ higher than MPC^a and MPC^b and MPCam. The value was observed to increase as the number of ring is increased to trimer, but decreases from tetramer pentimer this may be due to the fact that SO_3H group that removes electron density from a conjugated π system via resonance effect, thus making the π system more electrophilic. The high polarizability indicates that $MPSO_3H$ will show a higher strength of molecular interactions, chemical reactivity and high electro-optic response than pyrrole. The molecular area was also found to the higher than pyrrole, and its value increases as the value increase as the number of ring is increased.

The Log P value was found to be lower than that of pyrrole, MPC^a and MPC^b. The low value obtained, indicates a lower hydrophobicity and binding ability to serum protein. The straight line plot as shown in Fig. 4.15 also indicates a high solubility in aqueous phase and lower susceptibility to metabolism.

Table 4.15. QSAR properties of MPCOSH oligomers

No. of monomers	Polarizability α ($Å^3$)	Molecular area ($Å^2$)	Log P	Log (1/C)
1	51.21	158.68	0.43	2.62
2	61.29	280.41	-0.80	1.70
3	71.28	408.86	-2.04	0.77
4	81.12	525.37	-3.27	-0.15
5	40.54	649.12	-4.51	-1.08

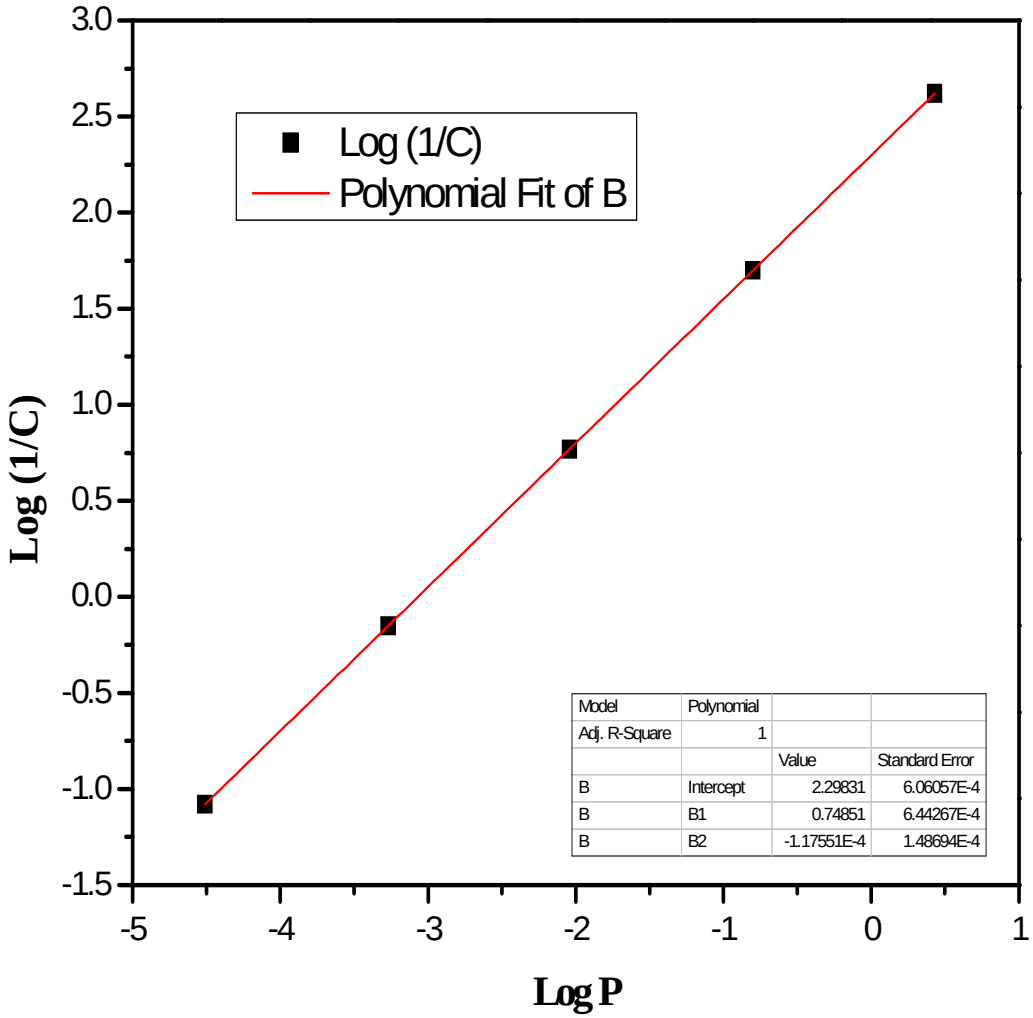

Fig 4.14. Plot of Log (1/C) vs. Log P showing the biological activity of MPCOSH

Table 4.16**.** QSAR properties of $MPSO_3H$ oligomers

No. of monomers	Polarizability α ($Å^3$)	Molecular area ($Å^2$)	Log P	Log (1/C)
1	51.11	168.43	-0.92	1.61
2	61.52	294.38	-3.51	-0.33
3	71.52	416.70	-6.10	-2.28
4	40.36	549.03	-8.69	-4.22
5	40.41	679.27	-11.28	-6.16

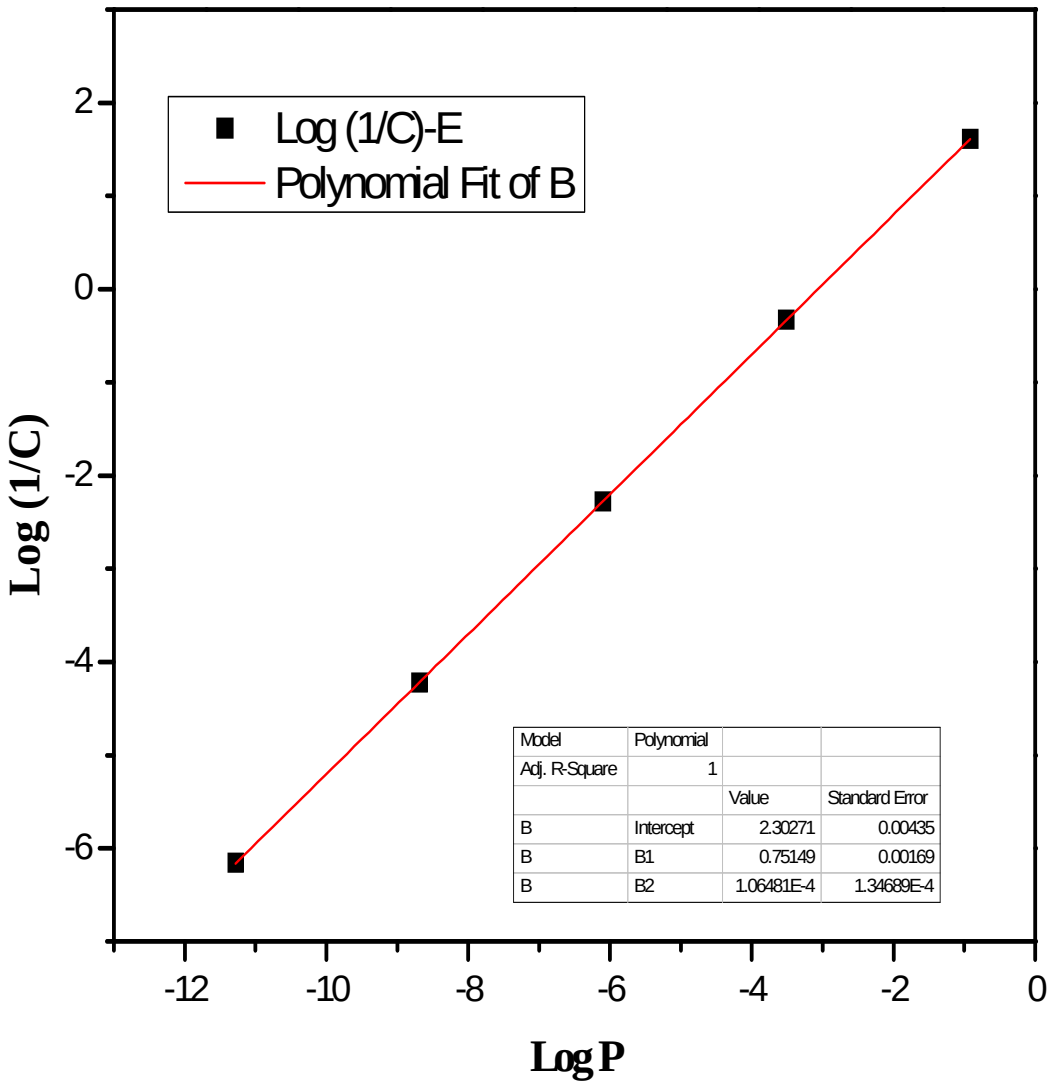

Fig 4.15. Plot of Log (1/C) vs. Log P showing the biological activity of $MPSO_3H$

4.3.7 QSAR properties of MPCHO

Table 4.17 shows the result of QSAR properties of MPCam polymer. From the result presented, it can be seen that the polarizability is about 3.53Å^3 and higher than pyrrole. The molecular area is lower than other studied molecules, and that the polarizability increases as the number of ring increases these indicates a lower reactivity and molecular interaction with the protein during binding. This is due to the fact that CHO groups are moderately electron withdrawing groups, therefore a more resonance effect is observed and the atom that is attached to the molecule is involved in a multiple bond.

From the results presented in Table 4.17, MPCHO has slightly lower values of Log P and Log (1/C) than pyrrole; therefore MPCHO will have a higher biological activity than pyrrole and a higher binding capacity is expected. As shown in Fig. 4.16, a straight line graph was observed, which indicates poor solubility in aqueous phase, higher ability to be trapped in fat deposit and higher susceptibility to metabolism.

Table 4.17. QSAR properties of MPCHO oligomers

No. of monomers	Polarizability α ($Å^3$)	Molecular area ($Å^2$)	Log P	Log (1/C)
1	49.84	141.92	-0.41	1.99
2	58.49	248.00	-2.48	0.44
3	67.04	354.30	-4.56	-1.12
4	75.55	461.27	-6.63	-2.67
5	84.13	564.59	-8.71	-4.23

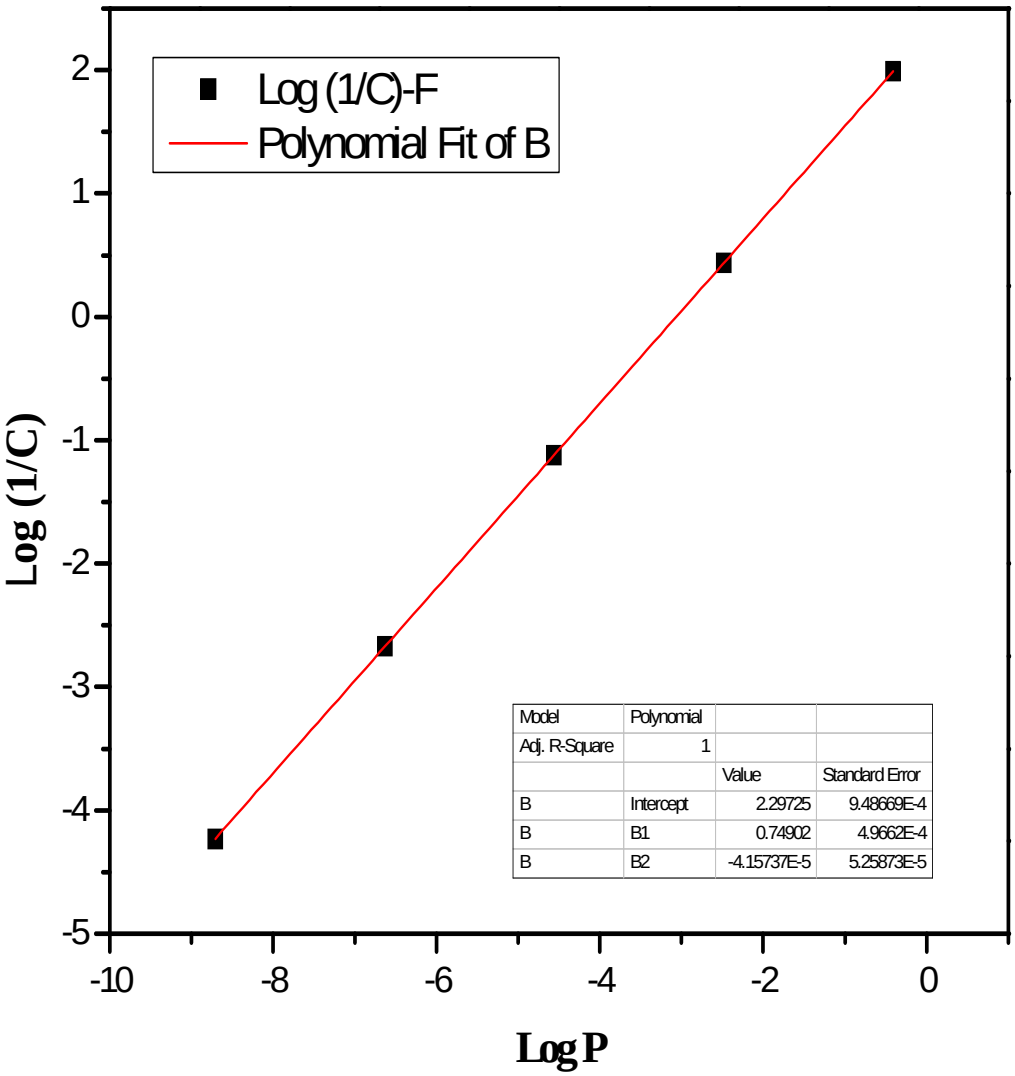

Fig 4.16. Plot of Log (1/C) vs. Log P showing the biological activity of MPCHO

4.4 Ionization Potential, Electron Affinity and Molecular Orbital Energy

4.4.1 Molecular energies of Pyrrole

The IP and EA of an atom or a molecule are the energy needed to remove or gain an electron and therefore can be referred to as the ability of the molecule to donate and accept electrons respectively. Table 4.18 shows the IP and EA of pyrrole. Table shows that all of the IPs from monomers up to five repeating units is positive values, whereas some of the EA values are negative. The negative EA means that the anionic state is unbound. It can be seen that most HOMO energies vary in the range of -4.4 to approximately -5.48, while LUMO energies vary significantly (from -0.31 to 1.39). As shown in Fig. 4.17, we find a linear relationship between the direct calculated vertical HOMO energies and 1/n calculated from DFT (with a correlation coefficient r^2 = 0.99) and the direct calculated vertical LUMO energies and 1/n calculated from DFT (with a correlation coefficient r^2 = 0.99). The LUMO; of π-nature is delocalized over the C-C bonds of the pyrrole ring, while the HOMO is located over the C=C bonds (Plate 4.8).

Energy gap between the Highest Occupied Molecular Orbital (HOMO) and the Lowest Unoccupied Molecular Orbital (LUMO), or simply HOMO-LUMO gap (HLG; ΔEg), also called Band gaps, is a key parameter which determines the molecular admittance because it is a measure of the electron density hardness (Hirata, 2003; Parr and Pearson, 1983).
The band gap of 5 pyrrole oligomers is extrapolated to polymer through second-degree polynomial fit equation. The band gap is obtained from the difference of the orbital energies (valence and conduction band). The experimental band-gap value of pyrrole ranges from 2.9-3.2 eV, are calculated by Zotti et al., (1992) and significantly correlates well with the calculated band gap of pyrrole, which is 2.9 eV, and this corresponds to π-π* transition energies.

A series of studies has shown that a small HOMO-LUMO gap corresponds to a high reactivity (Koopmans, 1933) and with anti-aromaticity (Haddon and Fuguhata, 1980**)**. According to De-Proft and Geerlings (2004), absolute hardness (half of HOMO/LUMO energies) is commonly used as a criterion of chemical reactivity and stability. They pointed out that aromatic rings influence the reactivity through aromatic π-electrons

delocalization of positive charge; increasing aromaticity causes the increase of hardness and the decrease of reactivity. A more reactive molecule is characterized by a lower value of μ, η. From result presented in Table 4.19, pyrrole exhibits high reactivity, low stability, anti-aromatic behaviour and it is a soft molecule.

Table 4.18. IPs, EAs, HOMOs, LUMOs, and Energy Gaps of pyrrole oligomers

No. of Monomers	EA (eV)	IP (eV)	E_{LUMO} (eV)	E_{HOMO} (eV)	Eg (eV)
1	-1.39	5.48	1.39	-5.48	6.87
2	-0.39	4.82	0.39	-4.82	5.21
3	-0.02	4.57	0.02	-4.57	4.57
4	0.16	4.48	-0.16	-4.48	4.32
5	0.31	4.40	-0.31	-4.40	4.09
∞			-1.20	-4.12	2.92
R^2			0.99	0.99	
[a]*Expt.*					2.9-3.2

[a] (Zotti et al., 1992)

Table 4.19. Calculated molecular hardness, electrophilicity, and chemical potential of pyrrole

No. of monomer	η (eV)	μ (eV)	ω (eV)
1	3.44	-2.05	0.61
2	2.61	-2.22	0.95
3	2.29	-2.28	1.14
4	2.16	-2.32	1.25
5	2.05	-2.36	1.36

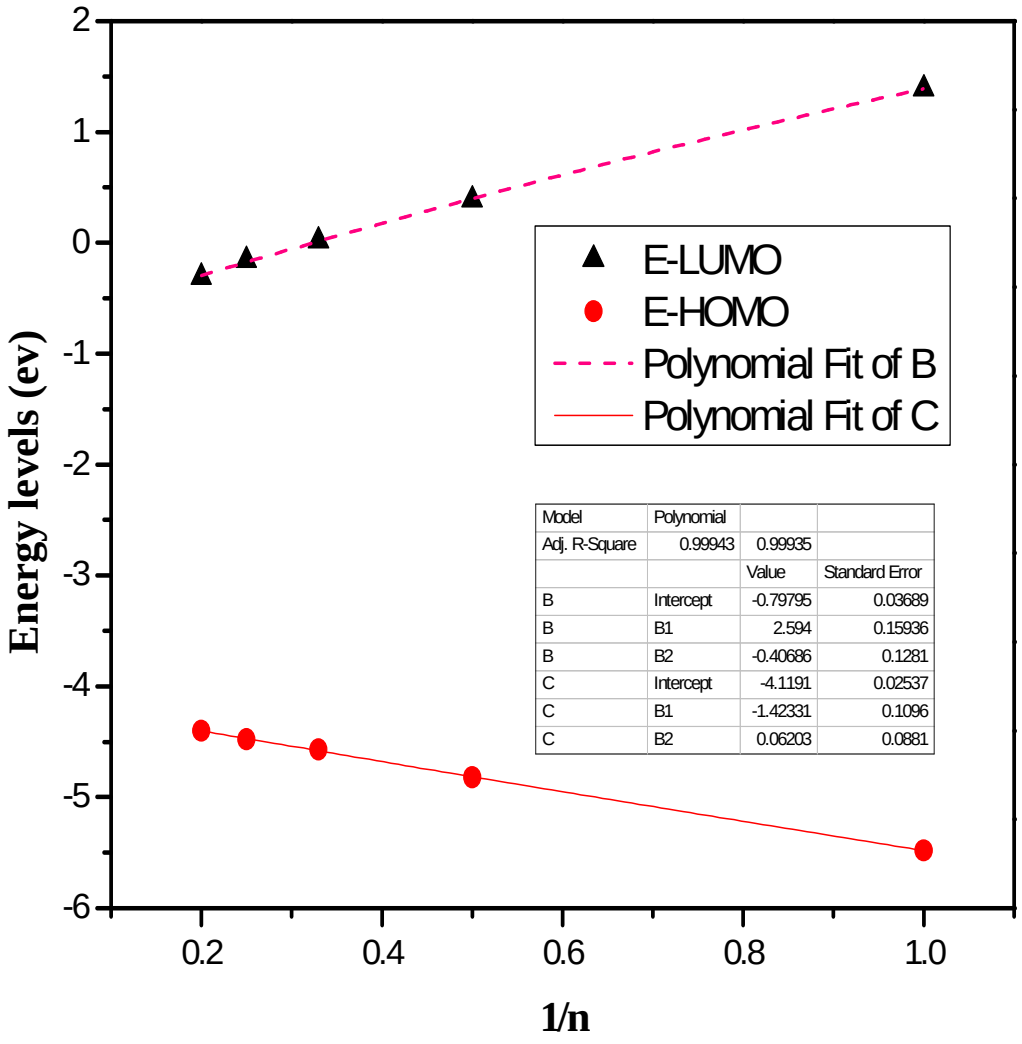

Model	Polynomial		
Adj. R-Square	0.99943	0.99935	
		Value	Standard Error
B	Intercept	-0.79795	0.03689
B	B1	2.594	0.15936
B	B2	-0.40686	0.1281
C	Intercept	-4.1191	0.02537
C	B1	-1.42331	0.1096
C	B2	0.06203	0.0881

Fig. 4.17. Plot of HOMO, LUMO energy level against 1/n of pyrrole oligomer.

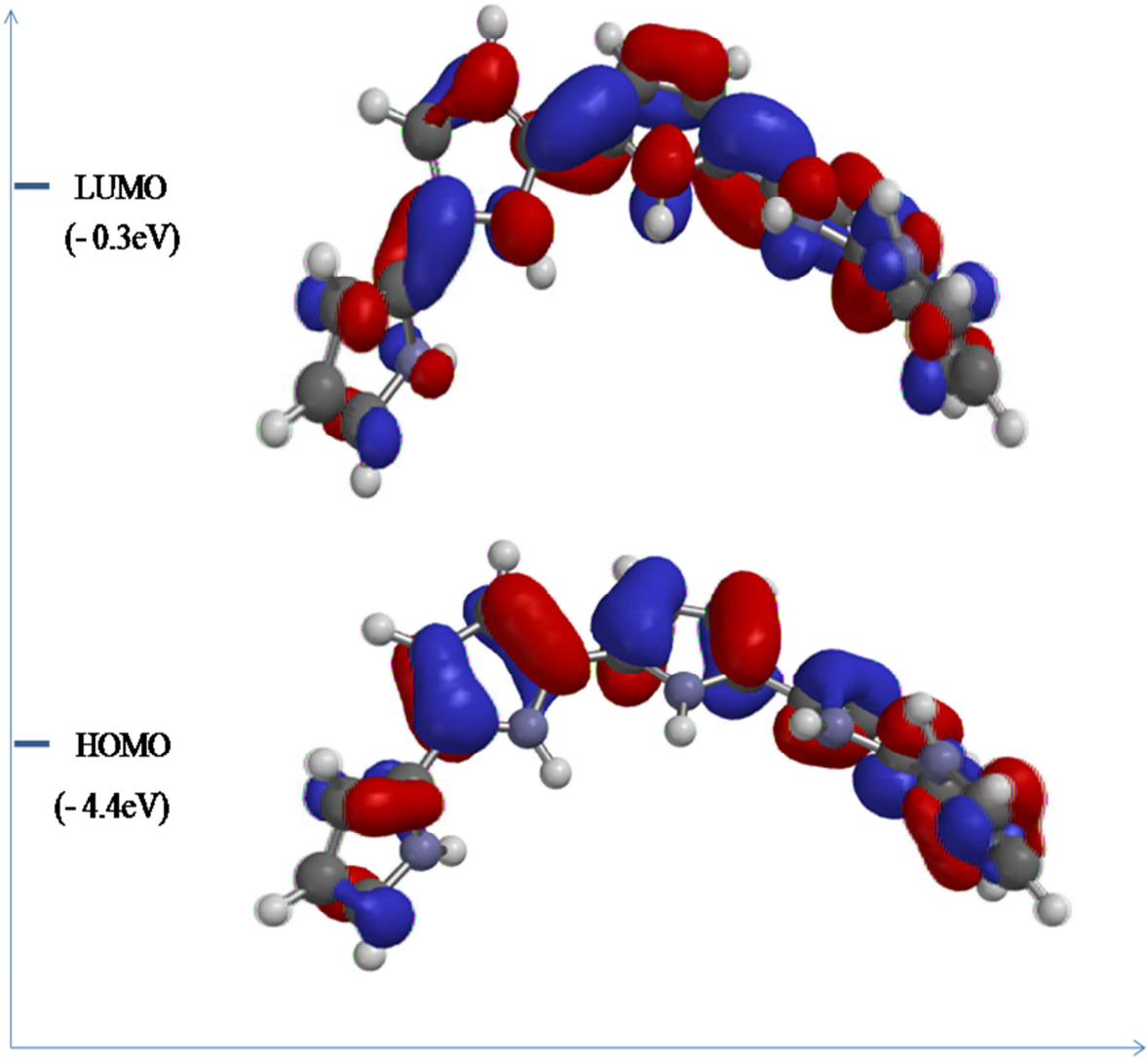

Plate 4.8. The frontier molecular orbital plot of pyrrole

4.4.2 Molecular energies of MPC[a]

The results for IP and EA of MPC[a] are presented in Table 4.20. Result also shows that all values of IPs and EA from monomers up to five repeating units are positive values. The HOMO energies vary within the range of -4.42 to -5.93, while LUMO energies vary significantly (from -0.23 to -1.89). Fig. 4.18, shows a linear relationship between the direct calculated vertical HOMO energies and 1/n calculated from DFT (with a correlation coefficient r^2 = 0.87) and the direct calculated vertical LUMO energies and 1/n calculated from DFT (with a correlation coefficient r^2 = 0.97). The LUMO extended over the C-C bonds, the nitrogen and oxygen atom, this involves delocalization over the entire molecule framework while the HOMO is located over the C=C bonds (Plate 4.9).

The band gap of 5 MPC[a] oligomers was also extrapolated to polymer through second-degree polynomial fit equation. The band gap is obtained from the difference of the orbital energies (valence and conduction band). A significant decrease in band gap of 2.9eV to 2.53eV was observed for MPC[a]. This difference is due the substitution of hydrogen atom in by a methyl group at C3 and the electron-withdrawing character of the carboxyl group which affects the π-conjugation in the pyrrole ring. Increase conjugation also contributes to the decrease in energy gap. This agrees with experimental results and it's comparable to the work of Guimarães *et al*., (2008). According to Koopmans, (1933), Haddon and Fuguhata, 1980) and De-Proft and Geerlings (2004), MPC[a] shows high reactivity, low stability, anti-aromatic behaviour and termed as a soft molecule as characterized by a lower value of band gap, μ and η as shown in Table 4.21, when compared with pyrrole.

Table 4.20. IPs, EAs, HOMOs, LUMOs, and Band Gaps of MPC[a] oligomers

No. of monomers	EA (eV)	IP (eV)	E_{LUMO} (eV)	E_{HOMO} (eV)	Band gap (eV)
1	0.23	5.93	-0.23	-5.93	5.7
2	1.1	5.91	-1.1	-5.91	4.81
3	1.56	5.61	-1.56	-5.61	4.04
4	1.53	5.51	-1.53	-5.51	3.98
5	1.58	5.11	-1.58	-5.11	3.53
∞	1.89	4.42	-1.89	-4.42	2.53
R^2			0.97	0.87	

Table 4.21. Calculated molecular hardness, electrophilicity, and chemical potential of MPC[a]

No. of monomer	η (eV)	μ (eV)	ω (eV)
1	2.85	-3.08	1.66
2	2.41	-3.51	2.65
3	2.02	-3.59	3.19
4	1.99	-3.52	3.11
5	1.77	-3.35	3.17

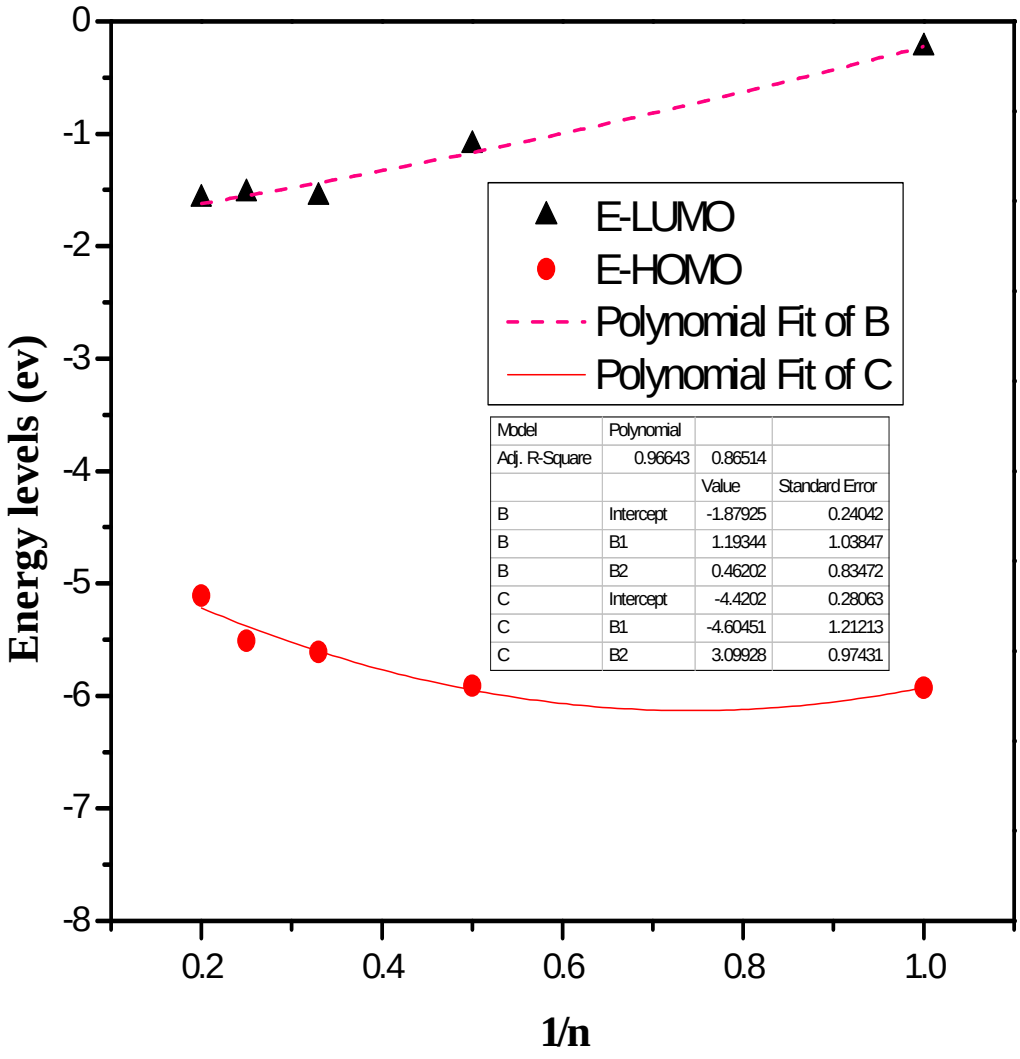

Fig 4.18. Plot of HOMO, LUMO energy level against 1/n of MPC[a] oligomer

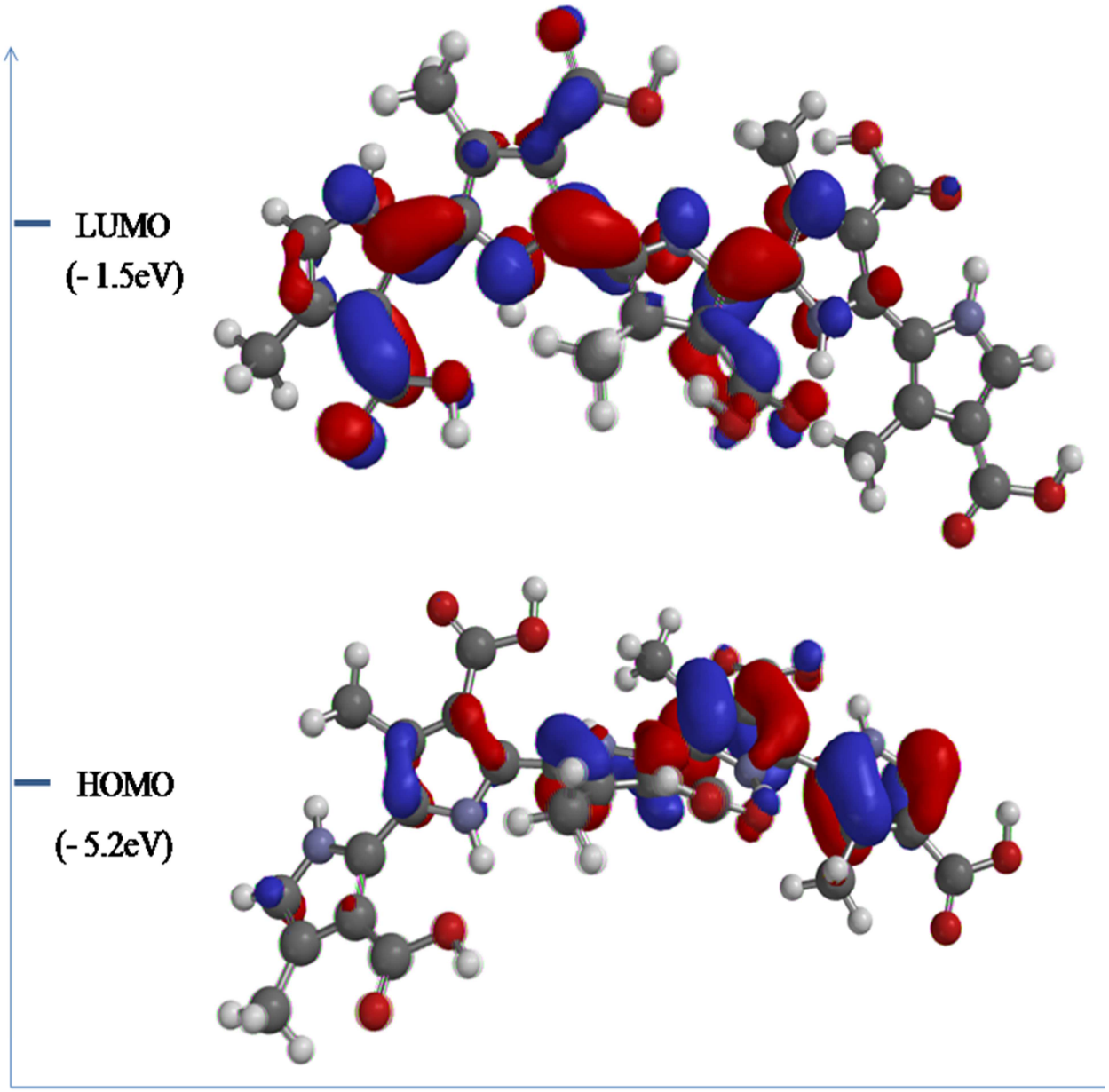

Plate 4.9. The frontier molecular orbital plot of MPC[a]

4.4.3 Molecular energies of MPC^b

Analysis of the results of IP and EA for MPC^b in Table 4.22 shows that all values of IPs and EA from monomers up to five repeating units are positive values. The HOMO energies vary within the range of -5.22 to -6.24, while LUMO energies vary (from -0.62 to -1.84). As shown in Fig. 4.19, a linear relationship exist between the direct calculated vertical HOMO energies and 1/n calculated from DFT (with a correlation coefficient r^2 = 0.76) and the direct calculated vertical LUMO energies and 1/n (with a correlation coefficient r^2 = 0.93). As shown in Plate 4.10, the LUMO of π-nature is delocalized over the C-C bonds of the ring, while the HOMO is located over the C=C bonds.

The energy gap of 5 MPC^b oligomers was extrapolated to polymer through second-degree polynomial fit equation. The band gap was also obtained from the difference between LUMO-HOMO. A significant decrease in band gap of 2.9eV to 2.61eV was observed for MPC^a. This difference observed will be due to the presence of an electron withdrawing group at N atom carrying the lone pair of electron. This result is also comparable to earlier findings of Guimarães *et al*., 2008. Also according to Koopmans, (1933), Haddon and Fuguhata, 1980) and De-Proft and Geerlings (2004), calculated result as shown in Table 4.22-4.23 reveals that MPC^b will demonstrate high reactivity, low stability, anti-aromatic behaviour and termed as a soft molecule as characterized by a lower value of band gap, μ and η when compared with pyrrole. From these features, MPC^b will have a higher spontaneous interaction and binding ability to the polymer than MPC^a and pyrrole. There are no experimental data for the modeled compound.

Table 4.22. IPs, EAs, HOMOs, LUMOs, and Band Gaps of MPC[b] oligomers

No. of Monomers	EA (eV)	IP (eV)	E_{LUMO} (eV)	E_{HOMO} (eV)	Band gap (eV)
1	0.62	6.24	-0.62	-6.24	5.62
2	0.88	5.62	-0.88	-5.62	4.74
3	1.21	5.22	-1.21	-5.22	4.01
4	1.42	5.55	-1.42	-5.55	4.13
5	1.84	5.27	-1.84	-5.27	3.43
E_{gap} ($n \rightarrow \infty$)			-2.65	-5.26	2.61
R^2			0.93	0.76	

Table 4.23. Calculated molecular hardness, electrophilicity, and chemical potential of MPC[b]

No. of Monomers	η (eV)	μ (eV)	ω (eV)
1	2.81	-3.43	2.09
2	2.37	-3.25	2.23
3	2.01	-3.22	2.59
4	2.07	-3.49	2.95
5	1.72	-3.56	3.69

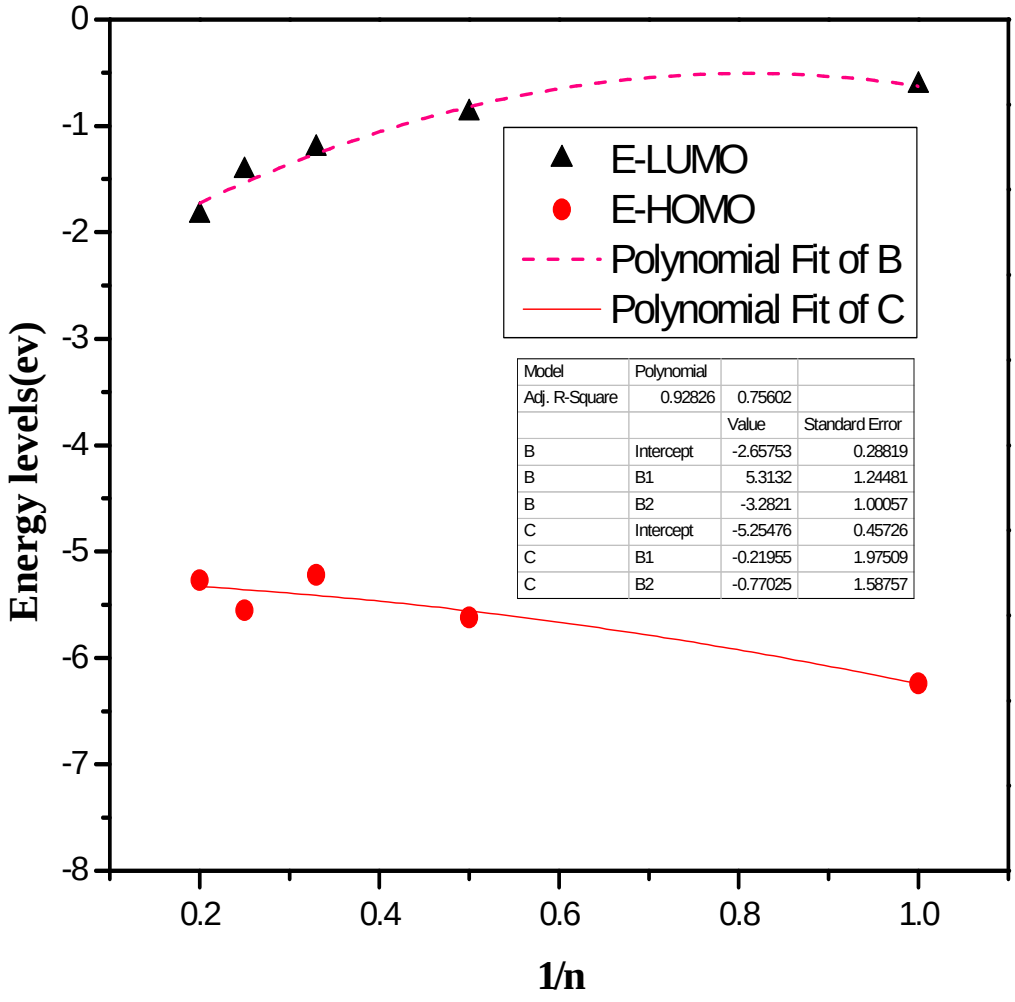

Fig. 4.19. Plot of HOMO, LUMO energy level against 1/n of MPC^b oligomer

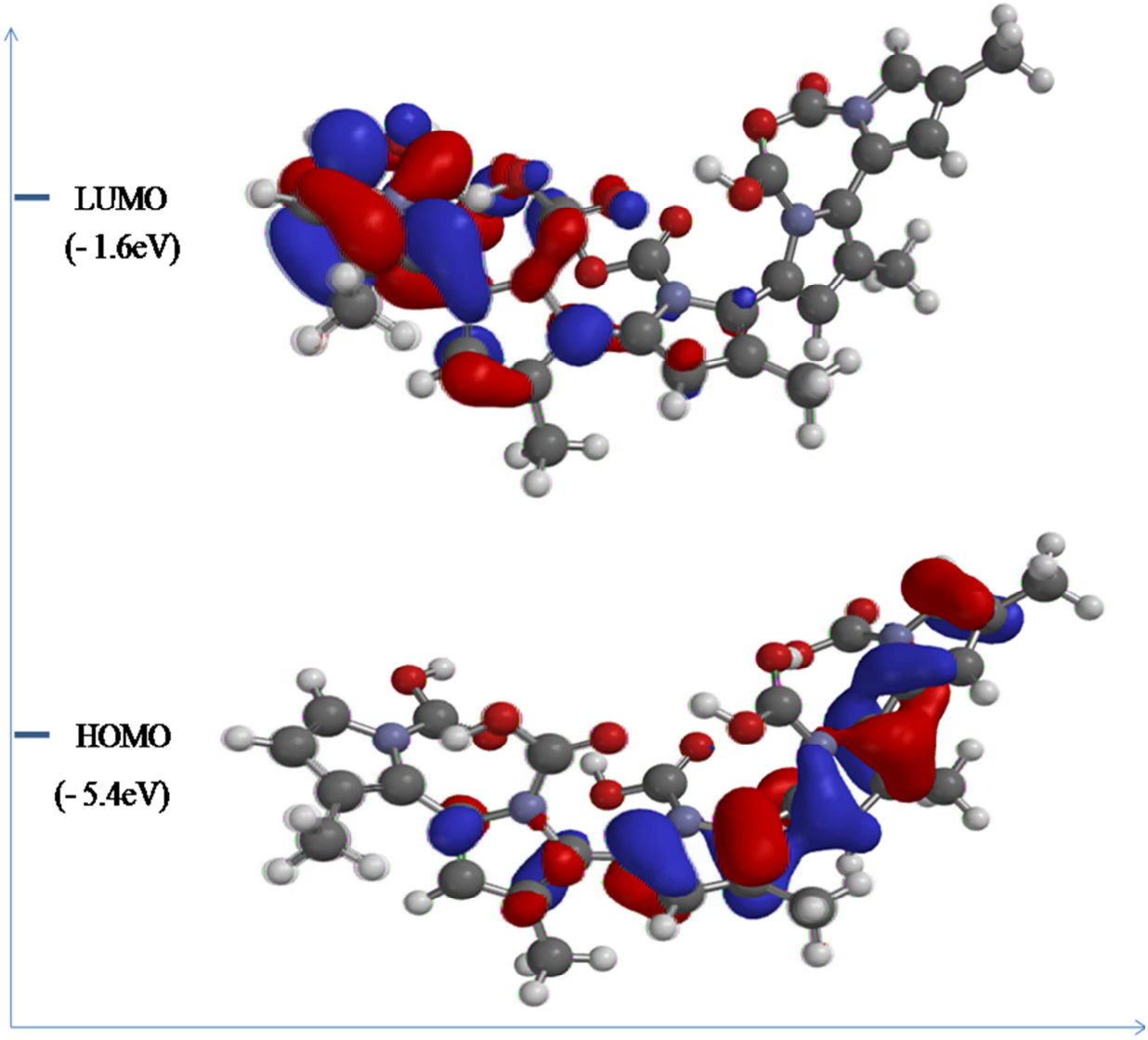

Plate 4.10. The frontier molecular orbital plot of MPC[b]

4.4.4 Molecular energies of MPCam

Calculated results for IP and EA of MPCam are shown in Table 4.24. These reveal that all values of IPs and EA from monomers up to five repeating units are also positive values. The HOMO energies vary within the range of -4.21 to -5.83, while LUMO energies vary significantly (from -0.01 to -1.07). As shown in Fig. 4.20, there is a linear relationship between the direct calculated vertical HOMO energies and 1/n calculated from DFT (with a correlation coefficient r^2 = 0.84) and the calculated vertical LUMO energies and 1/n calculated from DFT (with a correlation coefficient r^2 = 0.98). The LUMO frontier molecular orbital extended over the C-C bonds, the nitrogen and oxygen atom, this involve delocalization over the entire molecule framework while the HOMO is located over the C=C bonds (Plate 4.11).

The band gap of MPCam oligomers was also extrapolated to polymer through second-degree polynomial fit equation. The band gap was obtained and significant decrease in band gap from 2.9eV to 2.38eV was observed for MPCam. The substitution of hydrogen atom by an amide group at C4 ($CONH_2$) brings about a deactivating effect. The amide group been attached to the ring through the carbonyl carbon, brings about a partial positive charge on the carbon and has as a deactivating influence which also affects the π-conjugation in the pyrrole ring. Increased conjugation also contributes to the decrease in energy gap. This result is also comparable to the work of Guimarães *et al*., (2008). MPCam will exhibit a higher reactivity, lower stability, anti-aromatic behaviour and termed as a softer molecule as characterized by a lower value of band gap, μ and η as shown in Table 4.21, when compared with pyrrole, MPC^a, MPC^b.

Table 4.24. IPs, EAs, HOMOs, LUMOs, and Band Gaps of MPCam oligomers

No. of Monomers	EA (eV)	IP (eV)	E_{LUMO} (eV)	E_{HOMO} (eV)	Band gap (ev)
1	0.01	5.83	-0.01	-5.83	5.82
2	0.82	5.21	-0.82	-5.21	4.39
3	0.92	5.11	-0.92	-5.11	4.19
4	0.95	4.68	-0.95	-4.68	3.73
5	1.07	4.21	-1.07	-4.21	3.14
E_{gap} ($n \rightarrow \infty$)			-1.07	-3.45	2.38
R^2			098	0.84	

Table 4.25. Calculated molecular hardness, electrophilicity, and chemical potential of MPCam

No. of Monomers	η (eV)	M (eV)	ω (eV)
1	2.91	-2.92	1.47
2	2.20	-3.02	2.08
3	2.10	-3.02	2.18
4	1.87	-2.82	2.13
5	1.57	-2.62	2.19

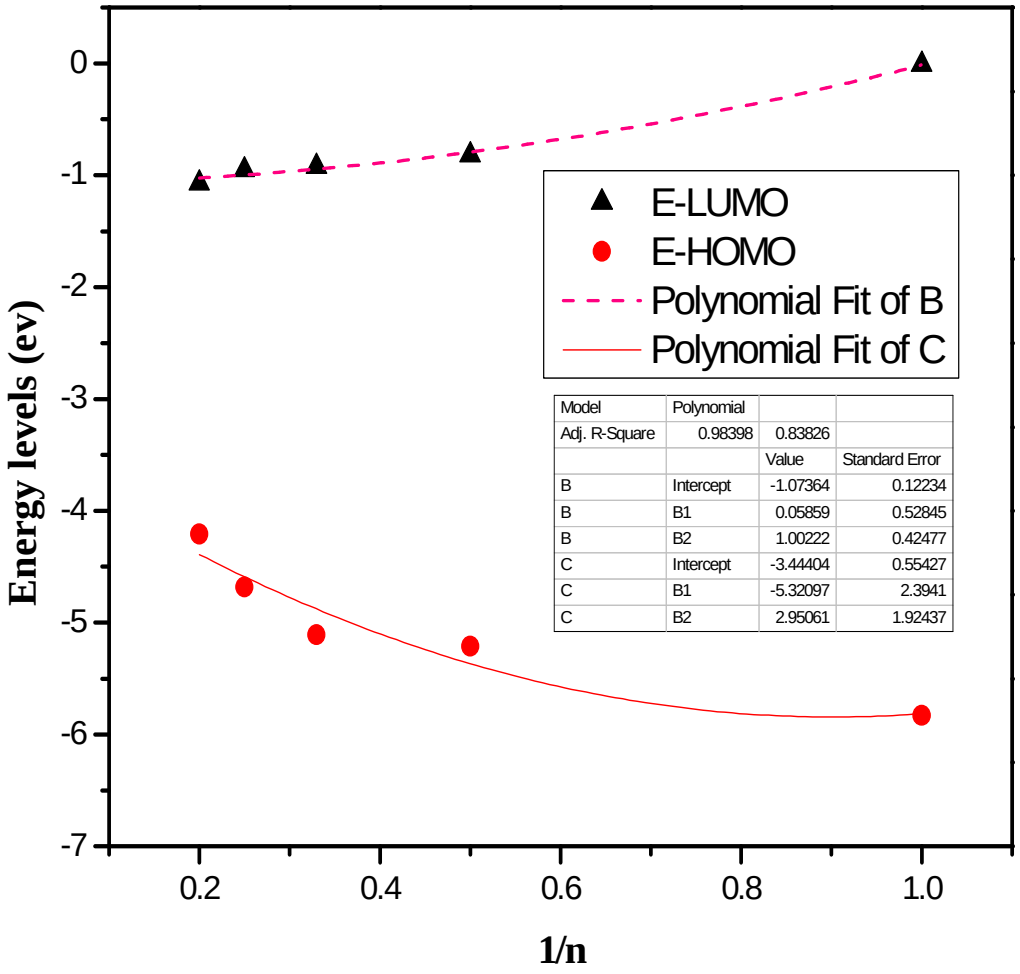

Fig. 4.20. Plot of HOMO, LUMO energy level against 1/n of MPCam oligomer

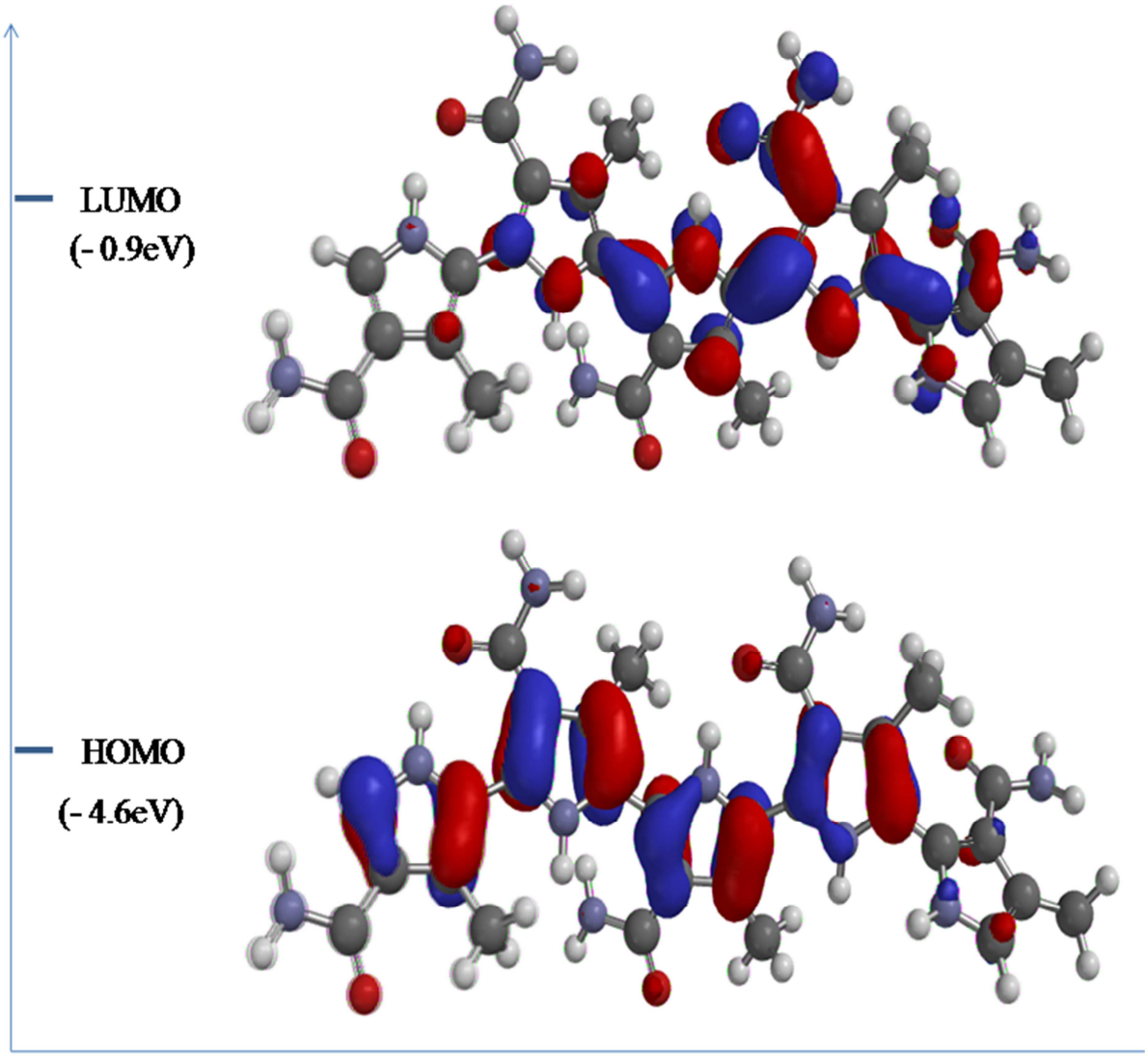

Plate 4.11. The frontier molecular orbital plot of MPCam

4.4.5 Molecular energies of MPCOSH

The IP and EA calculated results of MPCOSH are presented in Table 4.26. Data show that all values of IPs and EA from monomers up to five repeating units are positive values. The HOMO energies vary within the range of -5.06 to -6.21, while LUMO energies vary significantly (from -0.82 to -2.11). Fig. 4.21, shows a linear relationship between the direct calculated vertical HOMO energies and 1/n calculated from DFT (with a correlation coefficient r^2 = 0.99) and the direct calculated vertical LUMO energies and 1/n calculated from DFT (with a correlation coefficient r^2 = 0.99). The LUMO extended over the C-C bonds, the sulphur and oxygen atom, this involve delocalization over the entire molecule framework while the HOMO is located over the C=C bonds (Plate 4.12). MPCOSH shows more electron density distribution of HOMO orbital as compared to pyrrole, MPC^a, MPC^b and MPCam.

The energy gap of five MPCOSH oligomers was also extrapolated to polymer through second-degree polynomial fit equation. A significant decrease in band gap of pyrrole (2.9eV) to 1.66eV was observed for MPCOSH. This difference is due the substitution of hydrogen atom in by a methyl group at C3 and the electron-withdrawing character which affects the π-conjugation of the ring. Increase conjugation also contributes to the decrease in energy gap. This agrees with experimental results and it's comparable to the work of Guimarães *et al*., (2008). Also according to Koopmans, (1933), Haddon and Fuguhata, 1980) and De-Proft and Geerings, (2004), MPCOSH will display a higher reactivity, low stability, anti-aromatic behaviour and termed as a softer molecule based on the band gap value, μ and η as shown in Table 4.27, when compared with other modeled compounds. There are no experimental or theoretical data for these derivatives.

Table 4.26. IPs, EAs, HOMOs, LUMOs, and Band Gaps of MPCOSH oligomers

No. of monomers	EA (eV)	IP (eV)	E_{LUMO} (eV)	E_{HOMO} (eV)	Band gap (eV)
1	0.82	6.21	-0.82	-6.21	5.39
2	1.31	5.78	-1.31	-5.78	4.47
3	1.67	5.42	-1.67	-5.42	3.75
4	1.85	5.25	-1.85	-5.25	3.40
5	2.11	5.06	-2.11	-5.06	2.95
E_{gap} ($n \rightarrow \infty$)			-2.77	-4.43	1.66
R^2			0.99	0.99	

Table 4.27. Calculated molecular hardness, electrophilicity, and chemical potential of MPCOSH

No. of monomers	η (eV)	μ (eV)	ω (eV)
1	2.70	-3.52	2.30
2	2.24	-3.55	2.82
3	1.88	-3.55	3.36
4	1.70	-3.56	3.73
5	1.48	-3.59	4.37

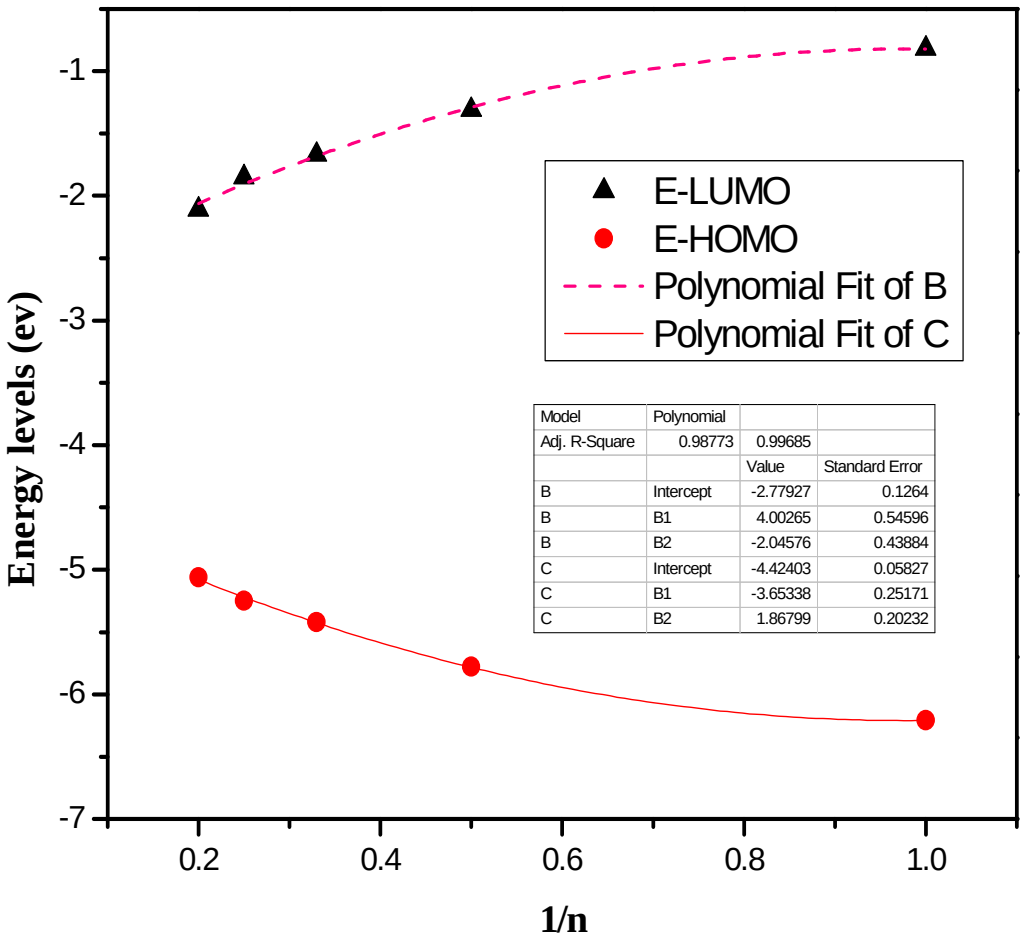

Fig. 4.21. Plot of HOMO, LUMO energy level against 1/n of MPCOSH oligomer

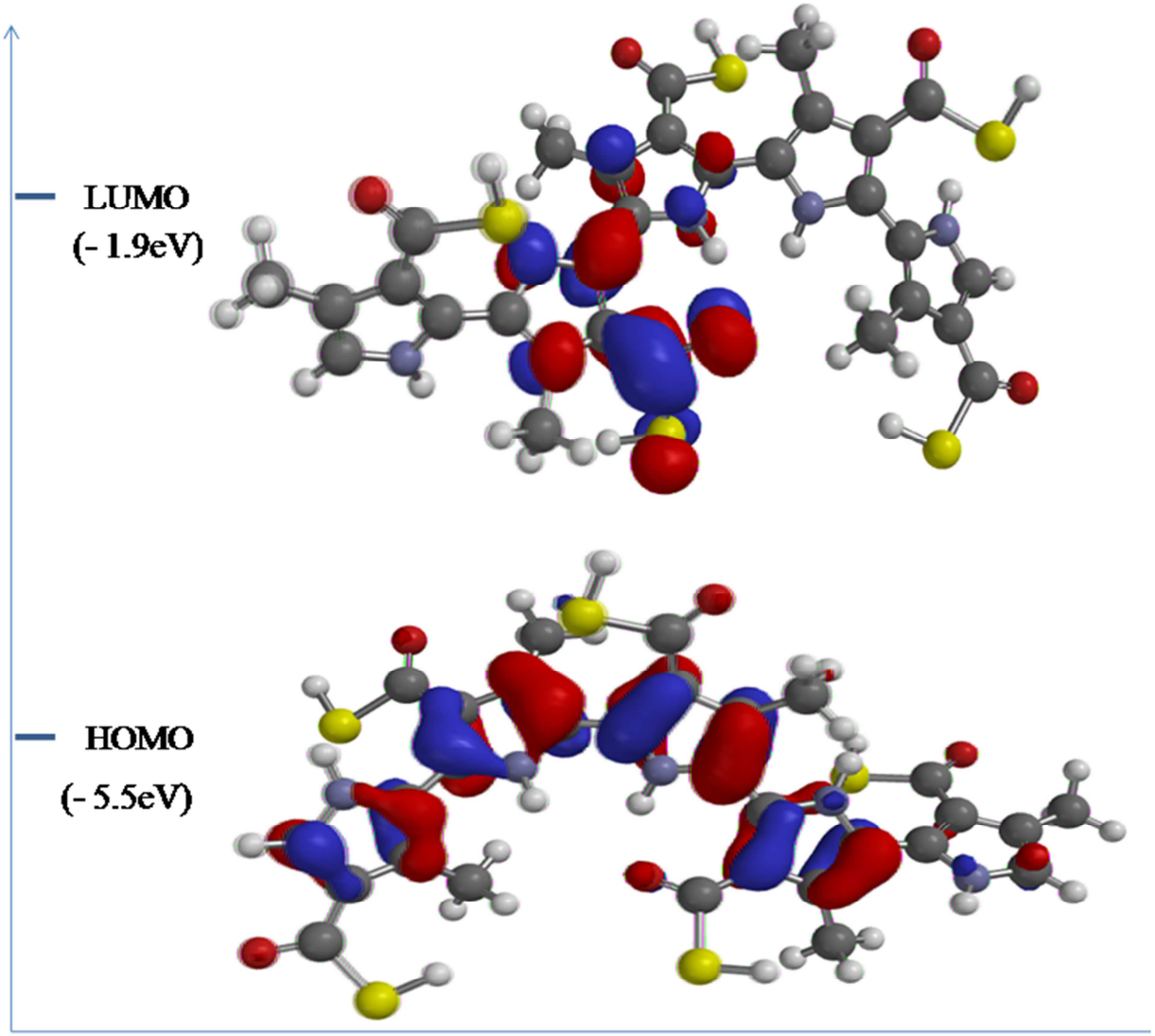

Plate 4.12. The frontier molecular orbital plot of MPCOSH

4.4.6 Molecular energies of $MPSO_3H$

Analysis of the results of IP and EA for $MPSO_3H$ in Table 4.28 shows that, all values of IPs and EA from monomers up to five repeating units are positive values. The HOMO energies range of -4.60-6.35, while LUMO energies vary from -0.95 to -2.50. As shown in Fig. 4.22, a linear relationship also exit between the direct calculated vertical HOMO energies and 1/n calculated from DFT (with a correlation coefficient r^2 = 0.99) and the direct calculated vertical LUMO energies and 1/n (with a correlation coefficient r^2 = 0.99). As seen in Plate 4.13, the LUMO; of π-nature is delocalized over the C-C bonds of the ring, while the HOMO is located over the C=C bonds.

The energy gap of five $MPSO_3H$ oligomers was extrapolated to polymer through second-degree polynomial fit equation. A decrease in energy gap from 2.9eV to 2.10eV was observed for $MPSO_3H$. This is also due to the fact that sulfonate (SO_3H) groups are moderately electron withdrawing groups as compared to amide groups (MPCam), therefore a more resonance effect is observed. This result is also comparable to earlier findings of Guimarães *et al*., 2008. Also according to Koopmans, (1933), Haddon and Fuguhata, 1980) and De-Proft and Geerlings (2004), calculated result as shown in Table 4.28-4.29 reveals that MPC^b will exhibits high reactivity, low stability, anti-aromatic behaviour and termed as a soft molecule as characterized by a lower value of band gap, μ and η when compared with pyrrole and MPCam.

Table 4.28. IPs, EAs, HOMOs, LUMOs, and Band Gaps of $MPSO_3H$ oligomers

N	EA (eV)	IP (eV)	E_{LUMO} (eV)	E_{HOMO} (eV)	Band gap (eV)
1	0.95	6.35	-0.95	-6.35	5.40
2	1.09	5.91	-1.09	-5.91	4.82
3	1.46	5.48	-1.46	-5.48	4.02
4	1.67	5.37	-1.67	-5.37	3.70
5	1.77	5.21	-1.77	-5.21	3.44
E_{gap} ($n \rightarrow \infty$)			-2.50	-4.60	2.10
R^2			0.99	0.99	

Table 4.29. Calculated molecular hardness, electrophilicity, and chemical potential of $MPSO_3H$

N	η (eV)	μ (eV)	ω (eV)
1	2.70	-3.65	2.47
2	2.41	-3.50	2.54
3	2.01	-3.47	3.0
4	1.85	-3.52	3.35
5	1.72	-3.49	3.54

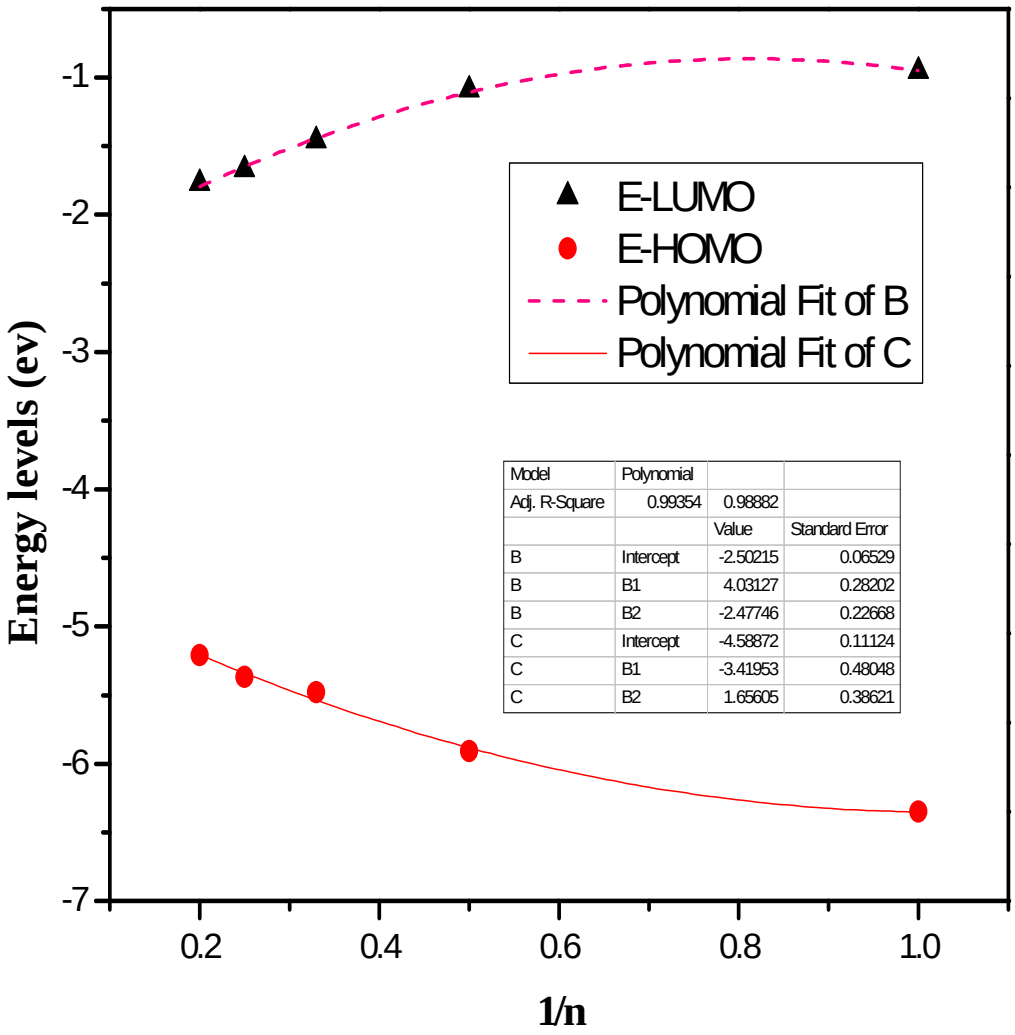

Model	Polynomial		
Adj. R-Square	0.99354	0.98882	
		Value	Standard Error
B	Intercept	-2.50215	0.06529
B	B1	4.03127	0.28202
B	B2	-2.47746	0.22668
C	Intercept	-4.58872	0.11124
C	B1	-3.41953	0.48048
C	B2	1.65605	0.38621

Fig. 4.22. Plot of HOMO, LUMO energy level against 1/n of $MPSO_3H$ oligomer

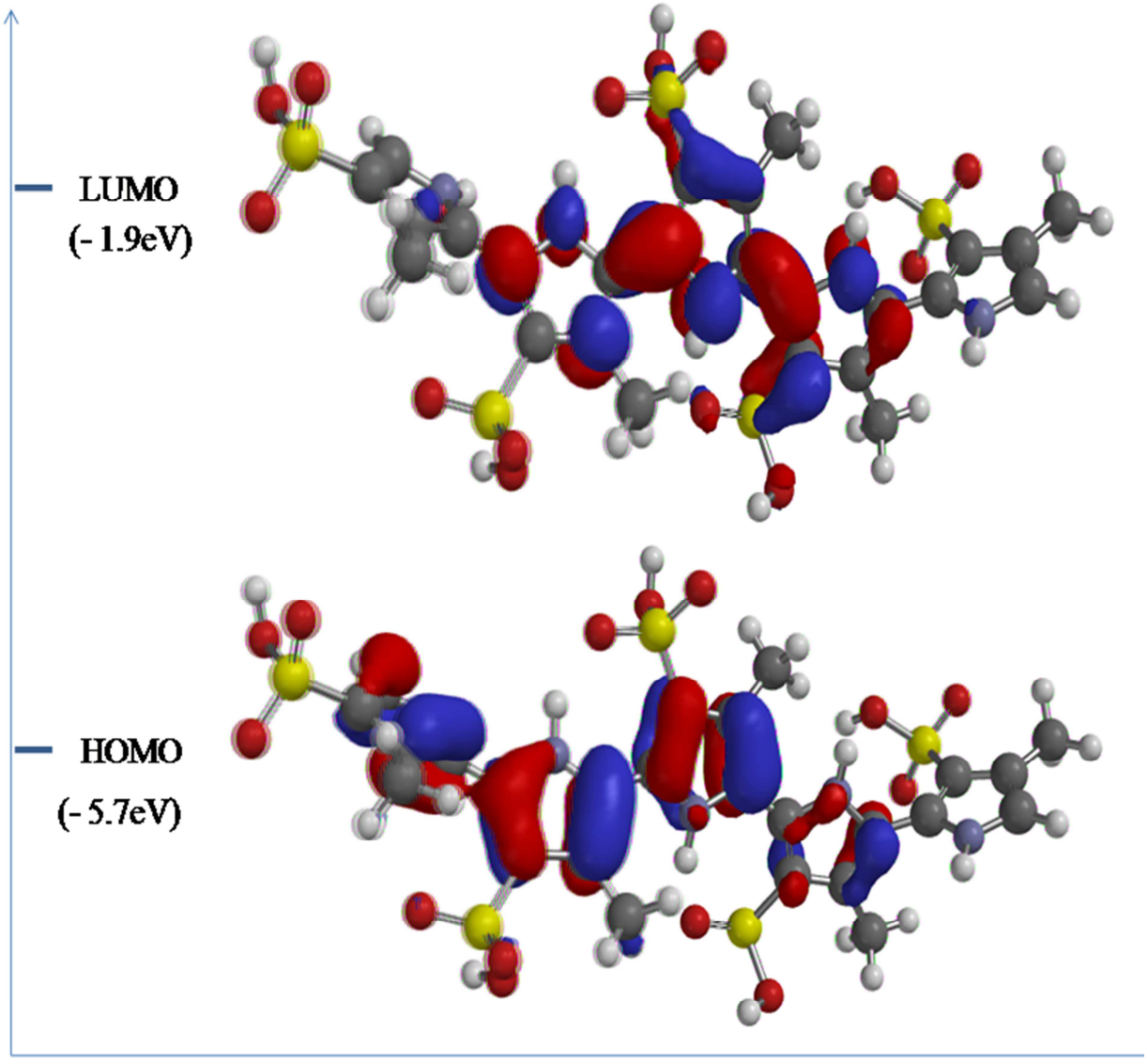

Plate 4.13. The frontier molecular orbital plot of $MPSO_3H$

4.4.7 Molecular energies of MPCHO

The results for IP and EA of MPCHO are presented in Table 4.20. Results also show that all values of IPs and EA from monomers up to five repeating units are positive values. The HOMO energies vary within the range of -4.60-6.35, while LUMO energies vary (from -0.95 to -2.50). Fig. 4.23, shows a linear relationship between the direct calculated vertical HOMO energies and 1/n calculated from DFT (with a correlation coefficient r^2 = 0.65) and the direct calculated vertical LUMO energies and 1/n calculated from DFT (with a correlation coefficient r^2 = 0.99). The LUMO extended over the C-C bonds, the nitrogen and oxygen atom, this involve delocalization over the entire molecule framework while the HOMO is located over the C=C bonds (Plate 4.14).

The energy gap of MPCHO oligomers was also extrapolated to polymer through second-degree polynomial fit equation. A slight increase in band gap of 2.9eV to 2.96eV was observed for MPCHO. According to Koopmans (1933); Haddon and Fuguhata, 1980) and De-Proft and Geerlings, (2004), MPCHO will exhibit low reactivity, high stability, aromatic behaviour and termed as a hard molecule as characterized by a higher value of band gap, μ and η as shown in Table 4.21, when compared with other modeled compounds.

Table 4.30. IPs, EAs, HOMOs, LUMOs, and Band Gaps of MPCHO oligomers

No. of Monomers	EA (eV)	IP (eV)	E_{LUMO} (eV)	E_{HOMO} (eV)	Band gap (eV)
1	0.7	6.05	-0.7	-6.05	5.38
2	1.08	5.78	-1.08	-5.78	4.7
3	1.44	5.86	-1.44	-5.86	4.42
4	1.71	5.67	-1.71	-5.67	3.96
5	1.91	5.71	-1.91	-5.71	3.80
E_{gap} ($n \rightarrow \infty$)			-2.69	-5.65	2.96
R^2			0.99	0.65	

Table 4.31. Calculated molecular hardness, electrophilicity, and chemical potential of MPCHO

No. of Monomers	η (eV)	μ (eV)	ω (eV)
1	2.69	-3.38	2.12
2	2.35	-3.43	2.50
3	2.21	-3.65	3.01
4	1.98	-3.69	3.44
5	1.90	-3.81	3.82

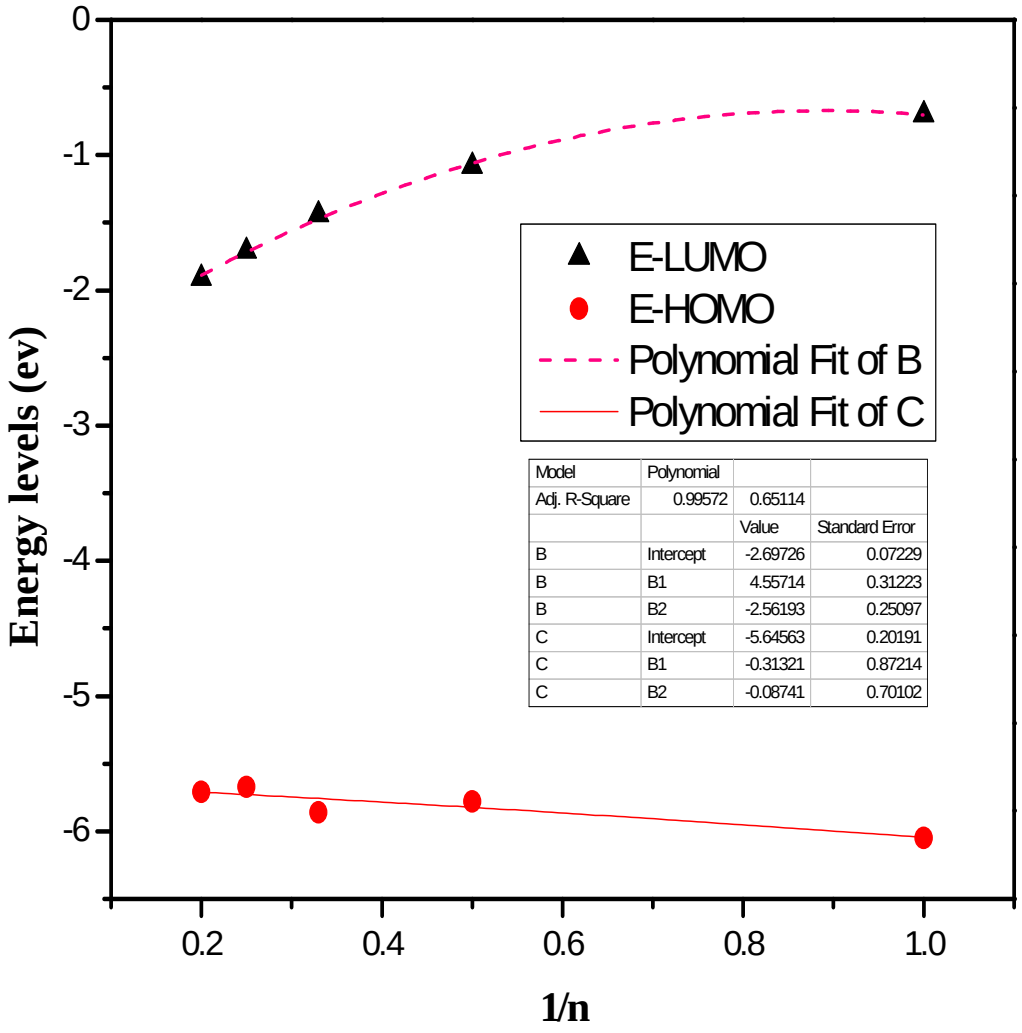

Model	Polynomial		
Adj. R-Square	0.99572	0.65114	
		Value	Standard Error
B	Intercept	-2.69726	0.07229
B	B1	4.55714	0.31223
B	B2	-2.56193	0.25097
C	Intercept	-5.64563	0.20191
C	B1	-0.31321	0.87214
C	B2	-0.08741	0.70102

Fig. 4.23. Plot of HOMO, LUMO energy level against 1/n of MPCHO oligomer

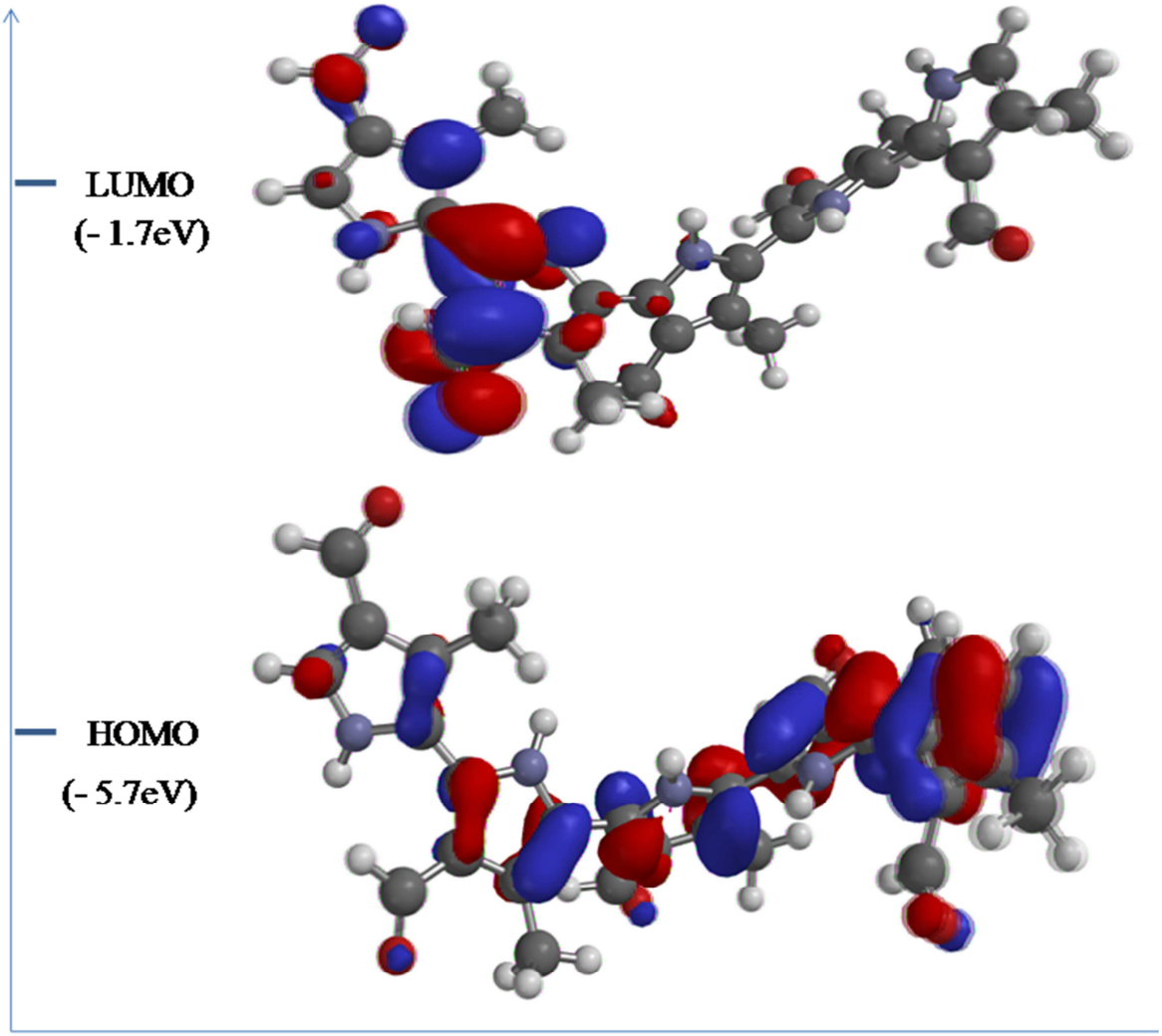

Plate 4.14. The frontier molecular orbital plot of MPCHO

4.5 Electronic absorption properties

The extent of absorption of a new material determines how it can orient the protein and enable electron transfer. This is an important factor for the application as a biosensor device. A good biosensor material should have broad and strong visible absorption characteristics (Liu *et al*., 2001).

On the basis of the optimized ground-state structures, we present in Table 4.32 the vertical excitation energy E_{ex} (eV), calculated absorption λ_{max} (nm) and oscillator strength (O.S) along with main excitation configuration of the oligomers. These values are calculated by TD-DFT method starting with optimized geometry B3LYP/6-31G(d) level.

4.5.1 Electronic absorption properties of pyrrole

The simulated absorption spectrum of pyrrole is presented in Plate 4.15. The calculated wavelength λ_{max} (nm) increases as the number of ring increases. The largest oscillator strengths (O.S) originate from $S_0 \rightarrow S_1$ electronic transition. Excitation to S_1 state corresponds exclusively to the promotion of an electron from the HOMO to the LUMO. As in the case of the oscillator strength, the absorption wavelength arising from $S_0 \rightarrow S_1$ electronic transition increases progressively with the increase in the conjugation. As seen in Table 4.32, the bands assigned at 190.59, 239.29, 279.44, 306.27, and 329.52 (nm) which is in agreement with the experimental values as obtained by Heeralal and Krishamurthi, (2014) (Appendices). These corresponds to the HOMO-LUMO transition and is of ICT (intramolecular charge transfer) character thus possessing averagely high transition intensity.

Table 4.32. Calculated electronic transition data for pyrrole

No. of Monomers	Electronic transition	λmax (nm)	E(exc) (ev)	O.S	MO/Character	Coefficient
1	$S_0 \rightarrow S_1$	190.59	6.51	0.00	HOMO → LUMO	0.99
	$S_0 \rightarrow S_2$	180.87	6.86	0.004	HOMO → LUMO+1	0.65
	$S_0 \rightarrow S_3$	172.98	7.17	0.194	HOMO → LUMO-1	0.94
2	$S_0 \rightarrow S_1$	239.29	5.18	0.693	HOMO → LUMO	0.97
	$S_0 \rightarrow S_2$	221.37	5.60	0.0001	HOMO → LUMO+1	0.89
	$S_0 \rightarrow S_3$	211.52	5.86	0.0009	HOMO-1 → LUMO	0.64
3	$S_0 \rightarrow S_1$	279.44	4.44	0.9818	HOMO → LUMO	0.99
	$S_0 \rightarrow S_2$	253.12	4.90	0.0092	HOMO → LUMO+1	0.81
	$S_0 \rightarrow S_3$	238.99	5.19	0.0014	HOMO → LUMO+2	0.93
4	$S_0 \rightarrow S_1$	306.27	4.05	1.0534	HOMO → LUMO	0.99
	$S_0 \rightarrow S_2$	277.90	4.46	0.0142	HOMO → LUMO+1	0.78
	$S_0 \rightarrow S_3$	251.79	4.92	0.0238	HOMO → LUMO+3	0.89
5	$S_0 \rightarrow S_1$	352.76	3.76	0.9379	HOMO → LUMO	0.99
	$S_0 \rightarrow S_2$	308.91	4.17	0.0373	HOMO → LUMO+1	0.76
	$S_0 \rightarrow S_3$	284.61	4.62	0.4973	HOMO-1 → LUMO	0.67

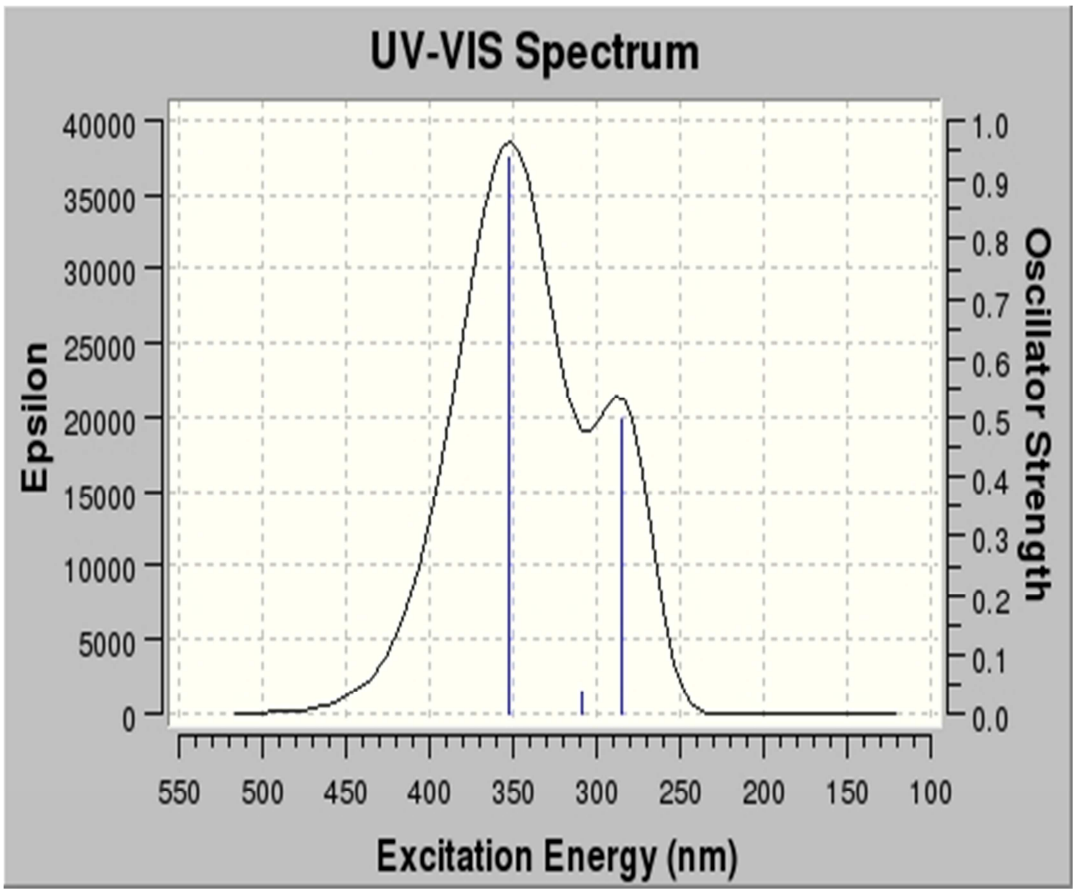

Plate 4.15. Calculated UV-VIS spectrum of pyrrole

4.5.2 Electronic absorption properties of MPC[a]

The simulated absorption spectrum of MPC[a] is presented in Plate 4.16. The calculated wavelength λ_{max} (nm) also increases as the number of ring increases. The largest oscillator strengths (O.S) also originate from $S_0 \rightarrow S_1$ electronic transition. Excitation to S_1 state corresponds exclusively to the promotion of an electron from the HOMO to the LUMO. As in the case of the oscillator strength, the absorption wavelength arising from $S_0 \rightarrow S_1$ electronic transition increases progressively with the increase in the conjugation. As seen in Table 4.33, the bands assigned at 235.05, 276.55, 317.70, 345.36, and 376.51 (nm) correspond to the HOMO-LUMO transition and is of ICT (intramolecular charge transfer) character, thus, possessing higher transition intensity. Also it is has been established that organic molecules (including biological molecules and conjugated molecules) have a strong triplet-triplet transition (Liu *et al*., 2001; Gerber *et al*., 1994). For two, three, four and five rings MPC[a] the singlet-singlet transition basically involves four (|H>, |H-1>, |L>and |L+1>) but preliminary calculations of spectra show an increase of the transition levels which can be used to orient the molecule and enable electron transfer.

Table 4.33. Calculated electronic transition data for MPC[a]

No. of Monomers	Electronic transition	λmax (nm)	E(exc) (ev)	O.S	MO/Character	Coefficient
1	$S_0 \rightarrow S_1$	235.05	5.28	0.0455	HOMO → LUMO	0.31
	$S_0 \rightarrow S_2$	233.76	5.30	0.0003	HOMO-1 → LUMO	0.99
	$S_0 \rightarrow S_3$	200.24	6.19	0.2639	HOMO → LUMO	0.89
2	$S_0 \rightarrow S_1$	276.55	4.48	0.4035	HOMO → LUMO	0.97
	$S_0 \rightarrow S_2$	268.21	4.62	0.0405	HOMO → LUMO+1	0.96
	$S_0 \rightarrow S_3$	251.66	4.93	0.0047	HOMO-1 → LUMO	0.65
3	$S_0 \rightarrow S_1$	317.70	3.90	0.4236	HOMO → LUMO	0.981
	$S_0 \rightarrow S_2$	290.57	4.27	0.2339	HOMO-1 → LUMO	0.23
	$S_0 \rightarrow S_3$	276.21	4.49	0.0286	HOMO → LUMO+2	0.97
4	$S_0 \rightarrow S_1$	345.36	3.59	0.4789	HOMO → LUMO	0.98
	$S_0 \rightarrow S_2$	320.70	3.87	0.3947	HOMO → LUMO+1	0.95
	$S_0 \rightarrow S_3$	303.01	4.09	0.1178	HOMO → LUMO+2	0.95
5	$S_0 \rightarrow S_1$	380.51	3.29	0.7449	HOMO → LUMO	0.97
	$S_0 \rightarrow S_2$	353.42	3.51	0.0698	HOMO → LUMO+1	0.96
	$S_0 \rightarrow S_3$	345.94	3.58	0.0627	HOMO → LUMO+2	0.96

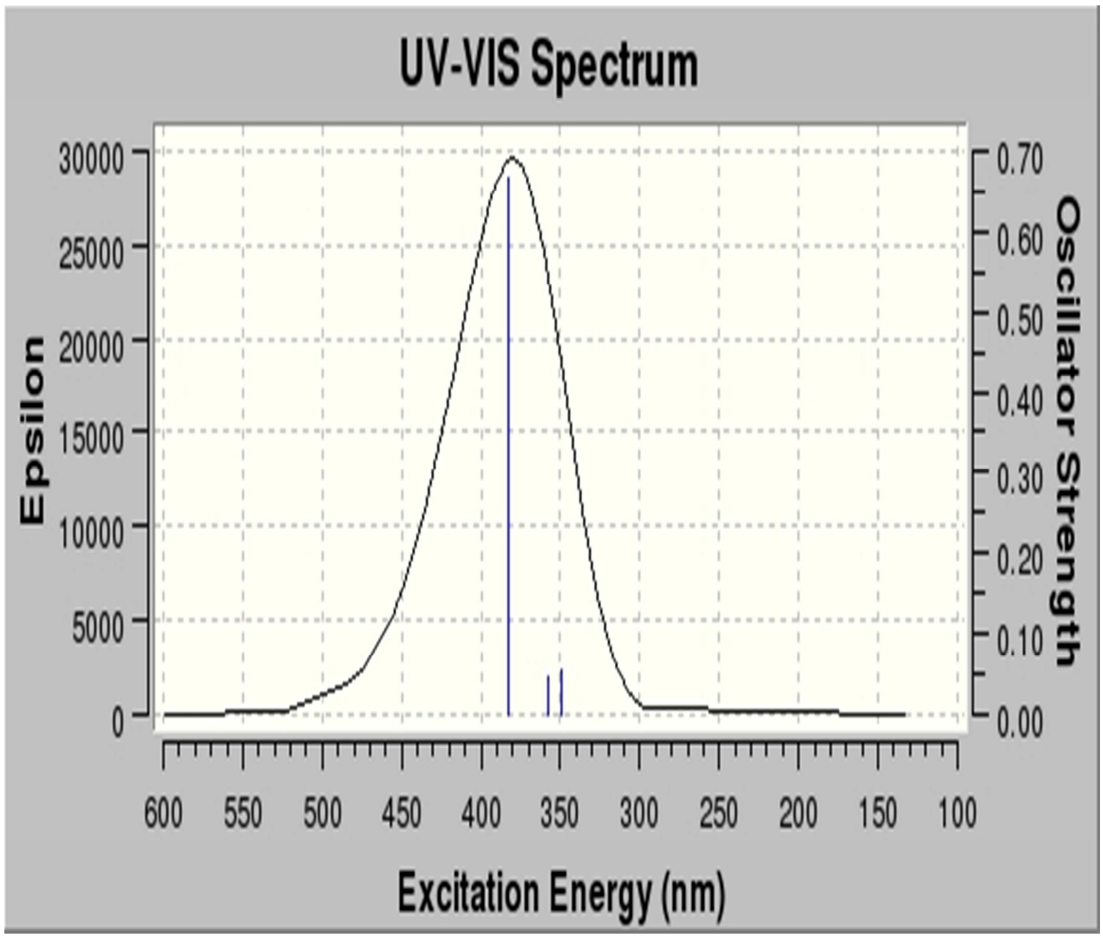

Plate 4.16. Calculated UV-VIS spectrum of MPC[a] (Pentamer)

4.5.3 Electronic absorption properties of MPC^b

The simulated absorption spectrum of MPC^b is presented in Plate 4.17. The calculated wavelength λ_{max} (nm) also increases as the number of ring increases. The largest oscillator strengths (O.S) also originate from $S_0 \rightarrow S_1$ electronic transition. As in the case of the oscillator strength, the absorption wavelength arising from $S_0 \rightarrow S_1$ electronic transition increases progressively with the increase in the conjugation. As seen in Table 4.33, the bands assigned at 236.02, 295.04, 330.59, 337.58, and 372.80 (nm) correspond to the HOMO-LUMO transition and is of ICT (intramolecular charge transfer) character In comparison with the maximum absorption of (MPC^a) (376.51nm), there is a difference about 3.71 nm for (MPC^b) (372.80 nm), which is attributed to the lower ICT. The singlet-singlet transition for three, four and five rings MPC^b basically involves four (|H>, |H-1>, |L>and |L+1>).

4.5.4 Absorption properties of MPCam

The absorption spectrum of studied compounds as seen in Plate 4.18 reveals that the largest oscillator strength and absorption wavelength also originates from $S_0 \rightarrow S_1$ electronic transition, these increases progressively with the increase in the conjugation. As shown in Table 4.34, the HOMO-LUMO transition bands are 251.55, 300.40, 312.63, 365.67, and 372.47 nm. In comparison with the maximum absorption of (MPC^a) (376.51nm), there is a difference about 4.04 nm for (MPCam) (372.47 nm), which is attributed to the low ICT. However, transition distributions have shown that in all cases for MPCam the |H>orbital contains significant contributions to the spectra.

Table 4.34. Calculated electronic transition data for MPC[b]

No. of monomers	Electronic transition	λmax (nm)	O.S	MO/Character	Coefficient
1	$S_0 \rightarrow S_1$	236.02	0.0428	HOMO → LUMO	0.95
	$S_0 \rightarrow S_2$	212.26	0.0717	HOMO-2 → LUMO	0.72
	$S_0 \rightarrow S_3$	205.65	0.0991	HOMO → LUMO	0.65
2	$S_0 \rightarrow S_1$	295.04	0.1190	HOMO → LUMO	0.99
	$S_0 \rightarrow S_2$	265.72	0.0498	HOMO-1 → LUMO	0.35
	$S_0 \rightarrow S_3$	237.96	0.0324	HOMO-1 → LUMO	0.86
3	$S_0 \rightarrow S_1$	330.59	0.2110	HOMO → LUMO	0.99
	$S_0 \rightarrow S_2$	292.54	0.0493	HOMO → LUMO+1	0.92
	$S_0 \rightarrow S_3$	280.34	0.1084	HOMO-1 → LUMO	0.90
4	$S_0 \rightarrow S_1$	337.58	0.2465	HOMO → LUMO	0.87
	$S_0 \rightarrow S_2$	326.16	0.0139	HOMO-1 → LUMO	0.85
	$S_0 \rightarrow S_3$	303.91	0.0552	HOMO → LUMO+1	0.88
5	$S_0 \rightarrow S_1$	408.87	0.1508	HOMO → LUMO	0.95
	$S_0 \rightarrow S_2$	371.07	0.0927	HOMO-1 → LUMO	0.95
	$S_0 \rightarrow S_3$	361.81	0.0941	HOMO → LUMO+2	0.92

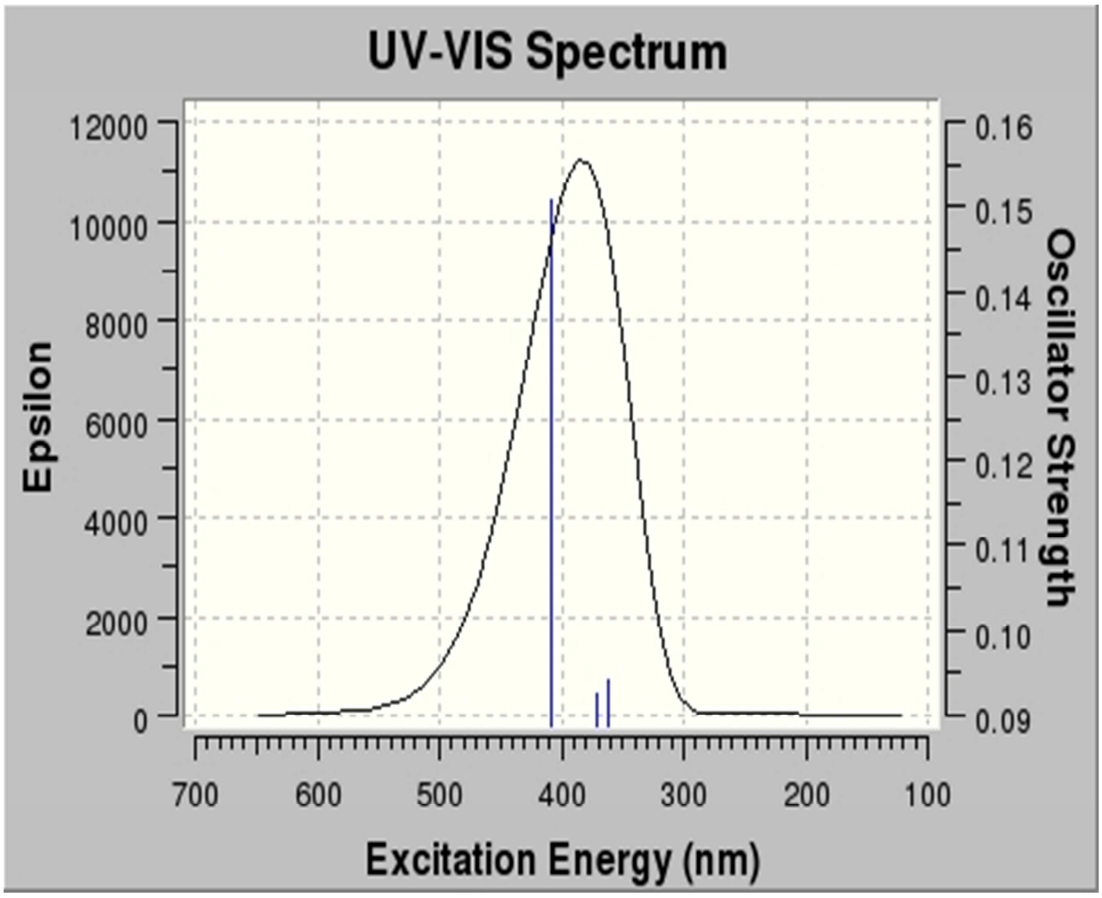

Plate 4.17. Calculated UV-VIS spectrum of MPC[b] (Pentamer)

Table 4.35. Calculated electronic transition data for MPCam

No. of Monomers	Electronic transition	λmax (nm)	E*exc* (ev)	O.S	MO/Character	Coefficient
1	$S_0 \rightarrow S_1$	251.55	4.93	0.0012	HOMO → LUMO	0.77
	$S_0 \rightarrow S_2$	232.49	5.33	0.0376	HOMO+1 → LUMO	0.92
	$S_0 \rightarrow S_3$	203.50	6.10	0.2019	HOMO-1 → LUMO	0.75
2	$S_0 \rightarrow S_1$	300.40	4.13	0.4614	HOMO → LUMO	0.97
	$S_0 \rightarrow S_2$	274.03	4.53	0.0177	HOMO → LUMO+1	0.94
	$S_0 \rightarrow S_3$	263.01	4.71	0.0041	HOMO-4 → LUMO	0.75
3	$S_0 \rightarrow S_1$	312.63	3.97	0.5506	HOMO → LUMO	0.97
	$S_0 \rightarrow S_2$	294.74	4.21	0.1948	HOMO → LUMO+1	0.98
	$S_0 \rightarrow S_3$	269.29	4.60	0.0595	HOMO-1 → LUMO	0.67
4	$S_0 \rightarrow S_1$	365.67	3.39	0.6315	HOMO → LUMO	0.99
	$S_0 \rightarrow S_2$	334.87	3.70	0.2365	HOMO-1 → LUMO	0.91
	$S_0 \rightarrow S_3$	323.22	3.84	0.1734	HOMO → LUMO+1	0.91
5	$S_0 \rightarrow S_1$	380.63	3.33	0.9062	HOMO → LUMO	0.98
	$S_0 \rightarrow S_2$	347.85	3.60	0.0334	HOMO → LUMO+1	0.78
	$S_0 \rightarrow S_3$	344.46	3.66	0.1027	HOMO → LUMO+3	0.75

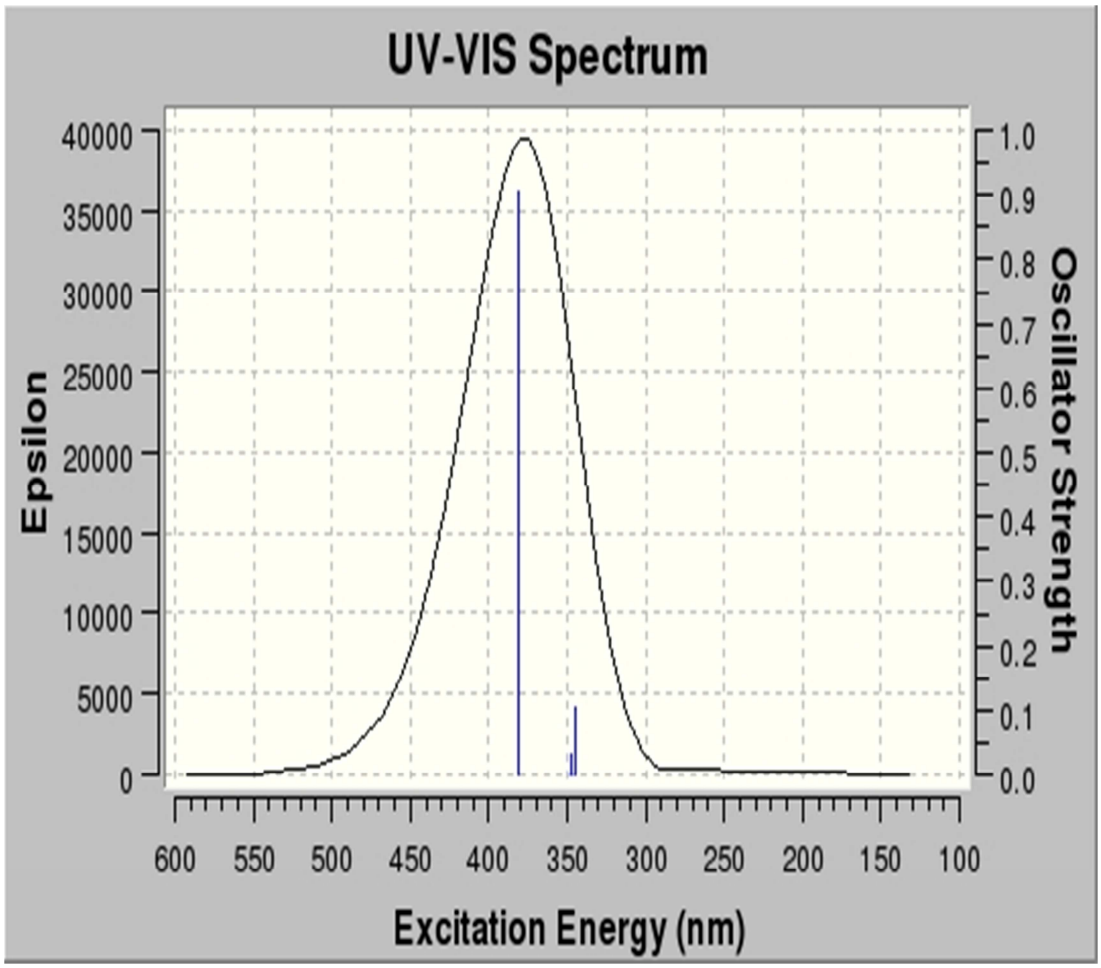

Plate 4.18. Calculated UV-VIS spectrum of MPCam (Pentamer)

4.5.5 Electronic absorption properties of MPCOSH

The calculated wavelength λ_{max} (nm) increases as the number of ring increases. The largest oscillator strengths (O.S) also originate from $S_0 \rightarrow S_1$ electronic transition, except for the monomer form which is forbidden. Excitation to S_1 state also corresponds to the promotion of an electron from the HOMO to the LUMO. The oscillator strength and the absorption wavelength arising from $S_0 \rightarrow S_1$ electronic transition; increases progressively with the increase in the conjugation as shown in Plate 4.19. As seen in Table 4.33, the bands assigned at 277.94, 319.80, 329.27, 367.28, and 395.05 (nm) corresponds to the HOMO-LUMO transition and is of ICT (intramolecular charge transfer) character. However, transition distributions have shown that in all cases for MPCam the |H>orbital contains significant contributions to the spectra. For MPC structures the most important absorption lines corresponds to different possible transitions, (|H, $\rightarrow$ L), |H-5 $\rightarrow$ L), |H L+2), |H-5 $\rightarrow$ L+1). In comparison with the maximum absorption of (MPC[a]) (376.51 nm), there is a difference about 18.54 nm for MPCOSH (395.05 nm), which is attributed to the stronger ICT.

Table 4.36. Calculated electronic transition data for MPCOSH

No. of Monomers	Electronic transition	λmax (nm)	E*exc* (ev)	O.S	MO/Character	Coefficient
1	$S_0 \rightarrow S_1$	276.94	4.48	0.0003	HOMO → LUMO	0.67
	$S_0 \rightarrow S_2$	249.83	4.96	0.0515	HOMO+2 → LUMO	0.91
	$S_0 \rightarrow S_3$	229.38	5.41	0.1383	HOMO+1 → LUMO	0.74
2	$S_0 \rightarrow S_1$	319.80	3.88	0.2184	HOMO → LUMO	0.91
	$S_0 \rightarrow S_2$	284.14	4.36	0.0820	HOMO-2 → LUMO	0.52
	$S_0 \rightarrow S_3$	279.20	4.44	0.0218	HOMO-4 → LUMO	0.31
3	$S_0 \rightarrow S_1$	329.27	3.77	0.3555	HOMO → LUMO	0.98
	$S_0 \rightarrow S_2$	318.83	3.89	0.1089	HOMO → LUMO+1	0.97
	$S_0 \rightarrow S_3$	290.40	4.27	0.0005	HOMO-5 → LUMO+1	0.67
4	$S_0 \rightarrow S_1$	367.28	3.38	0.2679	HOMO → LUMO	0.98
	$S_0 \rightarrow S_2$	332.77	3.37	0.2381	HOMO-1 → LUMO	0.88
	$S_0 \rightarrow S_3$	326.78	3.79	0.0559	HOMO → LUMO+2	0.89
5	$S_0 \rightarrow S_1$	402.63	3.14	0.1830	HOMO → LUMO	0.99
	$S_0 \rightarrow S_2$	365.21	3.42	0.2602	HOMO → LUMO+1	0.98
	$S_0 \rightarrow S_3$	349.24	3.61	0.1931	HOMO → LUMO+2	0.93

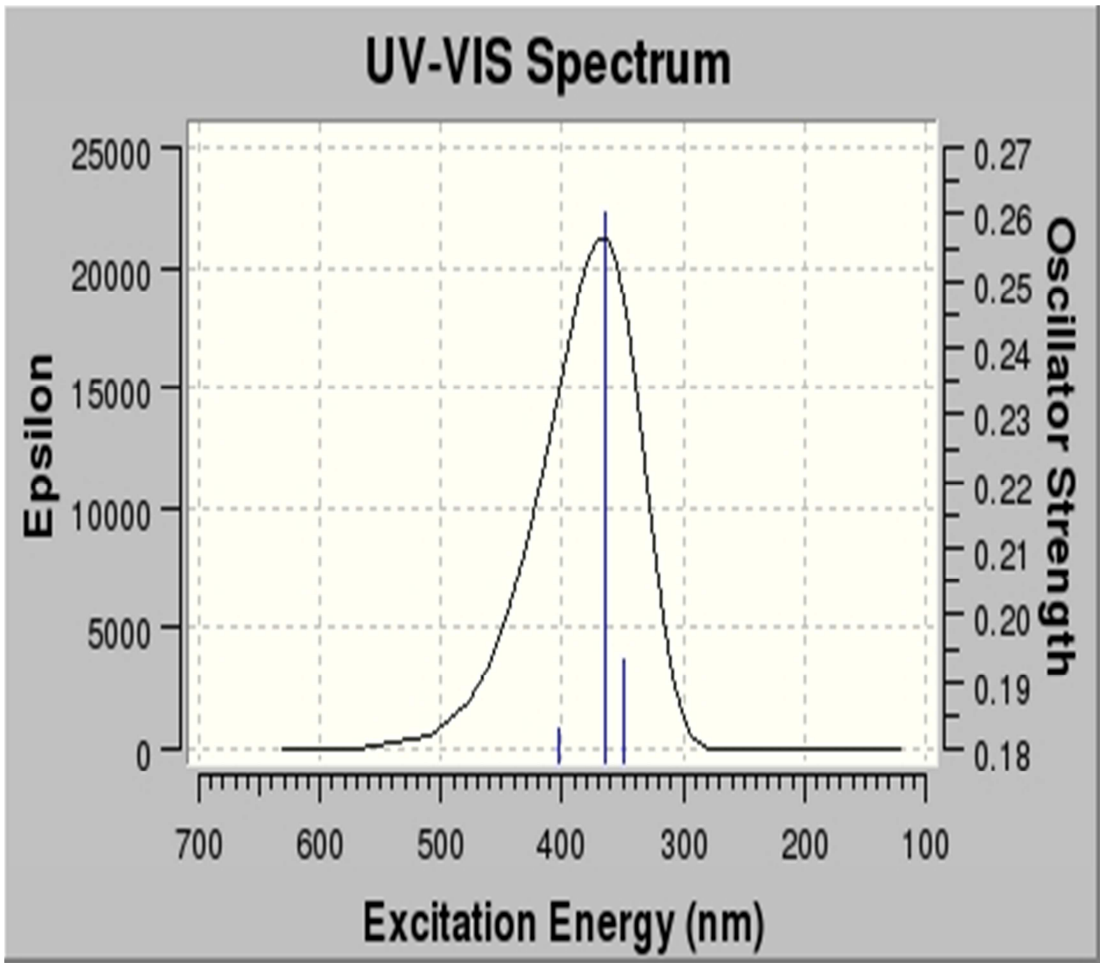

Plate 4.19. Calculated UV-VIS spectrum of MPCOSH

4.5.6 Electronic absorption properties of $MPSO_3H$

The simulated absorption spectrum of $MPSO_3H$ is presented in Plate 4.20. The calculated wavelength λ_{max} (nm) also increases as the number of ring increases. The largest oscillator strengths (O.S) also originate from $S_0 \rightarrow S_1$ electronic transition. As in the case of the oscillator strength, the absorption wavelength arising from $S_0 \rightarrow S_1$ electronic transition increases progressively with the increase in the conjugation. As seen in Table 4.37, the bands assigned at 199.86, 273.55, 308.94, 313.17, and 337.30 (nm) corresponds to the HOMO-LUMO transition and is of ICT (intramolecular charge transfer) character In comparison with the maximum absorption of (MPC^a) (376.51 nm), there is a difference about 39.21 nm for $MPSO_3H$ (337.30 nm), which is attributed to the lower ICT than other modeled compounds.

Table 4.37. Calculated electronic transition data of $MPSO_3H$

No. of Monomers	Electronic transition	λmax (nm)	E*exc* (ev)	O.S	MO/Character	Coefficient
1	$S_0 \rightarrow S_1$	199.86	6.20	0.0334	HOMO → LUMO	0.72
	$S_0 \rightarrow S_2$	191.78	6.47	0.0116	HOMO → LUMO+2	0.70
	$S_0 \rightarrow S_3$	185.26	6.69	0.0185	HOMO → LUMO+4	0.79
2	$S_0 \rightarrow S_1$	273.55	4.53	0.5933	HOMO → LUMO	4.53
	$S_0 \rightarrow S_2$	232.22	5.34	0.0029	HOMO-1 → LUMO	0.76
	$S_0 \rightarrow S_3$	219.59	5.64	0.0324	HOMO-2 → LUMO	0.72
3	$S_0 \rightarrow S_1$	308.94	4.01	0.7293	HOMO → LUMO	0.98
	$S_0 \rightarrow S_2$	284.36	4.36	0.1941	HOMO → LUMO+1	0.93
	$S_0 \rightarrow S_3$	244.44	5.07	0.1535	HOMO-1 → LUMO	0.77
4	$S_0 \rightarrow S_1$	313.17	3.96	0.8515	HOMO → LUMO	0.97
	$S_0 \rightarrow S_2$	283.82	4.37	0.2157	HOMO-1 → LUMO	0.91
	$S_0 \rightarrow S_3$	279.04	4.44	0.0135	HOMO → LUMO+2	0.95
5	$S_0 \rightarrow S_1$	345.78	3.68	0.821	HOMO → LUMO	0.98
	$S_0 \rightarrow S_2$	306.81	4.11	0.0772	HOMO → LUMO+1	0.97
	$S_0 \rightarrow S_3$	288.39	4.35	0.1365	HOMO → LUMO+2	0.75

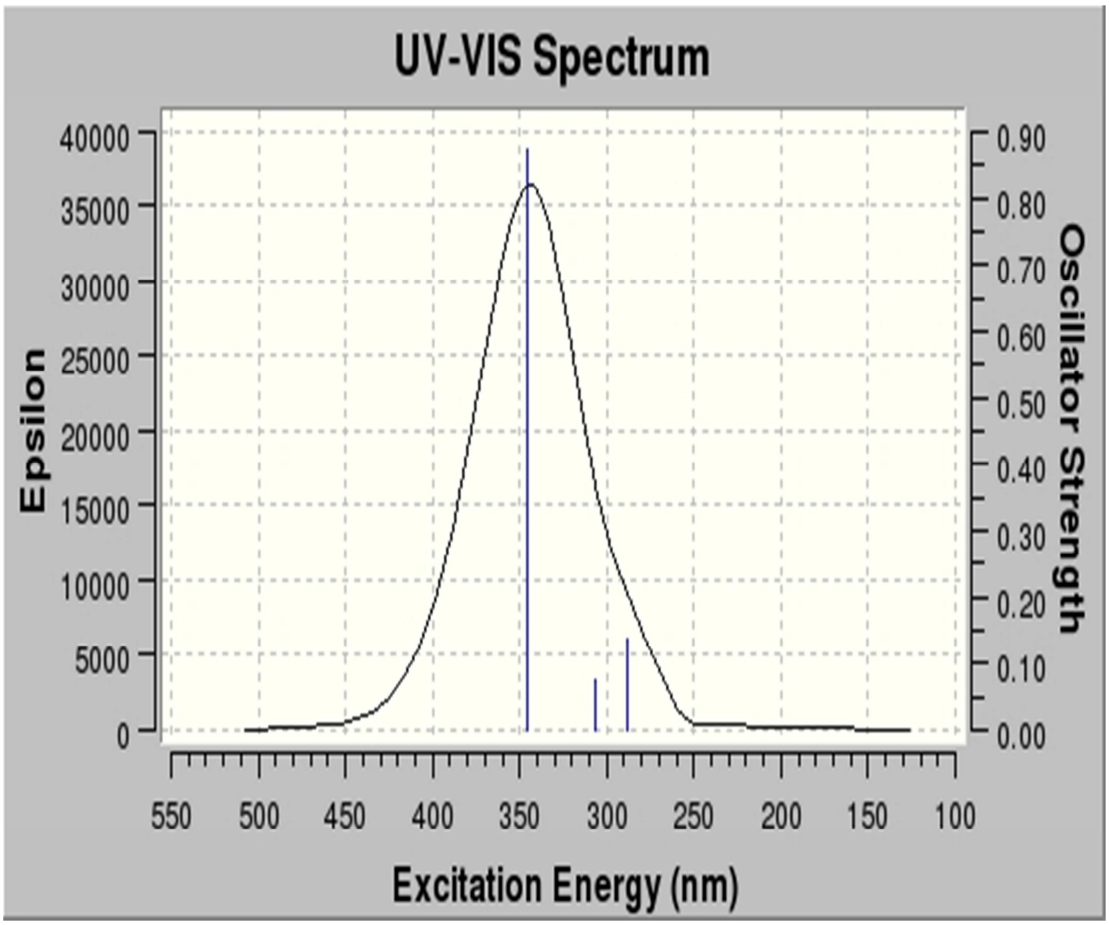

Plate 4.20. Calculated UV-VIS spectrum of $MPSO_3H$ (Pentamer)

4.5.7 Electronic absorption properties of MPCHO

The calculated wavelength λ_{max} (nm) increases as the number of ring increases. The largest oscillator strengths (O.S) also originate from $S_0 \rightarrow S_1$ electronic transition. Excitation to S_1 state also corresponds to the promotion of an electron from the HOMO to the LUMO. The oscillator strength and the absorption wavelength arising from $S_0 \rightarrow S_1$ electronic transition; increases progressively with the increase in the conjugation as shown in Plate 4.21. As seen in Table 4.38, the bands assigned at 308.60, 324.40, 326.10, 327.50, and 345.50 (nm) corresponds to the HOMO-LUMO transition and is of ICT (intramolecular charge transfer) character.

Table 4.38. Calculated electronic transition data for MPCHO

No. of Monomers	Electronic transition	λmax (nm)	E*exc* (ev)	O.S	MO/Character	Coefficient
1	$S_0 \rightarrow S_1$	308.60	4.02	0.00	HOMO → LUMO	0.99
	$S_0 \rightarrow S_2$	253.90	4.88	0.381	HOMO+1 → LUMO	0.91
	$S_0 \rightarrow S_3$	206.20	6.01	0.372	HOMO-1 → LUMO	0.88
2	$S_0 \rightarrow S_1$	324.40	3.82	0.0115	HOMO → LUMO	0.86
	$S_0 \rightarrow S_2$	311.60	3.98	0.0002	HOMO-1 → LUMO	0.91
	$S_0 \rightarrow S_3$	291.00	4.26	0.1634	HOMO+1 → LUMO	0.86
3	$S_0 \rightarrow S_1$	326.10	3.80	0.0440	HOMO → LUMO	0.94
	$S_0 \rightarrow S_2$	325.30	3.81	0.0046	HOMO-1 → LUMO	0.35
	$S_0 \rightarrow S_3$	312.20	3.97	0.0010	HOMO-2 → LUMO+1	0.94
4	$S_0 \rightarrow S_1$	327.50	3.77	0.0705	HOMO → LUMO	0.38
	$S_0 \rightarrow S_2$	325.60	3.81	0.0062	HOMO+1 → LUMO+1	0.31
	$S_0 \rightarrow S_3$	325.30	3.81	0.0162	HOMO+2 → LUMO+1	0.32
5	$S_0 \rightarrow S_1$	345.50	3.59	0.224	HOMO → LUMO	0.92
	$S_0 \rightarrow S_2$	336.90	3.68	0.2977	HOMO → LUMO+1	0.79
	$S_0 \rightarrow S_3$	329.00	3.77	0.0233	HOMO → LUMO+3	0.47

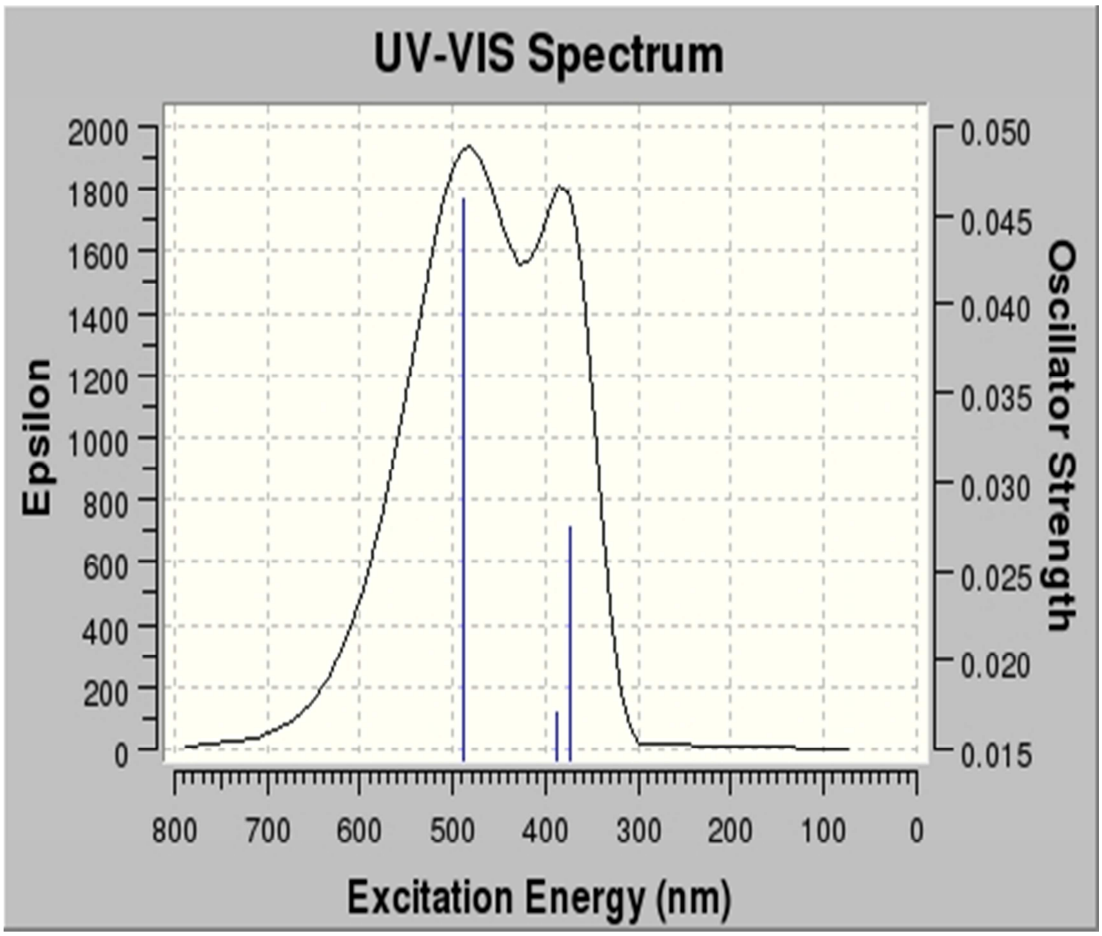

Plate 4.21. Calculated UV-vis spectrum of MPCHO (Pentamer)

4.6 The nature of the ground and excited state Properties

The nature of the ground state properties of pyrrole and MPC has been studied using DFT approach. Inorder to ascertain if the ground state is dominated by non dynamic (static) correlation (arising from near-degeneracies among electronic configuaration) or dynamic correlarion (arising from coulomb repulsion), T1 diagnostics and Natural bond orbital (Hajgató, 2009) coupled cluster tool was carried out. T1 diagnostics (< 0.02) indicates that the system is single reference (closed shell), while (>0.02) indicates that the system is multireference in nature (open shell).

An easy way to ascertain whether there are unpaired electrons in a correlated wave function is to examine the occupation numbers of the spinless natural orbitals; in a closed-shell configuration, these are always 2 doubly occupied or 0 unoccupied, while values close to 1 indicate single occupancy and unpaired electrons (Hachmann *et al*., 2007). In Fig. 4.24 and Fig. 4.25 we have plotted the occupancies of the natural orbitals for the studied systems. We have designated the two orbitals with occupancies closest to 1 the highest occupied natural orbital HONO with occupancy greater than 1 and lowest unoccupied natural orbital LUNO with occupancy less than 1, respectively.

These natural orbitals together with usual highest occupied molecular orbital HOMO and lowest unoccupied molecular orbital LUMO are shown in Fig. 4.38 and Fig. 4.39. The result shows that poly pyrrole is a single reference (dynamic correlation), closed shell system while other studied systems are multireference (static correlation), open shell in natureas seen in Table 4.39.

Table 4.39. T1 diagnostics for studied systems

No of monomers	Pyrrole	MPC[a]	MPC[b]	MPCAM	MPCOSH	$MPSO_4H$	MPCHO
1	0.002	0.011	0.011	0.020	0.010	0.017	0.010
2	0.004	0.022	0.023	0.021	0.011	0.023	0.026
3	0.007	0.034	0.044	0.032	0.030	0.039	0.037
4	0.008	0.045	0.047	0.040	0.037	0.049	0.044
5	0.013	0.060	0.053	0.062	0.042	0.070	0.066

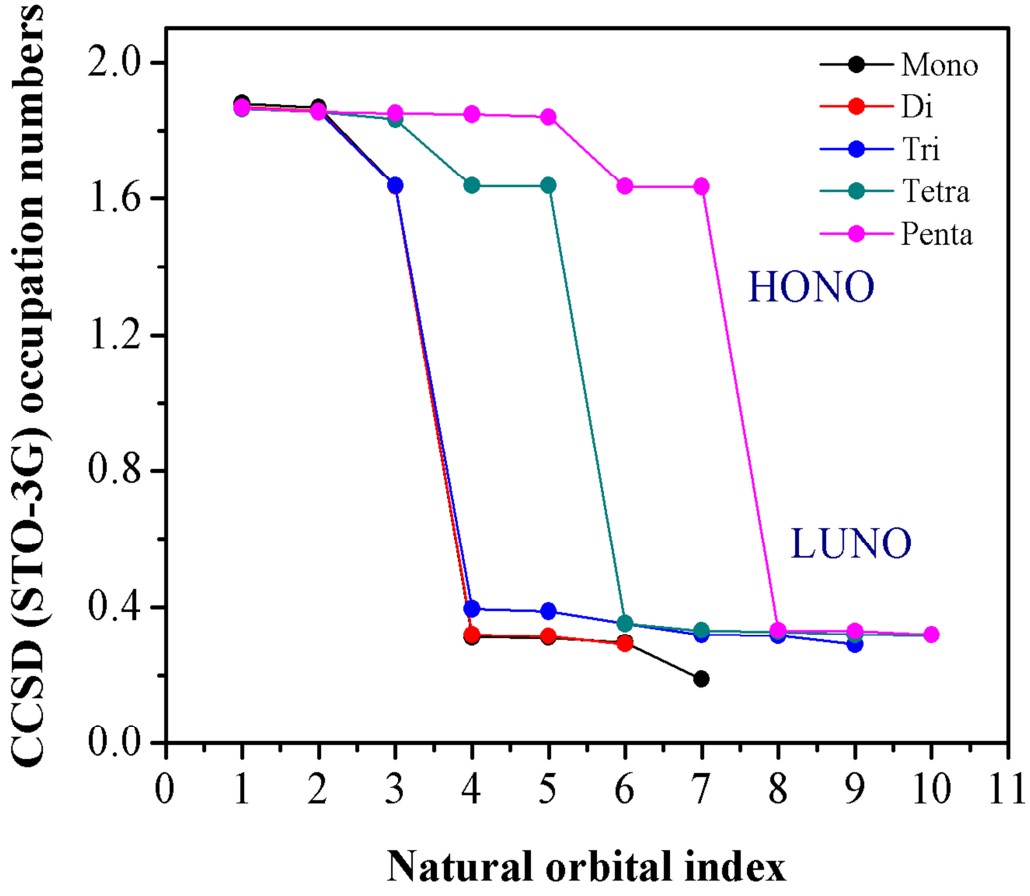

Fig. 4.24. Natural orbital occupation numbers for the doubly occupied orbitals of Unsubstituted Pyrrole as a function of chain length

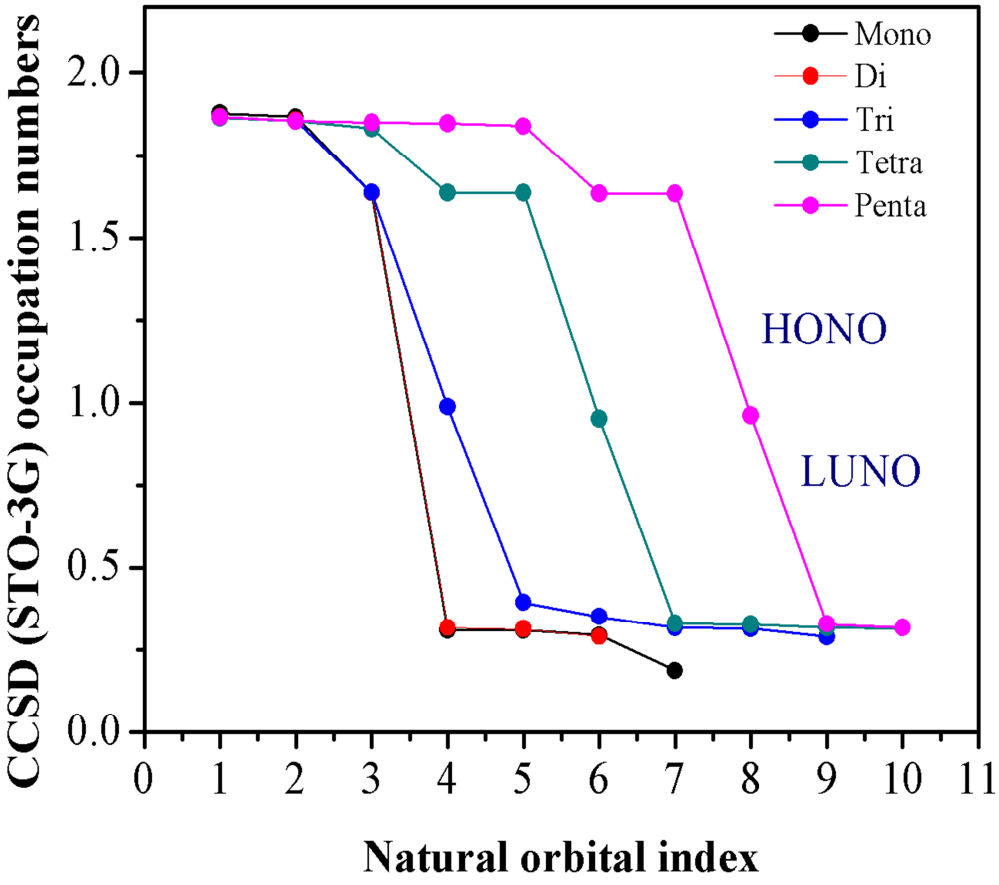

Fig. 4.25. Natural orbital occupation numbers for the near singly occupied orbitals of Substituted Pyrroles as a function of chain length

4.7 Vertical Singlet-triplet gap and First excited state Dipole moment

In order to accurately determine the nature of ground state of studied systems, the vertical singlet-triplet gap of systems were studied using SF-TDDFT. Also to establish the possibility of intermolecular charge transfer the first excited dipole moments were determined.

Result in table 4.40 shows that all studied systems have a singlet ground state, based on the fact that there is no cross over in the singlet-triplet energy gap (from positive value to negative value). This is in accordance with Hachmann *et al*., (2007).

Transtion dipole moment (d_{nm}) is a transition between two states. For a charged particle it is simply an off-diagonal matrix element of the position operator multiplied by the particle charge. This is useful for determining intermolecular interactions and if the transitions are allowed under the electric dipole interactions. Results in table 4.40 show a non-zero d_{nm} for pyrrole, MPC[a] MPCAM, monomer and tetramer (allowed transition), while d_{nm} decreases for trimer, dimer and pentmer, due to the triple integral returning an ungerade (odd) product and redistribute electrons within the same orbital and will return a zero product. The negative d_{nm} of MPC and $MPSO_4$ also reveals that there is no spatial overlap between the ground state and excited state orbitals resulting in a negative transition dipole moment. MPCOSH shows a difference sequence, in the sense that the transition dipole moment decreases sequencially from 0.3-0.1D, which is an implication that there are spatial overlap between the ground state and excited state orbitals. It can be concluded that in the polymeric form of systems based on the molecular orbitals that certain transitions are allowed and certain transitions are forbidden this is due to the symmetry of the ground and exited state.

Table 4.40. Vertical singlet-triplet gap (eV) and transition dipole moment (Debye) (in parenthesis) for studied systems

no of monomer	pyrrole	MPC	MPC[b]	MPCAM	MPCOSH	$MPSO_4H$	MPCHO
1	4.81	4.19	4.31	4.75	5.32	4.32	4.41
	(0.429)	(0.222)	(0.343)	(0.356)	(0.354)	(0.322)	(0.343)
2	3.67	3.74	3.98	3.69	4.81	3.63	3.98
	(0.035)	(-0.113)	(0.065)	(0.023)	(0.221)	(-0.033)	(0.025)
3	3.20	3.47	3.32	3.47	4.01	3.57	3.37
	(0.015)	(-0.037)	(0.035)	(0.045)	(0.185)	(-0.043)	(0.005)
4	3.17	3.45	3.21	3.43	3.25	3.34	3.42
	(0.202)	(-0.131)	(0.402)	(0.034)	(0.130)	(-0.091)	(0.287)
5	3.01	3.38	3.11	3.38	3.18	3.47	3.41
	(0.035)	(-0.003)	(0.032)	(0.03)	(0.110)	(-0.003)	(0.007)

CHAPTER FIVE
CONCLUSION AND RECOMMENDATIONS

In order to guide the synthesis of novel materials with low band gaps, the geometric, thermodynamic, electronic structures and absorption properties have been carried out. Quantum mechanical calculation for the structure elucidation of pyrrole and its derivatives using Semi-empirical methods, TD-DFT, DFT B3LYP/6-31G, CCSD and SFTDDFT/6-311++G(d,p) (d) level of theory from monomer up to five repeating units have been carried out.

The mutual comparison of the obtained equilibrium geometries showed that the DFT predicted C-C and C=C bond length are in agreement with the experimental values. In order to characterize the alternation of single or double carbon-carbon bonds within the two ring moieties, the Bond Length Alternation parameter (*BLA*) was used. The BLA values were also in agreement with the experimental values. However, substitution of hydrogen atom in pyrrole by a methyl group at C3 (in 3-methylpyrrole) and other functional groups at C4 causes fairly small changes in ring inter atomic distances. The estimated inter-ring bond length based on Badger's rule is 1.41Å indicating that the average structure is about 30% quinoid. The calculated geometries indicate that the strong conjugate effects and effective aromatic structure are formed in pyrrole, $MPSO_3H$, and MPC^b. The order is Pyrrole> $MPSO_3H$>MPCam> MPC^b>MPCHO> MPC^a>MPCOSH.

Substitution of some functional groups into the backbone of pyrrole structure led to an increased effective electronic stabilization.

The heat of formation of $MPSO_3H$ indicates that it is more thermodynamically stable and has a more effective electronic stabilization, while MPCHO has the lowest as compared to others. The order is $MPSO_3H$> MPCOSH> MPC^b> MPC^a>MPCam>MPCHO.

Polarizability which is a property that is associated with chemical reactivity and high electro-optic response was also studied for all the compounds. It can be concluded from the results that $MPSO_3H$ and MPCOSH have the highest polarizabilty compared to others and pyrrole which is the lowest. A low Log P value indicates high solubility in aqueous phase, low ability to be trapped in fat deposit and less susceptibility to metabolism. Based

on this fact, a polymer with low LogP and Log (1/C) show a molecule with a high biological activity, binding effect and its ability to orient the protein and enable electron transfer. Therefore it can be inferred that the decreasing order of activity is $MPSO_3H$> MPCam > MPCHO > MPC^a> MPCOSH>pyrrole> MPC^b

The Ionization potential (IP), Electron affinity (EA), HOMO, LUMO, and band gap of optimized structures have been calculated. The oligomers of simulated compounds were extrapolated to polymer through second-degree polynomial fit equation with r^2 value ranging from 0.66-0.99. Calculated band gap of pyrrole, which is 2.9 eV, significantly correlates with the experimental band-gap value which ranges from 2.9-3.2 eV and this corresponds to π-π* transition energies.

The substitution of methyl and some functional groups destabilized the HOMO and LUMO levels, decreased the band gaps, and increased the conjugation length, which are essential features in the design of low band gap conducting polymers. The substitution of nitrogen atoms on the backbone of (MPC^b) lowers the LUMO energy but results in the large band gap, as compared with MPC^a; this is due to electron localization. The calculated band gaps of the studied polymers decreases with the chain length, with MPCOSH and $MPSO_3H$ having the lowest energy gap 1.66 and 2.10 respectively. The increasing order of energy gap is MPCOSH<$MPSO_3H$< MPCam < MPC^a < MPC^b <pyrrole< MPCHO.

In general calculated values of E_g, μ, η and ω, according to koopman's theorem and Fukui function *f(r)*, which are reactivity descriptors lead to the conclusion that MPCOSH is more reactivity, lower stability and aromatic behaviour and termed as a softer molecule than other studied compounds.

The UV-Vis absorption spectra have been simulated by TD-DFT calculations. The oscillator strength and the absorption wavelength arising from $S_0 \rightarrow S_1$ electronic transition; increases progressively with the increase in the conjugation. Excitation to S_1 state also corresponds to the promotion of an electron from the HOMO to the LUMO. In comparison with the maximum absorption of other studied compounds, MPCOSH has the highest (395.05nm), which is attributed to the strong intramolecular charge transfer.

Analysis of the Natural bond orbitals reveals that Pyrrole is a single reference (dynamic correlation), closed shell system while other studied systems are multireference (static correlation), open shell in nature.

It can be concluded that in the polymers, certain transitions are allowed and certain transitions are forbidden due to the symmetry of the ground and exited states. The presence of substituents on polypyrrole decreased the energy gaps which led to the enhancement of their molecular properties making them suitable components of biosensor. MPCOSH will be the best choice out of the studied compounds, as components of biosensor.

RECOMMENDATIONS

i. We hope that our results may provide a reference for further experimental and theoretical work as well as effects directed towards the synthesis of these derivatives and their application in biosensor and other sensor devices.

ii. Further studies of many more substituted pyrroles are recommended to identify substituted pyrrole with much lower energy gap.

iii. Molecular docking of proteins with some of the substituted polypyrroles to explain the binding affinity and molecular interactions.

REFERENCES

Arslan, A., Türkarslan, Ö., Tanyeli, C., Akhmedov, İ. M. and Toppare, L. 2007. Electrochromic properties of a soluble conducting polymer: Poly (1-(4-fluorophenyl) -2,5- di(thiophen-2-yl) -1H-pyrrole). *Journal Chemical Physics* 104: 410-416.

Barker, P.D., Gleria, K.D., Hill, H.A.O. and Lowe,V.J. 1990. Electron transfer reactions of metalloproteins at peptide-modified gold electrodes. *European Journal of Biochemistry* 190.1: 171-175.

Bartlett, P.N. and Wang J.H. 1996. Electroactivity, stability and application in an enzyme switch at pH 7 of poly (aniline)–poly(styrenesulfonate) composite films. *Journal* of the *Chemical Society, Faraday Transactions* 92: 4137.

Bartlett, P.N. and Simon E. 2000. Poly(aniline)–poly(acrylate) composite films as modified electrodes for the oxidation of NADH. *Physical Chemistry Chemical Physics* 2: 2599.

Bartlett, P.N. and Wallace E.N.K. 2001. The oxidation of ascorbate at poly(aniline)–poly(vinylsulfonate) composite coated electrodes. *Physical Chemistry Chemical Physics* 3:1491.

Bax, D.V., Tipa, R.S., Kondyurin, A., Higgins, M.J., Tsoutas, K. Gelmi, A., Wallace, G.G., McKenzie, D.R., Weiss, A.S. and Bilek, M.M.M. 2012. Cell patterning via linker-free protein functionalization of an organic conducting polymer (polypyrrole) electrode. *Acta Biomaterialia* 8.7: 2538–2548.

Becke, A. D. 1988. Density-functional exchange-energy approximation with correct asymptotic behaviour. *Physical Review A* 38: 3098−3100.

Becke, A. D. 1993. Density-functional thermochemistry. III. The role of exact exchange. *Journal of Chemical Physics* 98: 5648-5652.

Bernard, M. C., Hugot-Le Goff, A., Joiret, S., Phong, P. V. 2001. Polyaniline films for protection against corrosion. *Synthetic Metals* 119:283-284.

Bidan, G., Billon, M., Livache, T., Mathis, G., Roget, A. and Torres-Rodriguez, L. M. 1999. Conducting polymers as a link between biomolecule and microelectronics. *Synthetic Metals* 102: 1363-1365.

Bird, C. W. 1997. Conceptual and Computational DFT in the study of Aromaticity. *Tetrahedron*. 53: 2497.

Blom A., Odnoblyudov, M. A., Yassievich, I. N. and Chao K. A. 2002. Resonant states induced by impurities in heterostructures. *Physical Review B* 65.15: 155302.

Brahim, S., Wilson, A. M., Narinesingh, D., Iwuoha,, E. I. and Guiseppi-Elie, A. 2003. Chemical and biological sensors based on electrochemical detection using conducting electroactive polymers. *Microchimica Acta* 143:123-137.

Cass, A. E. G., Davis, G., Francis, G. D., Hill, H. A. O., Aston, W. J., Higgins, I. J., Plotkin, E. V., Scott, L. D. L. and Turner, A. P. F. 2004. Ferrocene-mediated enzyme electrode for amperometric determination of glucose. *Analytical. Chemistry* 56: 667-671.

Chaubey, A. and Malhotra, B. D. 2002. Review: Mediated biosensors. *Biosensors & Bioelectronics* 17: 441-456.

Chong (editor), D. P. 1995. *Recent Advances in Density Functional Methods*, Part I, World Scientific Publishing Co. Pte. Ltd. Tokyo. P428

Cosnier, S. 2005. Biomolecule immobilization on electrode surfaces by entrapment or attachment to electrochemically polymerized films. A review. *Biosensors & Bioelectronics* 14: 443-456.

Cosnier, S., Ionescu, R. E. and Holzinger. M. 2008. Aqueous dispersions of SWCNTs using pyrrolic surfactants for the electro-generation of homogeneous nanotube composites. Application to the design of an amperometric biosensor *Journal of Material Chemistry* 18: 5129-5133

Cramer, C. J. 2002. *Essentials of Computational Chemistry: theories and models*, 1st edition, John Wiley & Sons Ltd. England 271-272

Cuff, L. and Kertesz, M. 1997. Evidence of quinonoid structures in the vibrational spectra of thiophene based conducting polymers. *Journal of Chemical Physics* 106.13: 5541-5553.

Darain, F., Park, J.S., Akutsu, H., Shim, Y.B. 2007. Superoxide radical sensing using a cytochrome c3 immobilized conducting polymer electrode. *Biosensors and Bioelectronics* 23: 161-167.

David, C. Y. 2001. *Computational Chemistry: A Practical Guide for Applying Techniques to Real-World Problems.* New York: John Wiley & sons, inc, publication. 32-38.

De-Proft, F. and Geerlings, P. 2004. Spin polarized conceptual density functional theory study of the regioselectivity in the [2+2] photocycloaddition of enones to substituted alkene) *Physical Chemistry* 6: 242.

Dewar, M. and Thiel. W. 1977. Ground States of Molecules. 38. The MNDO Method. Approximations and Parameters. *Journal of the American Chemical Society* 99: 4899.

Domingo, L. R., Aurell, M., Contreras, M. and Perez, P. J. 2002. Reactivity of Carbon-Carbon double bond toward nucleophilic addition. A DFT analysis, *Physical Chemistry A*. 106: 6871.

Dreizler, R. M., Gross, E. K. U. 1990. *Density Functional Theory*, Springer-Verlag, Berlin New York London 245-246

Foresman, J. B. Frisch, Æ. 1996. Exploring Chemistry with Electronic Structure Methods; Gaussian: Pittsburgh, PA. 23-43

Frenkel, M., Marsh, K.N., Wilhoit, R.C., Kabo, G.J. and Roganov, G.N. 1994. thermodynamics of Organic Compounds in the Gas State, Thermodynamics Research Center, College Station, TX

Frisch, M. J., Trucks, G. W., Schlegel, H. B., Scuseria, G. E., Robb, M. A. Cheeseman, J. R., Montgomery, J. A., Vreven, Jr., T., K. N. Kudin, J. C. Burant, J. M. Millam, S. S. Iyengar, J. Tomasi, V. Barone, B. Mennucci, M. Cossi, G. Scalmani, N. Rega, G. A. Petersson, H. Nakatsuji, M. Hada, M. Ehara, K. Toyota, R. Fukuda, J. Hasegawa, M. Ishida, T. Nakajima, Y. Honda, O. Kitao, H. Nakai, M. Klene, X. Li, J. E. Knox, H. P. Hratchian, J. B. Cross, C. Adamo, J. Jaramillo, R. Gomperts, R. E. Stratmann, O. Yazyev, A. J. Austin, R. Cammi, C. Pomelli, J. W. Ochterski, P. Y. Ayala, K. Morokuma, G. A. Voth, P. Salvador, J. J. Dannenberg, V. G. Zakrzewski, S. Dapprich, A. D. Daniels, M. C. Strain, O. Farkas, D. K. Malick, A. D. Rabuck, K. Raghavachari, J. B. Foresman, J. V.

Ortiz, Q. Cui, A. G. Baboul, S. Clifford, J. Cioslowski, B. B. Stefanov, G. Liu, A. Liashenko, P. Piskorz, I. Komaromi, R. L. Martin, D. J. Fox, T. Keith, M. A. Al-Laham, C. Y. Peng, A. Nanayakkara, M. Challacombe, P. M. W. Gill, B. Johnson, W., Chen, M. Wong, W., Gonzalez, C. and Pople, J. A. Gaussian 09 Revised Gaussian, Inc., Pittsburgh PA, 2009.

Genies, E. M., Tsintavis, C. 1985. Redox mechanism and electrochemical behaviour of polyaniline deposits. *Journal of Electroanalytical Chemistry* 195: 109-128.

Gerard, M., Chaubey, A., Malhotra, B. D. 2002. Application of conducting polymers to biosensors. *Biosensors & Bioelectronics* 17: 345-359.

Gerber, H.P., Seipel, K., Georgiev, O., Hofferer, M., Hug, M., Rusconi, S., Schaffner, W. 1994. Transcriptional activation modulated by homopolymeric glutamine and proline stretches *Science* 263: 808.

Godby, R.W., Schlüter, M. and Sham, L.J. 1986. Accurate exchange-correlation potential for silicon and its discontinuity on addition of an electron. *Physical Review Letters* 56**:** 2415.

Granot E., Basnar B., Cheglakov Z., Katz E. and Willner I. 2006. Enhanced Bioelectrocatalysis Using Single-Walled Carbon Nanotubes (SWCNTs)/Polyaniline Hybrid Systems in Thin-Film and Microrod Structures Associated with Electrodes. *Electroanalysis*, 18: 26.

Grimme S. 2011. Density functional theory with London dispersion corrections *Computational Chemistry and Molecular Modeling* 1.2 :211–228.

Guimarães, J., Jeconias R., Gama A., Carlos A., Brito S., Celso P., de M., Bernardo L. and Jordan D N. 2008. On the fluorescence of pyrrole derivative oligomer. *Materials Science and Engineering C* 28: 1076–1081.

Gunnarsson, O., Lundqvist, B. I. and Lundqvist, S. 1972. *Solid State Communicaion* 11: 149.

Hachmann, J. Dorando, J. J. Aviles, M. and Chan,G. K.L. 2007. The radical character of the acenes: A density matrix renormalization group study Journal Chemical Physics 127:104107.

Haddon, R. C. and Fuguhata, T.1980. Comparative molecular orbital study of lower annulenes, *Tetrahedron Letter* 21: 1191.

Hailin, G., Kerry, J., Gilmore, S.A., Chee, O.T., and Gordon G.W. 1993. Chemical polymerization of 3-methylpyrrole-4-carboxylic acid. *Polymer* 34.9: 2007-2010.

Hajgató, B. Szieberth,D. Geerlings, P. De Proft, F. and Deleuze M. S. 2009. A benchmark theoretical study of the electronic ground state and of the singlet-triplet split of benzene and linear acenes. Journal of Chemical Physics 131: 224321-19.

Havinga, W., Hoeve, T. and Wynberg, H. 1992. New Charge Transfer–Type π-Conjugated Poly (aryleneethynylene) Containing Benzo [2, 1, 3] thiadiazole as the Electron-Accepting Unit. *Polymer Bulletin* 29:119.

Heeger, A. J. 2001. Semiconducting and metallic polymers: the fourth generation of polymeric materials. *Reviews of Modern Physics* 73*:* 681–700.

Heeralal V. B. and Krishnamurthi M. 2014. Versatile metal complexes of 2,5-bis{*N*-(2,6-di isopropylphenyl)iminomethyl}pyrrole for epoxide–CO_2 coupling and ring opening polymerization of ε-caprolactone. *RSC Advances* 4: 6094-6102

Hehre, E and Ohlinger, S. 2011. Spartan' 10 for windows, machintosh and linux Tutorial and user's gui, Copyright © 2011 by Wavefunction, Inc. USA 43-44

Hirata, S., Zhan, C.G., Apra, E., Windus, T.L. and Dixon, D.A. 2003. A new, self-contained asymptotic correction scheme to exchange-correlation potentials for time-dependent density functional theory. *Journal of Physical Chemistry A.* 107: 10154-10158.

Hoa, D.T., Suresh Kunar T.N., Punekar N.S., Srinivasa R.S., Lal R. and Contractor A.Q. 1992. Biosensor Based On Conducting Polymers. *Analytical Chemistry* 64: 2645

Hohenberg, P and Kohn, W. 1964a. In homogeneous electron gas. *Physics Review B* 136: 864.

Hohenberg, P and Kohn, W. 1964b. In homogeneous electron gas. *Physical Review* 136.3B: B864–B871.

Hughes, J.P., Rees, S., Kalindjian, S.B. and Philpott, K.L. 2011. Principles of early drug discovery. *British Journal Pharmacology*. 162.6: 1239–1249.

Ivanov, A. N., Lukachova, L. V., Evtugyn, G. A., Karyakina, E. E., Kiseleva, S. G., Budnikov, H. C., Orlov, A. V., Karpacheva, G. P. and Karyakin, A. A. 2002.

Polyaniline-modified cholinesterase sensor for pesticide determination. *Bioelectrochemistry* 55: 75-77.

Iwuoha, E. I., Smyth, M. R. 1996. Polymer-based amperometric biosensors, in: Lyons, M. E. G. (Ed.), Electroactive Polymer Electrochemistry, Plenum Press, New York, pp. 297-325.

Iwuoha, E. I., de Villaverde, D. S., Garcia, N. P., Smyth, M. R. and Pingarron, J. M. 1997. Reactivities of organic phase biosensors. 2. The amperometric behaviour of horseradish peroxidase modified with an electrtosynthetic polyaniline film. *Biosensors & Bioelectronics* 12: 749-761.

Iwuoha, E.I., Williams-Dottin, A. R., Hall, L. A., Morrin, A., Mathebe, G. N., Smyth, M. R. and Killard, A. 2004a. Electrochemistry and application of a novel monosubstituted squarate electron-transfer mediator in a glucose oxidase-doped poly (phenol) sensor. *Pure* and *Applied Chemistry* 76: 789-799.

Iwuoha, E.I., Wilson, A., Howel, M., Mathebe, N. G. R., Montane-Jaime, K., Narinesingh, D. and Guiseppi-Elie, A. 2004b. Cytochrome P4502D6 (CYP2D6) bioelectrode for fluoxetine. *Analytical Letters* 37: 929-941.

Jacquemin D., Perpete E.A., Chermette H., Ciofini I. and Adamo C. 2007. Comparison of theoretical approaches for computing the bond length alternation of polymethineimine. *Chemical Physics* 332: 79.

Jayasree, R., Chandrasekar, R. and Cindrella, L. 2012. Synthesis and characterization of polypyrrole-platinum composite for use as electrode material. *Polymer Composites* 33.9: 1652–1657.

Jensen, F. 1999. *Introduction to Computational Chemistry*. England: John Wiley& Sons. 56-61

Juan, C. C. 2003. *Introduction to Density Functional Theory*. New york: John Wiley& Sons 1-44.

Karim, F., Fakhruddin, A.N.M. 2012 Reviews in Environmental Science and Bio-Technology, 11.3: 261–274.

Kim, H.N., Kang, D.H., Kim, M.S., Jiao, A., Kim, D.H., Suh, K.Y. 2012. Patterning methods for polymers in cell and tissue engineering. *Annals of Biomedical Engineering* 40.6: 1339–1355.

Knorr, W. and Godby, R.W. 1992. Investigating exact Density-Functional Theory of a Model Semiconductor. *Physical Review Letters* 68: 639

Koch, W., Holthausen, M. C. 2001. *A Chemist's Guide to Density Functional Theory*, 2nd editon, Wiley-VCH Verlag GmbH

Kohn, W. and Sham L. J. 1965. Self-Consistent Equations Including Exchange and Correlation Effects. *Physical Review* 140: 1133.

Koopmans, T. 1933. Combinatorial Optimization Polyhedral and Efficiency. *Physica* 1: 104.

Kose, M. E. 2001. Electronic structure analysis and density functional study of an alternating donor/acceptor polymer thesis for Master of Science, Bilkent University, Chemistry Department. P 19-22

Kraljić, M., Mandić, Z.and Duić, Lj. 2003. Inhibition of steel corrosion by polyaniline coatings. *Corrosion Science* 45:181-198.

Kudera, M., Aitken, A., Jiang, L., Kaneko, S., Hill, H. A. O., Dobson, P. J., Leigh, P. A. and McIntire, W. S. 2000. Electron transfer processes of redox proteins at inherently modified microelectrode array devices. Journal Electroanalytical Chemistry 495:36-41.

Kwon, N.H., Rahman, M. A. Won, M.S. and Shim, Y.B. 2006**.** Lipid-bonded conducting polymer layers for a model biomembrane: application to superoxide biosensors. *Analytical Chemistry* 78: 52-60.

Labanowski, J. K. 2004 Simplified and Biased Introduction to Density Functional Approaches in Chemistry see: http://www.ccl.net/cca/documents/DFT/dftoverview/dft2.pdf, August 2004.

Langer, J.J. and Langer K. 2005. Polyaninline nonbiodetector *Reviews on Advanced Materials Science* 10: 434.

Lee, C., Yang, W. and Parr, R.G. 1988. Development of the Colle-Salvetti correlation-energy formula into a functional of the electron density. *Physical Review B* 37: 785-789.

Lee, Y.T. and Shim, Y.B. 2001. Direct DNA hybridization detection based on the oligonucleotidefunctionalized conductive polymer. *Analytical Chemistry* 73: 5629-5632.

Levine, N. 2013. *Quantum Chemistry*. 7th ed. New Jersey, USA: Prentice Hall.. 7-10

Li, X. j., and Iiao, G. 2009. Theoretical studies of the functionalized derivatives of fullerene $C_{24}H_{24}$ by attaching a variety of chemical groups. *Journal of Molecular Structure*: *THEOCHEM* 893: 26–30.

Lin, P. Yan, F. 2012. Organic thin-film transistors for chemical and biological sensing. *Advanced* Materials 24.1: 34–51.

Lindfors, T. and Ivaska, A. 2002. Potentiometric and UV-vis characterisation of N-substituted polyanilines *Journal of Electroanalytical Chemistry* 535: 65.

Liu, M., Wen, Y.P Li, D. Yue, R.R. Xu, J.K and He, H.H. 2011. A stable sandwich-type amperometric biosensor based on poly(3,4-ethylenedioxythiophene)–single walled carbon nanotubes/ascorbate oxidase/nafion films for detection of L-ascorbic acid. *Sensors and Actuators B: Chemical* 159: 277–285.

Liu, Y.J., Yamamoto, S., Sueishi, Y. 2001. Photoinduced hydride transfer reaction between methylene blue and leuco violet. *Journal of photochemical A-chemisty* 143: 153.

Mader, S. S. 1996. *Biology, 5th ed.* Dubuque: Times Mirror Higher Education Group, Inc. Washington, D.C

Majumdar, G., Goswami, M., Sarma, T.K., Paul, A. and Chattopadhyay, A. 2005. Au nanoparticules and polyaniline coated resin beads for simultaneous catalytic oxidation of glucose and colorimetric detection of the product. Langmuir 21.5: 1663–1667.

Malinauskas A., Garjonyte R., Mazeikiene R. and Jureviciute I. 2004. Electrochemical response of ascorbic acid is conducting and electro generated polymer. *Talanta*, 64: 121.

Malki, Z. E., Hamidi, M., Lére-Porte, J-P., Serein-Spirau, F. L., Bejjit, M. Haddad and Bouachrine, M. 2012. Theoretical study of the geometric, electronic structure and properties of alternating donoracceptor conjugated oligomers: Carbazole (Cbz)-

based 3.4-ethylenedioxythiophene (Edot). *Advanced Material Letters* 3.4: 266-272.

Malta, M., Gonzalez, E. R., Torresi, R. M. 2002. Electrochemical and chromogenic relaxation processes in polyaniline films. *Polymer* 43: 5895-5901.

Matharu, Z., Sumana, G., Arya, S. K., Singh, S. P., Gupta, V. and Malhotra, B. D. 2007. Polyaniline Langmuir-lodgett film based cholesterol biosensor *Langmuir* 23: 13188-13192.

Mazeikiene R., Niaura G. and Malinauskas A. 2003. Voltammetric study of the redox processes of self-doped sulfonated polyaniline. *Synthetic Metals* 139: 89.

Menges N., Sari O., Abdullayev Y., Erdem S.S., Balci M., 2013. Design and synthesis of pyrrolotriazepine derivatives: an experimental and computational study. *Journal of Organic Chemistry* 78.11:5184-95.

Meuwly, M. and Karplus. M. 2004. Theoretical Investigations on *Azotobacter vinelandii* Ferredoxin I: Effects of Electron Transfer on Protein Dynamics. *Biophysical Journal* 86.4: 1987–2007.

Mirmohseni, A., Solhjo, R. 2003. Preparation and characterisation of aqueous polyaniline battery using modified polyaniline electrode. *European Polymer Journal* 39: 219-223.

Mishra, A. K. and Tandon, P. J. 2009. Density Functional Theory Study of Poly (o‑phenylenediamine) Oligomers. *Physical Chemistry B* 113: 9702−9707.

Molino, P.J., Higgins, M.J., Innis, P.C., Kapsa, R.M.I. and Wallace, G.G. 2012. Fibronectin and bovine serum albumin adsorption and conformational dynamics on inherently conducting polymers: A QCM-D study. *Langmuir* 28.22: 8433–8445.

Mu, S., Chen, C., Wang, J. 1997. The kinetic behaviour for the electrochemical polymerization of aniline in aqueous solution. Synt. Met., 88:249-254.

Muhammad-Tahir., Z. and Alocilja E.C. 2003. A conductometric *biosensor* for biosecurity *Biosensors & Bioelectronics* 18: 813.

Nandeesh, K.N., Chandra, M., Mahendra, K., Palani, and K. 2013. Ethyl 1,4-bis(4-chlorophenyl)-2-methyl-1H-pyrrole-3-carboxylate *Acta Crystallographica E* 69 :1269.

Nero, J. D., Galvao, D.S. and Laks, B. 2002. Electronic structure investigation of biosensor polymer. *Optical Materials* 21: 461–466.

Ngamna O., Morrin A., Moulton S.E., Killard A.J., Smyth M.R. and Wallace G.G. 2005. An HRP based biosensor using sulphonated polyaniline Synthetic *Synthetic Metals* 153: 185.

Nien, P. C., Chen, P.Y and Ho, K.-C. 2009. Fabricating an Amperometric Cholesterol Biosensor by a Covalent Linkage between Poly(3-thiopheneacetic acid) and Cholesterol Oxidase *Sensors* 9: 1794-1806.

Parr, R. G and Pearson, R. G. J. 1983a. Hardness, Softness and the Fukui Function in the Electronic Theory of Metal and Catalysis. *America Chemical Society* 105: 7512.

Parr, R. G. 1983b. Absolute hardness: comparrion parameter to electronegativity. *Journal American Chemical Society* 105: 7512-7516.

Parr, R. G and Yang, W. 1989. *Density Functional Theory of Atoms and Molecules*, New York: Oxford University Press. 45-46

Parr, R. G and Chattaraj, P. K. J. 1991. Density Functional Theory of Electronic Structure. *American Chemical Society* 113: 1854.

Pearson, R. G. J. 1985. Absolute Hardness and Absolute Hardness of Lewis Acids and bases, *America Chemical Society* 107: 6801.

Petrova, J., Romanova, J., Madjarova, G., Ivanova, A. and Tadjer, A. 2012. Absorption Spectra of Model Single Chains of Conducting Polyaniline. *Journal Physical Chemistry* B 116.22: 6543–655.

Que, Lawrence Jr. 2000. *Physical Methods in Bioinorganic Chemistry*. University Science Books. Sausalito. 556

Rahman, M. A. Won, M.S. and Shim, Y.B. 2005a The potential use of hydrazine as an alternative to peroxidase in a biosensor: comparison between hydrazine and HRP-based glucose sensors. *Biosensors & Bioelectronics* 21: 257-265.

Rahman, M. A., Kwon, N.H., Won, M.S., Choe, E. S. and Shim, Y.B. 2005b. Functionalized conducting polymer as an enzyme-immobilizing substrate: an amperometric glutamate microbiosensor for in vivo measurements, *Analytical Chemistry* 77: 4854-4860.

Reach, G., Wilson, G. S. 1992. Can continuous glucose monitoring be used for the treatment of diabetes. *Analytical Chemistry* 64: 381A

Rochefort, A., Salahub, D. R. and Avouris, P. 1999. The Effects of Finite Length on the Electronic Structure of Carbon Nanotubes. *Journal Physical Chemistry B* 103: 641-646.

Romanova, J., Petrova, J., Tadjer, A. and Gospodinova, N. 2010. Polyaniline–water interactions: A theoretical investigation with the polarisable continuum model. *Synthetic Metals*. 160: 1050−1054.

Rottmannováa, L., Kraiwan P., C, Rimarčíka, J., Vladimír Lukeša, Erik K. and Anne-Marie Keltererb. 2012. Theoretical study of 2-phenylpyrrole molecule using various quantum-chemical approaches Acta Chimica Slovaca, 5.1:21—28.

Rung, E. and Gross, E. K. U. 1984. Density-Functional Theory for Time-Dependent Systems. *Physical Review. Letter* 52.12: 997–1000.

Ryder, K.S., Schweiger, L.F. Glidle, A. and Cooper, J.M. 2000. Strategies towards functionalised electronically conducting organic copolymers: Part 2 Copolymerisation *Journal of Materials Chemistry* 10: 1785.

Sadekar, A.G. Mohite, D., Mulik, S., Chandrasekaran, N., Sotiriou-Leventis, C., Leventis, N. 2012. Robust PEDOT films by covalent bonding to substrates using in tandem sol-gel, surface initiated free-radical and redox polymerization. *Journal of Materials Chemistry* 22.1: 100–108.

Sadlej, J. 1985. *Semi-Empirical Methods of Quantum Chemistry*. New York: John Wiley & Sons 234-235.

Salzner, U., Lagowski, J. B., Pickup P. G. and Poirier. R. A. 1997. Design of low band gap polymers employing density functional theory—hybrid functionals ameliorate band gap problem. *Journal of Computational Chemistry* 18: 1943.

Salzner, U., Lagoswski, J. B., Pickup, P.G. and Poirier, A. 1998a. Comparison of Electronic Structures of Polycylopentadiene, Polypyrrole, Polyfuran, Polysilole, Polyphosphole, Polythiophene, Polyselenophene and Polytellurophene. *Synthetic Metals* 96: 177-189.

Salzner, U., Pickup, P., Poirier, R., Lagowski, J. J. 1998b. Accurate Method for obtaining Band Gaps in Conducting Polymers Using a DFT/Hybrid Approach. *Physical Chemistry A* 102: 2572−2578.

Salzner, U. 2008. Investigation of Charge Carriers in Doped Thiophene Oligomers through Theoretical Modeling of their UV/Vis Spectra. *Physical Chemistry A* 112: 5458−5466.

Salzner, U. 2010. Effects of Perfluorination on Thiophene and Pyrrole Oligomers. *Physical Chemistry A* 114: 5397−5405.

Salzner, U. and Aydin, A. J. 2011. Improved Properties of pi-Conjugated Systems with Range-Separated Density Functionals. *Journal of Chemical Theory and Computation* 7: 2568− 2583.

Santos, A. L. O. M. and Silva, Manuel A. V. R. 2013. Experimental and Computational Study on the Molecular Energetics of 2-Pyrrolecarboxylic Acid and 1-Methyl-2-pyrrolecarboxylic. *Physical Chemistry A* 117: 5195−5204.

Scheller, F. W. Schubert, F. and Fedowitz, J. 1997. Present state and frontiers in biosensorics, In: Frontiers in biosensorics I. Fundamental aspects, Scheller, F. W.; Schubert, F.; Fedowitz, J. Eds., Basel: Birkhauser Verlag, pp 1-12.

Schuhmann, W. 1991. Electron transfer between glucose oxidase and electrodes via redox mediators bound with flexible chains to the enzyme surface. *Journal of the American Chemical Society* 113.4: 1394–1397.

Schultz, J.S. and Taylor, R. F. 1996. Introduction to chemical and biological sensors, In: *Handbook of chemical and biological sensors*. Taylor, R. F.; Schultz, J.S. Eds., London: IOP, pp 1-10

Shao, Y. Molnar, L.F. Jung, Y. Kussmann, J. Ochsenfeld, C. Brown, S.T. Gilbert, A.T.B. Slipchenko, L.V. Levchenko, S.V. O'Neill, D.P. DiStasio Jr., R.A. . Lochan, R.C T. Wang, G.J.O. Beran, N.A. Besley, J.M. Herbert, C.Y. Lin, T. Van Voorhis, S.H. Chien, A. Sodt, R.P. Steele, V.A. Rassolov, P.E. Maslen, P.P. Korambath, R.D. Adamson, B. Austin, J. Baker, E.F.C. Byrd, H. Dachsel, R.J. Doerksen, A. Dreuw, B.D. Dunietz, A.D. Dutoi, T.R. Furlani, S.R. Gwaltney, A. Heyden, S. Hirata, C-P. Hsu, G. Kedziora, R.Z. Khalliulin, P. Klunzinger, A.M. Lee, M.S. Lee, W.Z. Liang, I. Lotan, N. Nair, B. Peters, E.I. Proynov, P.A.

Pieniazek, Y.M. Rhee, J. Ritchie, E. Rosta, C.D. Sherrill, A.C. Simmonett, J.E. Subotnik, H.L. Woodcock III, W. Zhang, A.T. Bell, A.K. Chakraborty, D.M. Chipman, F.J. Keil, A.Warshel, W.J. Hehre, H.F. Schaefer, J. Kong, A.I. Krylov, P.M.W. Gill and M. Head-Gordon, B.J Deepmer, A.J Driessen, T.S Hehre, J. A Johnson, Pietro, W. J. and Yu, J. 2011. SPARTAN '10, build 1.01 Wavefunction Inc. Irvine CA.

Shao, Y., Fusti-Molnar, L. Jung, Y. Kussmann, J. Ochsenfeld, C. S. Brown, A.T.B. Gilbert, L.V. Slipchenko, S.V. Levchenko, D.P. O'Neill, R.A. Distasio Jr, R.C. Lochan, T. Wang, G.J.O. Beran, N.A. Besley, J.M. Herbert, C.Y. Lin, T. Van Voorhis, S.H. Chien, A. Sodt, R.P. Steele, V.A. Rassolov, P. Maslen, P.P. Korambath, R.D. Adamson, B. Austin, J. Baker, E.F.C. Bird, H. Daschel, R.J. Doerksen, A. Dreuw, B.D. Dunietz, A.D. Dutoi, T.R. Furlani, S.R. Gwaltney, A. Heyden, S. Hirata, C.-P. Hsu, G.S. Kedziora, R.Z. Khalliulin, P. Klunziger, A.M. Lee, W.Z. Liang, I. Lotan, N. Nair, B. Peters, E.I. Proynov, P.A. Pieniazek, Y.M. Rhee, J. Ritchie, E. Rosta, C.D. Sherrill, A.C. Simmonett, J.E. Subotnik, H.L. Woodcock III, W. Zhang, A.T. Bell, A.K. Chakraborty, D.M. Chipman, F.J. Keil, A. Warshel, W.J. Hehre, H.F. Schaefer III, J. Kong, A.I. Krylov, P.M.W. Gill, M. Head-Gordon. 2014. Q-Chem 4.2: An Engine for Innovation. *Physical Chemistry Chemical Physics* 8.3172.

Shao, Y., Head-Gordon, M. and Krylov, A. 2003. Advances in methods and algorithms in a modern quantum chemistry program package. *Journal of Chemical Physics* 118: 4807–4818.

Sharma, S. K., Singhal, R., Malhotra, B. D., Sehgal, N and Kumar, A. 2004. Biosensor based on Langmuir-Blodgett films of poly(3-hexyl thiophene) for detection of galactose in human blood. *Biotechnology Letters* 26.8:645–647.

Shi, L. and Willner, I. 2004a. Electrical contacting of glucose oxidase by DNA-templated polyaniline wires on surfaces. *Electrochemistry Communications* 6: 1057-1060.

Shi, L., Xiao Y. and Willner I. 2004a. Electrical contacting of glucose oxidase by DNA surfaces. *Electrochemical Communication* 6: 1057.

Shirakawa, H. A. 2001. The Discovery of Polyacetylene Film: The Dawning of an Era of Conducting Polymers. *Angewandte Chemie International Edition* 40.14: 2574–2580.

Singh, S., Chaubey, A. and Malhotra, B. D. 2004. Amperometric Cholesterol Biosensor Based on Immobilized Cholesterol Esterase and Cholesterol Oxidase on Conducting Polypyrrole Films. *Analytica Chimica Acta* 502: 229-234.

Singh, S., Solanki, P. R., Pandey, M. K. and Malhotra, B. D. 2006. Covalent immobilization of cholesterol esterase and cholesterol oxidase on polyaniline films for application to cholesterol biosensor. *Analytica Chimica Acta* 568: 126-132.

Solanki, P. R., Singh, S., Prabhakar, N., Pandey, M. K. and Malhotra, B. D. 2007. Application of conducting poly(aniline-*co*-pyrrole) film to cholesterol biosensor. *Journal of Applied Polymer Science*. 105: 3211-3219.

Stewart, J.J. 1989. Optimization of parameter of semi-emperical methods 1. The MNDO-PM3 method. *Journal of Computational Chemistry* 10.2: 209-220.

Swann, M.J., Glidle, A., Gadegaard, N., Cui, L., Barker, J.R. and Cooper, J.M. 2000. Distribution of adsorbed molecules in electronic nose sensors. *Physica B* 276-357.

Tan, X., Li, Cai, M., P., Luo, L., and Zou, X. 2005. An amperometric cholesterol biosensor based on multiwalled carbon nanotubes and organically modified sol–gel/chitosan hybrid composite film. *Analytical Biochemistry* 337:111–120.

Targema, M. Obi-Egbedi, N.O. Moriam D. Adeoye. 2013. Molecular structure and solvent effects on the dipole moments and polarizability of some aniline derivatives. *Computational and theoretical Chemistry* 1012: 47-53.

Tian, F., Xu, B., Zhu, G. and Zhu, L. 2001. Hydrogen peroxide biosensor with enzyme entrapped within electrodeposited polypyrrole based on mediated sol–gel derived composite carbon electrode. *Analytica Chimica Acta* 443: 9-16.

Turner, A. F. P., Karube, I. and Wilson, G. S., (Eds.), 1987. *Biosensors: Fundamentals and Applications*. Oxford: Oxford University Press. 770.

Ullah, H., Anwar-ul-Haq A.S., Khurshid A. and Salma B. 2013. Density Functional Theory Study of Poly (o-phenylenediamine) Oligomers. *Journal Physical Chemistry C* 117: 4069−4078.

Ullrich, C. A. and Yang, Z. 2014. A brief compendium of time-dependent density-functional theory. *Brazilian Journal of Physics* 44.1: 154-188.

Vedrine, C., Fabiano, S and Tran-Minh., C. 2003. Amperometric tyrosinase based biosensor using an entrapment support. *Talanta* 59, 2003: 535-544.

Vidal, J.C., Espuelas, J. and Castillo. J.R. 2004. Amperometric cholesterol biosensor based on in situ reconstituted cholesterol oxidase on an immobilized monolayer of flavin adenine dinucleotide cofactor. *Analytical Biochemistry* 333: 88-98.

Vladimir B. K., Nadezhda M. V., Irina L. Z., Elena Y. L. and Boris A. T. 2002. Theoretical analysis of pyrrole anions addition to carbon disulfide and carbon dioxide. International *Journal of Quantum Chemistry* 88.5*:* 542–548.

Walatka, V. V., Labes, M. M. and Perlstein, J. H. 1973. Polysulfur nitride-a one-Dimensional Chain with a Metallic Ground State. *Physical Review Letters* 31: 1139-1142.

Wallace, G. G., G. M. Spinks, L. A. P. Kane-Maguire, and P. R. Teasdale. 2009. Conductive Electroactive Polymers. 3rd ed. New York : CRC Press. 111-113

Waltman, R. J. 1986. Electrically conducting polymers: a review of the electropolymerization reaction, of the effects of chemical structure of polymer film properties, and of applications towards technology *Canadian Journal Chemistry* 64: 76-95.

Wang, J. 2001. Glucose Biosensors: 40 Years of Advances and Challenges. *Electroanalysis*, 13, 983.

Wang, J. 1991. Modified electrodes for electrochemical sensors. *Electroanalysis* 3: 255-259.

Wang, S., Bao, H., Yang, P. and Chen, G. 2008. Immobilization of trypsin in polyaniline-coated nano-Fe_3O_4/carbon nanotube composite for protein digestion . *Analytica Chimica Acta* 612: 182- 189.

Warren, J. H. 2003. A Guide to Molecular Mechanics and Quantum Chemical Calculation in Spartan Wave Function, Inc, USA. 43-44

Waterhouse, R. N., 2003. Determination of lipophilicity and its use as a predictor of blood-brain barrier penetration of molecular imaging agents. *Journal of Molecular imaging biology* 5.6:376-89.

Yang, Y. and Mu, S. 1997. Bioelectrochemical responses of the polyaniline horseradish peroxidase. *Journal of Electroanalytical Chemistry* 432:71-78.

Young, D.C. 2001. Computational Chemistry: A Practical Guide for Applying Techniques to Real-World Problems. New York: John Wiley & Sons, Inc. 32-42

Zanuy, D. and Alemán, C. 2008. DNA−Conducting Polymer Complexes: A Computational Study of the Hydrogen Bond between Building Blocks *Journal of Physical Chemistry B* 112.10: 3222–3230.

Zhao, M., Wu. and Cai, C. 2009. Polyaniline nanofibers: synthesis, characterization, and application to direct electron transfer of glucose oxidase. *Journal of physical Chemistry C* 113.12:4987-4996.

Zhou, N. J., Wang, T., Chen, Z., Yu, and Li, G. 2006. Enzyme-functionalized gold nanowires for the fabrication of biosensors. *Analytical Chemistry* 78: 5227- 5230.

Zhou, Z. and Navangul, H. V. J. 1990 Quantum Derham cohomology Theory, *Physical, Organic Chemistry* 3: 784.

Zotti, G., Martina S., Wegner G. & Schluter A.D. 1992. Well-defined pyrrole oligomers: electrochemical and UV/Vis studies. *Advanced Materials* 4.12: 798-801.

APPENDICES

Optimized coordinates of studied compound

MPC

Title Card Required

Symbolic Z-matrix:
Charge = 0 Multiplicity = 1

C	0.96532	-0.70957	0. 0000
C	-0.09853	0.25617	0. 0000
C	0.50782	1.5024	0. 0000
C	2.15407	-0.00424	0. 0000
H	0.07615	2.49496	0. 0000
H	3.18137	-0.34477	0. 0000
N	1.86478	1.33254	0. 0000
H	2.54825	2.0791	0. 0000
C	0.81969	-2.19049	0. 0000
H	0.27454	-2.52186	0.88946
H	1.79676	-2.68465	0. 0000
H	0.27454	-2.52186	-0.88946
C	-1.53136	0.00588	0. 0000
O	-2.06667	-1.09278	0. 0000
O	-2.29623	1.12341	0. 0000
H	-3.20382	0.75933	0. 0000

MPC-1-monomer

Title Card Required

Symbolic Z-matrix:
Charge = 0 Multiplicity = 1

N	0.45404	-0.08261	-0.02672
C	-0.61048	0.81163	0.04931
C	-1.78302	0.10547	0.01719
C	-1.4261	-1.28443	-0.0987
C	-0.06298	-1.37569	-0.12206
H	-0.40996	1.86837	0.13519
H	-2.1132	-2.11772	-0.17241
H	0.57299	-2.23471	-0.28325
C	1.80029	0.33213	-0.01374
O	2.13598	1.4761	-0.17486
O	2.69736	-0.66031	0.19034
H	2.26106	-1.45648	0.53507
C	-3.17205	0.66813	0.08895

H	-3.15358	1.76054	0.15465
H	-3.71481	0.29031	0.9645
H	-3.76153	0.39815	-0.79623

MPC-1-Pentimer

Title Card Required

Symbolic Z-matrix:
Charge = 0 Multiplicity = 1

N	3.18348	0.47665	0.33801
C	2.63517	1.58977	-0.3238
C	3.5796	2.11161	-1.19622
C	4.71525	1.27586	-1.11811
C	4.45636	0.26198	-0.21714
H	5.6261	1.37971	-1.69632
C	2.55452	-0.27131	1.37112
O	1.34117	-0.31759	1.51683
O	3.42167	-0.89925	2.20471
H	4.35268	-0.61606	2.12177
C	3.43134	3.30109	-2.07949
H	3.39694	4.21829	-1.48316
H	2.51285	3.23297	-2.6714
H	4.2725	3.38234	-2.77567
C	1.32041	2.13129	-0.08119
N	0.10654	1.53422	-0.44538
C	-0.91568	2.31548	0.1236
C	-0.36038	3.4624	0.66924
C	1.04333	3.33695	0.53347
H	1.78637	4.03803	0.89368
C	-1.07814	4.58392	1.33266
H	-0.37436	5.292	1.78218
H	-1.73105	4.2097	2.12778
H	-1.68839	5.13028	0.60662
C	-0.08849	0.36278	-1.22141
O	-1.17137	-0.18629	-1.37103
O	1.04358	-0.07599	-1.79673
H	0.83738	-0.93094	-2.2247
C	-2.30713	1.93887	0.10872
N	-2.8235	0.77669	0.70048
C	-4.09927	0.59138	0.15611
C	-4.45753	1.72809	-0.55574
C	-3.32641	2.57954	-0.56347
H	-3.23437	3.52102	-1.09163
C	-5.75678	1.99612	-1.23205
H	-6.59176	1.84501	-0.54042
H	-5.88701	1.32742	-2.08876
H	-5.80583	3.0274	-1.59634
C	-2.13594	-0.11373	1.55903
O	-2.43882	-1.28591	1.70244

O	-1.09129	0.47968	2.16154
H	-0.47189	-0.22745	2.45143
C	-4.90983	-0.57321	0.36951
N	-5.20395	-1.56231	-0.57308
C	-6.14214	-2.4042	0.02557
C	-6.38061	-2.0193	1.32555
C	-5.60079	-0.8597	1.53499
H	-6.5407	-3.23488	-0.54461
H	-5.56367	-0.26919	2.44257
C	-7.28798	-2.67319	2.30048
H	-7.39291	-3.74145	2.08505
H	-8.28096	-2.21446	2.26022
H	-6.90246	-2.57198	3.32011
C	-4.75906	-1.75953	-1.90488
O	-5.34267	-2.54353	-2.6405
O	-3.67333	-1.04992	-2.27972
H	-3.12513	-0.63484	-1.58135
C	5.35534	-0.82963	0.07261
C	6.61551	-0.71445	0.65484
C	7.14716	-2.02158	0.7612
C	6.22258	-2.88838	0.23569
N	5.11526	-2.1809	-0.21627
H	8.10952	-2.30421	1.17161
H	6.25809	-3.96545	0.12943
C	7.29998	0.53454	1.0961
H	8.18831	0.30614	1.69404
H	6.63231	1.14697	1.71062
H	7.61737	1.1224	0.22916
C	3.98443	-2.7524	-0.83727
O	3.0105	-2.12094	-1.20858
O	4.09638	-4.09121	-0.96078
H	3.2594	-4.37785	-1.38183

MPCam –monomer

Title Card Required

Symbolic Z-matrix:
Charge = 0 Multiplicity = 1

N	0.45404	-0.08261	-0.02672
C	-0.61048	0.81163	0.04931
C	-1.78302	0.10547	0.01719
C	-1.4261	-1.28443	-0.0987
C	-0.06298	-1.37569	-0.12206
H	-0.40996	1.86837	0.13519
H	-2.1132	-2.11772	-0.17241
H	0.57299	-2.23471	-0.28325
C	1.80029	0.33213	-0.01374
O	2.13598	1.4761	-0.17486
O	2.69736	-0.66031	0.19034

H	2.26106	-1.45648	0.53507
C	-3.17205	0.66813	0.08895
H	-3.15358	1.76054	0.15465
H	-3.71481	0.29031	0.9645
H	-3.76153	0.39815	-0.79623

MPCam-pentimer

Title Card Required

Symbolic Z-matrix:
Charge = 0 Multiplicity = 1

C	6.07814	-1.19032	-0.65749
C	7.49623	-1.18241	-0.84257
C	7.94905	0.09578	-0.51747
C	5.72762	0.09977	-0.23545
H	8.95316	0.49397	-0.4781
N	6.88789	0.8448	-0.15318
H	6.85722	1.83099	0.13516
C	5.16571	-2.35969	-0.90703
H	5.72539	-3.17329	-1.36892
H	4.32524	-2.09265	-1.5615
H	4.74957	-2.76408	0.02792
C	8.33814	-2.3113	-1.29112
O	7.99211	-3.48926	-1.24508
N	9.60118	-1.96194	-1.74407
H	10.10576	-2.72156	-2.18333
H	9.72809	-1.05321	-2.16788
C	4.43844	0.66772	0.10799
N	3.35796	-0.15555	0.25004
C	2.2203	0.54704	0.60467
C	2.56663	1.88959	0.67451
C	3.9669	1.98401	0.34575
H	3.40758	-1.16349	0.23161
C	1.63947	2.98396	1.13261
H	0.83939	2.56662	1.75121
H	1.13673	3.5054	0.3058
H	2.17354	3.73095	1.72655
C	4.7524	3.22554	0.2386
O	5.98816	3.30337	0.34496
N	4.0439	4.38213	0.03257
H	4.60484	5.19991	-0.16483
H	3.1135	4.35447	-0.3558
C	0.9232	-0.09713	0.76787
N	-0.18661	0.51056	0.26716
C	-1.31259	-0.24976	0.47885
C	-0.91556	-1.41474	1.14574
C	0.5001	-1.32163	1.33138
H	-0.24127	1.39448	-0.25287
C	-1.80742	-2.5213	1.63809

H	-2.70902	-2.12629	2.12505
H	-1.276	-3.14949	2.352
H	-2.1206	-3.19249	0.82357
C	1.30941	-2.34249	2.03452
O	0.92865	-3.49748	2.21224
N	2.56919	-1.95463	2.46469
H	2.73969	-0.97945	2.67512
H	3.00897	-2.62168	3.08721
C	-2.61048	0.18246	0.00001
N	-3.64815	-0.70941	-0.05966
C	-4.81509	-0.10428	-0.50011
C	-4.52371	1.22152	-0.76384
C	-3.13418	1.42043	-0.44251
H	-3.60334	-1.6441	0.31635
C	-5.49434	2.19597	-1.36437
H	-6.27363	1.65825	-1.91343
H	-5.00242	2.88628	-2.05565
H	-6.01459	2.77751	-0.59221
C	-2.39611	2.69239	-0.54091
O	-1.17088	2.79133	-0.73326
N	-3.14219	3.83363	-0.43809
H	-2.62454	4.70075	-0.39871
H	-4.06411	3.81564	-0.02895
C	-6.00574	-0.91224	-0.71039
N	-5.88296	-2.13852	-1.32367
C	-7.1099	-2.74909	-1.42748
C	-8.0567	-1.9279	-0.86259
C	-7.36169	-0.75121	-0.39454
H	-7.21588	-3.72378	-1.88265
H	-5.03463	-2.45743	-1.76869
C	-9.51285	-2.28672	-0.75193
H	-9.67193	-3.32191	-1.07014
H	-10.15131	-1.66116	-1.39358
H	-9.88352	-2.19097	0.2746
C	-7.88255	0.38992	0.39581
N	-9.25536	0.50107	0.48498
H	-9.58013	1.3583	0.91257
H	-9.85337	0.09174	-0.21665
O	-7.15794	1.18746	0.98667

MPCOSH-monomer

Title Card Required

Symbolic Z-matrix:
Charge = 0 Multiplicity = 1

N	2.46716	-0.88149	-0.09395
C	2.37659	0.49403	-0.02472
C	1.04951	0.85067	0.03688
C	0.29922	-0.38718	0.00571
C	1.2246	-1.42314	-0.06984
H	3.26236	1.11315	-0.01579
H	1.04902	-2.4871	-0.11019
C	0.58691	2.27661	0.1463
H	1.44593	2.93976	0.29279
H	-0.09233	2.4295	0.99274
H	0.0721	2.62302	-0.7603
C	-1.12724	-0.74635	0.06024
O	-1.50829	-1.89103	0.212
S	-2.43965	0.50684	-0.11339
H	-1.69137	1.58829	-0.39695
H	3.32739	-1.40535	-0.15376

MPCOSH-pentimer

Title Card Required

Symbolic Z-matrix:
Charge = 0 Multiplicity = 1

N	-6.15524	-0.0601	0.51211
C	-4.89379	-0.27175	-0.02564
C	-4.74446	-1.63833	-0.24299
C	-5.97641	-2.25111	0.17878
C	-6.8183	-1.23178	0.61528
H	-7.82711	-1.29995	0.99285
C	-3.5479	-2.26429	-0.90603
H	-2.97679	-1.50981	-1.45446
H	-3.84952	-3.03416	-1.62299
H	-2.84922	-2.73074	-0.19836
C	-6.48017	-3.63555	0.20419
O	-7.66328	-3.89977	0.28089
S	-5.33378	-5.05145	0.16941
H	-4.16768	-4.39272	0.3075
H	-6.53765	0.85137	0.72083
C	-3.93131	0.80849	-0.20512
C	-3.95906	2.07417	-0.81929
C	-2.68233	2.704	-0.59927
C	-1.92	1.81138	0.13765

N	-2.69068	0.67695	0.34767
H	-2.4269	-0.09309	0.9475
C	-2.21957	4.02213	-1.1383
H	-2.73543	4.85407	-0.64833
H	-2.43261	4.10593	-2.20832
H	-1.14407	4.14537	-0.98009
C	-5.00153	2.69044	-1.64698
O	-4.98454	3.85581	-1.98819
S	-6.36401	1.60148	-2.23313
H	-6.94186	2.61345	-2.90973
C	-0.52229	1.7898	0.54937
C	0.33262	2.67546	1.2334
C	1.62519	2.05608	1.32068
C	1.50888	0.8058	0.71048
N	0.21388	0.6866	0.25239
H	-0.10964	-0.1521	-0.22683
C	2.83564	2.61004	2.01632
H	2.5482	3.22279	2.87247
H	3.41849	3.26968	1.35941
H	3.4912	1.80801	2.37042
C	0.02167	3.94989	1.89506
O	0.86528	4.77353	2.19193
S	-1.7232	4.21713	2.3829
H	-1.43462	5.39756	2.96543
C	2.47655	-0.25166	0.49703
C	2.37041	-1.66264	0.36797
C	3.70372	-2.18271	0.19198
C	4.56502	-1.09827	0.22289
N	3.80495	0.03813	0.43548
H	4.17492	0.97697	0.40286
C	4.13379	-3.5899	-0.12524
H	5.09131	-3.5779	-0.65445
H	3.40395	-4.09683	-0.76269
H	4.2654	-4.217	0.76725
C	1.10729	-2.40024	0.40575
O	0.03001	-1.98185	-0.01205
S	1.03774	-4.05468	1.13709
H	2.25807	-4.08239	1.7066
C	6.0194	-1.04461	0.11441
C	6.92141	-0.30141	-0.66782
C	8.25784	-0.64743	-0.24617
C	8.12138	-1.58611	0.74774
N	6.78087	-1.81526	0.95291
H	8.87273	-2.11086	1.32038
H	6.38942	-2.39729	1.67891
C	9.55793	-0.12857	-0.78389
H	9.64479	-0.29838	-1.86181
H	10.39899	-0.62331	-0.28657
H	9.65143	0.95175	-0.63476
C	6.66966	0.60659	-1.79134
O	7.52601	1.31142	-2.28614

S	4.97466	0.61333	-2.50633
H	5.30967	1.54184	-3.42312

$MPSO_4$ - monomer

Symbolic Z-matrix:
Charge = 0 Multiplicity = 1

N	2.3041	-1.35785	-0.00402
C	2.60438	-0.01096	0.01952
C	1.43021	0.70675	0.01729
C	0.38671	-0.27741	-0.00621
C	0.95233	-1.53706	-0.01889
H	3.62851	0.33336	0.03668
H	0.49274	-2.51184	-0.0509
H	2.98343	-2.10343	-0.01805
S	-1.32772	0.08597	-0.01538
O	-1.77266	0.57082	1.29458
O	-1.66016	0.83675	-1.21869
O	-1.94431	-1.44054	-0.16824
H	-2.51137	-1.56736	0.61554
C	1.27045	2.19783	0.0379
H	2.24504	2.69442	0.07015
H	0.69426	2.52206	0.9125
H	0.73484	2.55099	-0.85054

$MPSO_4$ - Pentimer

Title Card Required

Symbolic Z-matrix:
Charge = 0 Multiplicity = 1

N	2.949	-0.43337	-0.17921
C	1.81723	0.24191	0.24001
C	2.20746	1.52251	0.63848
C	3.61762	1.58271	0.42438
C	4.0634	0.34719	-0.05485
H	2.97116	-1.44878	-0.25435
S	4.59851	3.02602	0.6572
O	4.44013	3.5045	2.02339
O	5.91342	2.83343	0.05208
O	3.80254	4.12862	-0.28066
H	4.28577	4.17467	-1.12694
C	1.3539	2.6283	1.192
H	0.54392	2.22642	1.80973
H	0.90762	3.24137	0.39903
H	1.95316	3.29163	1.81908
C	0.48442	-0.33653	0.18556
C	-0.06002	-1.63958	0.17734
C	-1.48847	-1.55471	0.11034
C	-1.78633	-0.19576	0.08729

N	-0.59277	0.4972	0.13617
H	-0.54004	1.48861	-0.08219
C	-2.44427	-2.71305	0.05191
H	-2.63731	-3.13734	1.04559
H	-2.03256	-3.52281	-0.55485
H	-3.3994	-2.4278	-0.3967
S	0.76278	-3.17349	0.31991
O	2.21422	-2.98517	0.42565
O	0.09775	-4.04889	1.28127
O	0.44966	-3.78733	-1.18363
H	0.50055	-4.76066	-1.10318
C	-3.08119	0.47276	0.09736
N	-4.15567	-0.16347	0.65337
C	-5.31525	0.5804	0.5353
C	-5.00049	1.75865	-0.1135
C	-3.59103	1.70184	-0.36847
H	-4.11552	-1.07359	1.08755
C	-5.96841	2.84028	-0.49051
H	-6.99418	2.49534	-0.33699
H	-5.85774	3.1127	-1.54465
H	-5.8098	3.75028	0.09846
S	-2.76274	2.94889	-1.28445
O	-1.30658	2.85294	-1.07801
O	-3.31069	3.04239	-2.62549
O	-3.22358	4.32242	-0.50507
H	-2.46086	4.61338	0.02946
C	-6.58643	0.08731	1.06849
C	-7.53215	-0.80634	0.5664
C	-8.58554	-0.97179	1.52427
C	-8.2345	-0.16855	2.58924
N	-7.04288	0.45318	2.3078
H	-8.74706	-0.00047	3.52547
H	-6.5517	1.08861	2.92056
C	-9.82071	-1.82014	1.43883
H	-10.41169	-1.71456	2.35421
H	-9.57146	-2.87669	1.30446
H	-10.45168	-1.53702	0.59013
S	-7.52091	-1.46541	-1.06187
O	-8.46413	-2.57369	-1.11575
O	-7.56159	-0.40623	-2.07097
O	-5.98104	-2.07843	-1.12953
H	-5.62611	-1.78822	-1.99205
C	5.37004	-0.19992	-0.39111
C	6.55647	-0.26983	0.324
C	7.45152	-1.02382	-0.49628
C	6.80649	-1.39513	-1.65981
N	5.54168	-0.90282	-1.58015
H	7.16692	-1.94298	-2.51567
H	4.85987	-0.93598	-2.32413
C	6.84803	0.28305	1.6853
H	7.50459	1.15645	1.61792

H	7.34689	-0.46723	2.30835
H	5.93081	0.59328	2.19333
S	9.09697	-1.44516	-0.05179
O	9.86918	-0.23036	0.16073
O	9.11388	-2.51121	0.95358
O	9.59337	-2.14711	-1.46472
H	9.88339	-3.04496	-1.21621

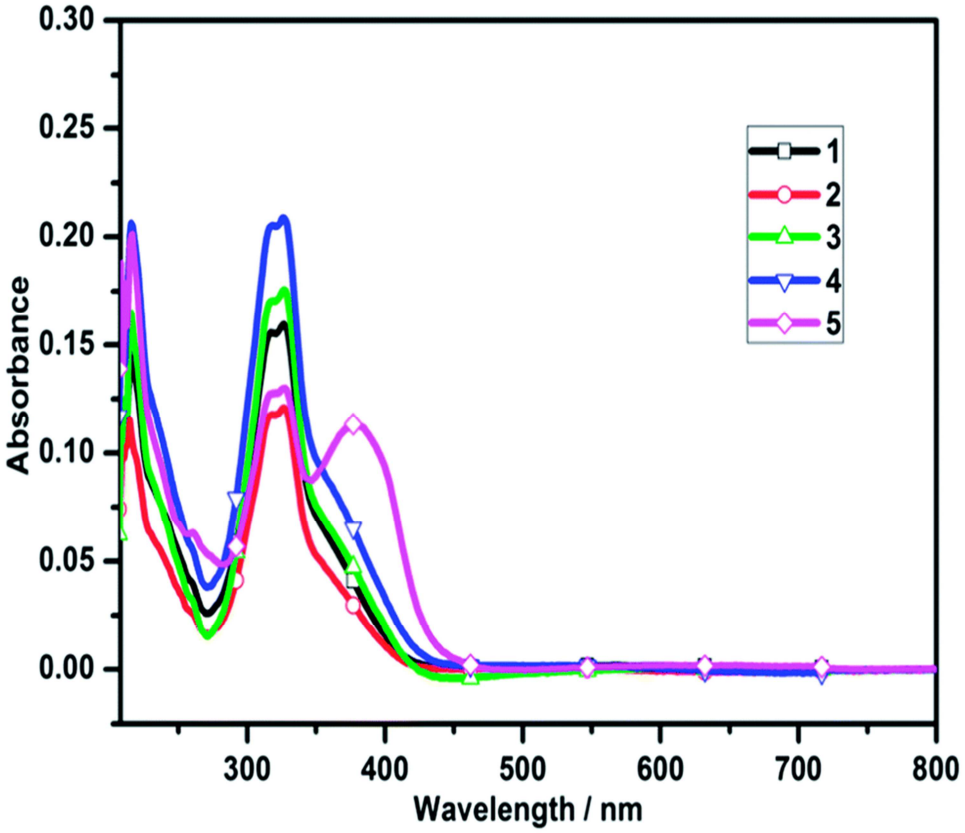

Experimental UV-VIS spectrum of pyrrole at different solvent phase (Heeralal and Krishamurthi, 2014)

UV/VIS Spectra for monomers

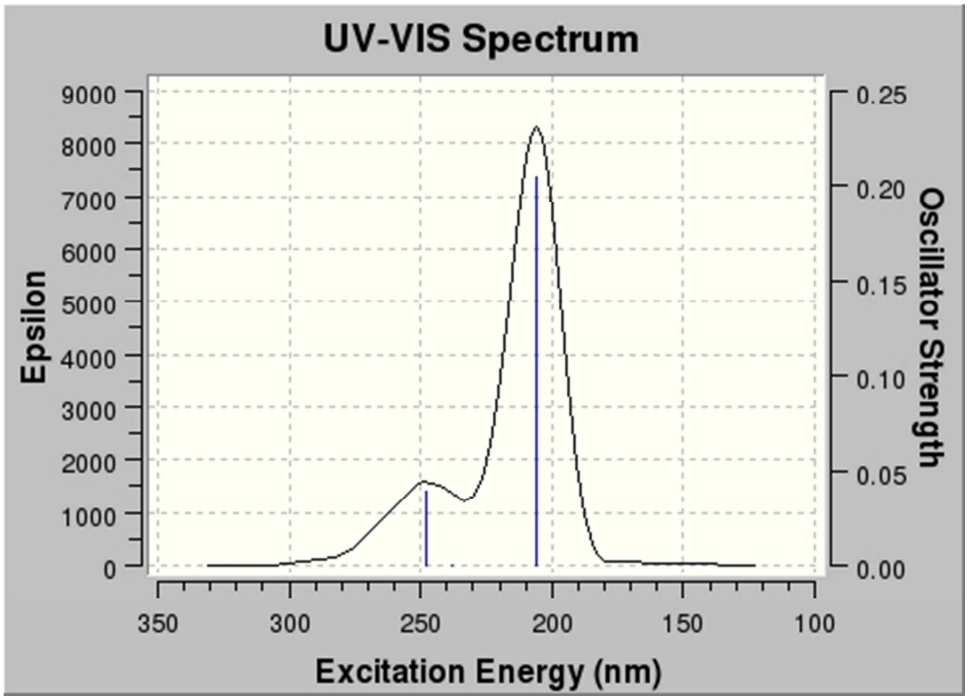

UV/VIS of MPC monomer

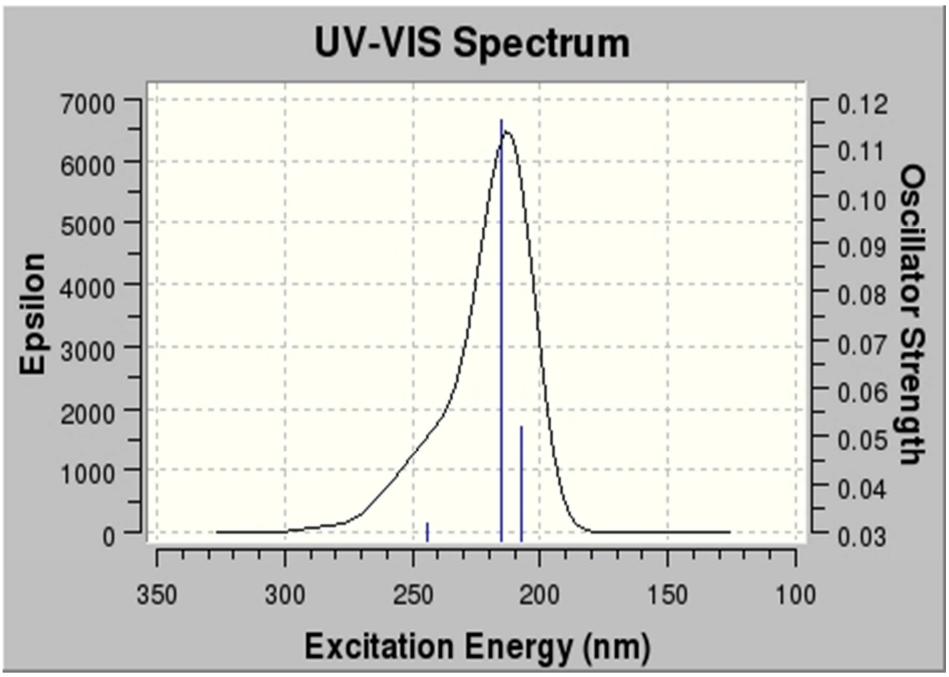

MPC[b] monomer

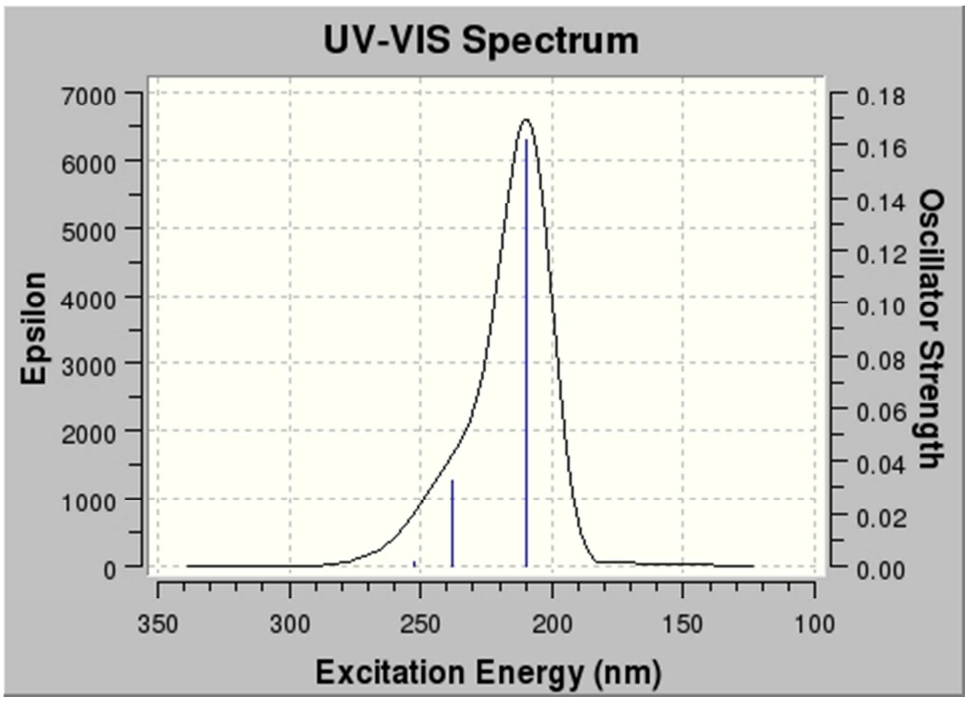

MPCam UV/VIS monomer

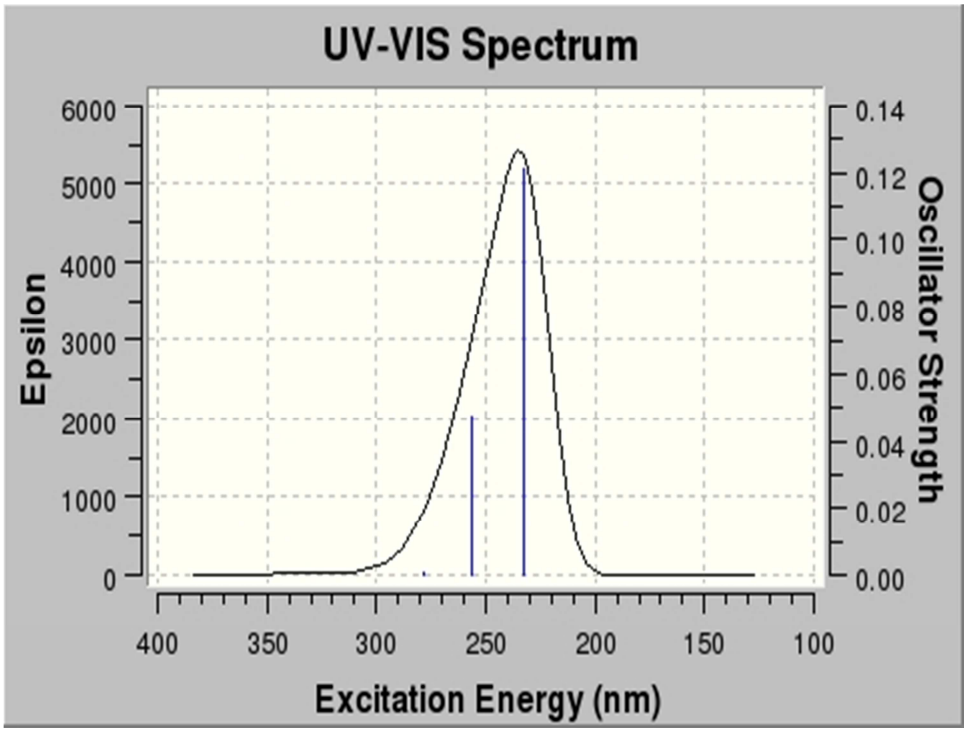

MPCOSH UV/VIS monomer

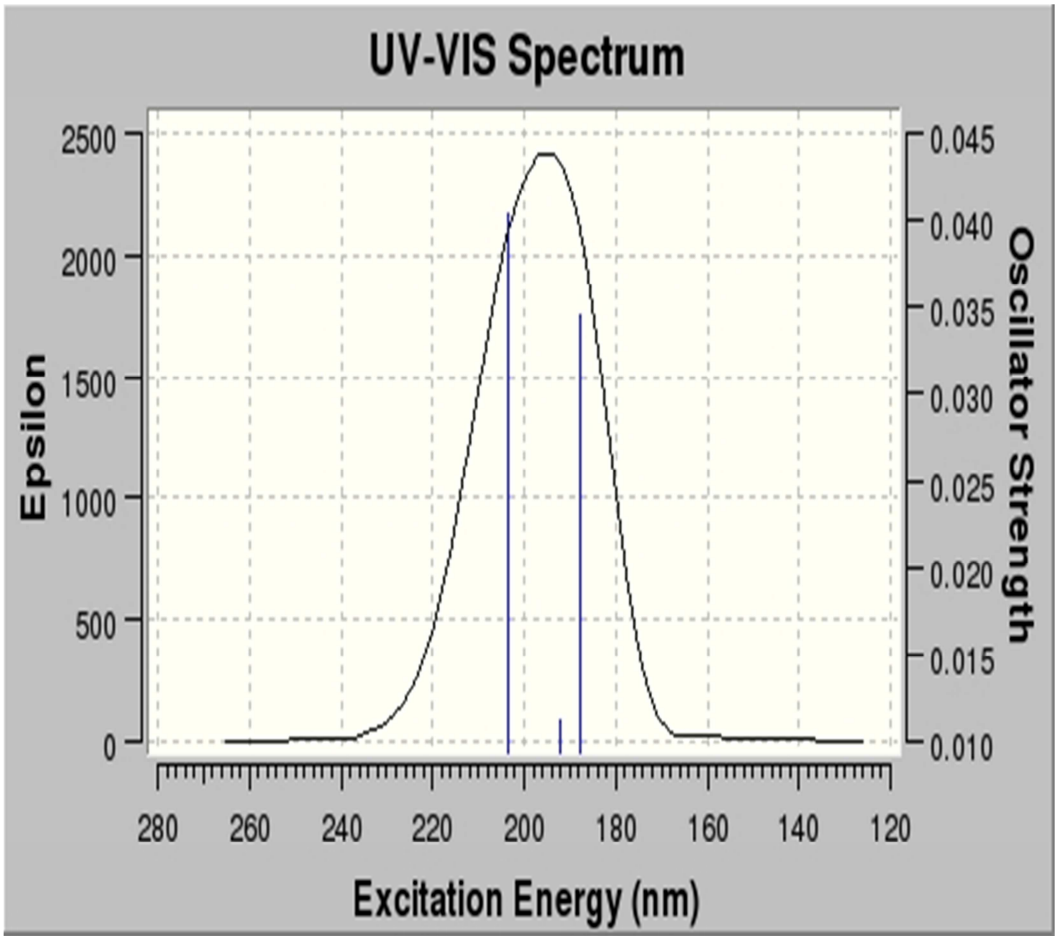

UV/VIS of $MPSO_3H$ monomer